mTOR SIGNALLING AND THE REGULATION OF FOXP3 EXPRESSION

A thesis submitted for the degree of

Doctor of Philosophy at the University of Oxford

Trinity Term 2012



CHRISTIAN PETER
Sir William Dunn School of Pathology
Lincoln College, Oxford

Acknowledgements

I thank my supervisors Professor Herman Waldmann and Professor Stephen Cobbold for giving me the opportunity to pursue my D.Phil studies in the Therapeutic Immunology Group. Their passion and knowledge were a constant inspiration over the last four years. Their belief in my scientific capabilities was a source of motivation and gave me the freedom to develop as a scientist. I also wish to thank Herman and Steve for the countless hours they devoted to scientific discussions and the revision of this dissertation.

None of this would have been possible without the funding provided by the Edward Penley Abraham trust.

I wish to thank all members of the Therapeutic Immunology Group. I am particularly thankful to Dr. Eleftherios Agorogiannis, Dr. Kathleen Nolan, Dr. Frederico Regateiro, Mrs. Susan Humm, Dr. Duncan Howie, Dr. Giovanni Piotti, Mr. Hugo Garcia-Rueda, Mr. Adrian Kendal and Dr. Elizabeth Adams. Thank you, Eleftherios, Kathleen, Frederico, Giovanni and Adrian for the great scientific and personal discussions, scientific advice and lots of fun! A special thanks to Kathleen for sharing her expertise in molecular biology and being always approachable and Sue for managing the lab so efficiently.

I wish to thank Professor Oreste Acuto for useful discussions regarding the phospho-proteomic experiments and for allowing me to use instruments in his lab.
Thanks to Dr. Konstantina Nika for the invaluable support with the luciferase assays and western blotting. Thank you Konstantina, Eleanor, Nadina and all the other"fresh air" enthusiasts for making the countless coffee breaks fun!

Thank you, Dr. Masahide and Yukiko Tone for the generous gift of the *Foxp3* luciferase reporter vectors and all their advice.
I wish to thank Dr. David Sabatini and Dr. Nathanael Gray for their kind gift of Torin 1.
I am grateful to Dr. Benjamin Thomas and Mrs. Svenja Hester for the support with the mass spectrometry-based phospho-proteomics experiments.

I wish to thank my graduate advisor Dr. Kevin Maloy for valuable discussions.

Thank you, Mrs. Lucinda Risius and Mrs. Gillian Helstrom for all the help with administrative requests.

Thank you, Naoki and Wei Hao for being fantastic housemates. I really felt at home living with you guys!

I am endlessly thankful to my parents! Without your unconditional support none of this would have been possible. This thesis is also dedicated to you!

Finally, I would like to thank my girlfriend Tine! Your love was a tremendous support and gave me the strength to see this through. I cannot wait until we finally share a daily life again, because I know with you by my side it will be great!

mTOR SIGNALLING AND THE REGULATION OF FOXP3 EXPRESSION

A thesis submitted for the degree of
Doctor in Philosophy at the University of Oxford

Trinity Term 2012

CHRISTIAN PETER
Sir William Dunn School of Pathology and Lincoln College

Abstract

Regulatory T-cells (Treg) are essential for the establishment of self-tolerance and they can be identified by the expression of FOXP3, the "master" transcription factor for the development of Treg. A number of essential signals, namely TCR engagement, TGFβ, as well as the inhibition of the kinase mTOR, have been shown to be crucial for the induction of FOXP3 in the peripheral immune system. Despite recent progress, the molecular mechanisms for induction of FOXP3 remains elusive due, at least in part, to the lack of a cell line that mimics the behavior of primary $CD4^+$ T-cells.

Here we report the isolation of a clone B02 from the mouse lymphoma line EL4 that can be induced to express high levels of FOXP3 in up to 50% of the cells. Pharmacological inhibition of mTOR and EAA depletion synergized with TGFβ in the induction, and led to reduced activity of both mTORC1 and mTORC2, which seemed to independently contribute to the enhanced FOXP3 expression. Luciferase reporter assays using *Foxp3* promoter and enhancer sequences indicated that the mTOR inhibition-mediated increase in FOXP3 expression resulted primarily from enhanced transcriptional activity.

In addition to the enhancement of FOXP3 induction, mTOR inhibition reduced the levels of IL-17A, presumably by SOCS-mediated inactivation of STAT3, which could also have accounted for increased *Foxp3* transcription. Although the precise targets of mTOR inhibition involved in the regulation of FOXP3 expression have yet to be identified, both luciferase assays and mass spectrometry-based quantitative phospho-proteomics using SILAC labelled B02 cells, have identified promising candidates. This unique EL4 clone could represent a special resource for investigating the signaling events leading to the induction of FOXP3 as well as events downstream of FOXP3 expression.

Abbreviations

4E-BP1	eIF4E-binding protein 1
7-AAD	7-Aminoactinomycin D
AA	amino acid
AMP	adenosine monophosphate
AMPK	AMP-activated kinase
ANOVA	analysis of variance
AP-1	activator protein 1
APC	antigen presenting cell
Arg	arginine
ATP	adenosine triphosphate
BCA assay	bicinchoninic acid assay
bp	base pair
BSA	Bovine serum albumin
CCR7	CC-chemokine receptor 7
CD	cluster of differentiation
CDS	coding sequence
CFSE	carboxyfluorescein succinimidyl ester
ChIP	Chromatin immune-precipitation
CNS	conserved non-coding sequence
CREB	cAMP response element-binding protein
DAPI	4’,6-diamidino-2-phenylindole
DC	dendritic cell
DEPTOR	DEP domain containing mTOR-interacting protein
DNA	desoxyribonucleic acid
DNMT1	DNA methyl transferase 1
EAA	essential amino acid
EAE	experimental autoimmune encephalomyelitis
EMSA	electrophoretic mobility shift assay
ERK	extracellular signal-regulated kinases
FACS	Fluorescence activated cell sorting
FCS	Fetal calf serum
FKBP12	FK506-binding protein 1A, 12kDa
FOXO1/3A	forkhead box O1/3A
FOXP3	forkhead box P3
GATA3	GATA-binding protein 3
GDP	guanosine diphosphate
GFP	green fluorescent protein
GM-CSF	granulocyte-macrophage colony-stimulating factor
GTP	guanosine triphosphate

h	hour
HIF1α	hypoxia inducible factor 1α
HPLC	High-performance liquid chromatography
HSV	herpes simplex virus
IFNγ	interferon γ
IL	interleukin
IMAC	immobilized metal ion chromatography
IRF1	interferon regulatory factor 1
iTreg	induced Treg
JNK	c-JUN N-terminal kinase
KD	knock-down
LCMV	lymphocytic choriomeningitis virus
LPS	lipopolysaccharide
Lys	lysine
LysC	endoproteinase LysC
MAD	median absolute deviation
MFI	mean or median fluorescence intensity (as indicated)
MHC	major histocompatibility complex
mLST8	mammalian lethal with sec-13 protein 8
MOG	myelin oligodendrocyte glycoprotein
mRNA	messenger RNA
mSIN1	mammalian stress-activated map kinase-interacting protein 1
mTOR	mammalian/mechanistic target of Rapamycin
mTORC	mTOR complex
NFAT	nuclear factor of activated T-cells
nTreg	natural Treg
P	phospho
PAF	platelet activating factor
PAT	proton-assisted amino acid-transporter
PBS	Phosphate buffer saline
PCR	polymerase chain reaction
PI3K	phosphoinositide 3-kinase
PKCα	protein kinase C α
PMA	Phorbol myristate acetate
PP2A	protein phosphatase 2A
PPAR-γ	peroxisome proliferator-activated receptor γ
PRAS40	proline-rich AKT substrate 40kDa
PROTOR 1/2	protein observed with RICTOR 1 and 2
pS6	phosphorylated RPS6
PTEN	phosphatase-and-tensin homolog deleted on chromosome 10
qPCR	quantitative PCR

RAG A-D	RAG-related GTP-binding-proteins A–D
RAPTOR	regulatory-associated protein of mammalian target of Rapamycin
RAR	retinoic acid receptor
REDD1	regulated in development and DNA damage response 1
RHEB	RAS homolog enriched in brain
RICTOR	Rapamycin-insensitive companion of mTOR
RNA	ribonucleic acid
RORγT	retinoic acid-related orphan receptor γ T
RQ	relative quantity
RT	room temperature
RUNX1	Runt-related transcription factor 1
S	serine
S1PR1	sphingosine-1-phosphate receptor 1
S6K1	S6 kinase 1
SCX	strong cation exchange
SDS-PAGE	sodium dodecyl sulfate polyacrylamide gel electrophoresis
Ser	serine
SGK1	serum- and glucocorticoid-induced protein kinase 1
shRNA	short hairpin RNA
SILAC	stable isotope labelling by amino acids in cell culture
SMAD3	Mothers against decapentaplegic homolog 3
SOCS	suppressor of cytokine signalling
SP-1	specificity protein 1
SREB1/2	sterol-regulatory element-binding protein 1/2
STAT	signal transducer and activator of transcription
T	threonine
TCR	T-cell receptor
TFA	trifluoroacetic acid
TGFβ	transforming growth factor β
Th	T-helper cell
TIEG1	TGFβ inducible early gene 1
TiO_2	Titanium dioxide
TK	thymidine kinase
TLR	toll-like receptor
TNFα	tumor necrosis factor α
TRAF6	TNFR-associated factor 6
Treg	regulatory T-cell
TSC 1/2	tuberous sclerosis 1/2
UTR	untranslated region
WB	western blot
Y	tyrosine

Table of Figures

Figure 1.	**Domain structure of mTOR and the composition of mTORC1 and mTORC2 signalling complexes**	**6**
Figure 2.	**Inputs and outputs of the mTOR signalling pathway**	**9**
Figure 3.	**The differentiation of naïve $CD4^+$ T-cells (Tn) into effector subsets is controlled by cytokines**	**25**
Figure 4.	**Regulation of $CD4^+$ T-cell differentiation by mTORC1 and mTORC2 activity**	**31**
Figure 5.	**The Foxp3 locus and the regulation of gene expression**	**33**
Figure 6.	**Stimulation of the T-cell line EL4 results in weak FOXP3 expression**	**79**
Figure 7.	**Isolation of a highly FOXP3 inducible clone G08 by limiting dilution cloning of EL4 cells and screening**	**81**
Figure 8.	**Isolation of a highly FOXP3 inducible reclone B02 by limiting dilution cloning of EL4 clone G08 and screening**	**83**
Figure 9.	**The induction of FOXP3 in EL4.B02 is highly dependent on TGFβ**	**86**
Figure 10.	**The mTORC1 inhibitor Rapamycin does not facilitate the induction of FOXP3 or reduce mTORC1 activity**	**88**
Figure 11.	**Enhanced FOXP3 induction coincides with decreased mTORC1 activity over time.**	**90**
Figure 12.	**Cell titration reveals cell density dependent mTORC1 inhibition and FOXP3 induction.**	**92**
Figure 13.	**Stimulation at high cell density enhances FOXP3 induction and reduces mTORC1 activity**	**94**
Figure 14.	**Stimulation at high density enhances *Foxp3* transcription**	**96**
Figure 15.	**Stimulation in conditioned medium enhances the induction of FOXP3**	**99**
Figure 16.	**Stimulation of cells at low density with TGFβ and in the presence of high cell numbers enhances the induction of FOXP3**	**101**
Figure 17.	**Stimulation of cells under limiting concentrations of EAA enhances the induction of FOXP3**	**104**
Figure 18.	**TGFβ reduces the levels of pS6 via activation of PP2A**	**105**
Figure 19.	**Stimulation of cells under low density and limiting amounts of EAA results in prolonged mTORC1 inhibition compared to stimulation at high density and normal levels of EAA**	**106**
Figure 20.	**Stimulation in limiting concentrations of EAA enhances *Foxp3* transcription**	**107**
Figure 21.	**Stimulation in limiting concentrations of EAA results in prolonged mTORC1 inhibition and enhances the induction of FOXP3**	**110**
Figure 22.	**Stimulation at high cell densities in limiting concentrations of EAA enhances the induction of FOXP3**	**112**
Figure 23.	**Rapamycin inhibits mTORC1 at low concentrations and enhances the induction of FOXP3**	**117**
Figure 24.	**The allosteric mTORC1 inhibitor Rapamycin enhances the induction of FOXP3**	**119**
Figure 25.	**Rapamycin increases the levels of *Foxp3* mRNA**	**120**
Figure 26.	**Rapamycin and TGFβ lower the phosphorylation levels of AKT at S473**	**127**
Figure 27.	**TGFβ reduces the levels of pAKT via activation of PP2A.**	**129**
Figure 28.	**EAA starvation reduces the levels of pAKT**	**130**
Figure 29.	**The ATP-competitive mTOR inhibitor Torin1 inhibits both mTORC1 and 2 and enhances the induction of FOXP3**	**134**
Figure 30.	**A time course analysis reveals differential kinetics of mTORC2 inhibition by Rapamycin and Torin1**	**138**
Figure 31.	**Torin 1 enhances FOXP3 expression with faster kinetics than Rapamycin**	**140**
Figure 32.	**Rapamycin and Torin 1 enhance *Foxp3* transcription at early time points during the stimulation**	**142**
Figure 33.	**Titration of Rapamycin reveals differential sensitivity of mTORC1 and 2 to the drug and highlights a role for mTORC1 in regulating FOXP3 expression**	**145**
Figure 34.	**Schematic illustration of the *Foxp3* locus, the transcription factors that bind to the regulatory elements that were investigate and the *Foxp3* luciferase vectors**	**150**

Figure 35.	**Luciferase control vectors do show any considerable responses upon stimulation**	**153**
Figure 36.	**mTOR inhibition enhances TGFβ and αCD3 stimulation induced CNS1 and 2 activation**	**155**
Figure 37.	**Significantly shortened CNS1 and 2 retain their TGFβ, CD3 and mTOR responsiveness**	**157**
Figure 38.	**Stimulation with αCD3, TGFβ and Torin 1 does not result in reduced levels of JUN B**	**160**
Figure 39.	**mTOR inhibition does not enhance AP-1 activation**	**162**
Figure 40.	**TIEG1 is constitutively expressed and translocated to the nucleus**	**164**
Figure 41.	**TIEG1 binds to *Foxp3* promoter oligos but the binding is not affected by mTOR inhibition**	**168**
Figure 42.	**SMAD3 phosphorylation is induced upon stimulation in the nuclear fraction but is unaffected by mTOR inhibition**	**170**
Figure 43.	**Only few cells translocate FOXO3A to the nucleus in response to PI3K or mTOR inhibition**	**172**
Figure 44.	**FOXO1 is consistently located in the cytoplasm and only few cells translocate FOXO3A to the nucleus in response to mTOR inhibition**	**174**
Figure 45.	**PP2A inhibition does not enhance αCD3 and TGFβ inducted FOXP3 expression.**	**176**
Figure 46.	**PP2A inhibition does not significantly increase the levels of pS6 and pAKT**	**177**
Figure 47.	**PP2A does not seem to be involved in the Rapamycin mediated enhancement of FOXP3 induction**	**178**
Figure 48.	**αCD3 stimulated EL4.B02 constitutively phoshporylates STAT3 and expresses high levels of IL-17A**	**180**
Figure 49.	**Exogenous IL-6 or TGFβ do not increase STAT3 phosphorylation levels or IL-17A expression**	**182**
Figure 50.	**IL-17A protein expression but *Il-17a* mRNA levels is independent of TGFβ**	**185**
Figure 51.	**Rapamycin reduces the levels of STAT3 phosphorylation**	**187**
Figure 52.	**Rapamycin inhibits stimulation induced phosphorylation of STAT3 in mouse $CD4^{+}FOXP3^{-}$ T cells**	**188**
Figure 53.	**Rapamycin reduced the expression of IL-17A**	**189**
Figure 54.	**Titration of Rapamycin indicates a role for mTORC1 in regulating IL-17A expression**	**191**
Figure 55.	**Torin 1 inhibits IL-17A in a concentration dependent manner**	**193**
Figure 56.	**TGFβ increases the expression of *Socs1* and *Socs3***	**195**
Figure 57.	**Rapamycin enhances the expression of *Socs1* and *Socs3***	**196**
Figure 58.	**EAA starvation enhanced the expression of *Socs1* and *Socs3***	**198**
Figure 59.	***Stat3* targeting shRNA 53 knocks down *Stat3* expression efficiently**	**200**
Figure 60.	**Screening of 48 sh53 *Stat3* targeting lines identifies several lines with increased *Stat3* knock-down efficiency**	**202**
Figure 61.	**Low cell density stimulation of sh53 *Stat3* knock down lines reveals unresponsiveness to stimuli inducing IL-17A and FOXP3 expression, which is partially restored at high cell density**	**204**
Figure 62.	**Constitutively active STAT3 dimers do not seem to affect the expression of FOXP3**	**207**
Figure 63.	**Double enhancer constructs retain the responsiveness of the individual enhancer by responding to their TGFβ, CD3 and mTOR inhibition**	**211**
Figure 64.	**The activity of the *Foxp3* promoter+CNS1 seems to be reduced in the presence of CNS2 and TGFβ.**	**213**
Figure 65.	**Mutation of the STAT3 binding site in CNS2 does not enhance the activity of double enhancer constructs**	**216**
Figure 66.	**mTOR inhibition by Rapamycin or EAA starvation does not inhibit *Il-17a* expression at intermediate time points.**	**218**
Figure 67.	**Rapamycin inhibits *Il-17a* expression at late time points and enhances *Foxp3* expression**	**219**
Figure 68.	**PMA partially blocks both the Rapamycin induced reduction of *Il-17a* expression and the enhancement of *Foxp3* induction.**	**222**
Figure 69.	**Workflow of the phosphoproteomics experiments**	**229**
Figure 70.	**Heavy SILAC labelled EL4.B02 cells retain their responsiveness with respect to mTOR inhibition mediated FOXP3 induction**	**230**
Figure 71.	**Massspectra of peptides derived from intermediate and heavy SILAC labelled EL4.B02 cells**	**233**

Figure 72.	**Massspectra of peptides derived from 1:1:1 (light:intermediate:heavy) mix of SILAC labelled cells**	**234**
Figure 73.	**SCX-fractionation separates peptides according to their solution charge**	**236**
Figure 74.	**Titanium dioxide incubation moderately enriches for phospho-peptides**	**238**
Figure 75.	**Titanium dioxide preferentially enriches for monophosphorylated peptides**	**240**
Figure 76.	**KEGG-pathway enrichment of 1st phospho-proteomics data set**	**244**
Figure 77.	**mTOR inhibition reduces and increases the levels of phosphorylation at a large number of phospho-sites.**	**245**
Figure 78.	**The adapted SCX-protocol fractionates peptides with lower solution charge over an increased number of fractions**	**252**
Figure 79.	**The adapted TiO_2-protocol enriches for phospho-peptides with very high efficiency**	**254**
Figure 80.	**The adapted TiO_2-protocoll shows increased efficiency to enrich for peptides with multiple phosphorylations**	**256**
Figure 81.	**KEGG-pathway enrichment of 2nd phospho-proteomics data set.**	**259**
Figure 82.	**Proteins annotated as components of the mTOR (A) and TCR (B) signalling pathway**	**260**
Figure 83.	**mTOR inhibition reduces and increases the levels of phosphorylation at a large number of phospho-sites**	**262**
Figure 84.	**Common and distinct phospho-proteins and phospho-peptides were detected in the two phospho-proteomics experiments**	**263**

Table of Contents

Acknowledgements I
Abstract III
Abbreviations V
Table of Figures IX
Chapter 1 | INTRODUCTION 1
1 | mTOR signalling and the immune system 3
1.1 | The mTOR signalling pathway 4
1.1.1 | mTOR as part of mTOR complexes 1 and 2 4
1.1.2 | Regulation of mTORC1 and mTORC2 activity 6
1.1.2.1 | Amino Acid sensing and AA induced activation of mTORC1 activity 10
1.1.3 | Downstream targets and effector functions of mTORC1 and 2 12
1.2 | mTOR and the regulation of antigen-presenting cell differentiation and function 14
1.3 | The effect of mTOR inhibition on other immune cells 17
1.4 | mTOR signalling regulates the differentiation and function of T-cells 19
1.4.1 | Costimulation, cytokine signalling and TCR engagement affect mTOR activity 19
1.4.2 | mTOR activity and the induction of anergy in T-cells 20
1.4.3 | mTOR in T-cell trafficking 21
1.4.4 | mTOR signalling and the differentiation of $CD8^+$ T-cells 22
1.4.5 | mTOR and the regulation of $CD4^+$ T-cell differentiation 23
1.4.5.1 | The role of the two mTOR complexes in regulating T-cell differentiation 28
1.5 | The molecular orchestration of the transcriptional activation of the *Foxp3* locus 31
1.6 | Aims and format of the thesis 37
Chapter 2 | MATERIALS AND METHODS 39
2.1 | Materials 41
2.1.1 | Consumables 41
2.1.2 | Reagents 42
2.1.3 | Antibodies 46
2.1.4 | Taqman-Assays 47
2.1.5 | Primers 48
2.1.5 | Mice 51
2.2 | Methods 51
2.2.1 | Schedule 1 termination 51
2.2.2 | Cell culture 51
2.2.2.1 | Culture media and incubation 51
2.2.2.2 | Regular culture medium (R-10 medium) 52
2.2.2.3 | Medium with limiting concentrations of EAA 52

2.2.2.4 | SILAC medium *52*
2.2.2.5 | Dialysis of fetal calf serum *53*
2.2.2.6 | Cell counting using Neubauer haemocytometer *53*
2.2.2.7 | Freezing and thawing of cells *53*
2.2.2.8 | Preparation of spleen cell suspensions *54*
2.2.2.9 | Isolation of $CD4^+$ T-cells from mouse spleens *54*
2.2.2.10 | Culture of EL4 and EL4.B02 cells *54*
2.2.2.11 | Limiting dilution cloning *54*
2.2.2.12 | Coating of tissue culture plastics with αCD3 antibodies *55*
2.2.2.13 | Stimulation of cells *55*
2.2.2.14 | Selection of stable transfectants using Puromycin and G418 *56*
2.2.4 | Fluorescence-activated cell sorting (FACS) analysis 56
2.2.5 | Staining of cells for confocal immuno-fluoresence microscopy 58
2.2.6 | Electroporation of cells 58
2.2.7 | Luciferase assay 59
2.3 | Methods of molecular biology **61**
2.3.1 | Mini, Midi and Maxi-preparation of plasmid DNA 61
2.3.2 | Total RNA isolation 61
2.3.3 | cDNA synthesis 62
2.3.4 | Real-time PCR using TaqMan® gene expression assays 62
2.3.5 | TOPO® TA cloning® of *Stat3* CDS 62
2.3.6 | Cloning of wildtype and mutant *Stat3* expression vectors 63
2.3.7 | Site-directed mutagenesis PCR 63
2.3.8 | Cloning of Firefly luciferase CNS1 and CNS2 double enhancer constructs 64
2.3.9 | Sequencing 64
2.3.10 | Electrophoretic mobility shift assay (EMSA) 65
2.4 | Proteomics techniques **67**
2.4.1 | Preparation of cytoplasmic and nuclear extracts 67
2.4.2 | Western Blot 67
2.4.3 | Mass spectrometry based phospho-proteomics 69
2.4.3.1 | SILAC labelling of EL4.B02 cells and confirmation of homogeneous labelling *69*
2.4.3.2 | Stimulation of cells *70*
2.4.3.3 | Workflow of 1^{st} phospho-proteomics experiment *70*
2.4.3.4 | Workflow of 2^{nd} phospho-proteomics experiment *71*
2.4.3.5 | Q Exactive Mass Spectrometry Analysis *72*
2.5 | Statistical analysis **74**

Chapter 3 | GENERATION AND CHARACTERIZATION OF THE FOXP3 INDUCIBLE EL4 CLONE B02 75

3.1 | Characterization of FOXP3 induction in EL4 cells and isolation of a highly responsive clone B02 77

3.2 | FOXP3 induction in EL4.B02 is dependent on TGFβ 84

3.3 | Cell density dependent mTORC1 inhibition is associated with upregulation of FOXP3 87

3.4 | Stimulation of cells in conditioned medium and in transwell conditions recapitulates the enhanced induction of FOXP3 under high cell density stimulation 98

3.5 | Stimulation of cells under limiting concentrations of EAA facilitates the induction of FOXP3 102

3.6 | The allosteric mTORC1 inhibitor Rapamycin enhances the induction of FOXP3 114

Chapter 4 | CONTRIBUTION AND KINETICS OF mTORC1 AND mTORC2-MEDIATED FOXP3 INDUCTION 123

4.1 | Stimulation in the presence of Rapamycin, Torin 1 and EAA starvation results in mTORC2 inhibition 125

4.2 | Kinetics of the enhancement of FOXP3 induction mediated by mTORC inhibition 136

4.2.1 | Rapamycin and Torin 1 display distinct kinetics of mTORC2 inhibition and enhanced FOXP3 induction 136

4.3 | mTORC1 inhibition by Rapamycin contributes to the induction of FOXP3 141

4.4 | Rapamycin titrations suggest roles for mTORC1 and mTORC2 mediated enhancement of FOXP3 induction 143

Chapter 5 | THE DOWNSTREAM TARGETS OF mTOR INVOLVED IN THE INDUCTION OF FOXP3 147

5.1 | Luciferase assays identify mTOR responsive regulatory elements in the *Foxp3* CNS1 and 2 149

5.2 | AP-1 does not seem to be involved in mTOR mediated induction of FOXP3 158

5.3 | TIEG1 constitutively localizes to the nucleus and seems to bind to *Foxp3* promoter sequences but neither is affected by mTOR inhibition 163

5.4 | SMAD3 phosphorylation at S423/425 is not regulated by mTOR inhibition 169

5.5 | The contribution of FOXO1 and FOXO3A to the induction of FOXP3 under mTOR inhibition conditions remains questionable 170

5.6 | The serine/threonine phosphatase PP2A does not seem to be involved in the mTOR inhibition mediated induction of FOXP3 175

5.7 | In the presence of TCR stimulation EL4.B02 constitutively phosphorylates STAT3 179

5.7.1 | STAT3 phosphorylation and IL-17A expression in EL4.B02 is independent of exogenous IL-6 181

5.7.2 | The expression of *Il-17a* mRNA is increased by TGFβ, whereas IL-17A protein expression is largely independent of TGFβ 183

5.7.3 | mTOR inhibition by Rapamycin reduces the levels of pSTAT3 and reduces the proportion of IL-17A$^+$ cells 186

5.7.4 | Both Rapamycin and Torin 1 reduce the proportion of IL-17A$^+$ cells in a concentration dependent manner 190

5.7.5 | Mechanism of mTOR mediated reduction of STAT3 phosphorylation: Rapamycin and EAA depletion upregulate *Socs1* and *3* expression and reduce IL-6 production 194

5.7.6 | An analysis of STAT3 knock-down and overexpression of STAT3 mutants fails to establish the role of STAT3 in the regulation of FOXP3 199

5.7.7 | Mutation of the STAT3 binding site in CNS2 of double enhancer constructs raises doubts over the involvement of STAT3 in the mTOR mediated induction of FOXP3 209

5.7.8 | mTOR inhibition by Rapamycin and EAA depletion do not reduce the levels of *Il-17a* mRNA early in the stimulation, but at later time points 217

5.7.9 | PMA partially circumvents Rapamycin mediated reduction of IL-17A and the enhancement of FOXP3 induction 219

Chapter 6 | A PHOSPHO-PROTEOMICS SCREEN TO IDENTIFY DOWNSTREAM TARGETS OF mTOR INVOLVED IN THE INDUCTION OF FOXP3 223

6.1 | EL4.B02 cells readily grow in SILAC labelling medium and retain their FOXP3 inducibility 230

6.2 | Selected proteins in intermediate and heavy SILAC EL4.B02 cells show more than 95% incorporation of the isotopically labelled AAs 231

6.3 | The first phospho-proteomics experiments 235

6.3.1 | SCX fractionation separates peptides based on their solution charge state 235

Figure 73. SCX-fractionation separates peptides according to their solution charge. Top panel (A,C,D) and bottom panel (B,D and F) show results for all peptides or phospho-peptides respectively. (A and B) The proportion of (phospho-)peptides with solution charges of 0 to +6 within the different SCX fractions. (C and D) The absolute number of (phospho-)peptides with solution charges of 0 to +6. (E and F) The absolute number of (phospho-)peptides identified in the SCX fractions. 236

6.3.2 | TiO_2 results in moderate enrichment of phospho-peptides 237

6.3.4 | TiO_2 enriches preferentially for monophosphorylated peptides 239

6.3.5 | Analysis of proteins with sites differentially regulated by Rapamycin and Torin 1 241

6.4 | The second, adapted phospho-proteomics experiment shows enhanced phospho-peptide enrichement, a greater number of identified phospho-peptides and phospho-sites, but little overlap with the 1st experiment 250

6.4.1 | The adapted SCX-protocol fractionates peptides with lower solution charge over an increased number of fractions 251

6.4.2 | The adapted TiO_2-protocol enriches for phospho-peptides with very high efficiency 253

6.4.3 | The adapted TiO_2-protocoll shows increased efficiency to enrich for peptides with multiple phosphorylations 255

6.4.5 | The adapted phospho-proteomics protocol identifies an increased number of phospho-peptides, phospho-sites and phospho-proteins 257

Chapter 7 | GENERAL DISCUSSION 267

References 293

Chapter 1 | INTRODUCTION

1 | mTOR signalling and the immune system

The importance of paracrine and cell-contact dependent signals in the regulation of immune homeostasis and immune responses has long been acknowledged. However, until recently the nutritional and energetic composition of the microenvironment, as well as the contribution of metabolic signals to these processes have largely been underestimated. In recent years, the mammalian/mechanistic target of Rapamycin (mTOR) pathway has emerged as a key sensor of nutritional and energetic signals as well as a major integrator of growth factor and cell surface receptor induced signals. The fact that mTOR affects a multitude of immune cells at various stages in their life cycle does not come as a surprise, considering the position of mTOR at the core of a signalling network that regulates the extensive changes in cellular metabolism during activation, maturation and differentiation of immune cells. By fine tuning metabolic pathways and gene expression profiles according to environmental stimuli, mTOR tightly controls cellular signalling events that ultimately regulate differentiation programs and cellular responses, thereby influencing the final outcome of immune responses [1].

1.1 | The mTOR signalling pathway

1.1.1 | mTOR as part of mTOR complexes 1 and 2

As the acronym TOR (target of Rapamycin) indicates, the discovery of the allosteric TOR inhibitor Rapamycin preceded the identification of its cellular target. Genetic screening of *Saccharomyces cerevisiae* for genes involved in Rapamycin-mediated cell cycle arrest, identified two TOR genes, *TOR1* and *2* [2-4]. Shortly afterwards the mammalian equivalent, mTOR, was purified by biochemical approaches and found to be inhibited by Rapamycin in complex with the immunophilin FK506-binding protein 1A, 12kDa (FKBP12) [5-7]. The evolutionary conserved serine/threonine kinase mTOR, an atypical member of the phosphoinositide 3-kinase (PI3K)-related kinase family, is constitutively expressed and its activity regulated through a variety protein-protein interactions and posttranslational modifications.

The amino terminal portion of mTOR is composed of huntingtin, elongation factor 3, a subunit of protein phosphatase 2A and TOR1 (HEAT) repeats. This cluster of repeats provides an interface for protein-protein interactions that are necessary for the formation of supramolecular complexes that regulate mTOR substrate specificity [8]. The C-terminal part of mTOR comprises a FRAP, ATM, and TRRAP (FAT) domain that interacts with the FATC domain at the C-terminal end of the protein, an interaction known to be essential for mTOR's autophosphorylation and catalytic activity [9, 10]. A FKBP12 Rapamycin-binding (FRB) domain and the kinase domain are located adjacent to the FAT domain [8]. (Figure 1A)

These domains enable mTOR to assemble in two structurally and functionally distinct complexes, mTORC1 and mTORC2. With the serine/threonine kinase at their core the

adapter proteins that form the two different complexes confer substrate specificity to the mTOR kinase, thereby enabling further diversification of downstream targets and upstream signals that can be integrated. However, both complexes share common proteins such as the mammalian lethal with sec-13 protein 8 (mLST8), DEP domain containing mTOR-interacting protein (DEPTOR) and the TTI1/TEL2 complex. In contrast, mTORC1 specific components consist of the regulatory-associated protein of mammalian target of Rapamycin (RAPTOR) and the proline-rich AKT substrate 40kDa (PRAS40), whereas the Rapamycin-insensitive companion of mTOR (RICTOR), the mammalian stress-activated map kinase-interacting protein 1 (mSIN1) and the protein observed with RICTOR 1 and 2 (PROTOR 1/2) are unique to the second TOR complex (mTORC2, Figure 1B) [11]. Rapamycin was originally thought to specifically disrupt the structure of mTORC1 and allosterically inhibit mTORC1 kinase function via its interaction with FKBP12 and the FRB domain of mTOR [12]. However, it has become evident that prolonged exposure to Rapamycin can, in some cell types, also result in the inhibition of mTORC2, presumably by reducing the levels of free mTOR protein necessary for the assembly of mTORC2 [13]. Despite the common use of Rapamycin to investigate mTOR signalling, this effect of Rapamycin is, surprisingly, frequently disregarded by researchers. Great care must therefore be taken when experimental data derived from Rapamycin treatment of cells is interpreted with respect to the involvement of the two mTOR complexes.

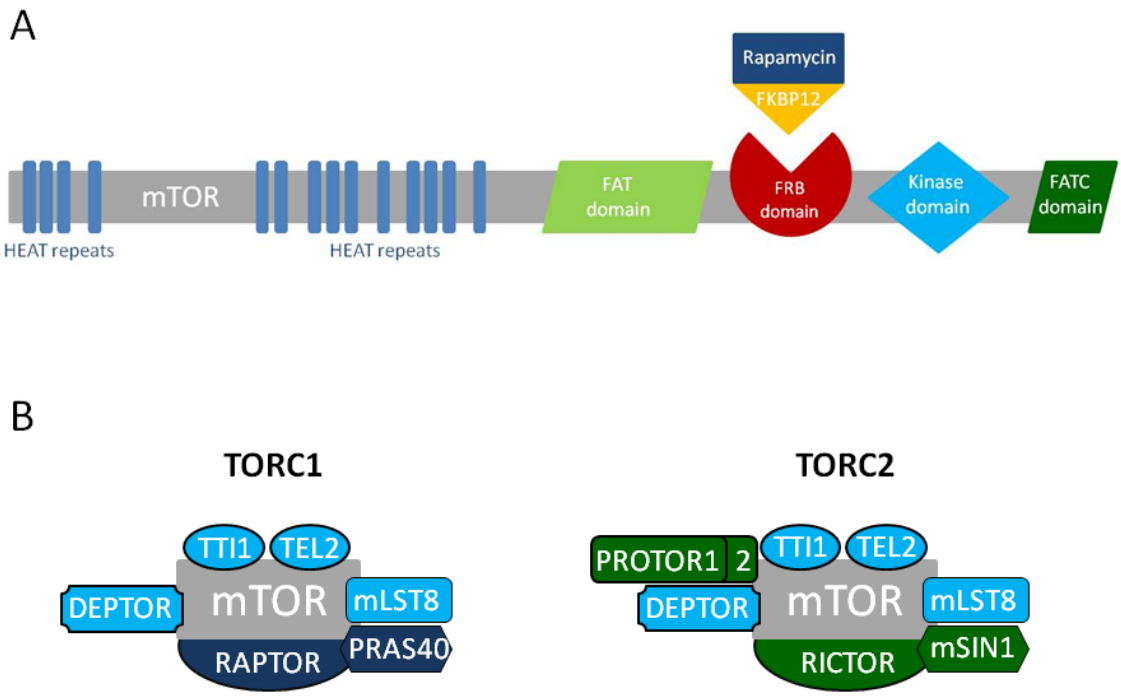


Figure 1. Domain structure of mTOR and the composition of mTORC1 and mTORC2 signalling complexes. (A) The serine/threonine kinase mTOR contains several N-terminal HEAT repeats (huntingtin, elongation factor 3, subunit of PP2A and TOR), a FAT domain (FRAP, ATM and TRRAP), a FKBP12 Rapamycin-binding domain (FRB), a kinase domain and a C-terminal FATC domain. (B) Both mTORC1 and 2 signalling complexes contain shared protein components: lethal with sec-13 protein 8 (mLST8), DEP domain containing mTOR-interacting protein (DEPTOR) and the TTI1/TEL2 complex (light blue). mTORC1 specific components are the regulatory-associated protein of mammalian target of Rapamycin (RAPTOR) and proline-rich AKT substrate 40kDa (PRAS40) (dark blue), whereas mTORC2 contains the unique components Rapamycin-insensitive companion of mTOR (RICTOR), the mammalian stress-activated map kinase-interacting protein 1 (mSIN1) and the protein observed with RICTOR 1 and 2 (PROTOR 1/2) (green).

1.1.2 | Regulation of mTORC1 and mTORC2 activity

The mTOR pathway has evolved to sense a variety of intracellular and extracellular signals including stress, energy status, oxygen, amino acids and growth factors, with the latter being the only firmly established cue that triggers mTORC2 activity (Figure 2). The characterization of mTORC2 activation as well as downstream signalling has at least in part been hampered by the lack of a specific inhibitor for mTORC2. The emergence of recently developed mTOR kinase inhibitors, such as Torin 1 and PP242, as well as knock-down and knock-out studies of mTORC2 components have begun to

shed more light on the regulation and function of mTORC2 [14-18]. Nevertheless the signalling events surrounding mTORC1 are far better characterized.

Many of the signals regulating mTORC1 activation converge at the level of the GTPase-activating protein complex formed by tuberous sclerosis 1 (TSC1) and TSC2. The TSC1/2 heterodimer in turn activates the GTPase activity of the RAS homolog enriched in brain (RHEB). Thereby the TSC complex negatively regulates mTORC1 activity since only the GTP-bound state of RHEB strongly activates mTORC1 [11]. Consequently, signals that activate TSC1/2 inhibit mTORC1 and signals that inhibit TSC1/2 activate mTORC1. Given that many of the signals downstream of cell surface receptors are at least partially transmitted via PI3K/AKT or ERK pathways, a diverse array of signals converge at the level of the TSC complex. Furthermore AKT can also activate mTORC1 signalling independent of TSC1/2 by phosphorylating PRAS40, a negative regulator of mTORC1 activity [19-21]. The mTORC1 activating signals include growth factors (insulin and insulin-like growth factors), various cytokines (IL-1, IL-2, IL-4, IL-12, IFNγ), costimulatory molecules (CD28) and antigen receptors (B-cell and T-cell antigen receptor) [22-27]. In addition to PI3K/AKT and ERK mediated mTORC1 activation via TSC1/2, TNFα induced IκB kinase β (IKKβ) activation results in TSC1 phosphorylation and mTORC1 activation [28]. This multitude of immunologically relevant molecules that activate mTORC1 highlights the importance of the mTOR signalling pathway in immune cells.

On the other hand signals that activate TSC1/2 and inhibit mTOR are transmitted via AMPK kinase pathways and the protein regulated in development and DNA damage response 1 (REDD1) [29-32]. AMP-activated kinase (AMPK) senses changes in the ratio of intracellular ATP/AMP concentrations and is activated in conditions indicating low energy levels (low ATP/AMP ratio) or low oxygen levels (hypoxia). Besides leading to

the activation of AMPK, hypoxia also activates REDD1, which in turn activates TSC2. In addition to the TSC1/2 mediated mTORC1 inhibition, AMPK can also reduce mTORC1 activation by phosphorylation of RAPTOR resulting in 14-3-3 binding and allosteric inhibition of mTORC1 [33]. AMPK signalling is furthermore involved in the DNA damage induced downregulation of mTORC1 activity, a process that is accompanied by increased p53-dependent transcription of *Tsc2* and phosphatase-and-tensin homolog deleted on chromosome 10 (*Pten*), resulting in reduced signalling of the PI3K-mTORC1 pathway [34-36].

The fact that the mTOR kinase acts as central signalling node by integrating a wide spectrum of different signals and controlling a variety of essential metabolic process downstream, places mTOR at the core of the regulation of cellular metabolism in response to external and internal stimuli . The integration of signals emanating from growth factor and cytokine receptors with signals reflecting the nutritional and energetic state of the cell, enables tuning of the cellular response in accordance to the current capabilities of the cell.

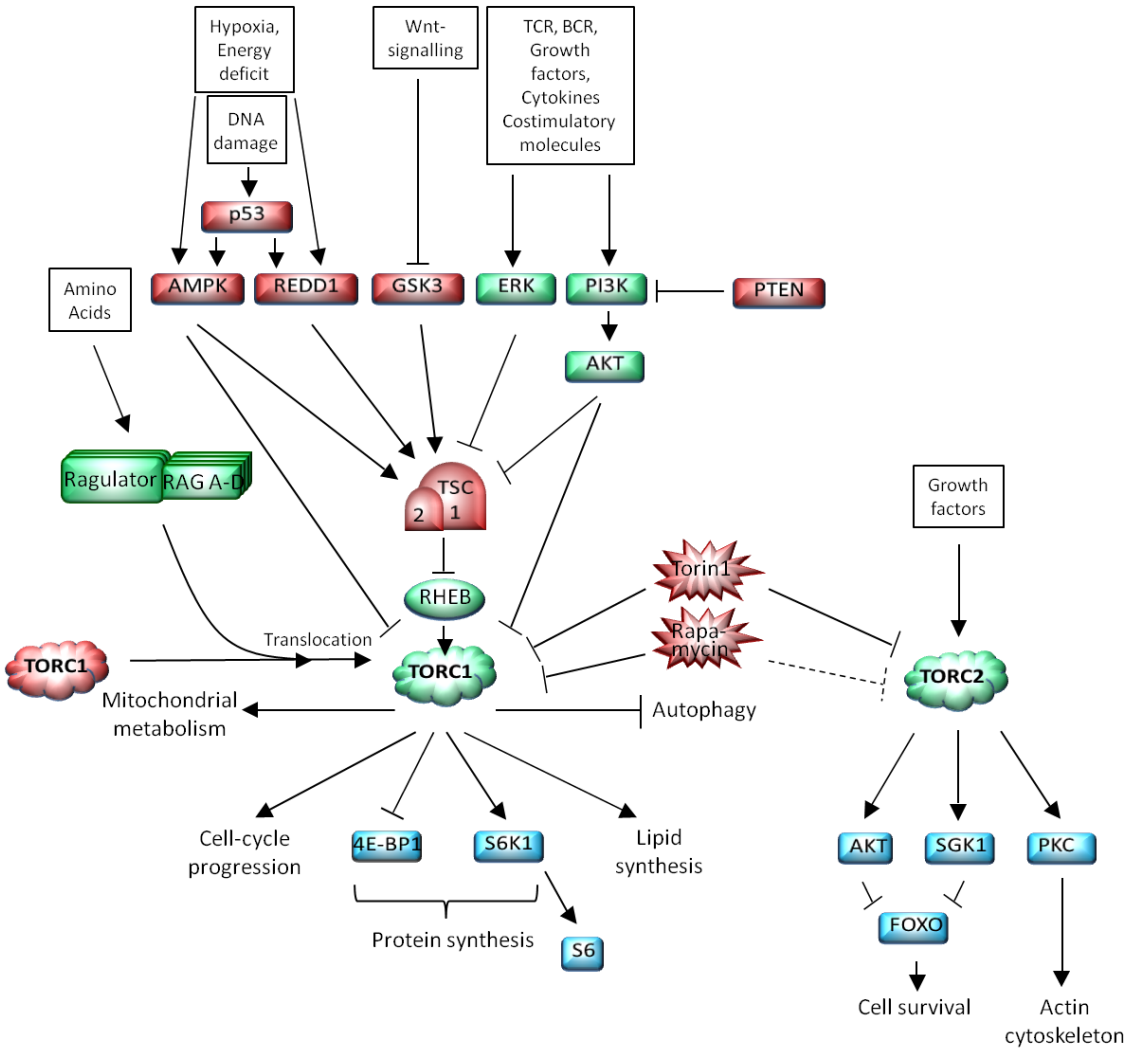


Figure 2. Inputs and outputs of the mTOR signalling pathway. A variety of signals including engagement of antigen receptors (TCR, BCR), as well as growth factor, cytokines and costimulatory molecule signalling activate the PI3K pathway, resulting in recruitment of AKT to the plasma membrane and the activation of AKT. Activated AKT along with signalling via ERK inhibits the TSC1/2 complex, enabling the activation of the mTORC1 by RHEB. Amino acid signalling via the Ragulator-RAG A-D complex resulting in translocation of mTORC1 to lysosomal, RHEB containing membranes is a prerequisite for mTORC1 activation. mTORC1 activity is activated by Wnt-signalling via GSK3, whereas it is inhibited under hypoxic, energy deficit and DNA damage conditions through the activity of AMPK and REDD1. Both AMPK and REDD1 activate the TSC1/2 complex to inhibit mTORC1, but AMPK can also inhibit mTORC1 directly. mTORC1 controls mitochondrial metabolism, cell-cycle progression, protein and lipid synthesis as well as autophagy through distinct downstream effector molecules. The only well established signal that activates mTORC2 are growth factors. mTORC2 activates downstream effectors AKT (S473) and SGK1 by phosphorylation thereby regulates cell survival. Activation of PKC downstream of mTORC2 is thought to be involved in the regulation of the actin cytoskeleton. The ATP-competitive mTOR inhibitor Torin 1 inhibits the kinase activity of mTOR in both complexes, whereas Rapamycin disrupts the structure of mTORC1 and in some cell types also that of mTORC2. Molecules involved in the activation of mTOR are coloured in green, whereas molecules that inhibit mTOR activity are displayed in red.

1.1.2.1 | Amino Acid sensing and AA induced activation of mTORC1 activity

Amino acids (AA) play a central role in cellular metabolism due to their role as basic building blocks for protein synthesis and as precursors and substrates for various metabolic processes. Therefore the presence of sufficient concentrations of AA represents an additional prerequisite that determines the cellular response to external stimuli.

The first indication for a role of the TOR kinase in AA sensing was obtained from studies in *Drosophila* that indicated that loss of TOR resulted in similar developmental and cellular phenotypes to those caused by AA deprivation [37, 38]. In fact AA not only act as potent stimulators of mTORC1 activity but are also required for mTORC1 activation by other stimuli, such as growth factors. This activation seems to be independent of TSC2, but appears to require RHEB activity [39]. AA do not seem to activate mTORC1 through regulation of RHEB activity but rather through intracellular translocation of mTORC1 to RHEB containing lysosomal membranes [40, 41]. This translocation process is regulated by the RAG-related GTP-binding-proteins A–D (RAG A–D), that form heterodimeric complexes which interact with mTORC1 via the RAPTOR component. The presence of AA induces the loading of RAG B with GTP, which enables the RAG B/D complex to establish the mTORC1 interaction [41, 42]. The translocation of the mTORC1-RAG complex from its diffuse cytoplasmic localization to lysosomal compartments is facilitated by another protein complex termed the Ragulator that is constitutively associated with the RAG proteins [40]. Recently the Ragulator complex was demonstrated to interact with the vacuolar ATPase (v-ATPase) in an AA-sensitive manner in which AA selectively strengthen the interaction between v-ATPase and the Ragulator-RAG protein complex which in turn allows mTORC1 translocation and activation [43]. This mechanism could

explain why the signalling of growth factors via mTOR seems to be dependent on the presence of AA, since a growth factor induced increase in RHEB activity in the absence of AA induced translocation to lysosomal membranes, would not affect mTORC1 activity.

The molecular sensor of AA has yet to be conclusively identified, although recent studies in *Drosophila* have revealed a potential role of proton-assisted amino acid-transporters (PAT) in sensing and transmitting an AA signal to mTORC1 [44, 45]. The same group recently demonstrated that PAT1 interacts with the RAG GTPases and seems to recruit mTOR to the lysosomal surfaces in an AA-dependent fashion. The authors hypothesis that the v-ATPase might cooperate with PAT1 to activate mTORC1 via RAG proteins, however they cannot exclude the contribution of other mechanisms regulating mTORC1 activity in an AA-dependent manner [46]. Given the dependency of PAT mediated AA transport on protons, as well as the proton transport activity of the v-ATPase, a functional link seems plausible. In line with the proposed mechanism of intraluminal sensing of AA, cells undergoing AA starvation-induced autophagy reactivate mTORC1 in a time dependent manner, presumably through the autophagy-induced accumulation of intraluminal AA [47]. Considering the fact that mTORC1 can regulate the activity of AA transporters, this model of PAT mediated AA sensing might also allow mTORC1 signals to feed back on its sensors [48, 49]. Furthermore, the apparent synergy between AA and growth factor signalling via mTORC1 could at least in part be explained by the observation that AKT can regulate the influx of nutrients that activate mTORC1, and the fact that increased PI3K/AKT signalling is known to result in enhanced endocytosis of PATs, increasing PAT-dependent mTORC1 activation [46, 50].

Irrespective of the precise mechanism that senses AA levels and results in AA mediated mTORC1 activation, the inhibition of mTORC1 activity by AA starvation and the dependency of growth factor signalling (via mTORC1) on the presence of AA are well established phenomena.

1.1.3 | Downstream targets and effector functions of mTORC1 and 2

The mTOR pathway has evolved to regulate a variety of crucial metabolic processes including protein and lipid synthesis, autophagy, mitochondrial metabolism and biogenesis, cell survival and cytoskeletal organization (Figure 2) [11]. This diverse set of outputs is mediated by an even larger set of downstream targets. In order to assess the contribution of mTOR complexes to the different effector functions, inhibitors such as Rapamycin or Torin 1, as well as knock-down and knock-out approaches have been utilized. The activity of the two complexes is routinely determined by evaluating the phosphorylation status of well-established mTORC1 and mTORC2 substrates. mTORC1 directly phosphorylates the translational regulators eIF4E-binding protein 1 (4E-BP1) and S6 kinase 1 (S6K1) [51]. The latter phosphorylates the ribosomal protein S6 at S235/236, which is also commonly used as mTORC1 activity readout. The phosphorylation events of 4E-BP1 at S65 and T37/46 were demonstrated to be insensitive to Rapamycin mediated mTORC1 inhibition and are therefore less frequently used for the measurement of mTORC1 activity, particularly in Rapamycin treated cells [16]. Whereas phosphorylation of 4E-BP1 enables cap-dependent translation by permitting the binding of eIF4F to the 5'cap of messenger RNAs (mRNA), S6K1 phosphorylation is thought to promote mRNA biogenesis as well as translation initiation and elongation through a variety of downstream targets [51].

An additional function of mTORC1 signalling lies in the regulation of the expression of genes involved in the fatty acid and cholesterol synthesis, which allows cells to generate membranes necessary for cell growth [52]. This effect is mediated by sterol-regulatory element-binding protein 1/2 (SREBP1/2), Lipin-1 and peroxisome proliferator-activated receptor γ (PPAR-γ) whose activity is controlled by mTORC1 directly or in part by S6K1 [53-57]. SREBP was further implicated in the regulation of the expression of components of the pentose-phosphate pathway [53]. Moreover, mTORC1 was demonstrated to induce the expression of many glycolytic genes through activation of hypoxia inducible factor 1α (HIF1α) transcription and translation [53, 58, 59]. This activation of ATP-generating mechanisms is further supported by an increase in the expression of genes associated with oxidative metabolism driven by the activation of YY-1 transcription factor by mTORC1 [60]. Besides managing energy and nutrient supplies under steady-state conditions, mTOR is also involved in regulating cellular resources during nutrient starvation by controlling autophagy. Autophagy enables cells to recycle cytoplasmic content such as proteins and (damaged) organelles in order to regenerate cellular building blocks and facilitate cell survival and function. mTORC1 inhibits autophagy and enables cell growth under steady-state conditions by suppressing the activity of the ULK complex that is key to the initiation of autophagy [61].

In contrast to these mTORC1 regulated processes, cell survival and cytoskeletal reorganization are thought to be downstream of mTORC2 (Figure 2). Its activity is measured by monitoring phosphorylation of the mTORC2 effector kinase AKT at a hydrophobic motif (S473) that is thought to be required for maximal activation of AKT. Importantly, AKT activation upstream of mTORC1 is induced by phosphorylation at

T308, allowing for differentiation of AKT activity upstream of mTORC1 and downstream of mTORC2 [62]. Mutation of S473A or depletion of mTORC2 that abolishes S473 phosphorylation revealed that a distinct set of AKT effector functions are regulated by mTORC2. Amongst these AKT targets are the forkhead box O1/3A (FOXO1/3A) transcription factors that are excluded from the nucleus in their phosphorylated form via association with 14-3-3 proteins and are known to control the expression of genes involved in stress resistance, metabolism and apoptosis [11, 63]. The serum- and glucocorticoid-induced protein kinase 1 (SGK1), another mTORC2 substrate, has also been demonstrated to be involved in the regulation of FOXO transcription factors [64]. The regulation of actin cytoskeleton organization represents another cellular function associated with mTORC2 activity. The mTORC2 substrates protein kinase C α (PKCα) along with paxilin and RHO GTPases have been implicated in this function [65, 66]. Bearing in mind the vital role of the cytoskeleton in molecular functions such as cell motility and cell division, this research area is likely to reveal novel insights into the role of mTORC2 activity.

1.2 | mTOR and the regulation of antigen-presenting cell differentiation and function

Given that antigen-presenting cells (APCs) survey the immune environment for cues in order to initiate and guide an appropriate adaptive immune response and the fact that mTOR acts as an integrator of environmental signals, one might predict a role for the mTOR pathway in the differentiation and function of APCs. Furthermore, the immunological context in which APCs encounter antigens has been demonstrated to be

of crucial importance for the differentiation of APCs and thereby the skewing of adaptive immune responses. As a consequence the role of the mTOR pathway in APC differentiation and function has been subject to extensive investigation in recent years.

Dendritic cells (DCs), as the epitome of a professional APC, constantly sample the microenvironment for antigens and consequently mature and present antigen-derived peptides on their cell surface. Upon maturation DCs express accessory signals, including costimulatory molecules and pro- and anti-inflammatory cytokines, that crucially shape the context in which the peptide-MHC complex is recognized by cells of the adaptive immune system [67]. The profound effect of mTOR inhibition on DC maturation was exemplified by Hackstein et al. who demonstrated that treatment of bone marrow-derived DCs (bmDCs) with Rapamycin *in vitro* and *in vivo* impaired interleukin 4 (IL-4)-dependent maturation indicated by reduced expression of costimulatory molecules, IL-12 and TNFα production as well as reduced T-cell stimulatory capacity [68]. Along the same lines Rapamycin inhibited maturation of bmDCs in the presence and absence of lipopolysaccharide (LPS) characterized by reduced upregulation of costimulatory molecules CD80 and CD86 as well as MHCII expression [69, 70]. Furthermore maturation induced by IL-1β and granulocyte-macrophage colony-stimulating factor (GM-CSF) was also impaired in the presence of Rapamycin, in the latter case even resulting in apoptosis [71, 72]. The diversity of signals that are regulated by mTOR, including those emanating from cytokine receptors and toll-like receptors (TLRs), highlights the essential role of the pathway as an integrator of signals that guide the maturation process in DCs.

The capacity of DCs to engulf antigen by various pathways such as receptor-mediated endocytosis and macropinocytosis, represents another crucial function of DCs. Rapamycin inhibits both endocytosis and macropinocytosis in immature bmDCs as well as splenic DCs [68, 73]. The precise mechanism that Rapamycin adopts so as to inhibit the uptake of antigen remains to be determined, but considering the importance of the actin cytoskeleton in these processes, it seems plausible that mTOR interferes with antigen uptake by influencing actin reorganization. However, since Rapamycin was also reported to decrease the expression of antigen uptake receptors (mannose receptor, CD32, CD46, CD91) in human monocyte-derived DCs, a similar mechanism might be engaged in mice [74].

In contrast to the negative effect of mTOR inhibition on T-cell stimulatory capacity and cytokine production during maturation, Rapamycin treatment of mature myeloid DCs results in enhanced IL-12 and decreased IL-10 production upon TLR ligation [75-77]. In line with these observations and the increased expression of CD86 and reduced levels of PD-L1, an inhibitory costimulatory molecule, myeloid DCs exhibited an enhanced activity to induce T-cell proliferation [75]. Conversely, hyper-activation of mTOR due to deletion of PTEN, a negative regulator of the PI3K/mTOR axis, or TSC2 results in decreased IL-12 secretion and increased IL-10 production [76, 77].

The immunosuppressive activities of Rapamycin have been extensively exploited in the prevention of transplant rejection and the treatment of autoimmune diseases [1]. Although this effect of *in vivo* Rapamycin administration is likely due to a concerted action of the drug on multiple cell types, evidence from *in vitro* and *in vivo* studies indicate that Rapamycin mediated mTOR inhibition facilitates the induction of a tolerogenic phenotype in DCs [75, 78]. Along these lines Rapamycin-matured DCs can

promote the generation of FOXP3^{+} Treg and transfer of Rapamycin-treated, allogeneic DCs can induce tolerance in mouse models of solid organ transplantation [69, 70, 79].

The comparability and interpretation of these results is however hampered by the different origin of the cells and the distinct differentiation and maturation protocols that were used by different groups. Moreover, the effect on T cell proliferation and polarization has to be interpreted with great care since residual Rapamycin from DC cultures might act on the T-cells themselves. Irrespective of these uncertainties, the evidence indicating a role for mTOR in the differentiation, maturation and function of DCs (and other APCs) is accumulating [80].

1.3 | The effect of mTOR inhibition on other immune cells

Besides the prominent effects of mTOR signalling on APCs and T-cells (discussed in the following sections), the function and proliferation of a variety of other immune cells is influenced by the mTOR pathway.

Neutrophils have a key role in the first line defence of the immune system by actively fighting infections via phagocytosis, degranulation and oxidative burst. Comparable to the effects of Rapamycin on DCs, GM-CSF and TLR signalling is at least partially suppressed by mTOR inhibition, resulting in reduced neutrophil migration and activation [81-83]. Besides direct interference with chemotatic and activating signals, mTOR also controls the platelet activating factor (PAF) induced translation of IL-6 receptor α (*Il-6rα*) as well as retinoic acid receptor α (*Rarα*) mRNA, a crucial transcription factor for neutrophils [84, 85].

A role for mTOR signalling in mast cell function, was described by Kim et al. The authors demonstrate that Rapamycin blocks FcεRI- and KIT-induced cytokine production, chemotaxis and cell survival [86]. In line with these findings, Shin and colleagues show that hyper-activation of mTOR in TSC1-deficient mast cells results in enhanced cytokine production in response to FcεRI engagement and increased cell death [87]. The role of mTOR in regulating chemotaxis was further validated and expanded by the observation that the dual TORC inhibitor Torin 1 and not Rapamycin inhibited prostaglandin E_2 induced chemotaxis, indicating that this function is regulated by Rapamycin insensitive mTORC1 or mTORC2 signalling [88]. Additional studies utilizing TORC inhibitors and knock-downs established that mTORC1 signalling is required for mast cell survival [89].

In addition to cells of the innate immune system, an important role of mTOR signalling in B-cells is beginning to emerge. Several studies investigating the effect of deletion of different components of the mTOR pathway in B-cells, clearly indicate the importance of mTOR signalling in the development and maturation of B-cells [90-92]. Accurately tuned mTOR signalling seems to be essential for normal maturation of B-cells, since B-cells from both mTOR hypomorph mice (reduced mTOR transcription/signalling) and TSC1 knock-out mice exhibit decreased numbers of marginal zone cells in the periphery [90, 91]. Similarly, functional disruption of mTORC2 by deletion of Sin1, partially blocked B-cell development [92]. In addition mTOR hypomorphs displayed impaired B-cell development at the large pre-B to small pre-B stage [90]. Furthermore B-cells from both hypomorph and $TSC1^{-/-}$ mice also showed decreased T-dependent and T-independent antibody production [90, 91]. The importance of mTOR signalling is further underlined by reports demonstrating that B-cell receptor (BCR)-, TLR- and CD40-mediated signalling activate the mTOR pathway [93-95]. Prolonged BCR-signalling resulting in robust mTOR activation

seems to be required for antigen driven expansion of B-cells, especially in the absence of CD40 ligation [93]. Furthermore, Rapamycin inhibits CD40- and LPS-induced B-cell proliferation [94, 95].

1.4 | mTOR signalling regulates the differentiation and function of T-cells

T-cells play an essential role in immune homeostasis as well as in the host response to pathogens and tumours. The key to the specificity of these adaptive T-cell responses lies in the highly precise recognition of antigen peptide presented by MHC molecules by the T-cell receptor (TCR) in conjunction with signals mediated by costimulatory molecules and cytokines in the local environment, that together induce naïve T cells to differentiate into distinct functional subsets. Each subset possesses discrete patterns of cytokine expression and other effector molecules, which provide the basis for the different immune functions of the diverse populations of T-cells. The ability of the mTOR complexes to integrate and fine tune a wide spectrum of environmental stimuli that impact the outcome of the differentiation process, has been demonstrated of crucial importance for the function of T-cells in a variety of different settings [1].

1.4.1 | Costimulation, cytokine signalling and TCR engagement affect mTOR activity

A multitude of stimuli that a T-cell encounters are known to signal via the PI3K-AKT-mTOR axis. Strikingly, many of the signals that are, according to the two-signal model of T cell activation [96, 97], required for full T-cell activation have been demonstrated to

induce phosphorylation cascades that also affect mTOR activity. Signal 1, namely TCR-engagement, activates both mTORC1 and mTORC2 within minutes of stimulation [23, 98-100]. Similarly, costimulation (Signal 2) via activatory receptors such as CD28 and OX40 or inhibitory receptor PD-1, activates and inhibits mTOR signalling respectively [23, 101-104]. Additional immunological signals are fed into the mTOR pathway through the action of cytokines receptors. Along these lines, IL-2 induced by CD28 engagement and the homeostatic cytokine IL-7 enhance mTOR activity, albeit with slower kinetics than TCR stimulation [105-108]. Furthermore, IL-12 was demonstrated to induce mTOR activation in antigen-stimulated $CD8^+$ T-cells [26]. Similarly, IL-4 and IL-1 increase mTOR activation in Th2 and Th17 cells respectively [24, 27].

1.4.2 | mTOR activity and the induction of anergy in T-cells

Besides central tolerance mechanism such as the negative selection of autoreactive cells in the thymus and peripheral tolerance mediated by regulatory T-cells, T cell anergy is thought to be another tolerance mechanism that controls immune homeostasis. T-cell anergy (that is the secondary unresponsiveness of T-cells to signals 1 and 2 with respect to proliferation and cytokine production) is classically induced via TCR stimulation in the absence of costimulation. In line with a role of mTOR in the signalling events underlying the full activation of T-cells, Rapamycin can facilitate the induction of T-cell anergy even in the presence of costimulation [23, 109-111]. Initially the anergic state was thought to result from TCR engagement in the absence of cell proliferation during the anergy induction process. However, experiments utilizing Rapamycin-resistant mTOR protein demonstrated that the anergy inducing effect of Rapamycin is due to inhibition of mTOR activity rather than the Rapamycin induced cell

cycle arrest [101]. Along these lines the induction of T-cell proliferation in the presence of Rapamycin does not reverse T-cell anergy and conversely cell cycle arrest in the absence of mTOR inhibition does not induce anergy [23, 109]. Besides the involvement of the cell cycle, an alternative explanation for the induction of anergy in T-cells was therefore proposed by by Zheng and colleagues. The authors demonstrate that inhibitor-mediated blockade of metabolic pathways, resulting in mTOR inhibition, induces anergy even in the presence of signal 1 and 2. Furthermore, anergic T-cells appear to fail to upregulate the metabolic machinery as required during the resource consuming processes of T cell activation [102, 112, 113]. These observations led Powell et al. to hypothesize that by integrating a wide spectrum of costimulatory, cytokine and environmental cues, mTOR evaluates the intensity of signal 2 and thereby determines the outcome of the antigen recognition (mTOR as signal 2). Consequently, TCR engagement in the absence of mTOR activity should result in anergy, whereas sustained mTOR activity should enable full T-cell activation and effector differentiation [114].

1.4.3 | mTOR in T-cell trafficking

The migration of naïve, effector and memory T-cells is tightly regulated in order to allow an effective and regulated immune response. This trafficking of T-cells between secondary lymphoid organs and other tissues requires signals that are transmitted through chemokine receptors and other trafficking molecules. Upon antigen encounter T-cells alter the expression pattern of these homing molecules as part of the activation induced differentiation process. In conjunction with the expression of adhesion

molecules, this allows them to leave the secondary lymphoid organs and migrate to sites of inflammation. The involvement of mTOR in the regulation of T-cell migration was demonstrated by experiments performed by Sinclair et al. and Rao et al. that showed that mTOR inhibition by Rapamycin prevented the homing of activated $CD8^+$ T-cells to non-lymphoid tissues [26, 115]. Rapamycin treated cells retained the expression of lymphoid tissue homing markers CC-chemokine receptor 7 (CCR7), CD62L and sphingosine-1-phosphate receptor 1 (S1PR1) rather than downregulating their expression in response to IL-2 signalling induced during their activation [115]. In line with these findings, hyper-activation of mTOR through deletion of negative regulators of mTOR signalling, PTEN and TSC1, results in enhanced downregulation of these receptors [115-117]. In addition to the pronounced effects of mTOR inhibition on $CD8^+$ T-cell trafficking, mTORC1 signalling in human $CD4^+$ T-cells was demonstrated to be essential for CCL5-mediated chemotaxis, highlighting that mTOR not only controls expression of homing receptors, but is also involved in the downstream signalling [118]. The retention of activated $CD8^+$ and $CD4^+$ T-cells in secondary lymphoid tissues might contribute to the immunosuppressive effects of Rapamycin.

1.4.4 | mTOR signalling and the differentiation of $CD8^+$ T-cells

Considering the well-established immunosuppressive effects of Rapamycin, the observation that the mTOR inhibitor also enhanced $CD8^+$ T-cell mediated antiviral immune responses in a mouse model of lymphocytic choriomeningitis virus (LCMV) infection was rather surprising [119]. The development of $CD8^+$ T cell responses can be dissected into distinct phases: A clonal expansion phase, which is accompanied by differentiation of $CD8^+$ cells into cytotoxic effector cells, and a contraction period in

which the effector cells apoptose and long-lived memory cells emerge [120]. Araki et al. demonstrate that Rapamycin administration to LCMV-infected mice improved not only the quantity but also the potency of virus specific $CD8^+$ T-cells. In a cell intrinsic, mTORC1-dependent manner Rapamycin seemed to both facilitate the generation of memory cell precursors and the survival of effector cells during the expansion phase as well as accelerate the differentiation of memory T-cell differentiation in the contraction phase [119]. Consistent with this data, constitutive AKT signalling interfered with the generation, function and survival of memory cells [121]. A similar, positive effect of Rapamycin on the generation of $CD8^+$ memory T-cells was described by Rao et al. and attributed to an increased expression of the transcription factor Eomesodermin. In contrast to the observations of Araki et al., Rapamycin also impaired the function of $CD8^+$ effector T-cells by downregulating the expression of the T-box transcription factor TBX21 (T-bet) that is important for the regulation of the effector cell phenotype [26]. Further support for the role of the mTOR pathway in the regulation of $CD8^+$ memory T-cells comes from studies utilizing T-cell specific TNFR-associated factor 6 (TRAF6) knock-out mice. Whereas the differentiation of effector cells is not affected by the deletion of TRAF6, the generation of memory cells in response to *Listeria monocytogenes* is severely impaired due to a failure to upregulate fatty acid oxidation pathways, an effect that can be rescued through administration of Rapamycin.

1.4.5 | mTOR and the regulation of $CD4^+$ T-cell differentiation

$CD4^+$ T-cells have the potential to differentiate into an ever growing number of effector T-cell subsets, each characterized by the expression of a set of transcriptional regulators and effector molecules (Figure 3). This differentiation process is thought to

be mainly guided by environmental signals that are perceived by the cells during or shortly after the activation event. The most prominent factors skewing the polarization of $CD4^+$ T-cells along their respective lineage are cytokines that are commonly produced by APCs.

Th1 cells that control cell-mediated immunity to target intracellular pathogens can be induced in the presence of IL-12, resulting in STAT1 and STAT4 signalling that culminates in the expression of T-bet, a transcription factor regulating the expression of many Th1 associated genes. The differentiation of Th2 cells, which are thought to coordinate humoral immune responses, is controlled by IL-4 induced STAT6 signalling that drives the expression of GATA3 as well as that of the Th2 effector cytokines IL-4, IL-5 and IL-13. Th9, Th17 and peripheral $FOXP3^+$ regulatory cells share the common requirement for transforming growth factor β (TGFβ) signalling to initiate their differentiation program. The induction of the recently identified Th9 cells requires additional IL-4 signals. However, it remains to be established whether Th9 cells represent a fully differentiated effector T-cell subset and whether they can be characterized by a distinct set of transcription factors that control their function. The Th17 differentiation program is elicited by TGFβ mediated SMAD3 and IL-6 induced STAT3 activation that ultimately result in the expression of Th17 signature cytokines IL-17A and IL-17F. Furthermore these signals induce the expression of the retinoic acid-related orphan receptor γ T (RORγT) which orchestrates Th17 cell function that targets extracellular bacteria and fungi. In contrast to these inflammatory T-cell subsets, the induction of $FOXP3^+$ regulatory T-cells in the periphery is dependent on STAT5 signalling induced by IL-2 and SMAD3 signalling activated by TGFβ. Induced regulatory T-cells (iTreg), similar to the thymic derived “natural” Treg (nTreg), express forkhead

box P3 (FOXP3), the master transcription factor required for their differentiation and function [122, 123].

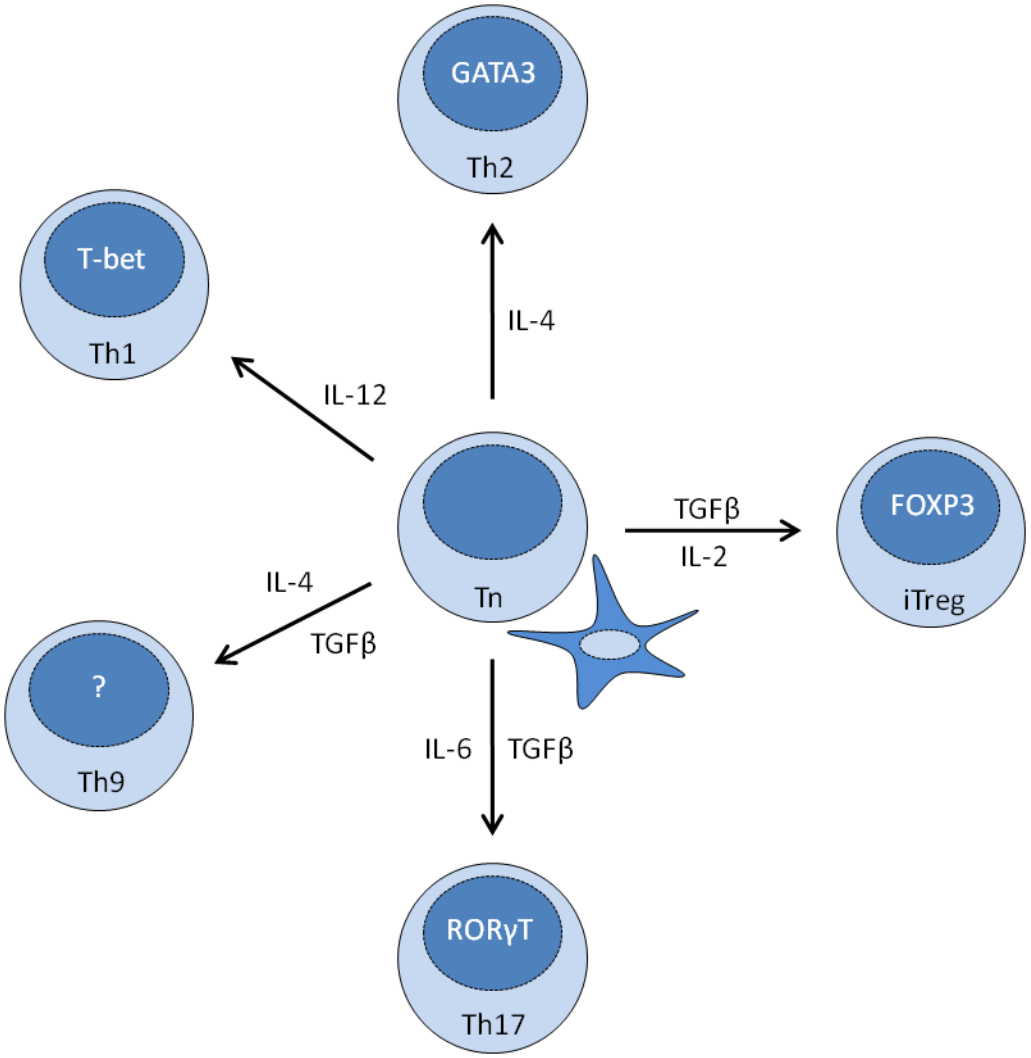


Figure 3. The differentiation of naïve CD4$^+$ T-cells (Tn) into effector subsets is controlled by cytokines. The different CD4$^+$ T-cell subsets (except for Th9) can be identified by the expression of lineage specific cytokines (not shown) and nuclear expression of lineage determining transcription factors: Th1 (T-bet), Th2 (GATA3), iTreg (FOXP3) and Th17 (RORγT). The expression of these transcription factors and thereby the differentiation program is amongst others controlled by antigen-recognition and costimulation (not shown) in the presence of polarizing cytokines that are produced by antigen presenting cells. For simplicity, the contribution of other signals, cytokines and transcription factors to the differentiation of CD4$^+$ T-cells has been omitted from the figure.

In contrast to the role of cytokines in the regulation of T-cell differentiation, the importance of the mTOR pathway for the outcome of T-cell differentiation events has only started to emerge in recent years.

Amongst the first to report an involvement of mTOR in skewing T-cell polarization, were Sauer et al. who demonstrated premature termination of TCR-signalling and inhibition of the PI3K/AKT/mTOR axis can enhance the induction of a $FOXP3^+$ regulatory T-cell (Treg) phenotype in naïve $CD4^+$ T-cells. This induction was independent of TGFβ since inhibition of SMAD signalling did not interfere with the induction of FOXP3 and no SMAD2 activation was detected. The authors proposed that mTOR inhibition enhanced the expression of FOXP3 by promoting transcriptionally permissive histone H3K4me2 and 3 and demethylation of the *Foxp3* promoter [124]. Further evidence that mTOR regulates FOXP3 expression through epigenetic mechanisms is provided by studies demonstrating that the "rapalog" everolimus reduces the activity of the DNA methyl transferase 1 (DNMT1) [125]. Consistent with the finding that constitutive activation of PI3K/AKT/mTOR signalling (as a result of genetic deletion of PTEN) inhibits the induction of FOXP3 [124], Haxhiansto et al. revealed that constitutive AKT signalling interferes with the TGFβ-induced upregulation of FOXP3 expression in $CD4^+$ T-cells. The reduced induction was partially rescued by Rapamycin-mediated mTOR inhibition, indicating a role for mTOR signalling in the process [126]. The interpretation of these experiments is however complicated by the fact that AKT acts both upstream of mTORC1 and downstream of mTORC2, which might explain the incomplete restoration of FOXP3 induction in the presence of Rapamycin.

A more physiologically relevant mechanism of mTOR mediated regulation of FOXP3 expression was presented by Cobbold et al., who demonstrate that mTOR inhibition

through depletion of essential amino acids (EAA) can synergize with TCR stimulation and TGFβ to induce FOXP3. Furthermore the authors proposed a mechanism for a phenomenon known as infectious tolerance, which describes the observation that tolerance in a $CD4^+$ T-cell population is passed on to another population of naïve T-cells, hence behaving as if infectious [127, 128]. According to the suggested mechanism, $FOXP3^+$ Treg would induce additional Treg by stimulating the expression of amino acid catabolizing enzymes in APCs, which then enhance the induction of FOXP3 through mTOR inhibition mediated by amino acid depletion in the local microenvironment [127].

Experiments utilizing mice with genetic deletion of mTOR in $CD4^+$ T cells further consolidate the role of mTOR activity in the regulation of FOXP3 expression. Stimulation of $mTOR^{-/-}$ $CD4^+$ T-cells with anti-CD3 antibody (αCD3) and APCs in the absence of any polarizing cytokines leads to an increased proportion of the $FOXP3^+$ cells compared to wildtype $CD4^+$ cells. In contrast to Sauer et al. this increase was dependent on small amounts of TGFβ in the culture medium, since the addition of a TGFβ neutralizing antibody significantly reduced the proportion of $FOXP3^+$ cells. However, since the $CD4^+$ T-cells that were used in these experiments contained $FOXP3^+$ nTreg it remained unclear whether the increased proportion of $FOXP3^+$ cells was due to a *de novo* induction of the Treg marker or solely a preferential expansion of the $FOXP3^+$ population under these conditions.

The preferential expansion of $FOXP3^+$ cells in the presence of Rapamycin was described by several groups and is thought to be due to the ability of $FOXP3^+$ cells to proliferate in the absence of mTOR activation [129-134]. This effect is thought to be mediated in part by the mTOR-independent but FOXP3-dependent upregulation of PIM2 kinase that controls cell survival and proliferation [129]. Furthermore, $FOXP3^+$ cells exhibit an

increased resistance to apoptosis due to upregulation of anti-apoptotic BCL-2 family members BCL-2 and BCL-XL under mTOR inhibition conditions, which might contribute to the preferential emergence of Treg in the presence of Rapamycin [132]. Evidence for an induction of FOXP3 in $mTOR^{-/-}$ $CD4^{+}$ cells was observed where cells exhibited hyper-activated SMAD3 signalling upon restimulation with TGFβ, indicating that $mTOR^{-/-}$ cells are hyper-sensitive to TGFβ. Likewise, Rapamycin can sensitize T-cells to TGFβ concentrations that in the absence of mTOR inhibition fail to facilitate the induction of FOXP3 [135].

In addition to the default differentiation along the Treg pathway under neutral conditions, the $mTOR^{-/-}$ cells also failed to differentiate into Th1, Th2 and Th17 under appropriate skewing conditions, due to an inability to activate STAT signalling [136]. In line with these findings two groups demonstrated that Rapamycin inhibits the differentiation of Th1 and Th17 cells [137, 138].

1.4.5.1 | The role of the two mTOR complexes in regulating T-cell differentiation

Genetic deletion of RHEB in $CD4^{+}$ T-cells, which results in specific inhibition of mTORC1 signalling, revealed that mTORC1 signalling was essential for the differentiation of Th1 and Th17 cells. The failure of the cells to express signature cytokines, IFNγ and IL-17A, as well as key transcription factors, T-bet and RORγT, was linked to the inability to activate the appropriate STAT transcription factors [139]. Th2 as well as Treg induction did not appear to be altered in $RHEB^{-/-}$ $CD4^{+}$ T-cells, indicating that mTORC1 signalling is not involved in the regulation of these T-cell lineages [136]. In line with these results,

RHEB$^{-/-}$ T-cells bearing a transgenic TCR for ovalbumin, failed to differentiate into IFNγ-secreting Th1 cells in response to *in vivo* infection with an ovalbumin expressing vaccinia virus, but expressed high levels of the Th2 cytokine IL-4. Consistent with their inability to generate Th17 responses, RHEB$^{-/-}$ mice were also resistant to myelin oligodendrocyte glycoprotein (MOG) peptide-induced experimental autoimmune encephalomyelitis (EAE), a disease model of multiple sclerosis that is usually driven by Th1 and Th17 cells. Rather than showing Th1 and Th17 infiltrates in the spinal cord, the mice developed "non-classical EAE", which is indicative of a Th2 response to the MOG peptide [139]. The role of mTORC1 in the regulation of Th17 differentiation was consolidated by studies performed by Lee et al. using RICTOR$^{-/-}$ CD4^{+} T-cells, which display impaired mTORC2 signalling through structural disruption of the second mTOR complex. The authors demonstrated that the skewing of naïve T-cells towards Th17 cells *in vitro* was unaffected. Furthermore, a reduced capacity of RICTOR$^{-/-}$ CD4^{+} T-cells to produce IFNγ and induce T-bet expression was observed, pointing towards an involvement of mTORC2 in the regulation of Th1 differentiation. This defect was demonstrated to be downstream of AKT signalling since the transduction of RICTOR$^{-/-}$ cells with constitutively active AKT constructs rescued the IFNγ production and T-bet expression. Moreover, RICTOR$^{-/-}$ CD4^{+} T-cells displayed impaired Th2 differentiation as demonstrated by reduced levels of GATA3 and IL-4 production *in vitro* and by impaired humoral responses *in vivo*. The former was revealed to be due to reduced activation of PKCθ downstream of inhibited mTOR complex 2 in RICTOR$^{-/-}$ cells [140]. In line with the inability to differentiate into Th2 cells in the absence of mTORC2 signalling, CD4^{+} T-cells from mice with a CD4 driven deletion of RICTOR (instead of LCK driven deletion used by Lee et al.) also showed a reduced propensity to differentiate along the Th2 lineage.

However, the defect was attributed to the incapacity to activate STAT6 rather than PKCθ. In contrast to the observation of Lee and colleagues that mTORC2 signalling is required for Th1 differentiation, the authors did not detect reduced levels of IFNγ or T-bet in their mTORC2 deficiency model [139]. With respect to the induction of the Treg marker FOXP3, neither of the two groups described a similar enhancement of FOXP3 induction in the absence of TGFβ in RICTOR$^{-/-}$ cells as was observed in mTOR$^{-/-}$ cells [136, 139, 140]. However, Lee at al. showed that a greater proportion of RICTOR$^{-/-}$ cells express FOXP3 in the presence of TGFβ when compared to the percentage that is induced in wildtype cells, indicating that mTORC2 activity inhibits TGFβ-induced FOXP3 expression [140]. A comparable increase in the proportion of FOXP3^{+} cells in the absence of exogenous TGFβ to that seen in mTOR knock-out T cells was only achieved when RICTOR$^{-/-}$ CD4^{+} T-cells were stimulated in the presence of low concentrations of Rapamycin that preferentially inhibited mTORC1, signifying that the putative increase in TGFβ sensitivity was only achieved when both complexes were inhibited [136, 139]. The precise mechanism that the inhibition of both complexes elicits to induce FOXP3 remains, unknown. The differential contribution of the two mTOR complexes to the differentiation of CD4^{+} T-cells into effector subsets is summarized in figure 4.

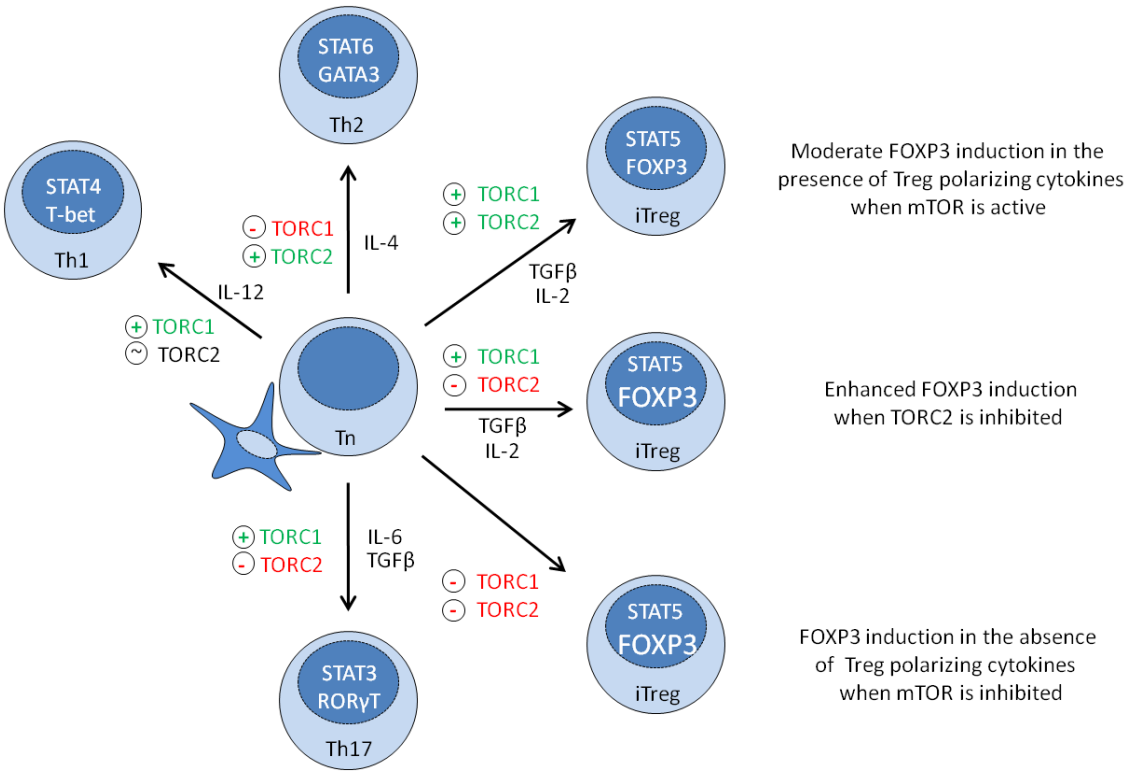


Figure 4. Regulation of CD4$^+$ T-cell differentiation by mTORC1 and mTORC2 activity. mTORC1 signalling is required for the differentiation of Th1 and T17 cells through regulation of the induction and activation of T-bet and STAT4 as well as RORγT and STAT3 respectively. mTORC2 signalling seems to be dispensable for the polarization of naïve T-cells (Tn) into Th17 cells, whereas it seems to be partially required for Th1 differentiation. In contrast, mTORC2 signalling is essential for STAT6 activation and GATA3 induction that mediate Th2 differentiation. mTORC1 signalling does not seem to be required for Th2 differentiation. The induction of the regulatory T-cell marker FOXP3 by TGFβ is independent of mTOR activity, but is enhanced when mTORC2 activity is inhibited. Treg differentiation and FOXP3 induction in the absence of polarizing conditions or under Th1, Th2 or Th17 conditions (not shown) occurs only when mTORC1 and mTORC2 are inhibited.

1.5 | The molecular orchestration of the transcriptional activation of the *Foxp3* locus

Immunological tolerance ensures that the immune system can develop a diverse set of antigen receptor specificities and maintain high levels of responsiveness to foreign antigens, but remains unresponsive to self-antigens. The breakage of these mechanisms unleashes the auto reactive potential of the immune system and leads to autoimmunity and damage to the host [141-143].

In the last two decades several different Treg subsets have been implicated as key players in the establishment of tolerance. Amongst them $CD4^+$ T_{reg} have been most extensively studied. Of these there are two major subsets: natural Treg (nTreg), generated in the thymus, and inducible Treg (iTreg) that can arise in the periphery [143, 144]. Both nTreg and a subset of iTreg can be identified by the expression of the transcription factor forkhead box P3 (FOXP3), a member of the forkhead/winged-helix family of transcription factors that confers the suppressive function to these cells [145, 146]. Despite extensive evidence for a crucial role of $CD4^+FOXP3^+$ Treg in controlling immunological tolerance, the knowledge of the signalling events underlying their induction is far from being completely understood [147]. What is known is that triggering of the T-cell receptor (TCR) in the presence of TGFβ [148-152] and IL-2 [153-155] and moderate to low co stimulation via CD28 [156-158], can induce a distinct set of transcription factors that activate regulatory elements in the *Foxp3* gene and thereby lead to the expression of FOXP3 in peripheral T-cells.

The basis for a detailed analysis of the complex regulatory signalling network that controls the expression of FOXP3 was established by a number of pivotal studies that identified and characterized 5 conserved non-coding sequences (CNS) in the *Foxp3* locus that regulate the rate of gene transcription [159-162] (Figure 5). Engagement of these CNS sequences by activated transcription factors as well as epigenetic modifications such as histone modifications regulate the expression of *Foxp3* which is driven by one of the CNSs', the *Foxp3* promoter.

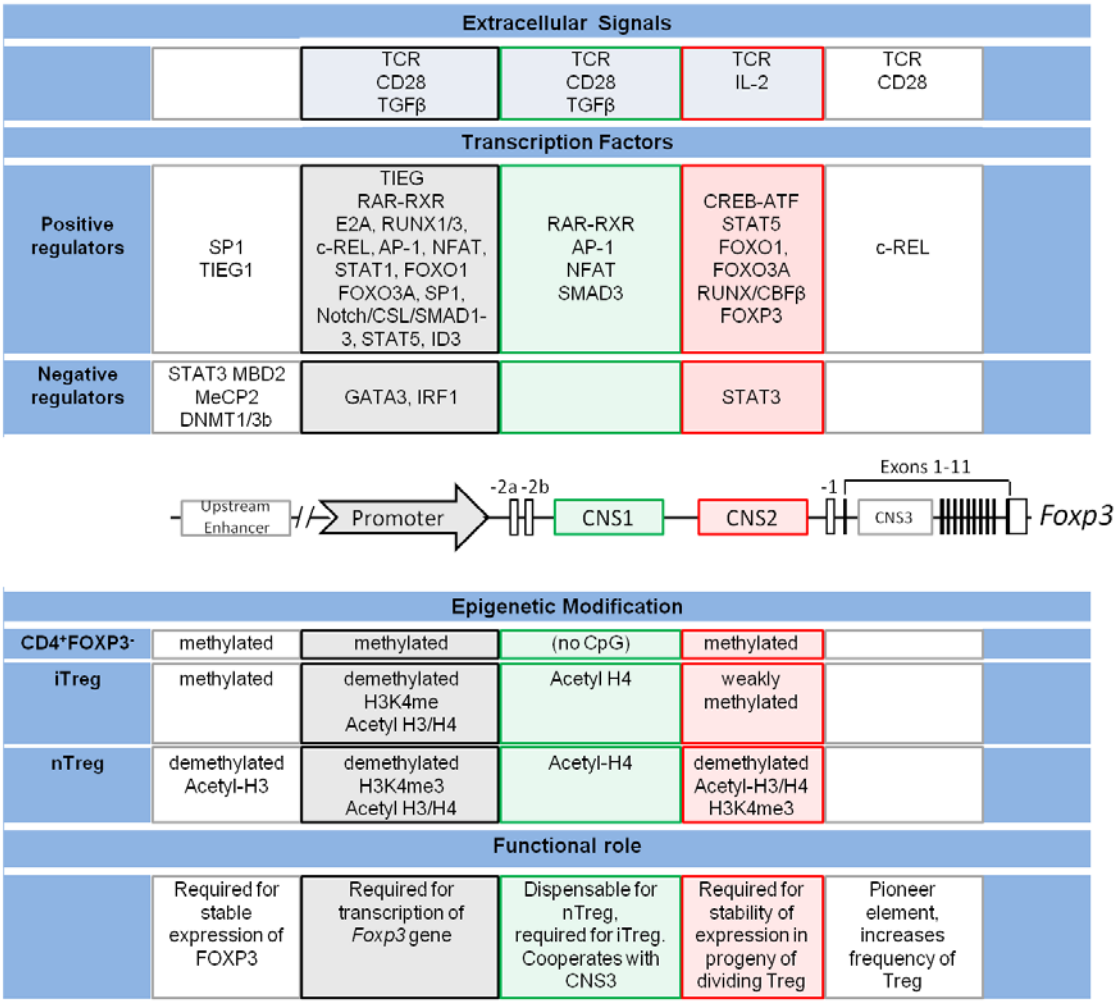


Figure 5. The Foxp3 locus and the regulation of gene expression. Extracellular signals regulate the induction and activation of intracellular transcription factors and protein complexes that bind to the regulatory regions and activate or inhibit transcription of *Foxp3* in induced and natural Treg (iTreg and nTreg). Epigenetic modifications control the stability of FOXP3 expression by influencing the accessibility of the locus to transcription factors. The figure was based on and adapted from Regateiro et al. [163].

Computational and experimental analysis of the promoter sequences indentified a multitude of functional transcription factor binding sites, including several activator protein-1 (AP-1), nuclear factor of activated T-cells (NFAT) and specificity protein 1 (SP-1) sites [159]. The *Foxp3* promoter alone however exhibits only negligible activity. This basal activity induced by TCR stimulation is however elevated in cooperation with CNS2 and sensitized to TGFβ in the presence of CNS1 [160, 164]. The former is thought to be the consequence of the formation of an "enhanceosome" consisting of c-REL, p65 and

NFATc2 bound to the promoter plus SMAD3 and CREB associated with CNS1. This process occurs in a sequential manner in that c-REL, p65 and NFATc2 are recruited to the promoter first, followed by their association with SMAD3 and CREB [165]. The TGFβ-dependent activation of FOXP3 expression was further demonstrated to be controlled by Notch1-mediated recruitment of CSL and SMAD1-3 to the *Foxp3* promoter. Consequently, the addition of γ-secretase inhibitors blocked the differentiation of iTreg, presumably by interfering with the formation of this transcription activating complex [166].

The essential role of FOXO1 and FOXO3A in the TGFβ dependent induction of FOXP3 was discovered following the observation that $FOXO1^{-/-}FOXO3A^{-/-}$ mice develop a fatal inflammatory disorder that is, in part, due to reduced Treg cell numbers and impaired function of the remaining Treg [167]. Subsequent experiments demonstrated that FOXO1 and FOXO3A bind and activate both the *Foxp3* promoter and CNS2 during the induction process [167-169]. A similar impairment in the induction of FOXP3 by TGFβ was detected in mice deficient in the E3 ubiquitin ligase ITCH. ITCH activates the transcription factor TIEG1 by ubiquitinylation, which enables TIEG1 to bind to *Foxp3* promoter sequences and activate transcription [170]. Furthermore TIEG1 was also demonstrated to bind to the upstream enhancer [171].

In line with the requirement of IL-2 in the TGFβ induced expression of FOXP3, STAT5 binds to both the promoter and CNS2 in the Foxp3 locus [172]. Similarly, STAT1, a member of the STAT family that is induced by the cytokine IL-27, was also shown to interact with human promoter sequences and enhance the induction of FOXP3 [173]. In contrast to this, IL-27 inhibits the induction of FOXP3 in mouse $CD4^{+}$ T-cells, raising the possibility that FOXP3 expression might be differentially regulated in mice and humans

[174, 175]. The negative effect of IL-27 on the induction of FOXP3 was at first demonstrated to be independent of STAT1 activation [175]. Subsequent studies revealed that the reduced induction was caused by activation of STAT3 and that STAT1 is, at least in part, responsible for inhibiting the negative effect of STAT3 on FOXP3 expression (in line with the reports of a positive role of STAT1 in the regulation of FOXP3 [173]) [174]. Further experiments will have to clarify the contribution of STAT1 in the activation of the *Foxp3* locus.

On the other hand, the role of IL-6 in the control of FOXP3 induction has been conclusively demonstrated. The addition of IL-6 to cultures otherwise suitable for the induction of FOXP3$^+$ Treg, inhibits the expression of FOXP3 and instead facilitates the differentiation of RORγT$^+$ Th17 cells [176-178]. This effect is thought to be due to activation of STAT3 by IL-6 [174]. The molecular mechanism with respect to the *Foxp3* locus was revealed by Xu and colleagues that demonstrated that IL-27 and IL-6 induced STAT3 activation facilitates the binding of the transcription factor to CNS2, which interferes with the binding of SMAD3 to CNS1. Deletion of the STAT3 site in CNS2 essentially converted CNS2 from acting as a silencer in the presence of IL-6 into an enhancing regulatory element. In the same study, Xu et al. also demonstrated the importance of an AP-1 site in CNS1 and two RAR-RXR sites in the promoter and CNS2, providing a mechanism for the long known effect of retinoic acid in enhancing FOXP3 induction.

In contrast to the inhibition of binding by IL-27 induced STAT3, both the AP-1 and RAR-RXR mediated activation of the *Foxp3* locus seem to facilitate the binding of SMAD3 to CNS1 [179]. Similar to the formation of the ”enhanceosome” [165], this observation emphasizes the importance of molecular interactions of the CNS regions and the factors that bind to them. These findings underscored the importance of SMAD3

binding to CNS1 for the induction of FOXP3. Tone et al. established the basis for these studies by identifying the core sequence of CNS1 that is necessary for the TGFβ-mediated induction and also discovered the SMAD3 site itself. By demonstrating that SMAD3 binding was dependent on the interaction with NFAT, the authors also established the crucial concept that the SMAD3 binding event is dependent on the interaction with other transcription factors [160].

As studies performed by Maruyama and colleagues showed, the effect of TGFβ-induced SMAD3 does not only directly control the expression of FOXP3. SMAD3 signalling enhances the binding of transcription activating E2A to the *Foxp3* promoter and also induces the expression of the DNA-binding inhibitor ID3 in $CD4^+$ T-cells. Besides the direct activation of the *Foxp3* locus by E2A, the TGFβ-induced ID3 prevents the expression of GATA3 that inhibits *Foxp3* promoter activity [180]. In addition to GATA3 and STAT3, the transcription factor IRF1 that is induced by the Th1-cytokine IFNγ has been demonstrated to bind to and inhibit the *Foxp3* promoter [181]. However, the precise mechanism of GATA3 and IRF1-mediated inhibition of *Foxp3* transcription remains elusive.

Another set of transcriptional regulators that is induced by TGFβ and is involved in the induction and maintenance of FOXP3 expression, is the RUNX family of transcription factors. RUNX1 and RUNX3 proteins are induced in response to TGFβ, interact with CBFβ and bind to the promoter as well as CNS2 to facilitate FOXP3 expression [182-184]. Furthermore the binding of the RUNX/CBFβ complex to CNS2 seems to be necessary for the inheritable expression of FOXP3 [161]. $CD4^+$ T-cells cannot maintain proper FOXP3 expression when transduced with a dominant negative RUNT domain that interferes with RUNX activity or when CBFβ was genetically deleted [183, 184]. In addition to its role

in the regulation of FOXP3 expression, RUNX is also required for Treg function by forming a complex with FOXP3 and regulating the Treg transcriptional program [185, 186].

The regulation of FOXP3 expression by transcription factors is dependent on both epigenetic marks that increase the accessibility of the locus as well as the recruitment of chromatin modifying enzymes by these transcription factors (reviewed in [187, 188]). The major epigenetic modifications that can be detected at the *Foxp3* locus are summarized in figure 5.

1.6 | Aims and format of the thesis

The work described in this thesis aims to establish a cell line model that reliably mimics the induction of FOXP3 in $CD4^+$ T-cells. The understanding of the precise signalling mechanisms that underlie the induction of FOXP3 has in part been hampered by the lack of such a cell line. Cell lines have proven to be a crucial tool in the study of TCR signalling due to their amenability to transfection and because they can easily provide large numbers of cells for biochemical analysis. A representative model should respond with FOXP3 expression only when stimulated with αCD3 antibody in the presence of TGFβ. Since our lab was amongst the first to describe that mTOR inhibition can enhance the induction of FOXP3, we have a keen interest in deciphering the contribution of the mTOR pathway in the induction process. Therefore the cell line model should also be responsive to mTOR inhibition via depletion of EAA or pharmacological inhibition.

The successful establishment of such a cell line would enable an analysis of the contribution of the two mTOR complexes in the regulation of FOXP3 expression. Moreover, this work aimed to identify downstream targets of the mTOR pathway that are involved in the control of FOXP3 expression. Despite recent, major advances in the field these targets remain to be identified.

In chapter 3 of this thesis the establishment of the FOXP3 inducible cell line model is described. Additionally, the conditions required for the induction of FOXP3 in the model are characterized and the responsiveness to mTOR inhibition demonstrated.

In the subsequent chapter the contribution of the two mTOR complexes to the induction of FOXP3 is probed, indicating a role for both complexes. The following chapter illustrates the attempts made to identify downstream targets of mTOR that are involved in the regulation of FOXP3 expression. The last results chapter describes a screen for mTORC1 and mTORC2 targets that regulated the induction of FOXP3 using a phospho-proteomics approach.

Considering the importance of mTOR signalling in shaping immune responses, particularly by shaping T-cells differentiation, as well as the clinal administration of the mTOR inhibitor Rapamycin as an immunosuppressant, a more detailed understanding of the role of mTOR in the regulation of FOXP3 could provide the basis for improved clinical protocols aiming to expand Treg populations.

Chapter 2 | MATERIALS AND METHODS

2.1 | Materials

2.1.1 | Consumables

Product	Supplier	Catalogue number
cl-Xposure film 18x24cm	Thermo Scientific	34089
Gene Pulser/MicroPulser Cuvettes, 0.4 cm gap	Bio Rad	165-2088
Microplates 96 well, white	SLS	MIC9016
NativePAGE™ Novex® 4-16% Bis-Tris Gels 1.0 mm, 10 Well	Invitrogen	BN1002BOX
NativePAGE™ Novex® 4-16% Bis-Tris Gels 1.0 mm, 15 Well	Invitrogen	BN1004BOX
Protein LoBind Tubes, 1.5ml Eppendorf tubes	Sigma-Aldrich	Z666505
Microcentrifuge tubes, 1.5ml	Appleton Woods	KC144
Microcentrifuge tubes, 0.5ml	Appleton Woods	KC123
Filter pipette tips, 10µl	Appleton Woods	4135
Pipette tips, 200µl	Appleton Woods	4804
Pipette tips, 1000µl	Appleton Woods	9032
Filter pipette tips, 30µl	Appleton Woods	4821
Filter pipette tips, 200µl	Appleton Woods	4823
Filter pipette tips, 1000µl	Appleton Woods	4809
Serilogical pipettes 5ml	Costar	4487
Serilogical pipettes 10ml	Costar	4488
Serilogical pipettes 25ml	Costar	4489
Serilogical pipettes 50ml	Costar	4490
Invitrolon sandwiches	Invitrogen	IC2005
NuPAGE® Novex 4-12% Bis-Tris Gels 1.0 mm, 17 well	Invitrogen	NP0329BOX
50ml tubes	Corning	430829
15ml tubes	BD Falcon	352097
96 well staining plate	BD Falcon	353910
FACS tubes	BD Falcon	352051
NuPAGE Bis-Tris 4-12% gel	Invitrogen	NP0335BOX
24-well tissue culture plate	Costar	3524

round bottom 96-well tissue culture plate	Costar	3799
Vented 25cm^2 tissue culture flask	Corning	3056
Vented 75cm^2 tissue culture flask	Corning	430641
Vented 175cm^2 tissue culture flask	Corning	431080
Nunc®cryogenic tubes	Thermo Scientific	375418
SnakeSkin® Pleated Dialysis Tubing	Thermo Scientific	68100
PES vacuum filtration device, 0.22µm	Corning	431097
Cell strainer 70µm	Falcon	352340

2.1.2 | Reagents

The following reagents were used in this thesis. The concentrations of the individual reagents that were used are indicated in the relevant figure legends, the main text or the "Materials and Methods" chapter. Were appropriate the reagents were resuspend according to manufacturer's recommendations or in the best available solvent.

Product	Supplier	Catalogue number
Iodoacetamide	Sigma-Aldrich	I-6125
Bovine serum albumin	Sigma-Aldrich	A-9647
Glycerol	Sigma-Aldrich	G-6279
MES hydrate	Sigma-Aldrich	M-2933
Ethanol	Fisher Scientific	20821.330
Methanol	Sigma-Aldrich	34860
Bis-Tris	Sigma-Aldrich	B-4429
Full Range Rainbow Molecular Weight Marker	GE Healthcare	RPN800E
cl-Xposure film 18x24cm	Thermo Scientific	34089
7-Aminoactinomycin D	Sigma-Aldrich	A-9400
Dual-Luciferase® Reporter Assay System 10-Pack	Promega	E1960
Recombinant human TGF-beta 1	Peprotech	100-21C
MagCellect Mouse CD4$^+$ T Cell Isolation Kit	R&D Systems	MAGM202

Goat serum	Sigma-Aldrich	G-9023
Rapamycin	Calbiochem	553211
MISSION® shRNA Bacterial Glycerol Stock, set of 5 clones	Sigma-Aldrich	
MISSION® Non-Target shRNA Control Vector	Sigma-Aldrich	SHC002
Puromycin dihydrochloride	Sigma-Aldrich	P-9620
Nupage antioxidant	Invitrogen	NP0005
LY294002	NEB	9901
Brefeldin A	Sigma-Aldrich	B-7651
RPMI1640 for SILAC	Thermo Scientific	PN89984
Acetonitrile	Sigma-Aldrich	34998
6ml syringe barrel style columns	Applied Seperations	2416
Hydrophobic polyethylene frits, 20µm	Applied Seperations	2426
Sep-Pak® Vac tC18 cartridge 3cc/200mg	Waters Ltd	WAT054925
Sep-Pak® Vac tC18 cartridge 1cc/50mg	Waters Ltd	WAT054960
Sodium Chloride	Sigma-Aldrich	73575
Trizma	Sigma-Aldrich	93349
Trizma hydrochloride	Sigma-Aldrich	93363
4-(2-Aminoethyl)benzenesulfonyl fluoride hydrochloride	Sigma-Aldrich	A-8456
Benzamidine	Sigma-Aldrich	12072
Leupeptin hemisulfate salt	Sigma-Aldrich	L-2884
Pepstatin A	Sigma-Aldrich	P-4265
β-Glycerophosphate disodium salt hydrate	Sigma-Aldrich	G-9422
Sodium fluoride	Sigma-Aldrich	71519
Glutamaic Acid	Sigma-Aldrich	
Calyculin A from *Discodermia calyx*	Sigma-Aldrich	C-5552
Potassium phosphate monobasic	Sigma-Aldrich	60221
Phosphoric acid	Sigma-Aldrich	79622
Potassium chloride	Sigma-Aldrich	60129
Lys-N Metalloendopeptidase	AMS Biotechnology Ltd	100965-1
L-arginine.HCl $^{13}C_6$ (Arg6)	CK Gas products	CLM-2265-H0.25
L-Arginine.HCl $^{13}C_6$ $^{15}N_4$ (Arg10)	CK Gas products	CNLM-539-H0.25
L-Lysine:2HCl $^{13}C_6$ $^{15}N_2$ (Lys8)	CK Gas products	CNLM-291-H0.25

L-Lysine:2HCL (4,4,5,5-D4) (Lys4)	CK Gas products	DLM-2640-0.5
L-lysine-2HCl	Thermo Scientific	88429
L-Arginine-HCl	Thermo Scientific	88427
Ionomycin	Sigma-Aldrich	I-0634
SV total RNA isolation system	Promega	Z3100
Potassium phosphate dibasic	Sigma-Aldrich	17835
One Shot® TOP10 Chemically Competent E. coli	Invitrogen	C4040-03
Torin1	Tocris Bioscience	4247
AP1(1) Luciferase Reporter Vector	Panomics	LR0002
AP1(2) Luciferase Reporter Vector	Panomics	LR0003
Restriction enzymes	NEB	
Active Motif nuclear extract kit	Active Motif	40010
Poly(deoxyinosinic-deoxycytidylic) acid sodium salt	Sigma-Aldrich	P-4929
Oasis HLB µElution plate	Waters Ltd	186001828BA
Micro BCA Protein Assay Kit	Thermo Scientific	23235
Microplate BCA Protein Assay Kit	Thermo Scientific	23252
Benzonase® Nuclease	Sigma-Aldrich	E-8263
Magnesium Chloride	Sigma-Aldrich	M-8266
Molecular biology grade trypsin	Sigma-Aldrich	T-6567
Titansphere, 5um, 500mg	Hichrom Ltd	75020-75000
Recombinant mouse IL-6	R&D Systems	406-ML-025
Stratagene PFU ULTRA II FUSION	Stratagene	600670
T4 DNA Ligase	Roche Diagnostics	11635379001
SuperScript III first strand synthesis system	Invitrogen	18080-051
RNaseOUT ™	Invitrogen	10777019
PP242 hydrate	Sigma-Aldrich	P-0037
QIAfilter Plasmid Maxi Kit	Qiagen	12263
QIAfilter Plasmid Midi Kit	Qiagen	12243
QIAprep Spin Miniprep Kit	Qiagen	27104
pGL4.74[hRluc/TK] Vector	Promega	E6921
Complete, Mini, EDTA-free	Roche	11836170001
Formaldehyde	Sigma-Aldrich	533998
Odyssey Blocking Buffer	Licor	927-40000

Prolong gold antifade with DAPI	Invitrogen	P36931
Foxp3 fixation/permeabilisation concentrate&diluent	eBioscience	00-5523-00
EZ-ECL kit 500ml	Geneflow	k1-0172
Pyrrolidine	Sigma-Aldrich	83240
Okadaic acid from *Prorocentrum concavum*	Sigma-Aldrich	O-9381
RPMI1640	PAA	E15-840
β-mercaptoethanol	Sigma-Aldrich	M-7522
penicillin/streptomycin	PAA	P11-010
L-glutamine	PAA	M11-004
Sodium pyruvate	PAA	S11-003
HEPES	PAA	S11-001
ultra low IgG fetal calf serum	Gibco	16250-078
Trypan blue solution	Sigma-Aldrich	T-8154
DMSO	Sigma-Aldrich	D2650
Dulbecco's PBS w/o Ca&Mg	PAA	H15-002
dNTPs	Bioline	BIO-39025
Puromycin dihydrochloride	Sigma-Aldrich	P-9620
Normal rabbit serum	Invitrogen	16120-099
Geneticin (G418)	Invitrogen	11811-031
Sodium azide	USB	21610
Tween 20	Sigma-Aldrich	P-1379
1M DTT solution	Invitrogen	43816
EDTA	VWR	100935V
Tris base	MP Biochemicals	819623
LDS	Sigma-Aldrich	L-4632
Bicine	Sigma-Aldrich	B-3876
Chlorobutanol	Sigma-Aldrich	91210
Pyrrolidine	Sigma-Aldrich	83240
Acetone	Sigma-Aldrich	650501
Urea	Sigma-Aldrich	U-4883
SDS	VWR	442444H
Orange G	Sigma-Aldrich	O-3765

2.1.3 | Antibodies

Antibodies were used at the concentration recommended by the manufacturer (WB, FACS and microscopy) or titrated to determine the optimal concentration (FACS). Isotype controls were used as a guide for the FACS analysis.

Product	Supplier	Catalogue number
IRDye® 800CW Goat (polyclonal) Anti-Mouse IgG (H+L),	Licor	926-32210
IRDye® 680CW Goat (polyclonal) Anti-Rabbit IgG (H+L),	Licor	926-32221
antipS6 (S235/236) Rabbit mAb (Alexa Fluor® 488 Conjugate)	NEB	4854
Rabbit (DA1E) mAb IgG Isotype Control (Alexa Fluor® 647 Conjugate)	NEB	2985
Rabbit (DA1E) mAb IgG Isotype Control (Alexa Fluor® 488 Conjugate)	NEB	2975
Anti-CD3e Hamster APC	BD Pharmingen	553066
Anti-pSMAD3 (Ser423/425) (C25A9) Rabbit mAb	NEB	9520
Rat IgG2a isotype control PE	eBioscience	12-4321-81
antiFOXP3 APC label	eBioscience	17-5773-82
antipAKT (Ser473) (D9E) XP™ Rabbit mAb (Alexa Fluor® 647 Conjugate)	NEB	4075
Rat IgG2a Isotype Control Allophycocyanin (APC)	eBioscience	17-4321-81
antiIL-6 Phycoerythrin (PE)	eBioscience	12-7061-81
antiFOXP3 antibody FITC	eBioscience	11-5773-82
Rat IgG2b, κ PE	BD Pharmingen	556925
Rat IgG2b, κ APC	BD Pharmingen	556924
FoxO3a (75D8) Rabbit mAb	NEB	2497
Anti-rabbit IgG (H+L), F(ab')2 Fragment (Alexa Fluor® 488 Conjugate)	NEB	4412
Anti-rabbit IgG (H+L), F(ab')2 Fragment (Alexa Fluor® 647 Conjugate)	NEB	4414
FoxO1 (C29H4) Rabbit mAb	NEB	2880

Anti-Mouse/Rat Foxp3 Alexa Fluor® 647	eBioscience	51-5773-82
Alexa Fluor® 647 Mouse anti-Stat3 (pY705)	BD Pharmingen	557815
PE Mouse anti-Stat3 (pS727)	BD Pharmingen	558557
Alexa Fluor 647 Mouse IgG2a, k isotype control	BD Pharmingen	558053
PE Mouse IgG1, k isotype control	BD Pharmingen	550617
pS6 S235/236) Rabbit mAb (Alexa Fluor® 647)	NEB	4851
Alexa Fluor 488 IgG1 k isotype control	BD Pharmingen	557720
PE anti-mouse/rat Foxp3 antibody	eBioscience	12-5773-82
Anti-Mouse/Rat Foxp3 Alexa Fluor® 488	eBioscience	53-5773-82
Rat IgG2a K Isotype Control Alexa Fluor® 488	eBioscience	53-4321-80
Histone H3 antibody	Abcam	ab1791
Alexa Fluor 488 rat anti-mouse IL-17A	BD Pharmingen	560220
Anti-KLF10 antibody	Abcam	ab73537
anti-JunB (C-11) antibody	Santa Cruz Biotechnology	sc-8051 X
anti-c-Jun (N) X	Santa Cruz Biotechnology	sc-45 X
Anti-GAPDH Mouse mAb (6C5)	Merck Bioscience	CB1001
Tieg1 antibody (H-13)	Santa Cruz Biotechnology	sc23159
PE rat anti-mouse IL-17A	BD Pharmingen	559502
Phospho-Stat Antibody Sampler Kit	NEB	9914

2.1.4 | Taqman-Assays

Gene	Assay ID
Socs1	Mm00782550_s1
Socs3	Mm00545913_s1
Il-17a	Mm00439619_m1
Foxp3	Mm00475162_m1
Hprt1	Mm00446968_m1
Stat3	Mm01219775_m1*
Rorc	Mm03682796_m1

2.1.5 | Primers

Primers were purchased from Sigma-Aldrich and Eurofins MWG Operon.

Name	Sequence	Mainly used for
Stat3 SalI fwd	GCCCGTCGACCAGTCGAGACCCCTGAC	*Stat3* amplification from cDNA
Stat3 rev FspI BamHI	GGATCCTCACATGGGGGAGGTTGCGCACT	*Stat3* amplification from cDNA
*Stat3*seq 1	AGTCTCGCCTCCTCCA	*Stat3* sequencing
Stat3 seq 2	CAGATCGCGTGCATC	*Stat3* sequencing
Stat3 seq 3	CCTGACCCTTAGGGAGC	*Stat3* sequencing
Stat3 seq 4	GGCCCTTTGGAATGAA	*Stat3* sequencing
Stat3 FLAG tag fwd	TCGACCTCGAGAGCGCTACCTCCCCCATGGATTACAAGGATGACGATGACAAGTGAG	FLAG tag into pEF1α-IRES-EGFP
Stat3 FLAG tag rev	GATCCTCACTTGTCATCGTCATCCTTGTAATCCATGGGGGAGGTAGCGCTCTCGAGG	FLAG tag into pEF1α-IRES-EGFP
Stat3 A661C-N663C fwd	TATAAGATCATGGATTGTACCTGCATCCTGGTGTCTCCACTT	*Stat3* constitutive dimer mutant
Stat3 A661C-N663C rev	AAGTGGAGACACCAGGATGCAGGTACAATCCATGATCTTATA	*Stat3* constitutive dimer mutant
M13F	TGTAAAACGACGGCCAGT	*Stat3* sequencing in pCR2.1 TOPO
M13R	CAGGAAACAGCTATGACC	*Stat3* sequencing in pCR2.1 TOPO

Enh1 fwd	TCGATAAGGATCCGTCGAC	CNS1 (both) amplification from pGL4
Enh1 L BamHI rev	CATCGGGATCCGGACTGATGC	CNS1 (long) amplification from pGL4
Enh1 S BamHI rev	GCATCGGGATCCGTTCCAGA	CNS1 (short) amplification from pGL4
RV3	CTAGCAAAATAGGCTGTCCC	Sequencing of luciferase constructs
RV4	GACGATAGTCATGCCCCGCG	Sequencing of luciferase constructs
RV5	CCGCTTCGAGCAGACATGATAAGA	Sequencing of luciferase constructs
GL4	AGCCCATAGCGTTCATAGCTTCT	Sequencing of luciferase constructs
E2 long seq	CTTGTTGCCGATGAAG	Sequencing of CNS2 constructs
E2S rev colony	ACGTCCATCTGGCTACCAT	Colony PCR of CNS2 containing constructs
E2L rev colony	CACAGACTCTGTAGGGTGCA	Colony PCR of CNS2 containing constructs
E2L dSTAT3 fwd	CAGGATAGACTAGCCAC**ggta**CCGAACGAAA CCTGTGGGGTAGATTAT	Mutation of STAT3 binding site in CNS2
E2L dSTAT3 rev	ATAATCTACCCCACAGGTTTCGTTCGG**tacc**G TGGCTAGTCTATCCTG	Mutation of STAT3 binding site in CNS2

TIEG fwd DY	AAAACTACAAGAACCCCCCCCCCACCCTGCA ATTATCAGCAC 5’ labelled with DY-682	EMSA (probe oligo)
TIEG rev DY	GTGCTGATAATTGCAGGGTGGGGGGGGGG TTCTTGTAGTTTT 5’ labelled with DY-682	EMSA (probe oligo)
TIEG comp fwd	AAAACTACAAGAACCCCCCCCCCACCCTGCA ATTATCAGCAC	EMSA (competing oligo)
TIEG comp rev	GTGCTGATAATTGCAGGGTGGGGGGGGGG TTCTTGTAGTTTT	EMSA (competing oligo)
TIEG comp fwd DY	AAAACTACAAGAACCCCCCCCCCACCCTGCA ATTATCAGCAC 5’ labelled with DY-782	EMSA (competing oligo)
TIEG comp rev DY	GTGCTGATAATTGCAGGGTGGGGGGGGGG TTCTTGTAGTTTT 5’ labelled with DY-782	EMSA (competing oligo)
TIEG Scram fwd	ACCTAACCACTCCACGACCACAACTAGACCT ACGACACCTCA 5’ labelled with DY-782	EMSA (competing oligo)
TIEG Scram rev	TGAGGTGTCGTAGGTCTAGTTGTGGTCGTG GAGTGGTTAGGT 5’ labelled with DY-782	EMSA (competing oligo)
TIEG cons fwd	GGTGTGGGGGTGTGGGGGTGTGGGGGTGT GGGGGTGTGGG 5’ labelled with DY-782	EMSA (competing oligo)
TIEG cons rev	CCCACACCCCCACACCCCCACACCCCCACAC CCCCACACC 5’ labelled with DY-782	EMSA (competing oligo)

2.1.5 | Mice

The mouse strain used in this thesis were C57Bl/6J(B6).FOXP3^{hCD2} (H2^{b}) in which all cells expressing FOXP3 coexpress a GPI anchored human CD2/52 fusion protein at the cell surface.

All mice were bred and maintained in the specific pathogen-free animal facility of the Sir William Dunn School of Pathology (Oxford, UK). All experiments were performed in accordance with the Home Office Animals (Scientific Procedures) Act 1986.

2.2 | Methods

2.2.1 | Schedule 1 termination

Sacrifice of mice for the provision of tissue was performed by exposing the mice to rising concentrations of carbon dioxide. Subsequently death was confirmed by cervical dislocation.

2.2.2 | Cell culture

2.2.2.1 | Culture media and incubation

Cells were cultured in a humidified incubator at 37°C in the presence of 5% carbon dioxide.

2.2.2.2 | Regular culture medium (R-10 medium)

Cells were cultured in RPMI 1640 supplemented with $5x10^{-5}$M β-mercaptoethanol, 1x penicillin/streptomycin, $2x10^{-4}$M L-glutamine, 10^{-4}M sodium pyruvate, 10^{-3}M HEPES and 10%vol/vol ultra low IgG fetal calf serum (R-10 medium).

2.2.2.3 | Medium with limiting concentrations of EAA

For stimulations performed under limiting concentrations of EAA, modified RPMI 1640 (custom made: lacking all essential amino acids (PAA)) was supplemented with 1x penicillin/streptomycin, $2x10^{-4}$M L-Glutamine, 10^{-4}M sodium pyruvate, 10^{-3}M HEPES and 10%vol/vol dialysed ultra low IgG fetal calf serum and the levels of EAA adjusted to the desired percentage (usually 5% of total volume) using R-10 medium.

2.2.2.4 | SILAC medium

Light, intermediate and heavy SILAC media were prepared using RPMI 1640 for SILAC (Thermo Scientific), which lacks L-Arginine and L-Lysine. By adding unlabelled or light (L-Lysine-2HCl, L-Arginine-2HCl), intermediate (L-Lysine:2HCL (4,4,5,5-D4) (Lys4), L-arginine.HCl $^{13}C_6$ (Arg6)) and heavy (L-Lysine:2HCL (4,4,5,5-D4) (Lys8), L-Arginine.HCl $^{13}C_6$ $^{15}N_4$ (Arg10)) labelled L-Lysine and L-Arginine to the level found in regular RPMI 1640 (L-Arg: 0.29mM, L-Lys: 0.219mM) isotopically labelled media were prepared. As described before, the media were also supplement with L-Glutamine, sodium pyruvate, HEPES and penicillin/streptomycin at the previously mentioned concentrations. In order to limit the amount of unlabelled amino acids that were introduced into the

isotopically labelled media, the media were supplemented with 10%vol/vol dialysed ultra low IgG fetal calf serum.

2.2.2.5 | Dialysis of fetal calf serum

Ultra low IgG fetal calf serum was dialysed against 4 changes of 5l PBS over 3 days at 4°C using snakeskin dialysis tubing. The dialysed FCS was filtrated through a 0.22µm PES vacuum filtration device.

2.2.2.6 | Cell counting using Neubauer haemocytometer

Single-cell suspensions were counted using a Neubauer-improved haemocytometer (Marienfeld) in a solution of 0.04-0.2% trypan-blue in order to exclude dead cells.

2.2.2.7 | Freezing and thawing of cells

For long term storage cells were resuspended at 2-5x10^6 cells/ml in ice-cold 90% ultra low IgG fetal calf serum and 10% DMSO and 1ml of the cell suspension transferred to cryo-vials. Cell stocks were stored in a -80C freezer or liquid-nitrogen at the Cell Bank Facility of the Sir William Dunn School of Pathology.

Cells were thawed in a 37°C water bath with continues shaking. Almost completely thawed cell suspensions were washed immediately with 50ml culture medium and then used for downstream applications.

2.2.2.8 | Preparation of spleen cell suspensions

Spleens were gently pushed through a 70µm nylon mesh cell strainer using the plunger of a 2ml syringe to produce a single-cell suspension. Cells were washed twice in culture medium and then used for downstream applications.

2.2.2.9 | Isolation of $CD4^+$ T-cells from mouse spleens

Splenic red blood cells were lysed by Tris-buffered ammonium chloride (0.144M NH_4Cl, 0.017M Tris HCl, pH 7.2) mediated lysis (3 minutes at RT). The mouse $CD4^+$ T-cell isolation kit (R&D systems) was used to isolate $CD4^+$ T-cells from spleens (single cell suspension). The biotinylated antibody cocktail supplied with the kit targets non-$CD4^+$ cells, which are then depleted using strepavidin ferrofluid and a magnet. The isolation was performed according to the manufacturer's protocol.

2.2.2.10 | Culture of EL4 and EL4.B02 cells

Cells were seeded at a density of ~$2x10^4$cells/ml/cm^2 (2 day culture) or ~$5x10^4$cells/ml/cm^2 (1 day culture) in R-10 medium (e.g. 40ml culture/75cm^2 flask). Cells were split 1:4 (1 day culture), 1:10 (2 day culture) or when they reached a density of ~$2x10^5$ cells/ml. Less frequent replacement of medium or seeding at higher density resulted in loss in inducibility with respect to FOXP3.

2.2.2.11 | Limiting dilution cloning

EL4 cells were diluted to 2.5 cells/ml in R-10 medium and 200µl of the suspension was added to each well of a round-bottom 96-well tissue culture plate. Cell growth was

monitored and cells transferred to a large tissue culture plate as soon as a visible population emerged. Until the cells were screened for FOXP3 inducibility, the putative clones were split 1:10 every other day in order to avoid overgrowth of the cultures and replace the spent medium.

2.2.2.12 | Coating of tissue culture plastics with αCD3 antibodies

Tissue culture plastic ware was coated with 5µg/ml αCD3 antibody (clone KT3) diluted in Dulbecco's PBS for at least 1h at 37°C. The volume used to coat the different tissue culture plastic ware was dependent on the surface (volume sufficient to cover entire surface). After the incubation the antibody solution was aspirated and the surface washed with at least 4x the coating volume of Dulbecco's PBS.

2.2.2.13 | Stimulation of cells

R-10 medium or medium containing limiting amounts of EAA were added to antibody coated tissue culture plates, dishes or flasks (950µl/well on 24-well plate or equivalent volume/surface area ratio). Additional reagents such as inhibitors, antibodies or growth factors were added to the medium at the indicated concentrations. Cells were resuspended at the appropriate concentration to achieve the desired final concentration when 50µl of cell suspension (24-well plate) were added to the stimulation medium, e.g. $2x10^5$ cells/ml for 10^4 cells/ml/well and $2x10^6$ cells/ml for 10^5 cells/ml/well. Cells were cultured in a humidified incubator at 37°C in the presence of 5% carbon dioxide for the indicated time periods.

2.2.2.14 | Selection of stable transfectants using Puromycin and G418

The most suitable concentration of puromycin and G418 was either determined by assessing cell survival of titrated amounts of the drugs by FACS analysis or was based on previous experience in the laboratory (optimal concentrations should be just sufficient to efficiently kill non-transfected cells). Concentrations that were used to select cells: ~2µg/ml Puromycin, 0.5-2mg/ml G418. After the transfection the cells were cultured without selection for 24-72h to enable the expression of resistance genes encode by plasmids. Transfected cells were then transferred into selection media, which was replaced in regular intervals. Alternatively, selection was performed by splitting the cells up into 24-well plates directly after electroporation. Again, puromycin or G418 were only added 24-72h after the transfection.

2.2.4 | Fluorescence-activated cell sorting (FACS) analysis

Buffers:	Blocking buffer:	415ml Dulbecco's PBS, 25ml heat-inactivated normal rabbit serum, 50ml 10% BSA, 10ml 5% sodium azide
	Washing buffer:	487ml Dulbecco's PBS, 5ml 10% BSA, 8ml 5% sodium azide
	Fixation reagent:	4% Formaldehyde mixed 1:1 with washing buffer just prior to use

All steps in the staining procedure were performed at 4°C. Surface and intracellular staining and Permeabilisation/Fixation were performed in 50µl volumes whereas in all washes steps and the final fixation step 200µl volumes were used.

Stimulated cells were collected, washed with Blocking buffer and transferred to 96-well staining plates. Antigens located at the cell surface were stained with the appropriate antibodies for 30 minutes. For the last 20 minutes of the surface staining the cell viability stain, 7-AAD (8µg/ml), was added. Following the two washes with Wash buffer, cells were fixed and permeabilized for at least 45 minute using the FOXP3 Fix/Perm reagent (eBioscience). The permeabilized cells were then washed twice with 1x Permeabilisation buffer (eBioscience) before the antibodies directed against intracellular targets were added (diluted in 1x Permeabilisation buffer). After a 45 minute incubation the cells were washed twice with 1x Permeabilisation buffer and fixed in the Fixation reagent.

Cells were analyzed on a 4-colour FACSCalibur flow cytometer (BD Biosciences). Data were analyzed using FlowJo flow cytometry analysis software (version 7.2.5) (Tree Star, Inc). In all FACS plots, numbers within the plot represent the percentage of cells within the gate.

The same staining protocol excluding the permeabilisation and fixation steps were used for MoFlow sorting of cells. After the staining, cells were resuspended at $2x10^7$cells/ml in MACS buffer (Dulbecco's PBS, 2mM EDTA, 0.5% w/v BSA) and sorted by Nigel Rust at the Flow Cytometry Facility of the Sir William Dunn School of Pathology.

For the detection of intracellular cytokines, stimulated cells were treated with 10µg/ml Brefelding A for 2h before the cells were collected.

2.2.5 | Staining of cells for confocal immuno-fluoresence microscopy

Two different protocols both yielding similar results were used for the staining. For simplicity only the one of the protocols is described here.

Stimulated cells were collected and then fixed and permeabilzed for 2h in cold Fix/Perm buffer (eBioscience). Following two washes with 1x Permeabilization buffer the primary antibodies directed against FOXO1 and FOXO3A, which were diluted 1:50 in 1x permeabilization buffer, were added. After an o/n incubation at 4°C (dark) the cells were washed twice with 1x Permeabilization buffer. Blocking of unspecific binding sites was performed using 5% goat serum in 1x Permeabilization buffer for 2h at 4°C (dark). The same buffer was also used to dilute the fluorochrome-conjugated goat anti-Rabbit secondary antibody. After a 2h incubation with the secondary antibody, cells were washes twice with 1x Permeabilization buffer and transferred onto glass slides. Excess liquid was removed using a tissue and a drop of Prolong gold antifade mounting medium with DAPI as well as a cover slip were gently placed on top of the cells. The slides were then cured for 24h in the dark and analyzed in the microscopy facility of the Sir William Dunn School of Pathology. Images were processed using the Carl Zeiss LSM Image Browser.

2.2.6 | Electroporation of cells

Cells were washed several times in RPMI 1640 and resuspended at $5x10^7$ cells/ml in RPMI 1640. Plasmids and 400µl of the cell suspension ($2x10^7$ cells) were added to Gene Pulser Cuvettes and both mixed by flicking the cuvette. Cells were electroporated in a Bio-Rad Gene Pulser with Capacitance Extender at 250V, 975µF.

Electroporated cells were resuspended in the cuvette and transferred to a tissue culture flask (selection of stable transfectants) or split up and directly added to several stimulation wells (luciferase assay).

2.2.7 | Luciferase assay

20µg Firefly reporter plasmid and 1µg *Renilla* reporter plasmid were electroporated as described above. Electroporated cells were then split up into up two 20 wells (24-well plate) containing the stimulation medium and coated antibody (usually two wells for each stimulation, pooled when collected for lysis). The stimulated cells were incubated for the indicated durations in a humidified incubator at 37°C in the presence of 5% carbon dioxide.

Transfected and stimulated cells were collected (pooling of identical stimulation and transfections) and a small quantity set aside for FACS staining in order to asses mTORC1 and mTORC2 activity. Cells were lysed in 60-80µl freshly prepared 1x Lysis buffer (Promega) at RT for 15 minutes. Lysates were centrifuged at maximum speed for 1 minute in a table top centrifuge and 50-70µl transferred to a fresh Eppendorf tube. Lysates were stored at -20C until they were analyzed.

2x20µl of each lysate were added to white 96-well luminometer plates. Freshly prepared LARII and Stop-and-Glow reagent were warmed to RT, the luminometer washed with EtOH/water and primed with the reagents. Luminescence was measured using an automated TriStar LB941 luminometer and a preset dual luciferase program. Ratios of Firefly to *Renilla* luminescence for each sample were calculated and averaged

for the two technical replicates. Ratios were normalized to ratios measured in untreated cells for each reporter construct.

2.3 | Methods of molecular biology

The basic molecular biology techniques, such as PCR techniques, gel extraction and purification, EtOH precipitation, Phenol/Chloroform extraction, restriction digest and ligation, were performed according to manufacturer protocols or adapted from protocols established In the laboratory as well as the "Molecular Cloning, A Laboratory Manual" textbook [189].

2.3.1 | Mini, Midi and Maxi-preparation of plasmid DNA

The isolation of plasmids was performed according to the manufacturer's protocols (Qiagen). However, the bacteria cultures used for plasmid preparation were in most cases 25-50% larger than the volumes suggested by Qiagen (higher yield). For mini-preparations of plasmids, bacteria were cultured in the nutrient rich TY- rather than LB-medium (obtained from "Stores" at the Sir William Dunn School of Pathology). The plasmid yield was determined using a NanoDrop ND-1000 spectrophotometer at 260nm (purity: 260/280nm and 230/280nm ratio).

2.3.2 | Total RNA isolation

DNase-treated total RNA was purified from cells using the spin purification protocol of the SV total RNA isolation system according to the manufacturer's instructions. The yield was determined using a NanoDrop ND-1000 spectrophotometer at 260nm. In cases where the concentrations or the purity (protein or other contaminats, 260/280nm and 230/280nm ratio) were low the RNA was EtOH-precipitated.

2.3.3 | cDNA synthesis

The SuperScript III first-strand synthesis system for real-time-PCR with random hexamers was used to synthesis cDNA from up to 1µg of total RNA. In order to rule out differential synthesis efficiency, the RNA of different samples was diluted to a similar concentration so that equal reaction volumes could be used.

2.3.4 | Real-time PCR using TaqMan® gene expression assays

TaqMan® gene expression assays (Applied Biosystems), each combining two unlabelled gene-specific primers and one specific FAM™ dye-labelled TaqMan® minor groove binder probe, were used for real-time-PCR in duplicate/triplicate wells on the Applied Biosystems 7500 Fast Real-Time PCR System with the SDS software v1.3.1. For each sample equal amounts of cDNA were used in a total reaction volume of 10-20µl. Gene expression levels were normalized to *Hprt1* and calculated with the sequence detection system software v1.3.1 or in Excel using the comparative CT method ($2^{-\Delta\Delta CT}$ method) [190].

2.3.5 | TOPO® TA cloning® of *Stat3* CDS

Stat3 CDS was amplified from cDNA samples prepared from EL4.B02 cells using touch-down PCR cycle program (gradually decreasing annealing temperature over cycles). Besides introducing the adenine overhangs necessary for TOPO TA cloning, the primers were designed to introduce 5' SalI and 3' FspI and BamHI restriction sites. The purified *Stat3* PCR product was cloned into the pCR®2.1-TOPO® vector and transformed according to the manufacturer's instructions (Invitrogen).

2.3.6 | Cloning of wildtype and mutant *Stat3* expression vectors

Wildetype *Stat3* as well as mutants generated by site-directed mutagenesis in the pCR®2.1-TOPO® vector were subcloned into the pEF1α-IRES-EGFP vector using SalI and BamHI restriction sites (pEF1α-*Stat3*-IRES-EGFP). Cloning of a *Stat3* FLAG tag oligo into a pEF1α-IRES-EGFP vector using SalI and BamHI restriction sites generated a pEF1α-FLAG-IRES-EGFP vector. Subcloning of *Stat3* from pEF1α-*Stat3*-IRES-EGFP digested with SalI and FspI into the SalI AfeI digested pEF1α-FLAG-IRES-EGFP vector resulted in the final expression plasmid pEF1α-*Stat3*-FLAG-IRES-EGFP, in which STAT3 proteins are c-terminally FLAG tagged and coexpressed with EGFP.

2.3.7 | Site-directed mutagenesis PCR

Site-directed mutagenesis was used to generate both Stat3 mutants and to mutate the STAT3 binding site in the firefly luciferase vectors.

Complementary mutagenesis primer pairs were designed to be 42bp long with the bp to be mutated located in the center of the primer and a melting temperature of ≥78°C. Two reactions were set up: one containing the forward mutagenesis primer and one containing the reverse mutagenesis primer (both at 0.8µM final concentrations). 50ng of plasmid containing the target sequence were mixed with each primer along with 0.2mM dNTPs, 1x polymerase buffer and at least 2.5 units Pfu Ultra II Fusion polymerase (50µl reaction volume). Both reactions were subjected to the following PCR cycle: [95°C, 1min (95°C, 1min; 55°C, 1min 30sec; 68°C, 3-5min (1min per kb of plasmid length))$_{10}$]. 25µl of each reaction were mixed in a new tube, additional 2.5 units of

polymerase added and the reaction mix subjected to another round of amplification with the following program: [95°C, 1min (95°C, 1min; 55°C, 1min 30sec; 68°C, 3-5min (1min per kb of plasmid length))$_{18}$]. Reactions were cooled on ice and 5µl NEB restriction enzyme buffer 4 as well as 1µl DpnI enzyme added. Tubes were incubated for at least 4h-o/n at 37°C before amplification and digestions were assessed on a 1% agarose gel. Bacteria were then transformed with 1-4µl of mutated DNA.

2.3.8 | Cloning of Firefly luciferase CNS1 and CNS2 double enhancer constructs

CNS1 (long) and CNS1 (short) sequences were amplified from luciferase constructs cloned in pGL4, provided by Tone et al. Both ends of the resulting PCR products contained BamHI restriction sites (5' from the pGL4 cloning vector, 3' introduced by reverse primer) and were cloned into a BamHI site located immediately upstream of the CNS2 (long) sequence in the Tone pGL4 Firefly luciferase CNS2 (long) reporter construct.

2.3.9 | Sequencing

All constructed sequences were confirmed by sequencing (as well as analytical digest and colony PCR). Sequencing was performed by submitting plasmid samples and sequencing primers to Source BioScience at the Department of Biochemistry of the University of Oxford. Sequences were analyzed using the Sequencher software version 4.9.

2.3.10 | Electrophoretic mobility shift assay (EMSA)

Complementary oligo pairs (fwd/rev) were resuspended at 20pmol/µl in TE-buffer and equal volumes mixed in one tube. The tube was placed in a heat block set to 100°C. After 3 minutes the heat block was turned off and allowed to slowly cool down to RT for several hours. The annealed oligos were then diluted 1:200 with RNase/DNase free water and stored at -20C.

Nuclear extracts were prepared and protein concentration determined as described later. Extracts were diluted to 1µg/µl. The composition of the binding mix was as follows (11µl per sample):

2µl 10x Binding buffer(100mMTris, 500mM KCl, 5mM DTT, pH7.5)

4µl Poli(dl.dC) (0.5µg/µl in 10mM Tris, 1mM EDTA, pH7.5)

1µl 2.5%Tween 20

0.2µl 10% BSA in water

3.8µl water

To each EMSA binding reaction 5µg nuclear protein from differentially stimulated cell was added. The DY782-labelled annealed oligos were diluted 1:100 in TE-buffer and 2µl added according to the plan in the figure 41. The mixture was incubated for 10min in the dark at RT. Subsequently 2µl of 1:8000 diluted, annealed probe oligo (80-fold less than competing oligos) was added to each sample, followed by 20min incubation in the dark at RT. 2µl of orange loading dye (65% Sucrose, 10mM Tris HCl pH7.5, 10mM EDTA, 0.3% w/v Orange G) were added to each sample. The samples were loaded on a Native

4-16% Bis-Tris polyacrylamide gel that was prerun at 80V for at least 1 hour. Electrophoresis was performed at RT in the dark at 80V until the dye front reached the bottom of the gel. Gels were scanned on the Odyssey imager.

2.4 | Proteomics techniques

2.4.1 | Preparation of cytoplasmic and nuclear extracts

The preparation of nuclear extracts was performed using the Active Motif nuclear extract kit. Except for a few instances in which the cytoplasmic and nuclear lysis was performed in smaller volumes in order to obtain more concentrated extracts, the manufacturer's protocol was followed.

2.4.2 | Western Blot

Buffers:

2x LDS buffer: 0.2g/ml glycerol, 0.034g/ml Tris base, 0.033g/ml Tris HCl, 0.04g/ml LDS, 0.3mg/ml EDTA, 0.000375% Serva blue 250, 0.000125% Phenol red, 0.1M DTT, pH8.5

20x MES-SDS Running buffer: 0.1952g/ml MES (pH7.2), 0.121g/ml Tris Base, 0.02g/ml SDS, 0.006g/ml EDTA

20x NuPAGE Transfer buffer: 0.0816g/ml Bicine, 0.1048g/ml Bis-Tris, 0.006g/ml EDTA, 0.15mg/ml Chlorobutanol

TTBS: 0.0121g/ml Tris HCl, 0.008625g/ml NaCl, 0.1% Tween 20

In order to achieve even loading of gels, the protein concentration of cytoplasmic and nuclear extracts were quantified using BCA assay. Before loading of the samples on the polyacrylamide gel, they were supplemented with an equal sample volume 2xLDS sample buffer to reduce proteins and facilitate loading. The samples were then boiled for 8 minutes at 95°C and pulse spun. The reduced samples and the Rainbow molecular

weight marker were loaded on a NuPAGE 4-12% Bis-Tris gradient polyacrylamide gel immersed in 1x MES-SDS Running buffer (inner chamber supplemented with 500µl NuPAGE antioxidant). The electrophoresis was performed at 200V for approximately 40 minutes or until the dye front reached the bottom of the gel. PVDF-membranes were soaked in methanol to break the surface tension, rinsed with water and along with Whatman-paper immersed in 2x Transfer buffer (100ml 20x buffer, 200ml methanol, 700ml water and 500µl NuPAGE antioxidant). For the wet transfer of the protein from the gel onto the membrane the individual components were stacked as following (all components were wetted with Transfer buffer): Anode, sponges, Whatman-paper, gel, membrane, Whatman-paper, sponges, cathode. A maximum of two gels were transferred at once. The blotting assembly was then submerged in Transfer buffer and the proteins transferred at 30V for 30 minutes to 1 hour. Subsequently the membranes were blocked for 1-2h with 5%BSA in TTBS (Odyssey imager: Odyssey blocking buffer) with agitation. Antibodies were diluted in blocking buffer and added to the membranes. The duration of the incubation ranged from 2h to o/n, depending on the antibody that was used (anti-phospho antibodies: o/n at 4°C). The membranes were then washed trice for 5 minutes with TTBS (Odyssey: PBS instead of TBS) and incubated with appropriate secondary antibodies (either HRP conjugated for ECL detection or fluorochrome-conjugated for Odyssey imager) for 30 minutes to 1 hour. After another 6 washes with TTBS the membranes were either incubated with a freshly prepared ECL solution and exposed to X-ray films for different durations (developed in X-OMAT film developer) or scanned using an Odyssey imager.

2.4.3 | Mass spectrometry based phospho-proteomics

As part of this thesis two sets of mass spectrometry based phospho-proteomics experiments were performed. Both experiments were based on the buffers and protocols described by Dephoure et al. [191].

2.4.3.1 | SILAC labelling of EL4.B02 cells and confirmation of homogeneous labelling

EL4.B02 cells were cultured in light, intermediate and heavy SILAC media for at least 10 cell divisions. In order to confirm that the homogeneous labelling of the cells, the "light", "intermediate" and "heavy" cells were lysed and subjected to SDS-PAGE as described before. The polyacrylamide gel was stained with Coomassie Brilliant Blue R-250 and bands of equal molecular weight from "light", "intermediate", "heavy" and 1:1:1 mixed lysate lanes excised. The gels slices were diced and subjected to in gel digest using trypsin. The protocol and reagents were provided by the Proteomics Facility at the Sir William Dunn School of Pathology. In brief, Coomassie stain was washed out of the cubes using 25mM ammonium bicarbonate in 50% acetonitrile (solution B) and gel pieces dehydrated using 100% acetonitrile. After evaporation of the acetonitrile in a SpeedVac, 10mM DTT was added for 30min (37°C), gel pieces washed twice with solution B and several times using acetonitrile. Following alkylation in iodoacetamide the gel pieces were washed with solution B, dehydrated using acetonitrile and digested with trypsin at 37°C o/n. Digest was stopped by acidification and proteins extracted using 0.1% formic acid (FA) in 50% acetonitrile. Dried peptides were submitted to the Proteomics Facility for analysis.

2.4.3.2 | Stimulation of cells

The differentially labelled cells were stimulated on 3x5 10mm diameter petri dishes using plate bound αCD3 antibody, 5ng/ml TGFβ and 250U/ml IL-2 (X-63 supernatant) in the respective SILAC medium ($1x10^6$ cells/ml, 20ml per dish). Two of the three 2 hour stimulations were either supplemented with 5nM Rapamycin or 250nM Torin1.

2.4.3.3 | Workflow of 1st phospho-proteomics experiment

In the first experiment the three differentially labelled and stimulated cells were lysed, the protein amount quantified (BCA assay) and lysates mixed at 1:1:1 protein ratio (7mg total protein). Reduction of disulfide bonds, alkylation, Lys-C digestion, desalting and SCX fractionation was performed essentially as described by Dephoure et al.[191]

Rather than using the IMAC-mediated enrichment of phospho-petides, a protocol provided by the Proteomics Facility that was originally developed by Dean Hammond, Roman Koerner and Francis Barr (available at http://www.proteomics.ox.ac.uk/documents/TiO2_enrichment.pdf) based on self-made micro columns containing a C8-silica matrix and titanium dioxide was used. In brief, after preparation, washing and conditioning of the micro columns the glycolic acid acidified, SCX-fractionated peptides were loaded onto the columns. The flow speed was controlled by carefully adjusting the centrifugation speed in a table top centrifuge. Peptide fractions were passed through the same column twice, with each round taking roughly 5 minutes. Two 5 minute washes with glycolic acid and 0.2% FA 80% acetonitrile were followed by a 2 minute washing step with 20% acetonitrile. Peptides were eluted during 15 minute long centrifugation using 0.6% ammonium

hydroxide, a 5 minute elution with 60% acetonitrile, a 15 minute elution with 1% Pyrrolidine and a 5 minute elution with 60% acetonitrile. Eluted phospho-peptide enriched fractions were then dried in a SpeedVac and submitted to the Proteomics Facility for analysis.

2.4.3.4 | Workflow of 2nd phospho-proteomics experiment

Based on the results of the 1st experiment and with the help of Dr. Mogjib Salek, the experimental protocol was adapted. The stimulation was performed as described before but the stimulation conditions were swapped between the "light", "intermediate" and "heavy" labelled cells. Furthermore rather than mixing cell lysates, the stimulated cells were mixed at equal numbers so that cytoplasmic and nuclear extracts (Active motif) could be prepared from the 1:1:1 cell mix. The cytoplasmic extract was immediately precipitated using 5x volumes of ice-cold acetone (precipitation at -30C o/n). Instead of using the nuclear lysis buffer provided by the Active Motif kit, the nuclear pellet was lysed in 4M Urea lysis buffer (Dephoure et al.) and supplemented with 1000 units Benzonase. After a 15min incubation the Urea concentration was topped up to 8M and lysis continued for an additional 15 minutes. The cleared nuclear lysate was then diluted 2.5-fold with water and acetone-precipitated o/n. Cytoplasmic and nuclear protein pellets were resolubilized in 8M urea lysis buffer, denaturated and alkylated as described by Dephoure et al. [191]. In the meantime the protein content was determined by BCA assay (10mg of cytoplasmic and 8mg of nuclear protein were used for the experiment). Both extracts were diluted 2.5-fold with 25mM Tris HCl (pH 8.8) and Lys-C digested for 4h at protein to enzyme ratio of 200:1. The digests were diluted 2-fold with 25mM Tris HCl (pH 8.8) and trypsin

added at a protein to enzyme ration of 100:1 (digest o/n). Additional trypsin was added for the last 4 hours (110:1) and the digest acidified. Desalting and SCX fractionation was performed as described by Dephoure et al. [191], however additional salt steps (2, 5, 15mM) were introduced (10 SCX-fractions per extract). The additional desalting step was omitted and SCX-fractions were directly subjected to titanium dioxide (TiO_2)-mediated phospho-peptide enrichment. TiO_2-beads were washed in 2% TFA 80% acetonitrile, conditioned with 1.5% ammonium hydroxide 40% acetonitrile and washed twice more with 2% TFA 80% acetonitrile. The SCX-fractions were acidified with 0.75x volumes saturated glutamic acid in 3% TFA 80% acetonitrile and 2.4mg TiO_2-beads adder per fractions. Following the 45min incubation the beads were transferred to an Oasis HLB µElution plate and a second round of phospho-peptide extractions performed as described. The beads from both extractions were pooled, washed with 2% TFA 80% acetonitrile and 0.2% FA 80% acetonitrile. Phospho-peptides were eluted in two steps using 1.5% ammonium hydroxide 40% acetonitrile (5 minute incubation) and 1.5% FA 40% acetonitrile. Eluted peptides were acidified and dried in a SpeedVac. Dried phospho-peptides were submitted to the Proteomics Facility for mass spectrometry analysis.

2.4.3.5 | Q Exactive Mass Spectrometry Analysis

The description of the Q Exactive Mass Spectrometry analysis method was kindly provided by Dr. Benjamin Thomas of the Proteomics Facility at the Sir William Dunn School of Pathology.

Samples were analysed on a Q Exactive Orbitrap mass spectrometer (Thermo, Hemel Hempstead, UK) coupled to a Dionex Ultimate 3000 RSLC nanoHPLC system (Dionex,

Camberley, UK). The HPLC system was run in direct injection mode without a trapping column in order to ensure efficient capture of hydrophilic compounds. Peptides were resolved on a home packed 25 cm long by 75 µm internal diameter PicoTip Emitter (New Objective) packed with 3 µm bead, 120 Angstrom pore, C18 material (Bischoff Chromatography, ProntoSil 120-3-C18). Columns were manufactured using a high-pressure helium packing bomb. Samples were typically resolved on a 140 min gradient method. The Q exactive mass spectrometer was operated as follows. The instrument was run in a "top 10" data dependent acquisition mode in which 1+ charged ions were excluded from isolation and fragmentation. HCD fragmentation was used to fragment the peptides. HCD collision energy was set to 25. Dynamic exclusion was enabled and allowed for 40 s in order to minimise repeat sequencing. The MS resolution was set at 70,000 (fwhm) and 17,500 (fwhm) for MSMS resolution. Fill times were set at 60 ms for MS and 120 ms for MSMS with targets of 1E06 for both. Raw instrument files were then analysed using MaxQuant version 1.2.2.5 [192]. Searches were performed against Ensemble mouse database version NCBIM37 release 67. Maxquant was used to perform quantitation and Andromeda identification. Default settings were used unless specified otherwise. Under the "modifications & labels" tab the following settings were applied: variable modifications: oxidation, acetylation, phospho STY, multiplicity: 2, maximum labelled AAs: 3, enzyme: LysC (1st exp.), trypsin (2nd exp.), first search ppm: 20, main search ppm: 6, maximum number of modifications per peptide: 5, maximum number of missed cleavages: 2, maximum charge: +7, light AA label: Lys4, Arg6, heavy AA label: Lys8, Arg10. Under the "MS/MS & sequences" tab the following settings were applied: fixed modifications: carbamidomethyl-L-I Under the " identifications &

quantifications" tab the following settings were applied: peptide+site+protein FDR: 0.01.

2.5 | Statistical analysis

Where indicated, statistical analysis was performed using GraphPad Prism (version 5.04) for Windows (GraphPad Software, www.graphpad.com). Statistical tests used include one-way analysis of variance (ANOVA) and repeated measures ANOVA with Dunnett's or Bonferroni's multiple comparison post test. Where applicable data was subjected to D'Agostino and Pearson omnibus normality test and outliers were identified using Grubb's test. The statistical significance is indicated as follows: *p<0.05, **p<0.01, ***p<0.001, ****p<0.001.

Chapter 3 | GENERATION AND CHARACTERIZATION OF THE FOXP3 INDUCIBLE EL4 CLONE B02

3.1 | Characterization of FOXP3 induction in EL4 cells and isolation of a highly responsive clone B02

The transcription factor FOXP3 and its central role in immune homeostasis has been extensively studied ever since it was discovered more than a decade ago. FOXP3 is specifically expressed in $CD4^+$ T-cells and has been demonstrated to be crucial for the differentiation, maintenance and function of Treg [145, 193, 194], a subset of T-cells that lie at the core of peripheral tolerance mechanisms. Although substantial progress has been made in understanding the signals and mechanisms that underlie the induction of *Foxp3* transcription in T-cells, a detailed picture of the molecular network and the factors involved in the control of FOXP3 expression is only beginning to emerge [195].

FOXP3 expression can be induced in the thymus in a process thought to be largely regulated by high affinity binding of the TCR to antigen MHC class II complexes [196-198], giving rise to a fate-committed population of $FOXP3^+CD4^+$ cells referred to as natural Treg (nTreg). In addition naive $CD4^+$ T-cells circulating in the periphery can be induced to express the Treg lineage specification factor FOXP3 *de novo* through the engagement of the TCR in the presence of TGFβ [199]. In order to distinguish the peripherally induced cells from nTreg, these $FOXP3^+$ Treg have been termed induced Treg (iTreg). They can also be readily generated *in vitro* from naive $CD4^+$ T-cells where TCR stimulation is accompanied by the exposure to TGFβ, IL-2 as well as CD28 costimulation [148, 152-154].

Despite having these well defined conditions for the induction of $FOXP3^+$ iTreg differentiation, the investigation of the molecular events underlying induction remain poorly understood, in part due to the lack of a valid and truly representative cell line

model of Treg differentiation. Cell lines have proven to be useful tools in deciphering early TCR signalling events [200], being experimentally amenable to over expression and knock-down studies, and providing large numbers of cells for biochemical analysis. Indentifying the TGFβ responsive element in the *Foxp3* locus Tone et al. demonstrated that the mouse lymphoma T-cell line EL4 can be induced to express *Foxp3* transcripts in response to CD3, CD28 and TGFβ stimulation whilst also showing a similar degree of histone 4 acetylation at the *Foxp3* promoter compared with primary FOXP3$^+$ cells [160]. These findings led me to explore whether the T-cell line EL4 could provide a suitable model system to study the breath of signalling events underlying the regulation of FOXP3 expression.

Stimulation of EL4 cells with plate-bound αCD3 with or without soluble αCD28, resulted in the induction of FOXP3 in a very small fraction of cells and the level of FOXP3 expression in the FOXP3$^+$ population was also low (Figure 6). In the presence of TGFβ the proportion of FOXP3$^+$ cells remained unchanged when compared to cells stimulated with αCD3 and αCD28 alone, however the MFI of these FOXP3$^+$ cells appears to be visibly higher. This might indicate that the TGFβ exposure enhanced the induction of FOXP3, but not the proportion of cells that responded (Figure 6).

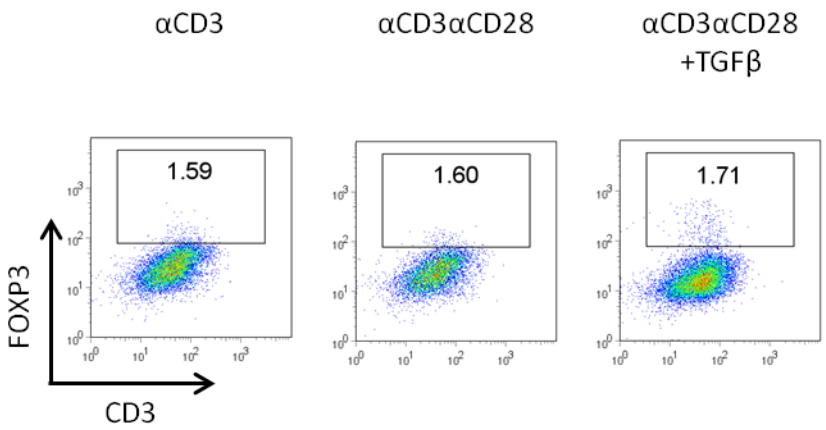


Figure 6. Stimulation of the T-cell line EL4 results in weak FOXP3 expression. FACS analysis of FOXP3 and CD3 expression in EL4 cells stimulated for 4 days at 10^5 cells/well in the presence of plate bound αCD3 (KT3, 5µg/ml), soluble αCD28 (37.51, 1µg/ml), and TGFβ (5ng/ml). Dot plots show live cells. Dead cells were excluded by gating on 7-AAD low cells.

In a setting in which only a population of ≤2% responds to the FOXP3 inducing stimuli, a detailed study of the signalling events underlying the induction of FOXP3 was not considered feasible. Therefore the EL4 cell line was subjected to limiting dilution cloning in the hope that in some of the isolated clones, a larger proportion of cells would upregulate FOXP3 upon stimulation. Cells were seeded at 0.5 cells per well and their growth monitored over an 11 day period. As expected from a seeding density of 0.5 cells per well, clones with considerable growth were observed in 46 out of 96 wells, indicating a cloning efficiency of 47.9%. When appropriate, the culture medium was refreshed and clones expanded by transferring them to large volume tissue culture plates. On day 12, a roughly equal number of cells from each of the 43 clones was stimulated with plate-bound αCD3, soluble αCD28 and 5ng/ml TGFβ for 4 days.

Screening of the isolated and stimulated clones by FACS analysis revealed that out of the 43 stimulated clones, 27 clones showed increased (≥2%) and 16 showed similar (≤2%) responsiveness compared to the parental EL4 line (Figure 7A). Strikingly, some of the isolated clones showed an up to 15-fold enrichment in the population of FOXP3

inducible cells (Figure 7B), indicating that the limiting dilution approach was successful in isolating cells biased to FOXP3 expression. However, neither of the clones responded homogeneously to the stimuli by FOXP3 upregulation. This could indicate that either the samples were in fact not of clonal origin or that the stimulation conditions were suboptimal. Furthermore it is also possible that responsive clones partially reverted to a non-inducible state during the expansion or that FOXP3 inducibility could never reach 100% due to the stochastic nature of such complex signalling events. The most responsive clones were expanded and stocks frozen and stored at -80C.

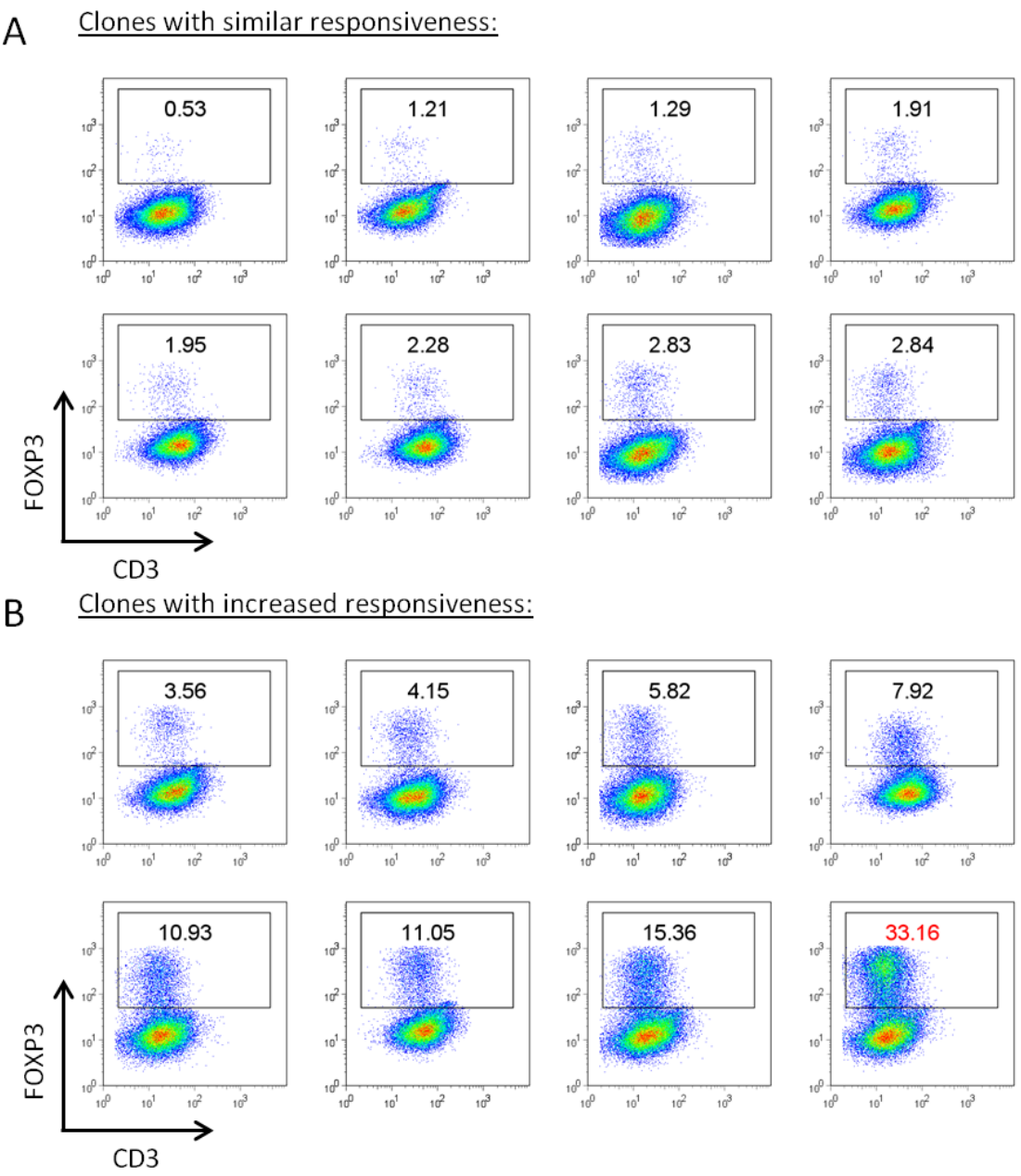


Figure 7. Isolation of a highly FOXP3 inducible clone G08 by limiting dilution cloning of EL4 cells and screening. FACS analysis of FOXP3 and CD3 expression in EL4 clones stimulated for 4 days in the presence of plate bound αCD3 (KT3, 5µg/ml), soluble αCD28 (37.51, 1µg/ml) and TGFβ (5ng/ml). Out of the 43 EL4 clones that were screened, 8 representative clones with similar (A) and increased responsiveness (B) are shown. The percentage of $FOXP3^+$ cells of the most responsive clone G08 is highlighted in red. Dot plots show live cells. Dead cells were excluded by gating on 7-AAD low cells.

In order to rule out that the most responsive EL4 clone G08 (Figure 7B, highlighted in red), exhibiting FOXP3 expression in more than 30% of the live cells, was not a true clone, and in an attempt to further enrich for FOXP3 inducibility , G08 was subjected to another round of limiting dilution cloning and screening (as described earlier). The

unstimulated clone G08 was screened along with the 24 stimulated subclones of G08, so that constitutive FOXP3 expression in clone G08 could be ruled out.

In line with the assumption that the expression of FOXP3 in clone G08 was induced through signals emanating from the engagement of CD3, CD28 and the TGFβ receptor, clone G08 did not exhibit any FOXP3 expression in the absence of the stimuli (Figure 8A). Analysis of the G08 subclones revealed that all but one clone exhibited similar or higher proportion $FOXP3^+$ cells after stimulation when compared to the clone G08 (Figure 8B and C). The 23 subclones with similar or higher inducibility, 11 displayed an increased proportion of responsive cells, with some clones upregulating FOXP3 in as many as 43% of the cells (Figure 8C, reclone B02). As observed in the previous screen, none of the subclones showed a homogeneous response to the stimuli. The fact that, with the exception of one reclone, all subclones responded at least as well as the clone G08, demonstrated that the FOXP3 inducibility is a relatively stable feature of the cells. Since all subclones were cloned twice at 0.5 cells per well, it seemed unlikely that the non homogeneous responsiveness of the screened G08 subclones was due to a lack of clonality. In line with this, further cloning of the most responsive reclone B02 did not further enrich for FOXP3 inducible cells (data not shown). It therefore seemed more likely that some feature of the stimulation conditions determined that not all cells could upregulate FOXP3 or that some of the cells reverted to an unresponsive state due, for example, to genetic instability.

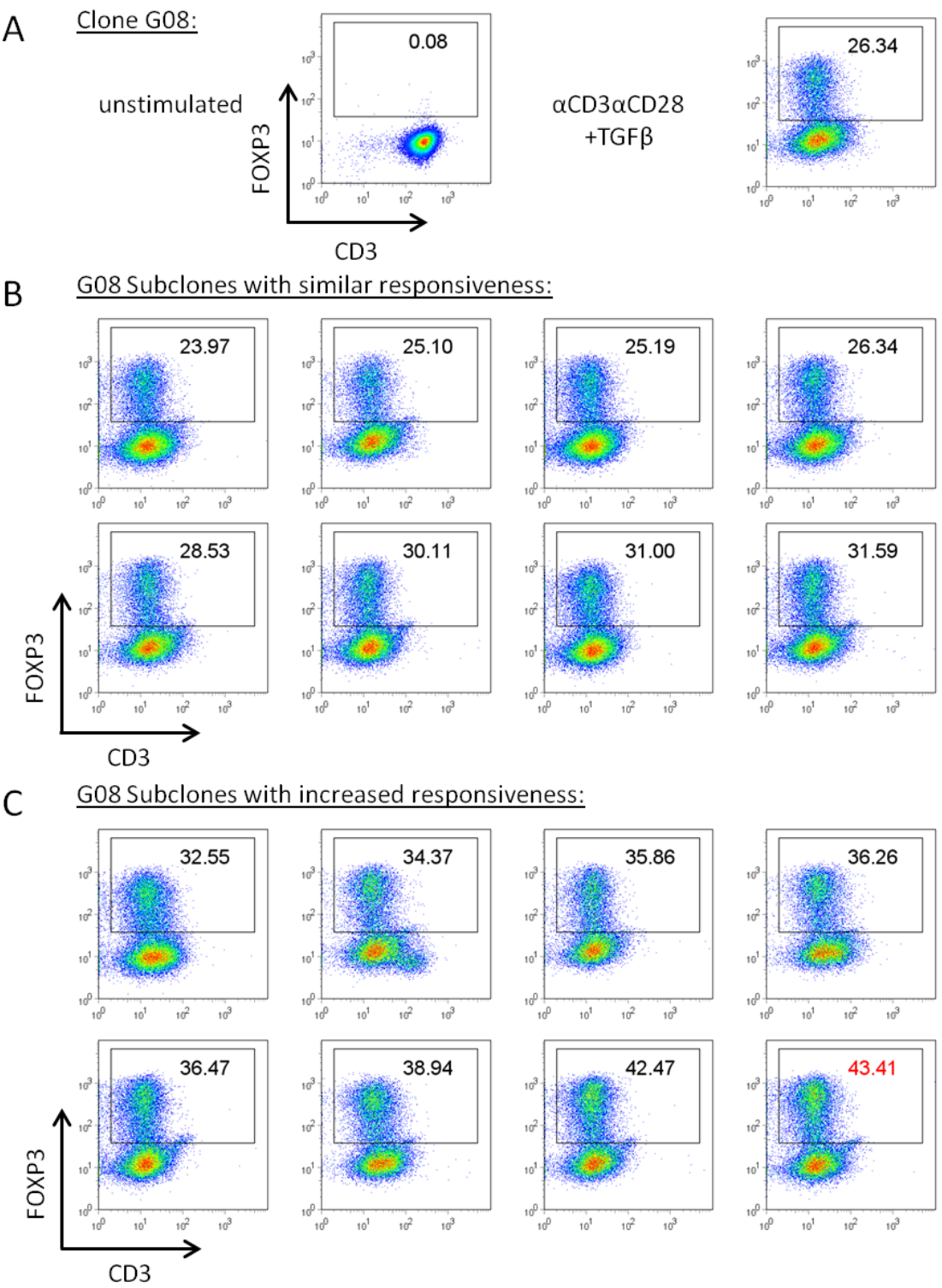


Figure 8. Isolation of a highly FOXP3 inducible subclone B02 by limiting dilution cloning of EL4 clone G08 and screening. FACS analysis of FOXP3 and CD3 expression in EL4 clone G08 (A) and EL4 subclones (B and C) either left unstimulated (A) or stimulated for 4 days in the presence of plate bound αCD3 (KT3, 5µg/ml), soluble αCD28 (37.51, 1µg/ml) and TGFβ (5ng/ml) (A, B and C). Out of the 23 EL4 subclones that were screened, 8 representative clones with similar (B) and increased responsiveness (C) are shown. The percentage of $FOXP3^+$ cells of the most responsive subclone B02 is highlighted in red. Dot plots show live cells. Dead cells were excluded by gating on 7-AAD low cells.

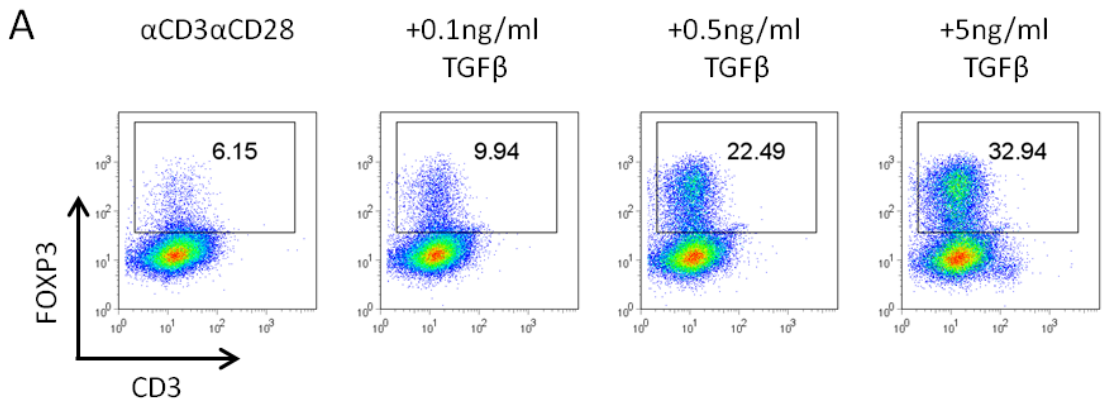
Clearly, the limiting dilution cloning approach enabled me to select clones where the proportion of cells responding with FOXP3 expression increased by 25-fold. The EL4 reclone B02 therefore represent a considerably better model system to study the molecular events underlying the induction of FOXP3 than the parental EL4 line. In fact, experiments in our laboratory using *in vitro* co-cultures of primary TCR-transgenic $CD4^+$ T-cells with antigen primed bone marrow derived dendritic cells in the presence of TGFβ show that induction of FOXP3 is not routinely achievable in more than 50% of the $CD4^+$ cells (data not shown). Therefore the established system provides a good basis for the investigation of cellular signalling in the context of the induction of FOXP3.

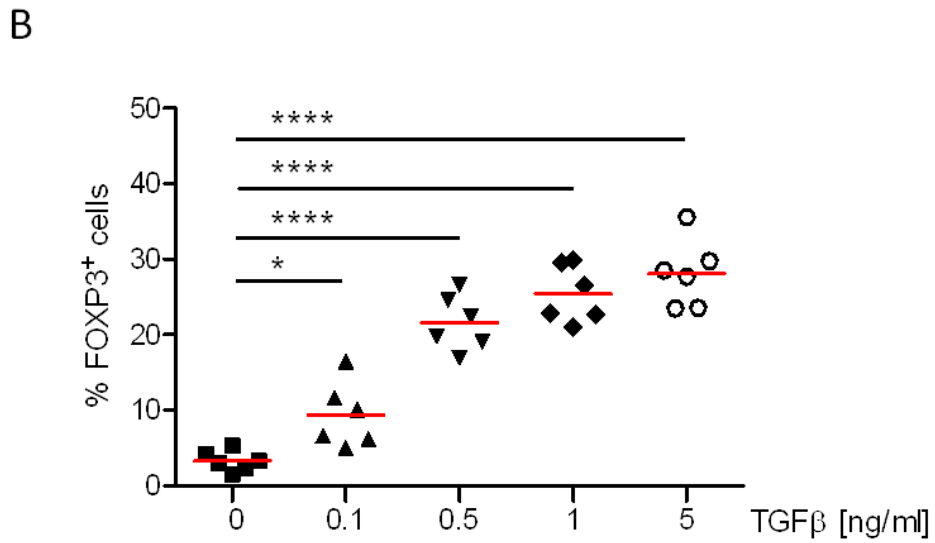
3.2 | FOXP3 induction in EL4.B02 is dependent on TGFβ

Based on the established conditions known to facilitate the induction of FOXP3 in primary $CD4^+$ T- cells, namely TCR and CD28 stimulation in the presence of TGFβ and IL-2 [148, 152-154], the dependency of FOXP3 induction on these factors was tested in the EL4 reclone B02.

Whilst altering one parameter e.g. the concentration of TGFβ, while keeping all other parameters constant, the effect of the test parameter could be tested. As expected, the induction of FOXP3 was highly dependent on TGFβ (Figure 9A). The proportion of $FOXP3^+$ cells increased with higher concentrations of TGFβ and plateaued at around 1ng/ml TGFβ (Figure 9B). Concentrations of 0.5ng/ml TGFβ and above induced a highly statistically significant increase in the proportion of cells responding with FOXP3 induction ($p<0.0001$), whereas concentrations of 0.1ng/ml enhanced the percentage of cells expressing FOXP3 to a lesser extent ($p<0.05$). When comparing the induction

within the different concentrations of TGFβ, a strong positive effect was observed at all higher concentrations of TGFβ with respect to the percentage of $FOXP3^+$ cells induced at 0.1ng/ml TGFβ ($p<0.0001$). However, a statistically significant enhancement in the induction of FOXP3 was only seen between stimulations containing 0.5 and 5ng/ml TGFβ ($p<0.05$: 0.5 versus 5ng/ml, ns: 0.5 versus 1 or 1 versus 5ng/ml), indicating that the FOXP3-inducing effect of TGFβ saturated at around 1ng/ml TGFβ. In line with this observation, increasing concentrations beyond 5ng/ml did not further enhance the induction of FOXP3 (data not shown).





Bonferroni's Multiple Comparison Test	Significant (p<0.05)
0ng/ml TGFβ vs 0.1ng/ml TGFβ	*
0ng/ml TGFβ vs 0.5ng/ml TGFβ	****
0ng/ml TGFβ vs 1ng/ml TGFβ	****
0ng/ml TGFβ vs 5ng/ml TGFβ	****
0.1ng/ml TGFβ vs 0.5ng/ml TGFβ	****
0.1ng/ml TGFβ vs 1ng/ml TGFβ	****
0.1ng/ml TGFβ vs 5ng/ml TGFβ	****
0.5ng/ml TGFβ vs 1ng/ml TGFβ	ns
0.5ng/ml TGFβ vs 5ng/ml TGFβ	*
1ng/ml TGFβ vs 5ng/ml TGFβ	ns

Figure 9. The induction of FOXP3 in EL4.B02 is highly dependent on TGFβ. (A) Representative FACS plots of FOXP3 and CD3 expression in EL4 reclone B02 stimulated at 10^5 cells/well for 4 days in the presence of plate bound αCD3 (KT3, 5µg/ml), soluble αCD28 (37.51, 1µg/ml) and 0, 0.1, 0.5 and 5ng/ml TGFβ. Dot plots show live cells. Dead cells were excluded by gating on 7-AAD low cells. (B) Summary of the percentage of $FOXP3^+$ cells induced in EL4.B02 cells stimulated as described in (A). Graph contains data of 6 independent experiments. The mean is indicated by a red bar. Statistical analysis was performed to compare all stimulation conditions using repeated measure one-way ANOVA with Bonferroni's multiple comparison post test (*p<0.05, ****p<0.0001). The level of significance compared to 0ng/ml TGFβ is indicated in the graph. All results of the statistical analysis are summarized in the table below.

3.3 | Cell density dependent mTORC1 inhibition is associated with upregulation of FOXP3

In addition to the well established FOXP3 inducing stimuli, TCR stimulation and TGFβ, a novel signal, namely inhibition of the mTOR pathway, has recently been described. Sauer et al. demonstrated that inhibition of PI3K/AKT pathway as well as the mTOR pathway can facilitate the induction of FOXP3 [124]. By using a more physiologically relevant system of EAA starvation-induced mTOR inhibition Cobbold et al. emphasized that activation of the mTOR pathway negatively regulates the expression of FOXP3 in an *in vitro* coculture system [127]. These exciting new findings in conjunction with observations made by Hashinaxo et al. that the expression of a constitutively active form of AKT in T-cells can block the induction of FOXP3, and that the effect can be partially reversed by addition of the allosteric mTORC1 inhibitor Rapamycin [126], raised the question whether the mTOR pathway can regulate FOXP3 expression in EL4.B02 cells.

In order to test whether mTORC1 inhibition is capable of facilitating induction of FOXP3, the allosteric mTORC1 inhibitor Rapamycin was added at different concentrations to cells stimulated with the canonical FOXP3 inducing signals. Surprisingly, the addition of the inhibitor did not enhance the induction of FOXP3 under these conditions, irrespective of the amount of Rapamycin (1-100nM) or TGFβ (0-5ng/ml) (Figure 10A: 1ng/ml TGFβ, 5C: 5ng/ml). In contrast to reports in the literature [201], Rapamycin did not reduce the levels of S235/236 phosphorylation of the ribosomal protein S6 (Figure 10B and D), a well-known substrate of the mTORC1 effector S6K1, which was used as a measure of mTORC1 activity in the experiments.

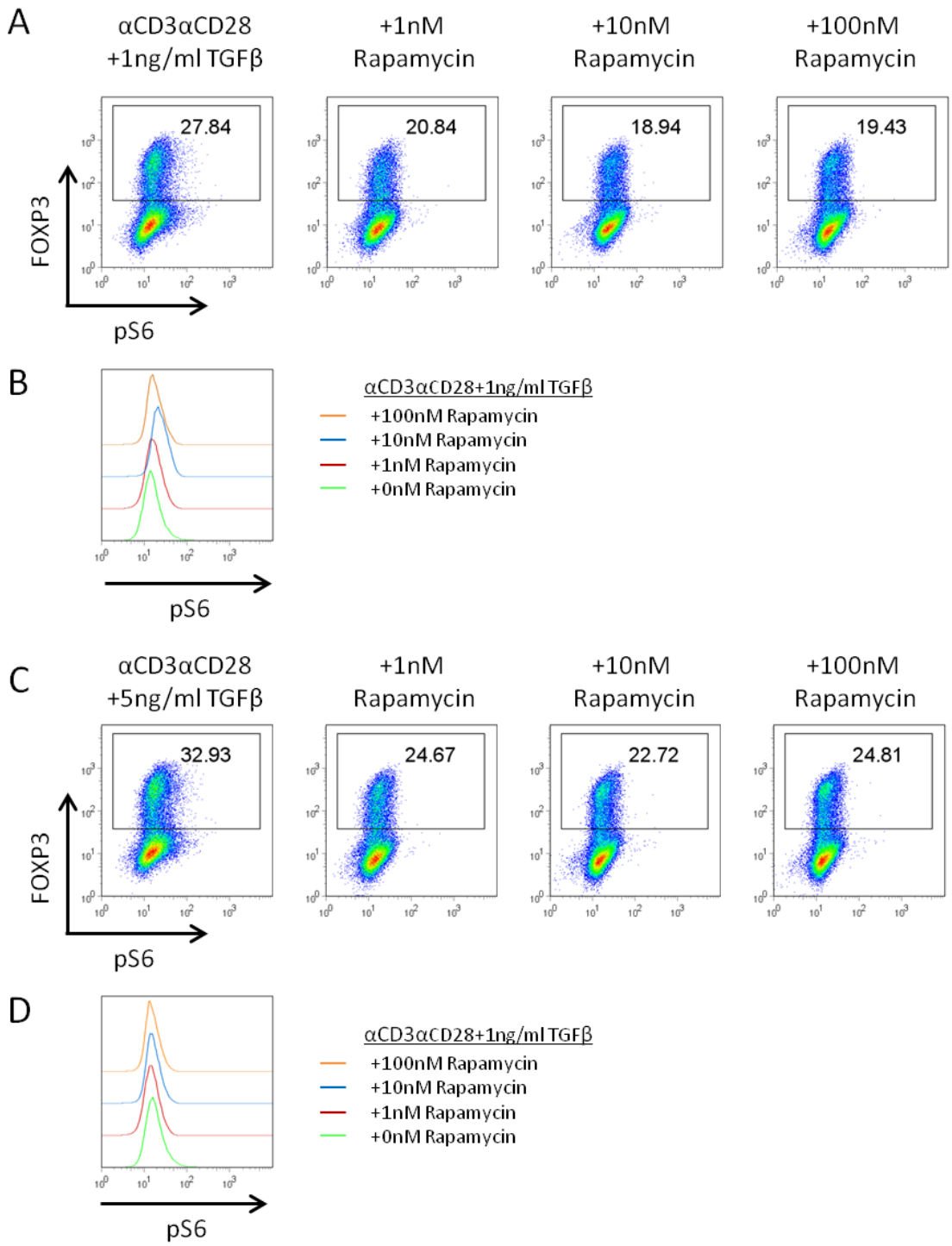


Figure 10. The mTORC1 inhibitor Rapamycin does not facilitate the induction of FOXP3 or reduce mTORC1 activity. EL4.B02 cells were stimulated at 10^5 cells/well for 4 days in the presence of plate bound αCD3 (KT3, 5µg/ml), soluble αCD28 (37.51, 1µg/ml), 1 (A and B) or 5ng/ml TGFβ (C and D) and with or without Rapamycin (1-100nM). Representative FACS plots of FOXP3 expression and S6 phosphorylation (A and C) and histograms of S6 phosphorylation (B and D) are shown. Data is representative of at least two independent experiments. Dot plots and histograms show live cells. Dead cells were excluded by gating on 7-AAD low cells.

mTORC1 has been demonstrated to be sensitive to a wide variety of signals including growth factors, nutrients as well as cellular energy levels [202]. The observation that even without added Rapamycin the cells already exhibited low levels of pS6, led me to consider that under the stimulation conditions used, depletion of nutrients by the cells resulted in "system intrinsic" mTORC1 inhibition. This nutrient-depletion induced inhibition of mTORC1 would render additional mTORC1 inhibition by Rapamycin obsolete.

In order to assess whether "system intrinsic" mTORC1 inhibition was occurring over the duration of the 4 day stimulation, a time course analysis was performed. The cells were stimulated under the previously described conditions, but analyzed in 24h intervals over the 4 day stimulation (Figure 11). The experiment revealed that mTORC1 activity was high 24h into the stimulation, but dropped significantly over the next 48h resulting in minimal residual mTORC1 activity beyond 72h (Figure 11A and B, 72 and 96h: $p<0.05$). The proportion of cells expressing FOXP3 increased over the course of the experiment in a pattern mirroring the declining mTORC1 activity, supporting the hypothesis that "system intrinsic" mTORC1 inhibition occurred and that this inhibition could facilitate the induction of FOXP3 (Figure 11A and C, 72 and 96h: $p<0.001$). A similar pattern of mTORC1 activity and proportion of $FOXP3^+$ cells was observed at all the TGFβ concentrations that were tested (data not shown), signifying that the effect was independent of the concentration TGFβ.

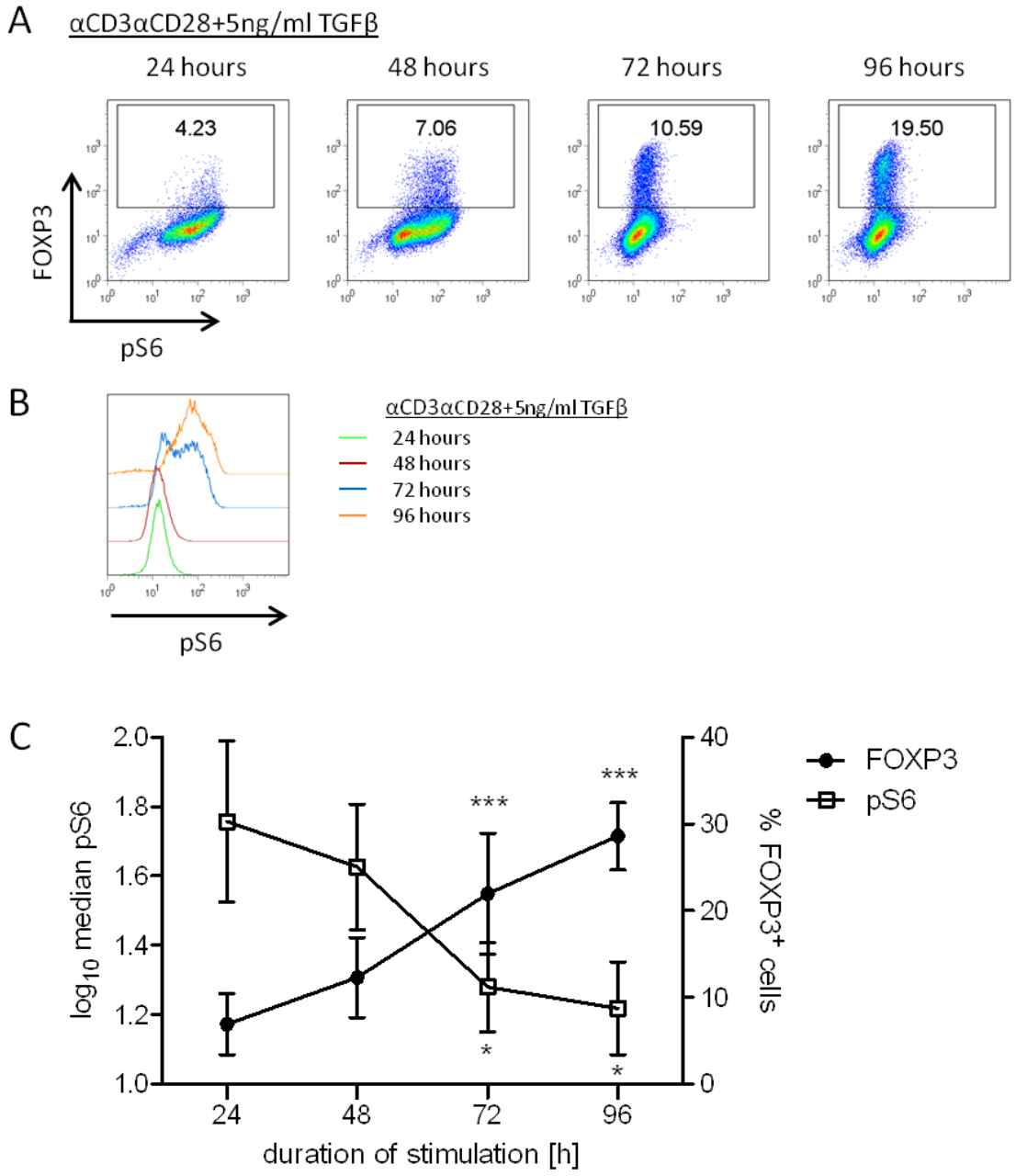


Figure 11. Enhanced FOXP3 induction coincides with decreased TORC1 activity over time. EL4.B02 cells were stimulated at 10^5 cells/well for 1,2,3, and 4 days in the presence of plate bound αCD3 (KT3, 5µg/ml), soluble αCD28 (37.51, 1µg/ml) and 5ng/ml TGFβ. Representative FACS plots of FOXP3 expression and S6 phosphorylation after 24, 48, 72 and 96 hours of stimulation (A) and pS6 histograms (B) are shown. Dot plots and histograms show live cells. Dead cells were excluded by gating on 7-AAD low cells. (C) Summary of experiments described in (A). Graph contains data of 4 (FOXP3) and 3 (pS6) independent experiments. The mean is indicated by a filled circle for the percentage of $FOXP3^+$ cells and an empty square for the levels of pS6 respectively. Error bars show the standard deviation. Statistical analysis was performed by comparing the values measured at each stimulation time point to the values detected at 24h using repeated measure one-way ANOVA with Dunnett's post test (*p<0.05, ***p<0.001).

Since the diametrically opposing trend of mTORC1 activity and the percentage of induced FOXP3$^+$ cells observed in the time course experiments is merely a correlation, additional experiments were performed to provide more definite evidence for the hypothesis. Given that the potential to deplete the culture medium of nutrients should decrease proportionally with decreasing cell density, the number of cells stimulated with αCD3 and TGFβ was carefully titrated from 10^5 cells per well (normal conditions) to 10^4 cells per well . Cells stimulated at lower cell density should therefore deplete the medium more slowly, and consequently retain higher mTORC1 activity and exhibit a smaller proportion of FOXP3$^+$ cells at the end of the 4 day stimulation period.

Indeed, the levels of pS6 and therefore mTORC1 activity remained high at lower cell densities and decreased with increasing cell density (Figure 12A). This drop in mTORC1 activity with increasing cell density was concomitant with augmented FOXP3 induction at higher cell densities, providing further evidence for the hypothesis that “system intrinsic” mTORC1 inhibition mediated an enhancement of FOXP3 induction. Similar cell titration experiments in which ¾ of the stimulation medium was replaced daily showed a shift of the pS6 curve towards higher cell densities when compared to cell titrations in which the medium was not replaced (Figure 12C). In addition refreshment of the stimulation medium resulted in a reduced proportion of FOXP3$^+$ cells at higher cell densities, indicating that the delayed mTORC1 inhibition caused by the medium refreshment largely prevented mTORC1 mediated enhancement of the induction of FOXP3. It is however important to note, that despite the daily replacement of the stimulation medium mTORC1 inhibition at higher densities could not be completely avoided. Furthermore it also seemed plausible that refreshment of ¾ of the medium

diluted an endogenous factor that acts on the induction of FOXP3, particularly at high cell density.

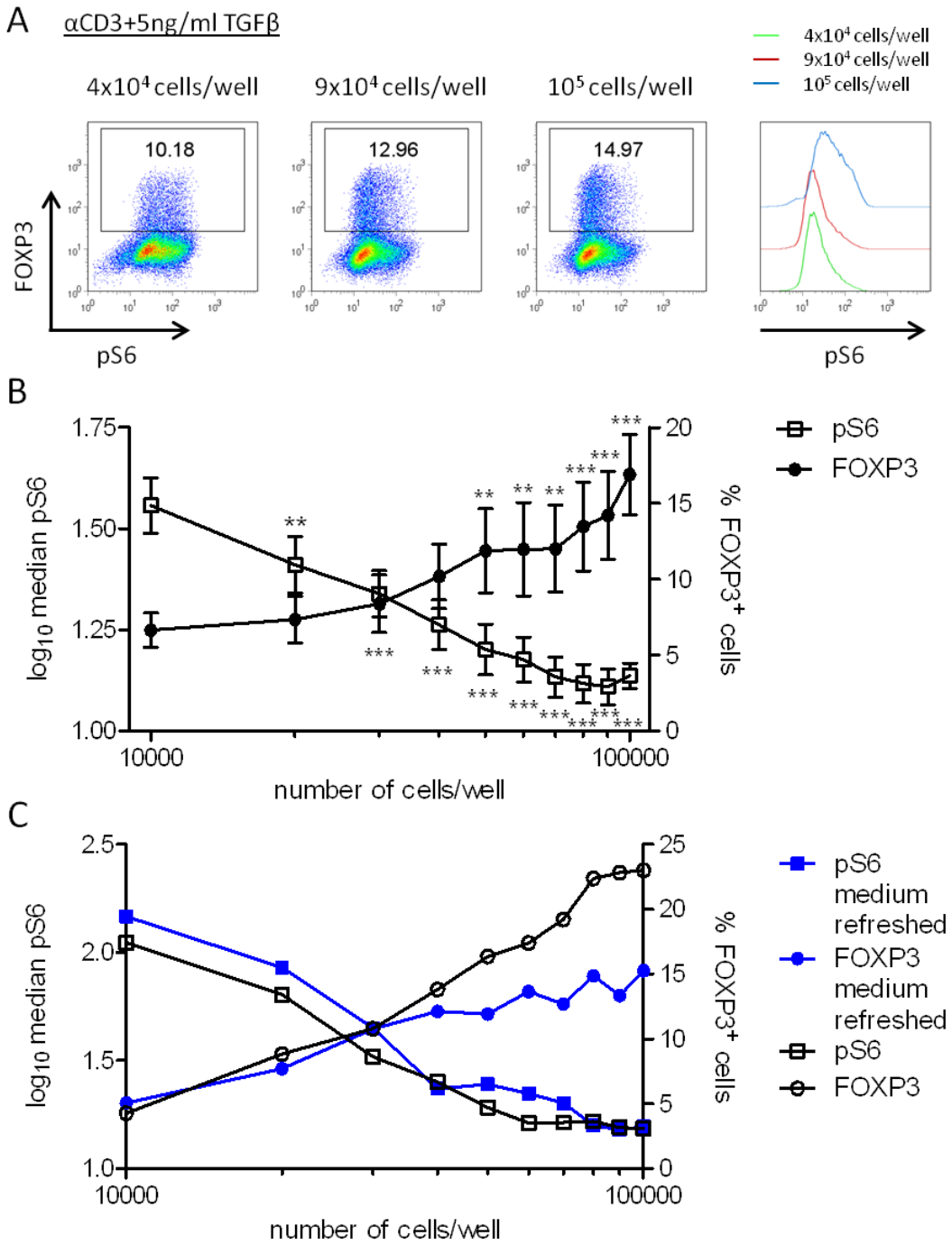


Figure 12. Cell titration reveals cell density dependent TORC1 inhibition and FOXP3 induction. EL4.B02 cells were stimulated at the indicated cell density for 4 days in the presence of plate bound αCD3 and 5ng/ml TGFβ. (A) Representative FACS plots of FOXP3 expression and pS6 histogram at selected cell densities are shown (live cells). (B) Summary of experiments described in (A). Graph contains data of 9 independent experiments. The mean is indicated by a filled circle for the percentage of FOXP3$^+$ cells and an empty square for the levels of pS6 respectively. Error bars show the standard error. Statistical analysis was performed by comparing the values measured at each stimulation time point to the values detected at 10^4 cells/well using repeated measure one-way ANOVA with Dunnett's post test (**p<0.01, ***p<0.001). (C) Cells were stimulated as in (A and B), but ¾ of stimulation medium was refreshed daily. One representative experiment of 5 is shown. Symbols used as in (B). Blue lines and symbols show the values detected in stimulations in which the medium was refreshed.

Based on the kinetics of mTORC1 activity and FOXP3 induction observed in the cell titration and time course studies, the stimulation conditions were adapted. Since most of the FOXP3 induction occurred within the first 72h, the stimulation period was reduced from 4 to 3 days. In combination with a 10-fold reduction of the number of cells that were stimulated per well this was thought to prevent "system intrinsic" mTORC1 inhibition and would therefore allow testing of the role of mTORC1 in regulating FOXP3 in future experiments.

Indeed, the stimulation of cells at low (10^4 cells per well) and high (10^5 cells per well) densities confirmed that the induction of FOXP3 was enhanced and mTORC1 activity reduced at high densities (Figure 13). The density dependent effect on the induction of FOXP3 was only observed in the presence of TGFβ (0ng/ml: $p>0.05$, 0.5ng/ml: $p<0.01$, 1 and 5ng/ml $p<0.0001$), indicating that the signal induced during high density stimulation (possibly mTORC1 inhibition) acts on TGFβ signalling pathways to facilitate the induction. Conversely, mTORC1 activity was significantly higher even in the absence of TGFβ at lower density ($p<0.0001$), demonstrating that the effect of TGFβ on pS6 levels was negligible.

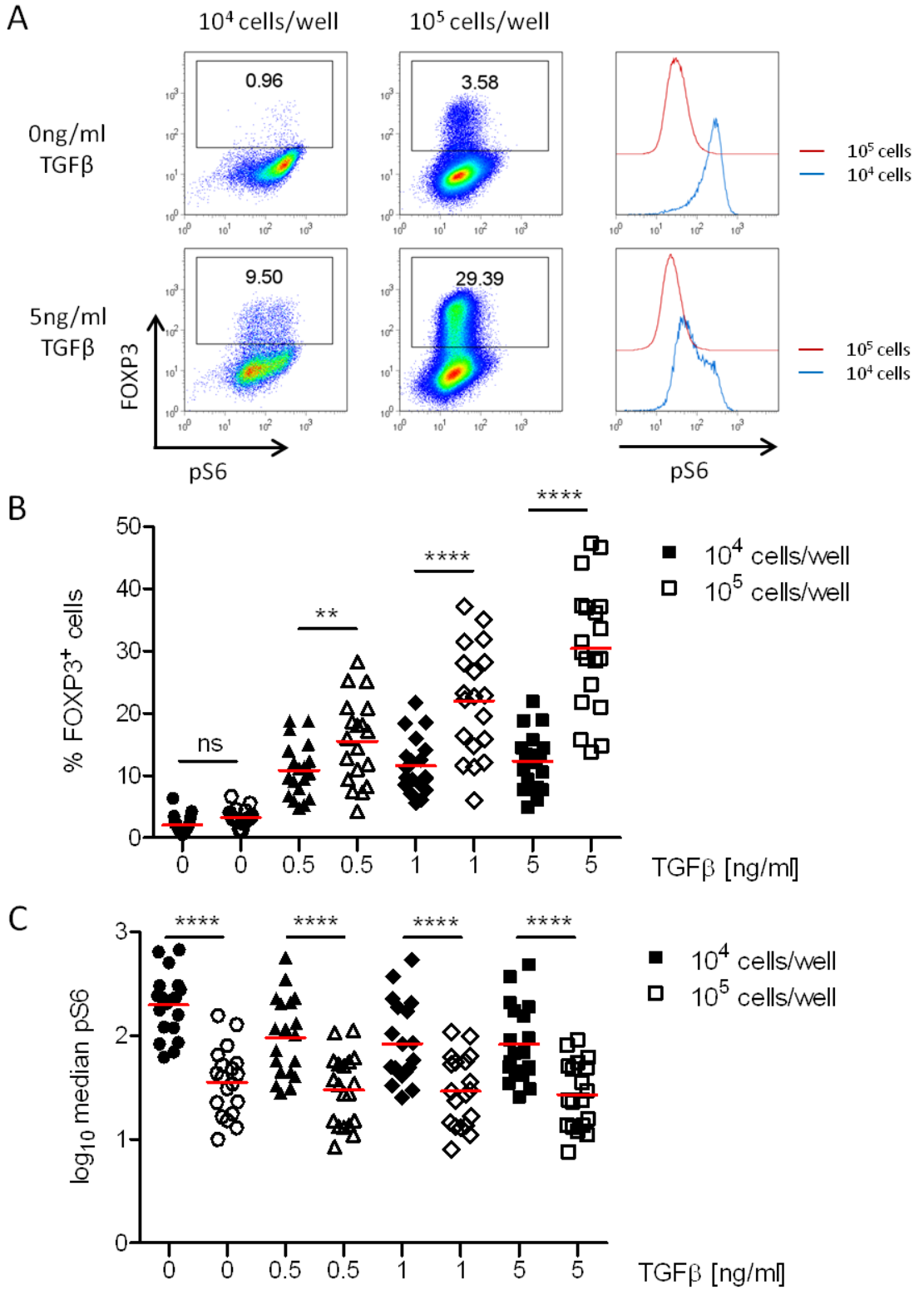


Figure 13. Stimulation at high cell density enhances FOXP3 induction and reduces TORC1 activity. EL4.B02 cells were stimulated at the indicated cell density for 3 days with αCD3 and the indicated TGFβ concentrations (A) Representative FACS plots of FOXP3 expression and pS6 levels and pS6 histogram of live cells (7-AAD low) are shown. (B and C) Summary of the percentage of FOXP3$^+$ cells and pS6 levels measured in the experiments described in (A). Graphs contain data of 19 independent experiments. The mean is indicated by a red bar. Filled symbols: low cell density, empty symbols: high cell density. Statistical analysis was performed by comparing high versus low density stimulation at each condition using repeated measure one-way ANOVA with Bonferroni's multiple comparison post test (**p<0.01, ****p<0.001).

A similar effect with respect to the FACS data analysing FOXP3 expression was observed on the levels of *FOXP3* transcripts measured by qPCR (Figure 14A). In comparison to low density stimulation, high density stimulation in the presence of TGFβ resulted in a significant increase of *FOXP3* mRNA levels at all time points (12h: $p<0.01$, 24h: $p<0.001$, 36h: $p<0.0001$, 48h: $p<0.001$). It is important to note that at least at the early time points, this increase in *Foxp3* mRNA could not be explained by "system intrinsic" mTORC1 inhibition. Therefore it seemed likely that an endogenous factor that accumulated to higher concentrations in high cell density stimulations, enhanced the induction of FOXP3. The nature of this factor will be subject of further investigation. In contrast to the results obtained by FACS, high density stimulation in the absence of TGFβ also led to a significant increase in *FOXP3* transcripts at 24 and 48h (24h: $p<0.05$, 48h: $p<0.01$), but not at 12 and 36h ($p>0.05$). The apparent discrepancy between FACS and qPCR results in the absence of TGFβ could be explained by the higher sensitivity of the qPCR method compared to the FACS analysis. An effect of autocrine TGFβ production seemed unlikely since qPCR results of cultures stimulated at high densities with and without neutralizing αTGFβ did not show significant differences (Figure 14B). However, it could not be ruled out that autocrine TGFβ signalling was efficiently blocked by the addition of the neutralizing antibody.

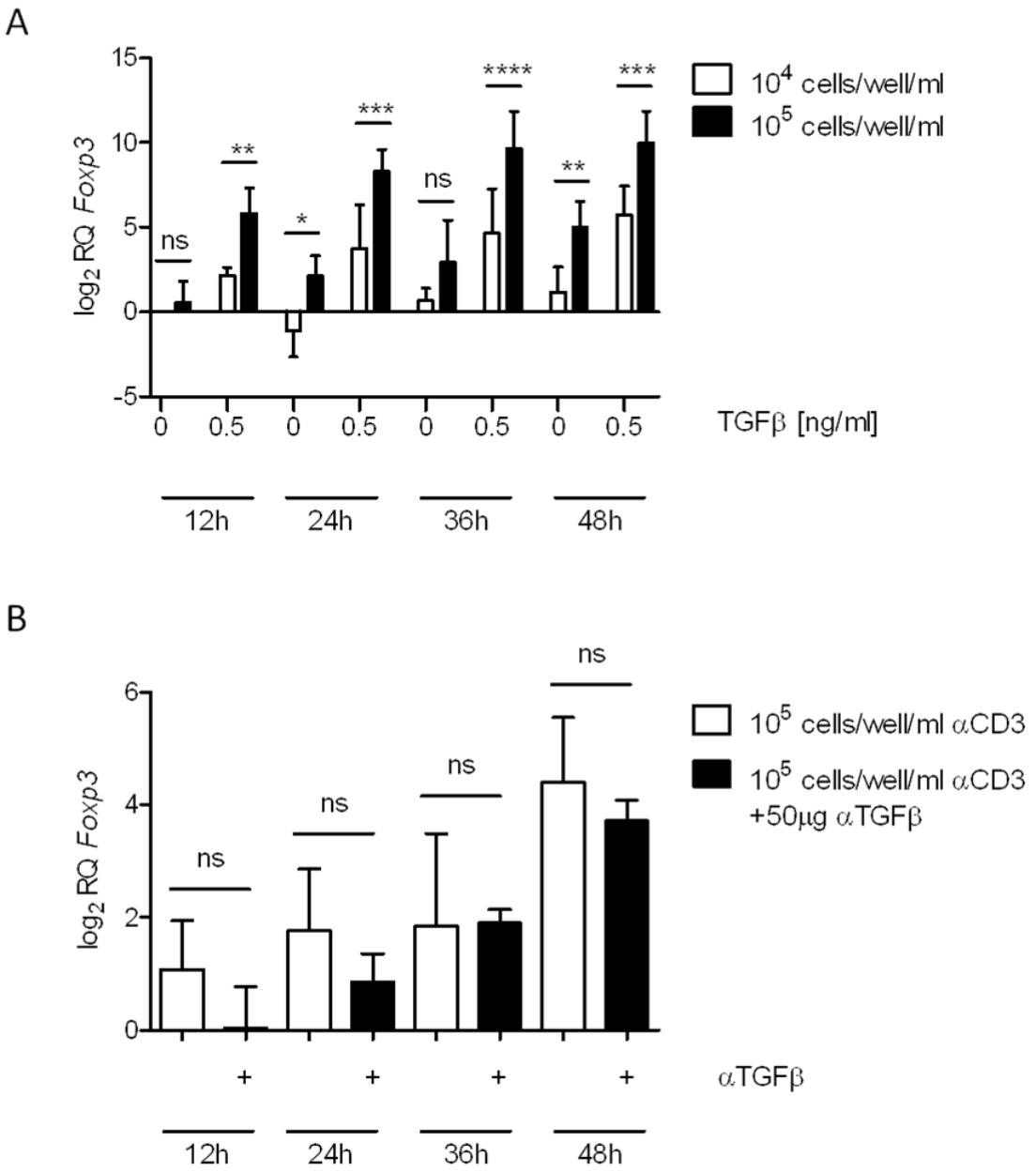


Figure 14. Stimulation at high density enhances *Foxp3* transcription. (A) Real-time PCR analysis *Foxp3* expression in cDNA samples prepared from EL4.B02 stimulated for the indicated durations and at cell densities and TGFβ concentrations. Data was normalized to *Hprt1* cDNA levels and is presented relative to cells stimulated at low density (10^4 cells/well/ml) with αCD3 for 12 hours. Mean and standard deviation of 4 biological replicates is presented. (B) Real-time PCR analysis *Foxp3* expression in cDNA samples prepared from EL4.B02 stimulated for the indicated durations at 10^5 cells/well/ml with αCD3 in the presence or absence of 50µg/ml αTGFβ antibody (1D11). Data was normalized to *Hprt1* cDNA levels and is presented relative to cells stimulated at low density (10^4 cells/well/ml) with αCD3 for 12 hours. Mean and standard deviation of 3 biological replicates is presented. Statistical analysis was performed to compare low cell density versus high cell density samples (A) and samples at high density with or without αTGFβ antibody (B) using repeated measure one-way ANOVA with Bonferroni's multiple comparison post test (*p<0.05, **p<0.01, ***p<0.001, ****p<0.001).

In summary, both time course and cell titration experiments revealed that stimulation of cells at high densities that were used in previous experiments resulted in mTORC1 inhibition and enhanced FOXP3 induction when compared to early time points (time course) or lower cell densities. This effect was likely to be due to cellular depletion of the stimulation medium of essential nutrients leading to mTORC1 inhibition, since daily refreshment of stimulation medium lowered mTORC1 inhibition and reduced FOXP3 induction at high cell densities. However, at this point the secretion of a putative soluble factor into the stimulation medium that enhances the induction of FOXP3 and/or reduces mTORC1 activity by the cells cannot be ruled out. A role for autocrine secretion and action of TGFβ seemed unlikely since the enhancement effect on FOXP3 was seen even when saturating concentrations of exogenous TGFβ were added to the stimulated cultures. Selective neutralization of putative endogenous versus exogenous TGFβ in the culture was technically not feasible. However, it would be useful to determine the levels of endogenously produced active TGFβ, in order to decisively rule out any involvement. Another aspect not considered in stimulations at different densities, was the obvious difference in the contact between cells. This will be addressed in the following section.

3.4 | Stimulation of cells in conditioned medium and in transwell conditions recapitulates the enhanced induction of FOXP3 under high cell density stimulation

Despite the significant effect of cell density on mTORC1 activity and FOXP3 induction that was seen in the cell titration experiments, the question whether cell contact dependent mechanisms are causative for the enhanced FOXP3 induction and/or mTORC1 inhibition observed at high cell densities remained. To address this issue, medium of cells left untreated or stimulated at high density was collected and used for stimulations of cells at low densities. If the stimulation medium was able to enhance the induction of FOXP3 in cells stimulated at low density compared to cells stimulated in fresh culture medium, this would provide further evidence that either depletion of nutrients or secretion of an unknown factor into the stimulation medium (or both) and not cell contact dependent mechanisms were responsible for the increased FOXP3 induction at high density.

Stimulation of cells in 95% conditioned stimulation medium of αCD3 and αCD3+0.1ng/ml stimulated cells (+/- TGFβ), resulted in significantly enhanced FOXP3 induction compared to cell stimulated in fresh medium. This increased induction was only seen when TGFβ was present (Figure 15, $p<0.01$). This experiment further underscored the hypothesis that depletion of the medium or secretion of a soluble factor capable of enhancing FOXP3 and not cell contact dependent mechanism are responsible for the observed effect.

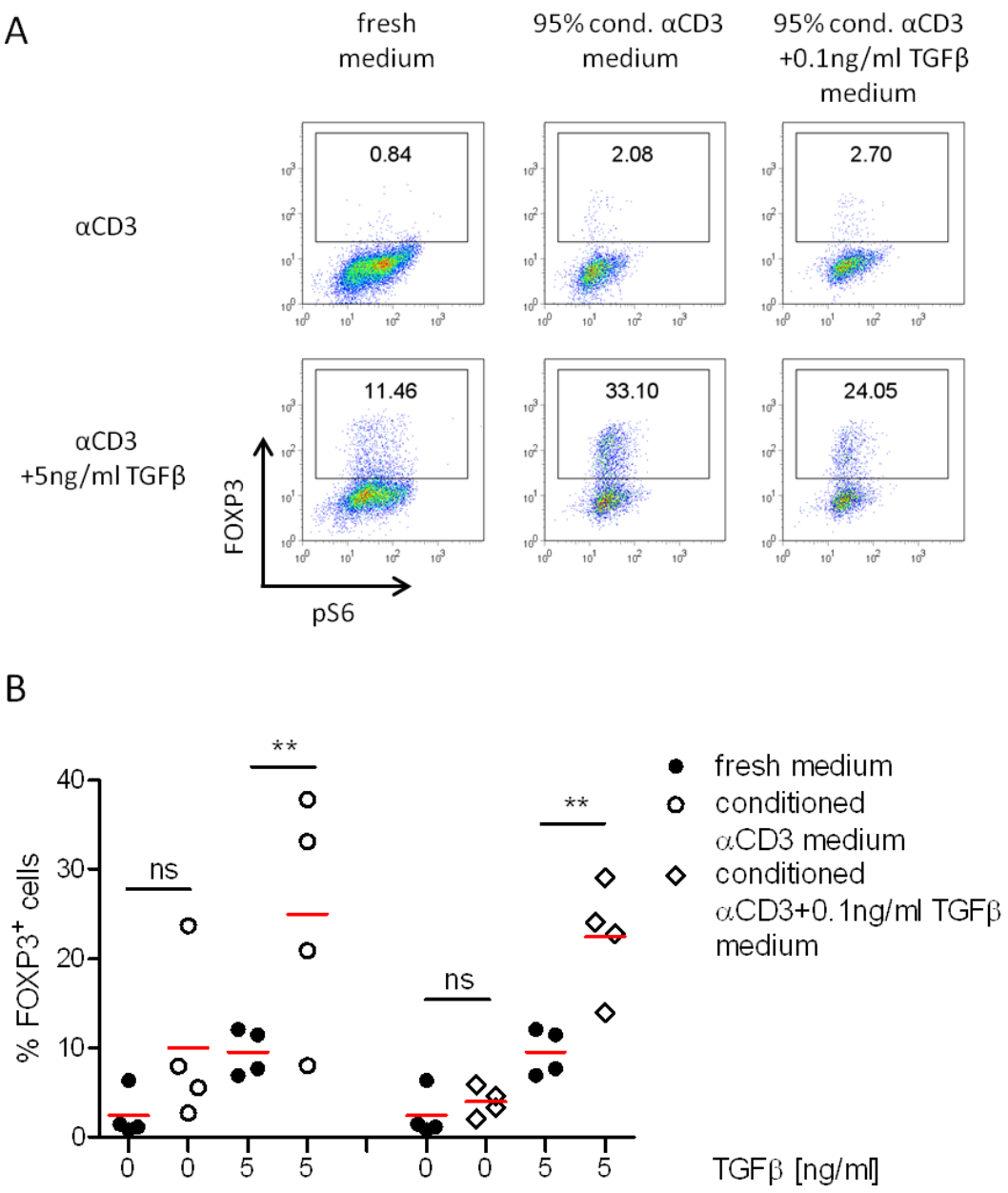


Figure 15. Stimulation in conditioned medium enhances the induction of FOXP3. EL4.B02 cells were stimulated at 10^4 cells/well/ml for 3 days in fresh medium or 95% conditioned medium (from stimulations at 10^5 cells/well/ml with αCD3 or αCD3+0.1ng/ml TGFβ) with αCD3 and the indicated TGFβ concentrations (A) Representative FACS plots of FOXP3 expression and pS6 levels are shown. Dot plots show live cells. Dead cells were excluded by gating on 7-AAD low cells. (B) Summary of the percentage of $FOXP3^+$ cells measured in the experiments described in (A). Graphs contain data of 4 independent experiments. The mean is indicated by a red bar. Statistical analysis was performed by comparing the percentage of $FOXP3^+$ cells detected in fresh medium at a given concentration of TGFβ versus the percentage measured in conditioned medium using repeated measure one-way ANOVA with Bonferroni's multiple comparison post test (**p<0.01).

An additional way of demonstrating that the medium and not cell contact was responsible for the observed enhancement of FOXP3 induction and mTORC1 inhibition at high densities was to make use of transwell tissue culture plates. Cells were stimulated at the bottom of the well, additional cells were seeded in the transwell insert that physically separated both cell populations.

Stimulation of cells at low density in the absence or presence of 10^4 or 10^5 cells in the transwell insert, resulted in a marked and significant increase in the proportion of $FOXP3^+$ cells only when 10^5 cells were seeded in the transwell insert (Figure 16, $p<0.01$). The induction in the presence of 10^4 cells was elevated slightly, but did not reach statistical significance. The activity of mTORC1 was analyzed in two of the experiments and showed the opposite trend compared to the percentage of $FOXP3^+$ cells. A noticeable drop in pS6 staining was only observed when 10^5 cells were placed in the transwell insert. Possibly, only the larger number of cells was able to deplete the medium of nutrients to a degree sufficient to inhibit mTORC1 and thereby enable enhanced FOXP3 induction. However, none of these experiments rule out that factors secreted by the cells were causing the mTORC1 inhibition or the increased FOXP3 induction.

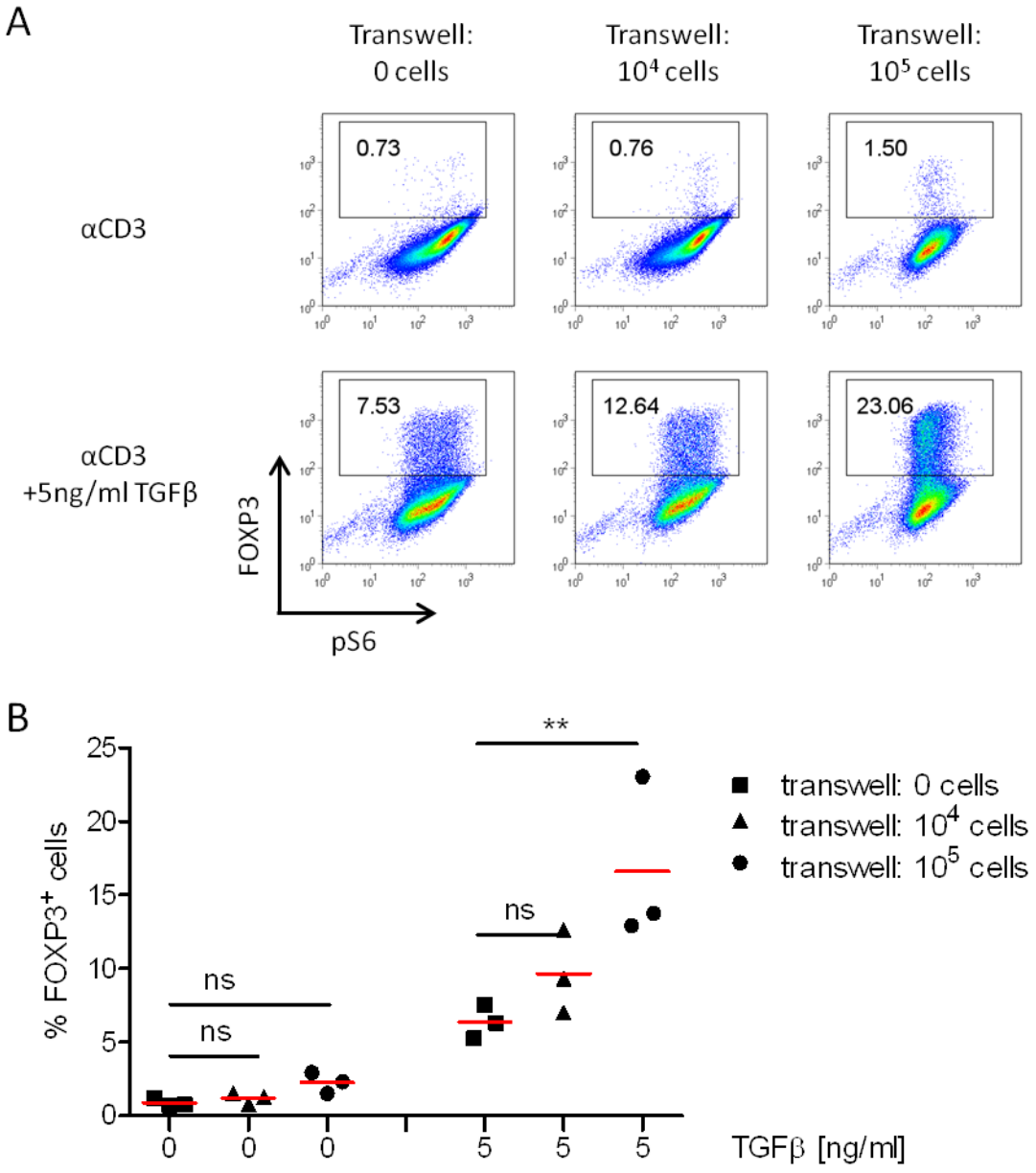


Figure 16. Stimulation of cells at low density with TGFβ and in the presence of high cell numbers enhances the induction of FOXP3. EL4.B02 cells were stimulated at 10^4 cells/well/ml for 3 days with αCD3 and the indicated TGFβ concentrations in tissue culture plates with transwell inserts. Inserts were left empty, 10^4 or 10^5 cells added. (A) Representative FACS plots of FOXP3 expression and pS6 levels are shown. Dot plots and histograms show live cells. Dead cells were excluded by gating on 7-AAD low cells. (B) Summary of the percentage of FOXP3$^+$ cells measured in the experiments described in (A). Graphs contain data of 3 independent experiments. The mean is indicated by a red bar. Statistical analysis was performed by comparing the percentage of FOXP3$^+$ cells detected samples with empty transwell insert at a given concentration of TGFβ versus the percentage measured in samples with 10^4 or 10^5 cells in the transwell using repeated measure one-way ANOVA with Bonferroni's multiple comparison post test (**p<0.01).

3.5 | Stimulation of cells under limiting concentrations of EAA facilitates the induction of FOXP3

Having established that stimulation of EL4.B02 cells at lower cell density avoided "system intrinsic" mTORC1 inhibition, a more direct approach was devised in order to test whether nutrient deprivation, particularly starvation of EAA, can facilitate the induction of FOXP3 via mTORC1 inhibition. By artificially limiting the concentrations of all EAAs using custom made RPMI devoid of EAAs and dialysed FCS, the effect of EAA starvation on mTORC1 activity and FOXP3 induction was tested. Preliminary experiments in which the concentration of EAA was titrated by supplementing 0% EAA medium with varying volumes of normal culture medium indicated that the optimal conditions with respect to FOXP3 induction were achieved when the concentration of EAA was limited to 5% of the concentration in normal culture medium (data not shown). By comparing the proportion of $FOXP3^+$ cells and the levels of pS6 detected by FACS at the end of the stimulation with those values obtained from cells stimulated in medium containing 100% EAA, the effect of EAA starvation on the induction of FOXP3 and mTORC1 activity could be assessed.

Stimulation of cells under limiting EAA resulted in highly significant decrease in pS6 levels especially in the absence of TGFβ (Figure 17C, $p<0.0001$). The drop in pS6 levels was less pronounced in cultures containing TGFβ. Nonetheless mTORC1 activity was significantly downregulated by limiting the amounts of EAA to 5% of the normal concentrations at all TGFβ concentrations analyzed ($p<0.01$). The reduced size of the effect on pS6 levels in the presence of TGFβ could be explained by the fact that addition of TGFβ itself, even in regular culture medium, reduced the MFI of pS6. Closer

analysis of the reduction of pS6 levels by TGFβ showed however that TGFβ, in contrast to EAA starvation, did not uniformly inhibit the phosphorylation of the ribosomal protein, but rather reduced the levels of a subpopulation (Figure 18A, histograms). This might be due to the activation of a negative regulator of the S6K1 pathway rather than signalling through mTORC1. In line with hypothesis TGFβ signalling was demonstrated to lead to the activation of serine/threonine phosphatase PP2A, which in turn associated with S6k1 resulting in its inactivation [203, 204]. Addition of a PP2A inhibitor, okadaic acid, to cells stimulated with TGFβ led to a significant, concentration-dependent increase in the levels of pS6 that almost reached the levels detected in the absence of TGFβ (Figure 18B). In absence evidence in the literature that TGFβ itself regulates mTORC1 activity, it is conceivable that the reduced pS6 levels observed in the presence of TGFβ could well be due to inactivation of S6K1 rather than mTORC1 inhibition.

With respect to the induction of FOXP3, stimulation of cells in limiting concentrations of EAA in the presence of TGFβ led to a highly significant enhancement of the expression of the Treg cell marker (Figure 17B, $p<0.0001$). In fact, the proportion of cells that upregulated FOXP3 under these conditions was comparable to those seen when cells were stimulated at high cell density (Figure 9).

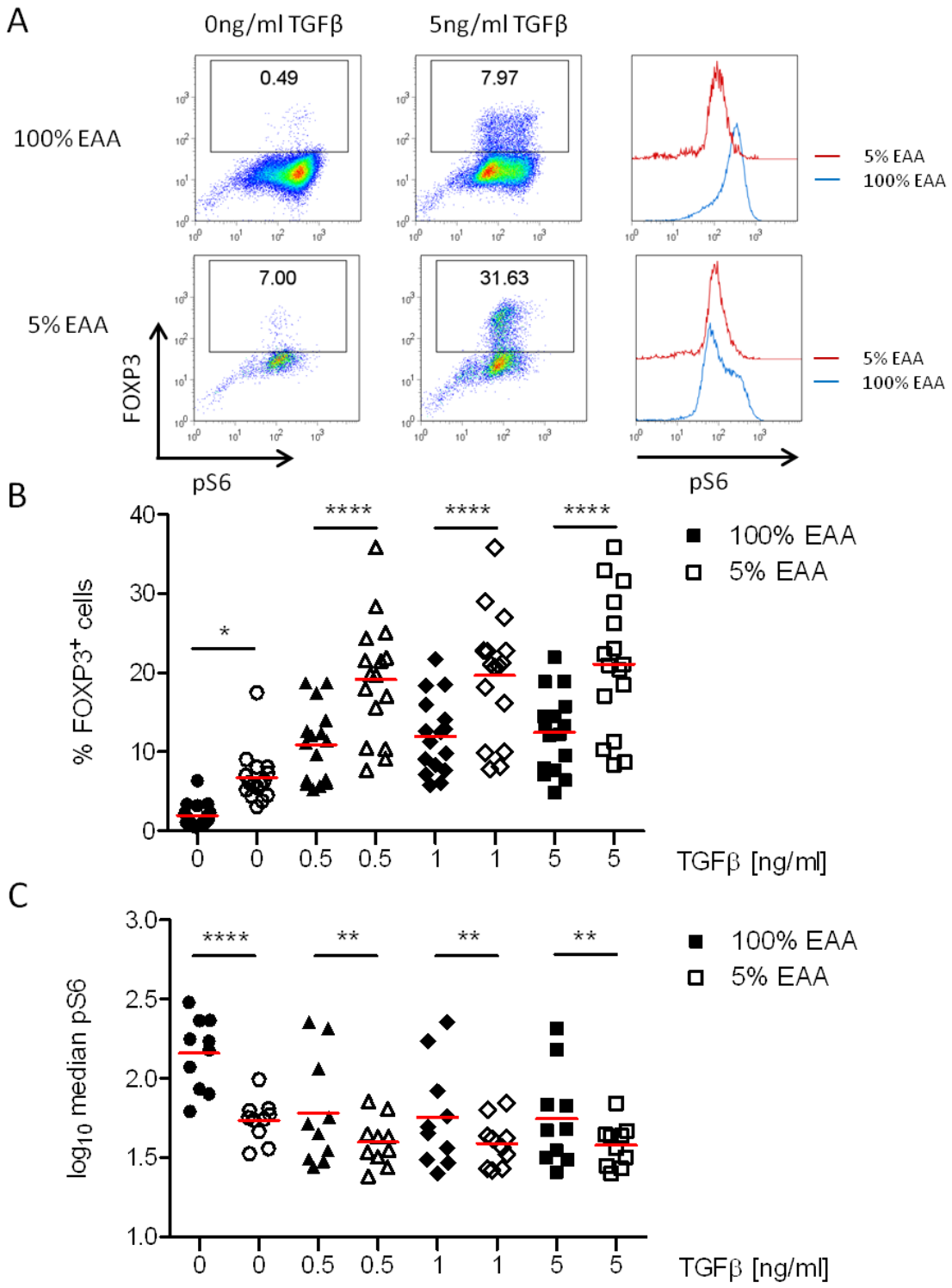


Figure 17. Stimulation of cells under limiting concentrations of EAA enhances the induction of FOXP3. EL4.B02 cells were stimulated at 10^4 cells/well/ml for 3 days with αCD3 and the indicated TGFβ concentrations in medium containing 100%EAA or 5% EAA. (A) Representative FACS plots of FOXP3 expression and pS6 levels and pS6 histograms are shown. Dot plots and histograms show live cells. Dead cells were excluded by gating on 7-AAD low cells. (B and C) Summary of the percentage of $FOXP3^+$ cells and levels of pS6 measured in the experiments described in (A). Graphs contain data of 16 (FOXP3) and 10 (pS6) independent experiments. The mean is indicated by a red bar. Statistical analysis was performed by comparing the percentage of $FOXP3^+$ cells and levels of pS6 of cells stimulated in 100% EAA and 5%EAA using repeated measure one-way ANOVA with Bonferroni's multiple comparison post test (*p<0.05, **p<0.05, ****p<0.0001).

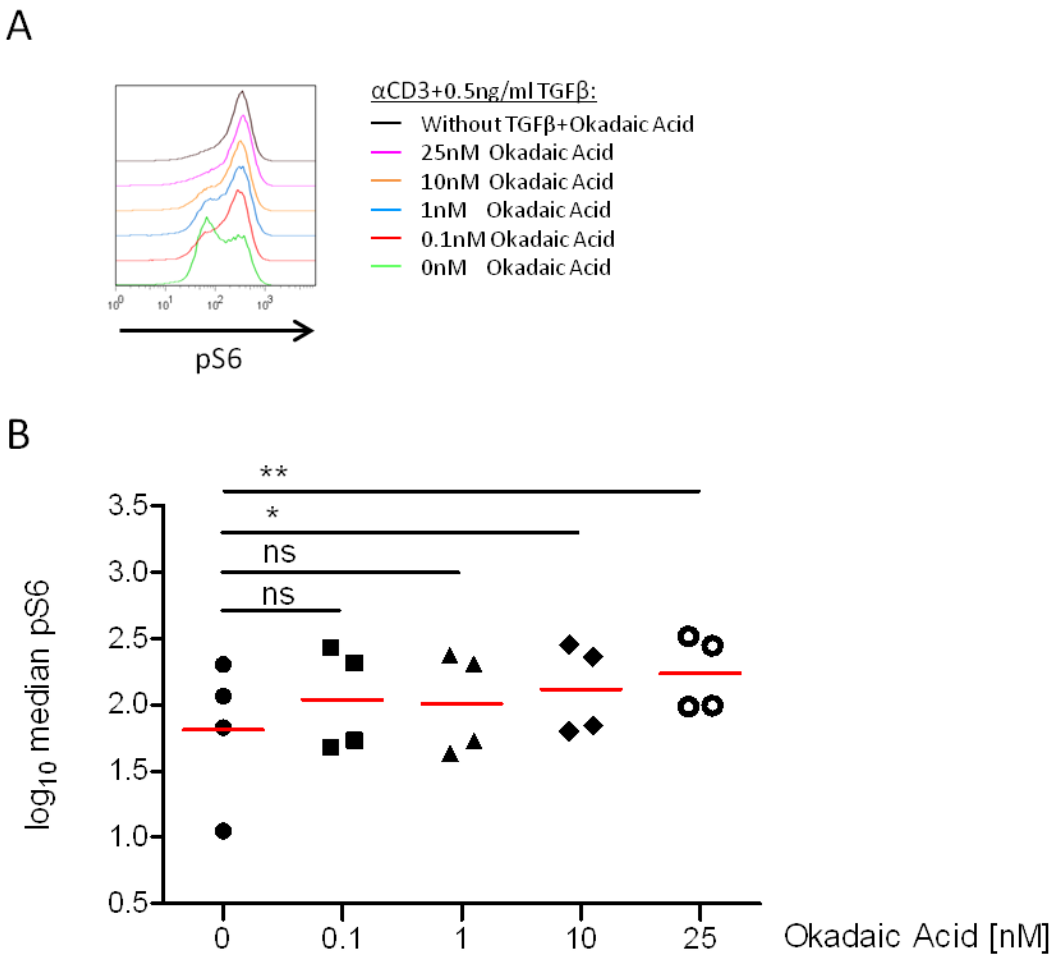


Figure 18. TGFβ reduces the levels of pS6 via activation of PP2A. (A) EL4.B02 cells were stimulated at 10^4 cells/well/ml for 3 days in the presence of plate bound αCD3 (KT3, 5µg/ml), with or without 0.5ng/ml TGFβ and the indicated concentrations of Okadaic Acid. Representative and pS6 histogram are shown. Histograms show live cells. Dead cells were excluded by gating on 7-AAD low cells. (B) Summary of experiments described in (A) (all stimulated with 0.5ng/ml TGFβ). Graph contains data of 4 independent experiments. The mean is indicated by a red bar. Statistical analysis was performed by comparing the values measured in the absence of Okadaic Acid to the values detected at the different Okadaic Acid concentrations using repeated measure one-way ANOVA with Dunnett's post test (*p<0.05, **p<0.01).

Compared to the stimulation of cells at high density under which FOXP3 induction saturated at TGFβ concentrations between 1 and 5ng/ml (Figure 9), maximal induction under EAA starvation conditions was reached at 0.5ng/ml (0.5 vs 5ng/ml: p>0.05). This could be due to the fact that cells stimulated in medium containing 5% EAA inhibited mTORC1 at an earlier time point and therefore experience mTORC1 inhibition for longer periods during the stimulation than those stimulated in regular medium at high

density (Figure 19). This could, in turn, allow for a longer period in which mTORC1 inhibition can enhance the induction of FOXP3. However, it could not be ruled out that the saturation of the TGFβ induced FOXP3 expression at higher concentrations of TGFβ in high density cultures was caused by insufficient engagement of TGFβ receptors by small amounts of TGFβ that were however sufficient for maximal induction at lower cell numbers. Additional support for the notion that EAA starvation provides a stronger signal than high density stimulation with respect to FOXP3 upregulation, was provided by the observation that EAA starvation facilitated the induction of FOXP3 even in the absence of exogenous TGFβ ($p<0.05$). This could indicate that either low levels of TGFβ in the medium were sufficient to synergize with the EAA depletion signal or that a TGFβ independent mechanism was engaged.

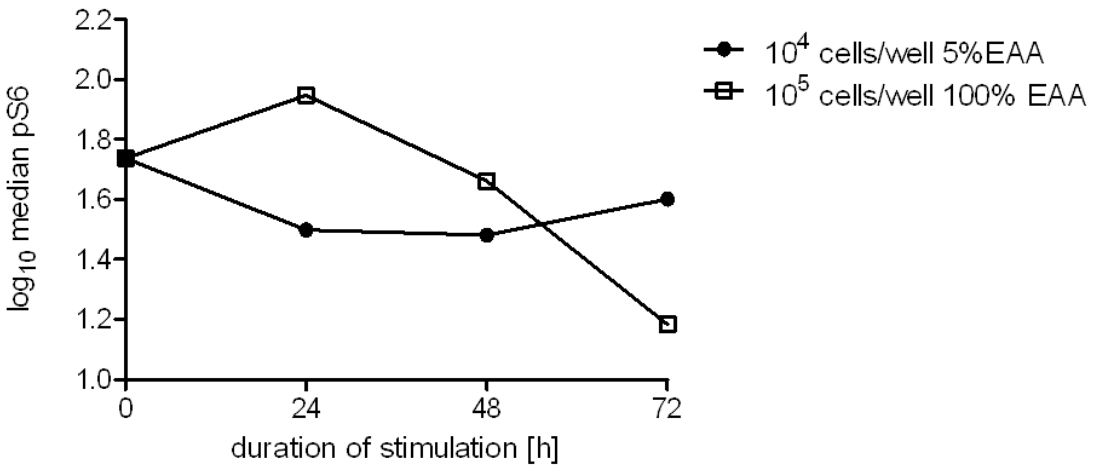


Figure 19. Stimulation of cells under low density and limiting amounts of EAA results in prolonged TORC1 inhibition compared to stimulation at high density and normal levels of EAA. EL4.B02 cells were stimulated at 10^4 cells/well/ml for 1,2,3 days with αCD3 and 5ng/ml TGFβ concentrations in medium containing 5% EAA and at 10^5 cells/well/ml for 1,2,3 days with αCD3 and 5ng/ml TGFβ concentrations in medium containing 100% EAA. Mean of the $\log_{10}$ median of pS6 measured in 2 independent experiments are shown.

The enhancement of FOXP3 expression by EAA depletion in the absence of TGFβ was confirmed by qPCR (Figure 20). EAA starvation significantly enhanced the levels of *Foxp3* transcripts as early as 24h after the stimulation was set up (24 and 36h: $p<0.01$, 48h: $p<0.001$). Although the same effect was observed in the presence of TGFβ, surprisingly the effect only reached statistical significance 36h after the start of the stimulation (36 and 48h: $p<0.001$). The delay in the enhancement in TGFβ treated cells compared to cells stimulated in the absence of TGFβ could be explained by the fact that the induction in the first 24h seems to be predominantly mediated by TGFβ, which could initially mask the effect of EAA depletion. However, it is also conceivable that the EAA starvation effect on the induction of FOXP3 is mediated by early, TGFβ-independent and late, TGFβ-dependent mechanism.

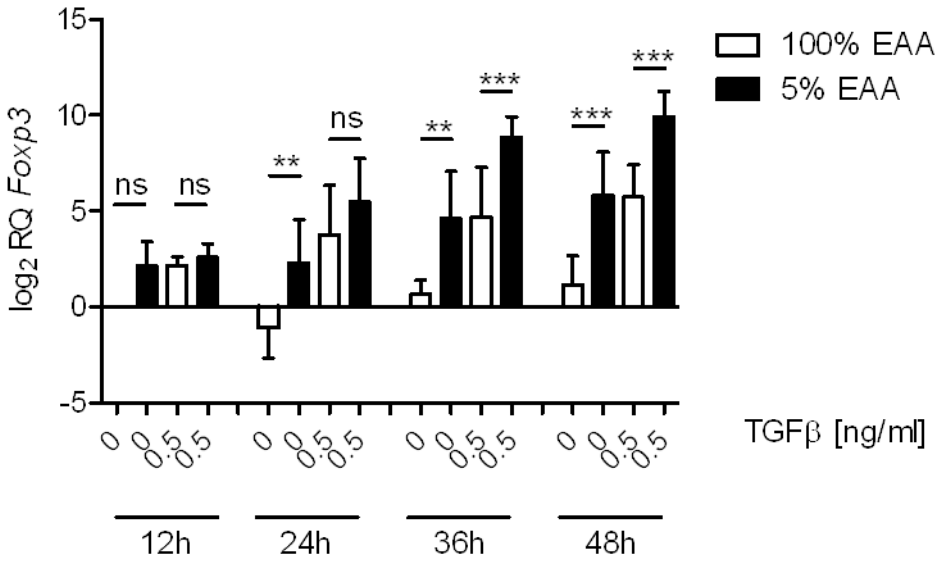


Figure 20. Stimulation in limiting concentrations of EAA enhances *Foxp3* transcription. Real-time PCR analysis *Foxp3* expression in cDNA samples prepared from EL4.B02 stimulated either in 100% EAA or 5% EAA containing medium for the indicated durations and TGFβ concentrations at 10^4 cells/well/ml. Data was normalized to *Hprt1* cDNA levels and is presented relative to cells stimulated at low density (10^4 cells/well/ml) with αCD3 for 12 hours in 100% EAA containing medium. Mean and standard deviation of 4 biological replicates is presented. Statistical analysis was performed to compare samples generated from cells stimulated in 100% and 5% EAA containing medium using repeated measure one-way ANOVA with Bonferroni's multiple comparison post test (**$p<0.01$, ***$p<0.001$).

Further evidence for the hypothesis that stimulation in 5% EAA resulted in a longer lasting mTORC1 inhibition signal and therefore a stronger enhancement of FOXP3 induction, came from experiments in which the induction of FOPX3 at high cell density in regular and 5% EAA containing medium was compared. If EAA starvation was forced to occur earlier during the stimulation by limiting the amount of EAA that were available, the proportion of cells responding with upregulation of FOXP3 should be increased compared to cells stimulated in regular medium.

In line with this hypothesis, stimulation under EAA starvation conditions in the presence of TGFβ resulted in reduced pS6 levels at early time points and therefore a longer mTORC1 inhibition period (Figure 21A). This prolonged inhibition was accompanied with a highly significant enhancement of the induction of FOXP3 under EAA starvation conditions even at high densities (Figure 21B and C, $p<0.0001$). Similarly to experiments analysing the induction under low cell density and high density conditions (Figure 13), the increase in the upregulation of FOXP3 was dependent on TGFβ. The apparent discrepancy of the strictly TGFβ dependent upregulation of FOXP3 under high cell density-EAA starvation conditions on the one hand, and the additional, at least partially TGFβ independent effect observed under conditions of low cell density EAA starvation could be explained by the fact that in the former both populations experienced significant mTORC1 inhibition, whereas in the latter, only the cells stimulated in 5% EAA medium exhibited significantly reduced mTORC1 inhibition. A similar argument could be applied to explain the TGFβ dependency of high versus low cell density stimulation in regular medium. Even though high density stimulation did result in significant mTORC1 inhibition, it is conceivable that the inhibition did not

occur as early in the stimulation as in cells stimulated under limiting EAA conditions therefore resulting in a lesser effect on the induction of FOXP3.

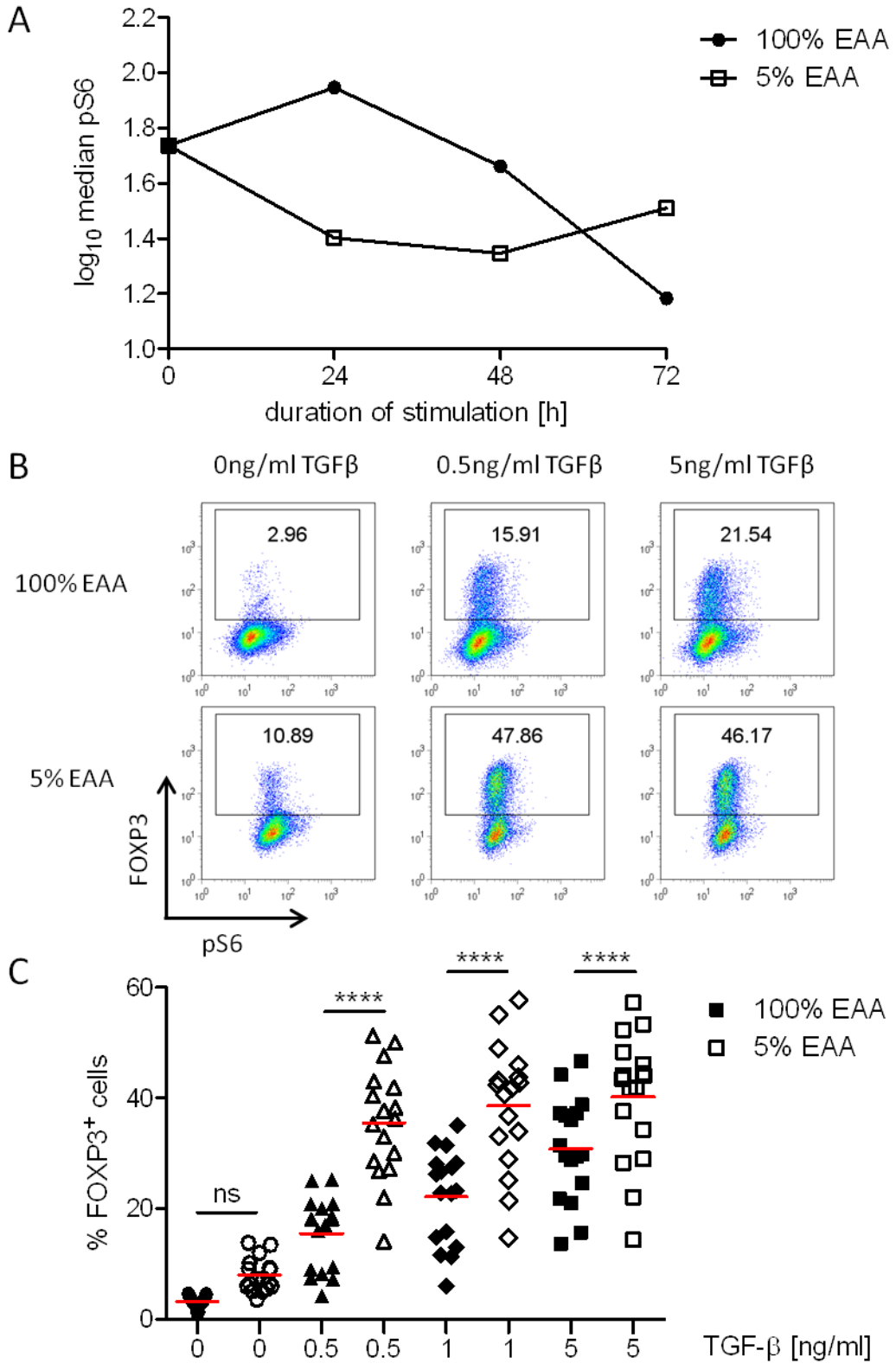


Figure 21. Stimulation in limiting concentrations of EAA results in prolonged TORC1 inhibition and enhances the induction of FOXP3. EL4.B02 cells were stimulated at 10^5 cells/well/ml for 1,2,3 days with αCD3 and the indicated TGFβ concentrations in medium containing 100%EAA or 5% EAA. (A) Mean of the median of pS6 measured in 2 independent experiments at day 1, 2, 3 are shown. (B) Representative FACS plots of FOXP3 expression and pS6 levels at day 3 are shown. (C) Summary of the percentage of $FOXP3^+$ cells and levels of pS6 measured at day3 (A). Graphs contain data of 17 independent experiments. The mean is indicated by a red bar. Statistical analysis was performed by comparing the percentage of $FOXP3^+$ cells stimulated in 100% EAA and 5%EAA medium using repeated measure one-way ANOVA with Bonferroni's multiple comparison post test (****p<0.0001).

Based on the assumption that a larger number of cells can deplete the 5% EAA culture medium of the remaining EAA faster, and would therefore be stimulated under mTORC1 inhibition for longer periods, one would expect an increased induction of FOXP3 at higher cell densities (similar to the cell density effect observed in normal medium). The FACS analysis revealed that at all tested TGFβ concentrations the proportion of induced $FOXP3^+$ cells was significantly greater when cells were stimulated at higher densities (Figure 22A and B, $p<0.0001$). Similar results were obtained at the level of *Foxp3* transcripts in qPCR time course analysis (Figure 22C). Except for the 48h time point, *Foxp3* mRNA levels were significantly higher in cells stimulated at high density in the presence of TGFβ (12h: $p<0.001$, 24h: $p<0.0001$, 36h: $p<0.001$).

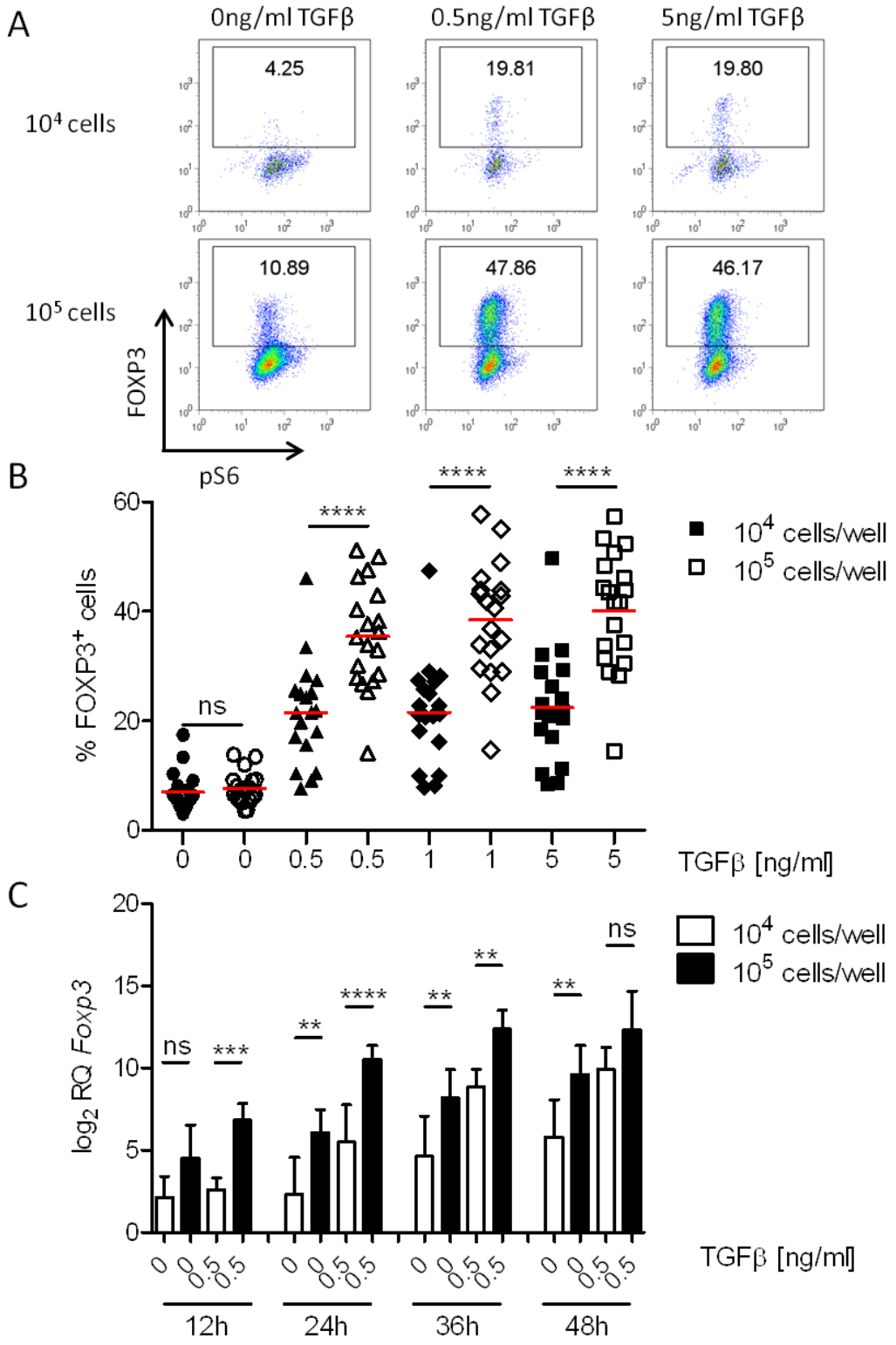


Figure 22. Stimulation at high cell densities in limiting concentrations of EAA enhances the induction of FOXP3. (A and B) EL4.B02 cells were stimulated at 10^4 and 10^5 cells/ml for 3 days with αCD3 and the indicated TGFβ concentrations in 5% EAA medium. (A) Representative FACS plots at day 3 are shown. (B) Summary of the % FOXP3$^+$ cells measured at day 3. Graphs contain data of 19 independent experiments. The mean is indicated by a red bar. (C) Real-time PCR analysis *Foxp3* expression in cDNA samples prepared from EL4.B02 stimulated as indicated in (A) for the indicated durations. Data was normalized to *Hprt1* and is presented relative to cells stimulated at 10^4 cells/ml with αCD3 for 12 hours. Mean and standard deviation of 4 biological replicates is presented. Statistical analysis was performed by comparing the % of FOXP3$^+$ cells (B) and *Foxp3* levels (C) stimulated 10^4 vs 10^5 cells/ml using repeated measure one-way ANOVA with Bonferroni's multiple comparison post test (**p<0.01, ***p<0.001, ****p<0.0001).

In Summary, EAA starvation significantly inhibited mTORC1 activity and enhanced the induction of FOXP3 in the EL4 clone B02. EAA starvation synergized with αCD3 and TGFβ in the induction of FOXP3 at both low and high cell density. Simulation of cells in 5% EAA medium at low density resulted in similar proportion of cells expressing FOXP3 to that where cells were stimulated at high density in medium containing normal levels of EAA, so raising the possibility that enhanced FOXP3 induction in the latter mentioned stimulation conditions might also be a results of EAA depletion. However, the stimulation in the presence of limited amounts of EAA represents a more controlled setting, since depletion of EAA is most likely to occur under these conditions. Although EAA depletion is a likely scenario under high density stimulation conditions, other nutrients such as glucose might also be depleted and thereby contribute to the induction.

Data obtained by FACS and qPCR indicated that EAA depletion in the absence of TGFβ also resulted in a significant enhancement of FOXP3 induction at low density. However, it remains to be determined whether this effect is due to low levels of TGFβ in the serum containing medium or represents a truly TGFβ-independent mechanism. This could be tested using neutralizing antibodies or by measuring active TGFβ concentrations in the supernatant of stimulated cultures. Quantitative PCR results from cultures stimulated at high cell density in the presence or absence of TGFβ neutralizing antibody demonstrated however that, at least in high density stimulation conditions endogenous TGFβ was unlikely to contribute to the enhanced induction of FOXP3 in the absence of exogenous TGFβ. Furthermore, the qPCR results indicated that both the "system intrinsic" as well as the EAA starvation induced enhancement effect at protein level were a result of increase *Foxp3* transcription. Although, EAA starvation resulted in

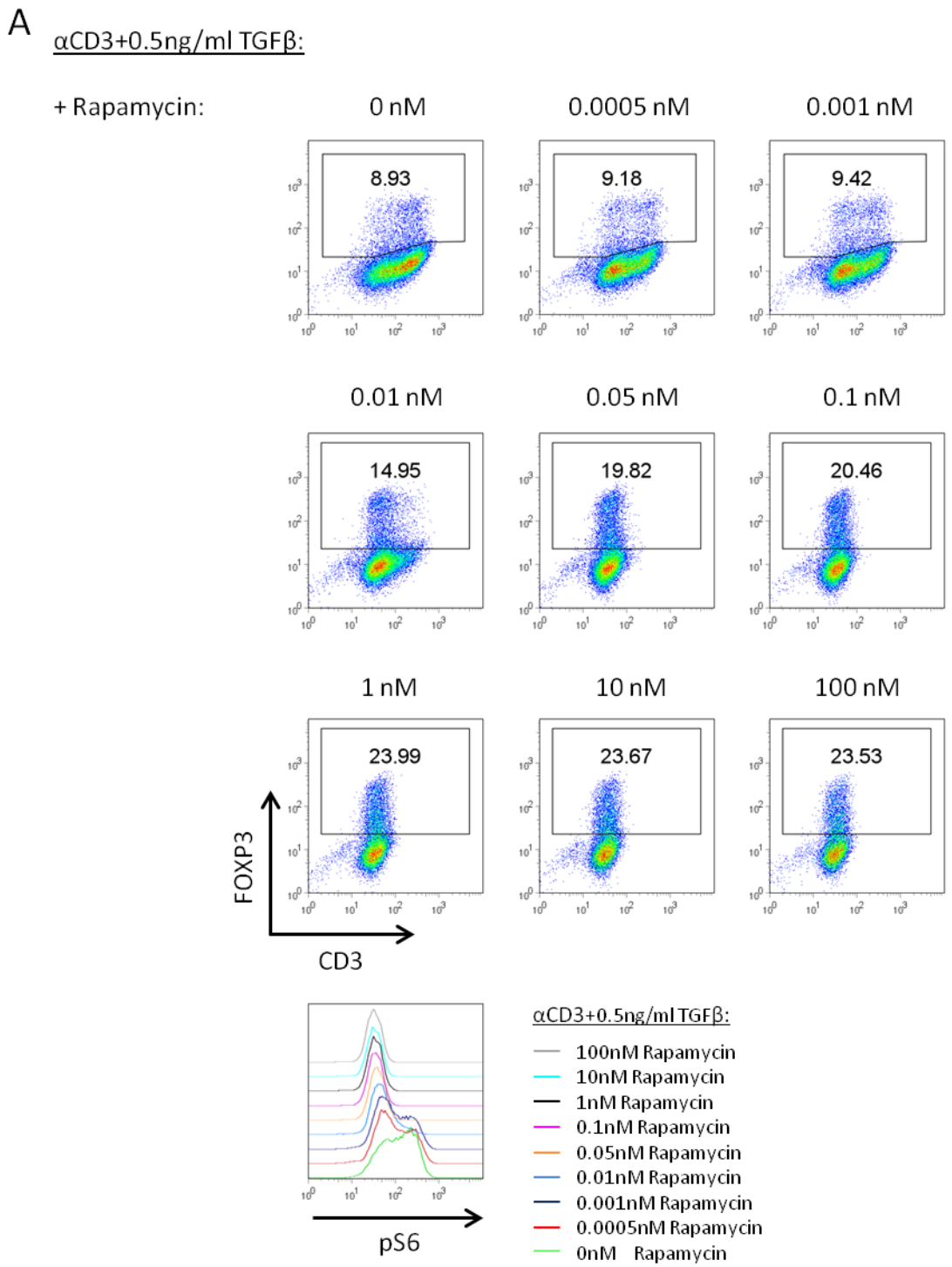
a significant increase in cell death at the end of the stimulation period, at least at the early time points that showed significantly elevated levels of *Foxp3* mRNA, there was no detectable difference in the survival rate of the cells (data not shown). Nevertheless, a partial contribution of preferential survival of FOXP3$^+$ cells to the increase in the proportion of FOXP3$^+$ cells at the end of the culture could not be ruled out. Irrespective of the underlying mechanism, the coincidence of mTORC1 inhibition resulting from EAA starvation and the increased proportion of FOXP3$^+$ cells at the end of the culture remains a pure correlation.

3.6 | The allosteric mTORC1 inhibitor Rapamycin enhances the induction of FOXP3

A screen in yeast aiming to identify targets of the Rapamycin mediated cell cycle arrest led to the discovery of the TOR proteins, *TOR1* and *2* [2]. The mammalian equivalent of the TOR proteins was named the mammalian target of Rapamycin (mTOR). Rapamycin has ever since been used *in vitro* and *in vivo* to study mTOR related functions. Although the immunopressive properties of Rapamycin were established decades ago and the bacterial metabolite is widely used as an immunosuppressant in clinical transplantation [205], the mechanism underlying the immunsuppressive effects of Rapamycin remain poorly understood. Several groups including our laboratory have shown recently that Rapamycin can facilitate the differentiation of FOXP3$^+$ Treg and thereby shedding some light on how Rapamycin might exert some of its immunosuppressive effects [124, 126, 127]. Since mTORC1 inhibition under high cell density cultures and EAA starvation could not be functionally linked to the induction of FOXP3, the involvement of mTORC1 in this

process was tested using the allosteric mTORC1 inhibitor Rapamycin. In order to determine the concentration range in which mTORC1 activity was effectively inhibited, different concentrations of Rapamycin were added to cells stimulated with αCD3 and increasing TGFβ concentrations. FACS analysis revealed that at all TGFβ concentrations tested a significantly reduced MFI for pS6 was measured at Rapamycin concentrations as low as 10pM (Figure 23B). However, analysis of pS6 levels across the population showed that uniform mTORC1 inhibition was only achieved at 50pM and above (Figure 23A). In line with the proposed functional link between mTORC1 inhibition and the enhanced FOXP3 induction, a significant increase in the proportion of $FOXP3^+$ cells was observed when mTORC1 activity was significantly inhibited (Figure 23B and C).

A


αCD3+0.5ng/ml TGFβ:
+ Rapamycin:
0 nM
0.0005 nM
0.001 nM
8.93
9.18
9.42
0.01 nM
0.05 nM
0.1 nM
14.95
19.82
20.46
1 nM
10 nM
100 nM
23.99
23.67
23.53
FOXP3
CD3
pS6
αCD3+0.5ng/ml TGFβ:
100nM Rapamycin
10nM Rapamycin
1nM Rapamycin
0.1nM Rapamycin
0.05nM Rapamycin
0.01nM Rapamycin
0.001nM Rapamycin
0.0005nM Rapamycin
0nM Rapamycin

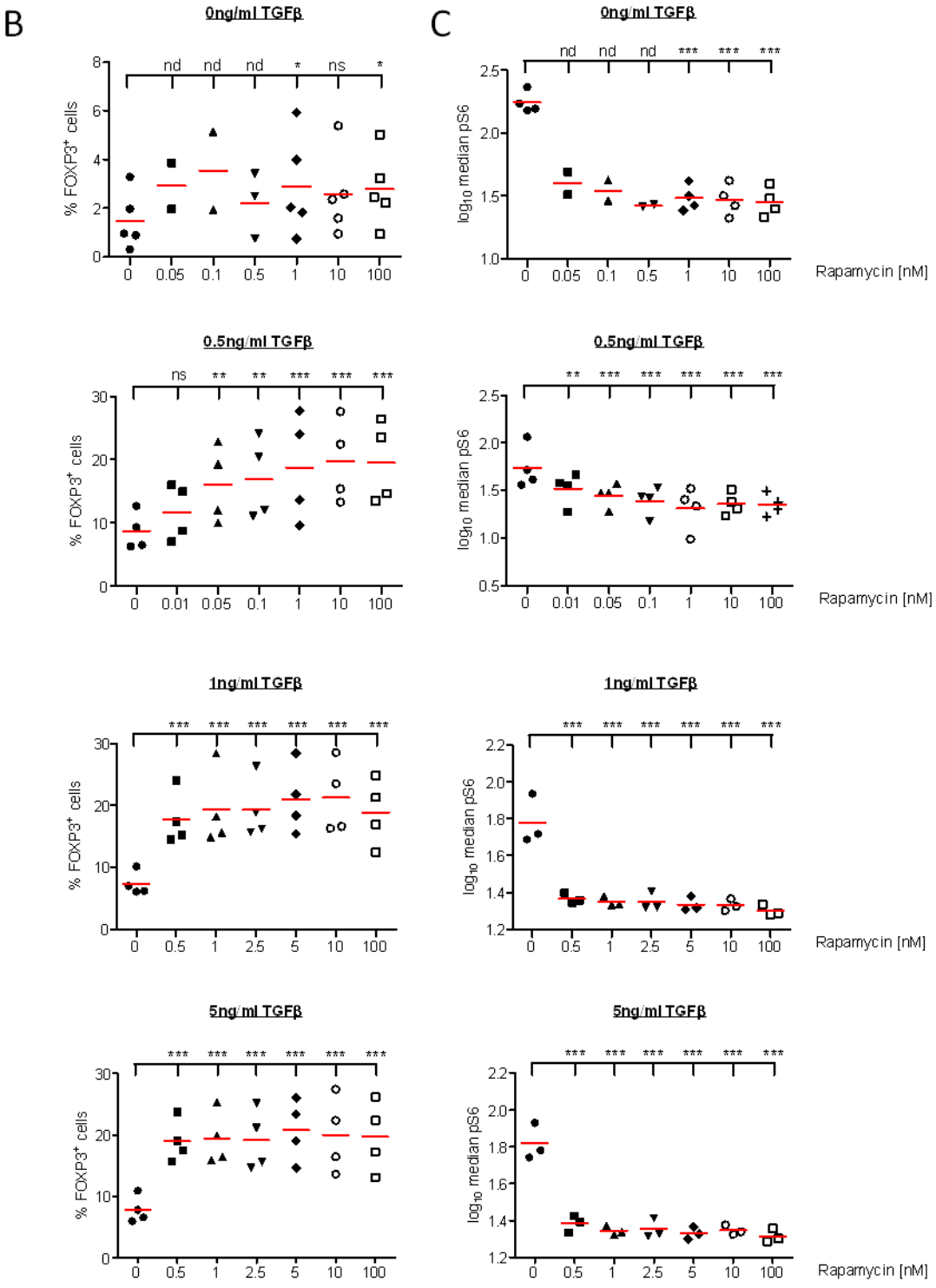


Figure 23. Rapamycin inhibits TORC1 at low concentrations and enhances the induction of FOXP3. EL4.B02 cells were stimulated at 10^4 cells/ml for 3 days with αCD3 and the indicated TGFβ and Rapamycin concentrations. (A, overleaf) Representative FACS plots of FOXP3 expression and pS6 levels and pS6 histograms are shown. Dot plots and histograms show live cells. Dead cells were excluded by gating on 7-AAD low cells. (B and C) Summary of the percentage of $FOXP3^+$ cells and levels of pS6 measured in the experiments described in (A). Graphs contain data of at least 2 independent experiments. The mean is indicated by a red bar. Statistical analysis was performed by comparing the percentage of $FOXP3^+$ cells and levels of pS6 of cells stimulated without Rapamycin to those stimulated with increasing Rapamycin concentrations using repeated measure one-way ANOVA with Dunnett's multiple comparison post test (*p<0.05, **p<0.01, ***p<0.001, ****p<0.0001, nd: statistical testing due to low number of replicates not possible).

Since, a robust and reproducible mTORC1 inhibition was desired, Rapamycin was used at 5nM in most of the following experiments. It is important to note that the survival of cells was not significantly affected at this concentration of Rapamycin when compared to lower concentrations that completely inhibited mTORC1 activity (data not shown). Furthermore, time course studies indicated that the inhibition of mTORC1 by Rapamycin was effectively immediately, since pS6 levels decreased to minimal intensity within 0.5h (data not shown).

The addition of 5nM Rapamycin to cells stimulated at low density with varying concentrations of TGFβ showed that the allosteric mTORC1 inhibitor significantly enhanced the induction of FOXP3 at all concentrations but not in the absence of TGFβ (Figure 24A and B, $p<0.0001$). Furthermore, the effect seemed to saturate at low TGFβ concentrations since no significant increase in the proportion of $FOXP3^+$ cells was detected between the different TGFβ concentrations. As expected pS6 levels were significantly reduced in the presence of the inhibitor irrespective of the presence of TGFβ in the cultures (Figure 24A and C, $p<0.0001$).

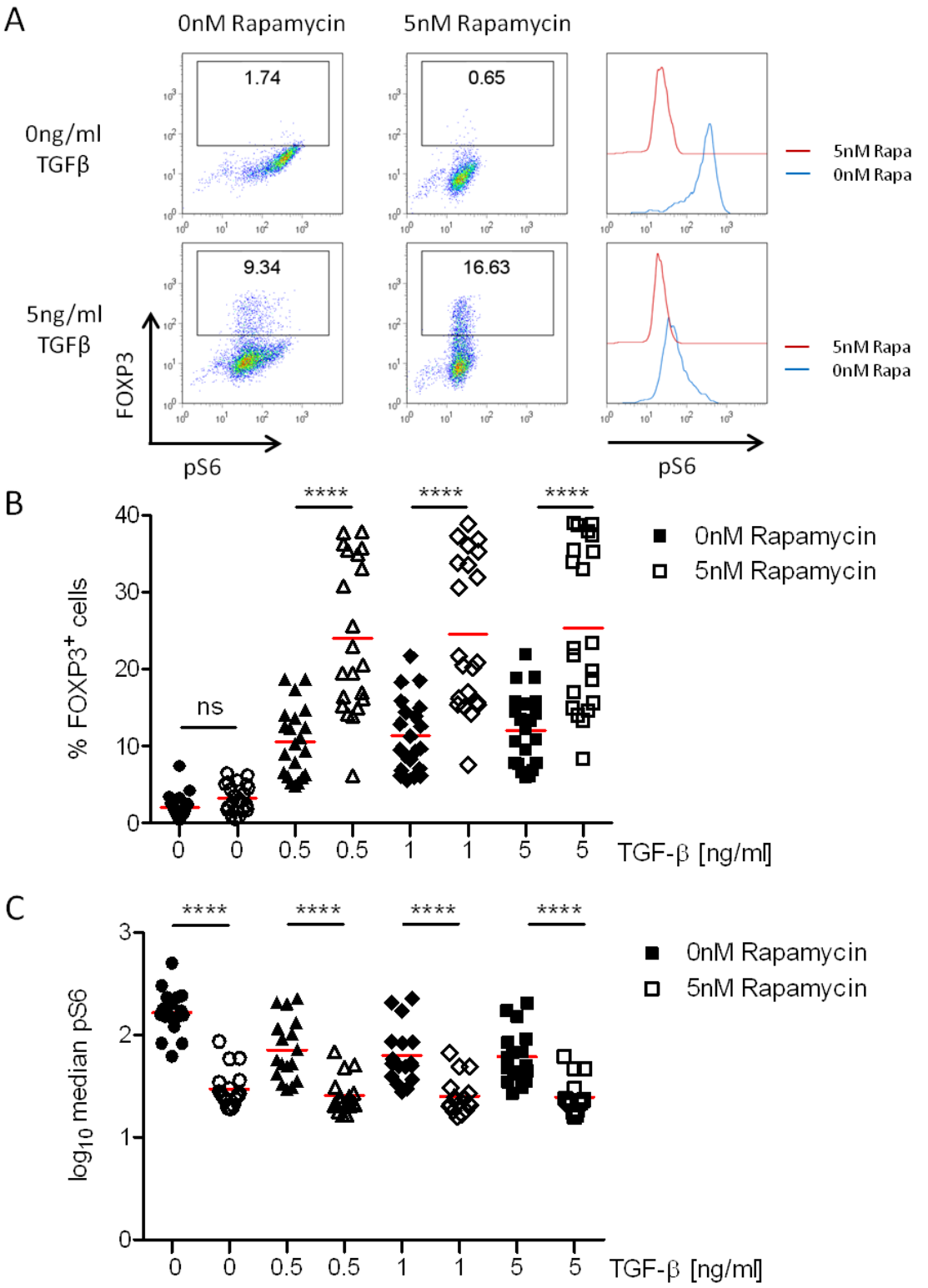


Figure 24. The allosteric TORC1 inhibitor Rapamycin enhances the induction of FOXP3. EL4.B02 cells were stimulated at 10^4 cells/ml for 3 days with αCD3, the indicated TGFβ concentrations and with or without 5nM Rapamycin. (A) Representative FACS plots of FOXP3 expression and pS6 levels and pS6 histograms are shown. Dot plots and histograms show live cells. Dead cells were excluded by gating on 7-AAD low cells. (B and C) Summary of the percentage of $FOXP3^+$ cells and levels of pS6 measured in the experiments described in (A). Graphs contain data of 21 (FOXP3) and 17 (pS6) independent experiments. The mean is indicated by a red bar. Statistical analysis was performed by comparing the percentage of $FOXP3^+$ cells and levels of pS6 of cells stimulated without Rapamycin to those stimulated with the indicated Rapamycin concentrations using repeated measure one-way ANOVA with Bonferroni's multiple comparison post test (****p<0.0001)

In order to test whether the enhanced induction of FOXP3 mediated by Rapamycin that was observed by FACS was at least in part a result of an increase in *Foxp3* transcription, a time course analysis of *Foxp3* mRNA by qPCR was performed. The analysis revealed that Rapamycin enhanced the expression of *Foxp3* at all time points, although levels measured at 12h did not reach statistical significance (Figure 25, 24 and 48h: $p<0.01$, 36h: $p<0.001$).

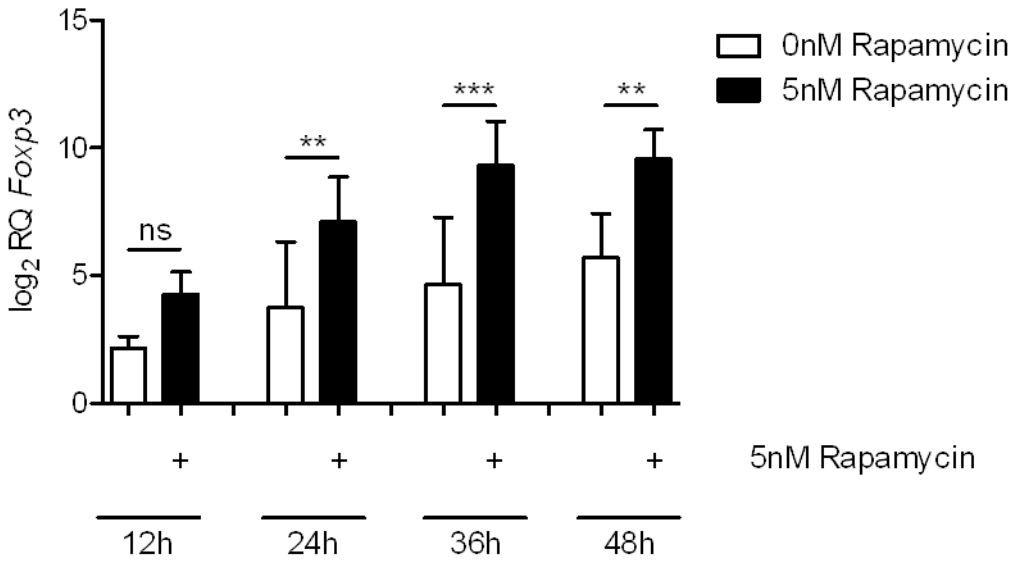


Figure 25. Rapamycin increases the levels of *Foxp3* mRNA. Real-time PCR analysis *Foxp3* expression in cDNA samples prepared from EL4.B02 stimulated at 10^4 cells/well/ml for the indicated durations with 0.5ng/ml TGFβ and with or without 5nM Rapamycin. Data was normalized to *Hprt1* cDNA levels and is presented relative to cells stimulated at low density (10^4 cells/well/ml) with αCD3 for 12 hours in regular medium. Mean and standard deviation of 4 biological replicates is presented. Statistical analysis was performed to compare samples generated from cell stimulated without Rapamycin with those with Rapamycin treatment using repeated measure one-way ANOVA with Bonferroni's multiple comparison post test (**p<0.01, ***p<0.001).

Several reports in the literature have demonstrated that Rapamycin can enrich for $FOXP3^+$ Treg by promoting their survival over $FOXP3^-$ cells by differentially regulating signalling and sensitivity to apoptosis [129-133]. The effect observed in this system however is likely to be due to increased *Foxp3* transcription, rather than preferential survival of $FOXP3^+$ cells since Rapamycin did not consistently decrease survival rates at the analyzed time points. Besides differential survival, preferential proliferation of FOXP3 expressing cells in the presence of Rapamycin could also account for the increase in $FOXP3^+$ cells or the increased levels of *Foxp3* transcripts. Analysis of CFSE labelled cells stimulated with or without Rapamycin did not, however indicate a differential proliferation rate of $FOXP3^+$ and $FOXP3^-$ cells in the cultures (data not shown). Although a role of preferential survival and proliferation effects seems unlikely, it could not conclusively be ruled out that these mechanisms contribute, at least in part, to the increase in the proportion of $FOXP3^+$ cells.

Chapter 4 | CONTRIBUTION AND KINETICS OF mTORC1 AND mTORC2-MEDIATED FOXP3 INDUCTION

4.1 | Stimulation in the presence of Rapamycin, Torin 1 and EAA starvation results in mTORC2 inhibition

The evolutionary conserved serine/threonine kinase mTOR nucleates two structurally and functionally distinct complexes, mTORC1 and mTORC2. Whereas the nutrient sensor mTORC1 was thought to be sensitive to Rapamycin due to the binding of the drug to the essential mTORC1 component FKBP12, resulting in the structural disruption of mTORC1, mTORC2 was initially thought to be Rapamycin insensitive [206]. This idea was challenged by studies of Sarbassov et al., who demonstrated that prolonged exposure to Rapamycin also seemed to inhibit the assembly of mTORC2 in some but not all cell lines [13].

With respect to the induction of FOXP3 in T-cells, the afore-mentioned effect of Rapamycin on mTORC2 had not been addressed at the time the following experiments were performed. Neither Cobbold nor Sauer et al. studied the role of mTORC2 activity in the regulation of FOXP3 expression in their experiments [124, 127]. Although Hashinaxo et al. did not directly test the hypothesis that mTORC2 is involved in regulating the induction of FOXP3, the authors discussed a potential role for mTORC2 by reflecting on the fact that the negative effect of a constitutively active form of AKT on the induction of FOXP3 was only partially reversible by Rapamycin [126]. However, a detailed analysis of the role of mTORC2 seemed difficult in an experimental system in which the serine/threonine kinase AKT that acts both upstream of mTORC1 and downstream of mTORC2 is constitutively active. Furthermore the Hashinaxo et al. failed to acknowledge and test the potential inhibition of mTORC2 by Rapamycin in their

experiments, for example by analysing the phosphorylation of AKT at the mTORC2 specific site S473 [207].

Therefore the effect of Rapamycin on the activity of mTORC2 in the EL4.B02 system was tested and a potential contribution of this inhibition to the induction of FOXP3 was investigated. The FACS analysis of cell stimulated in the presence of Rapamycin with or without TGFβ demonstrated that Rapamycin not only led to an increased percentage of $FOXP3^+$ cells and mTORC1 inhibition (Figure 24A and B), but also resulted in marked reduction of AKT S473 phosphorylation levels, indicating significant mTORC2 inhibition (Figure 26, $p<0.0001$). As in the case of pS6 levels, TGFβ itself significantly reduced the levels of pAKT ($p<0.0001$).

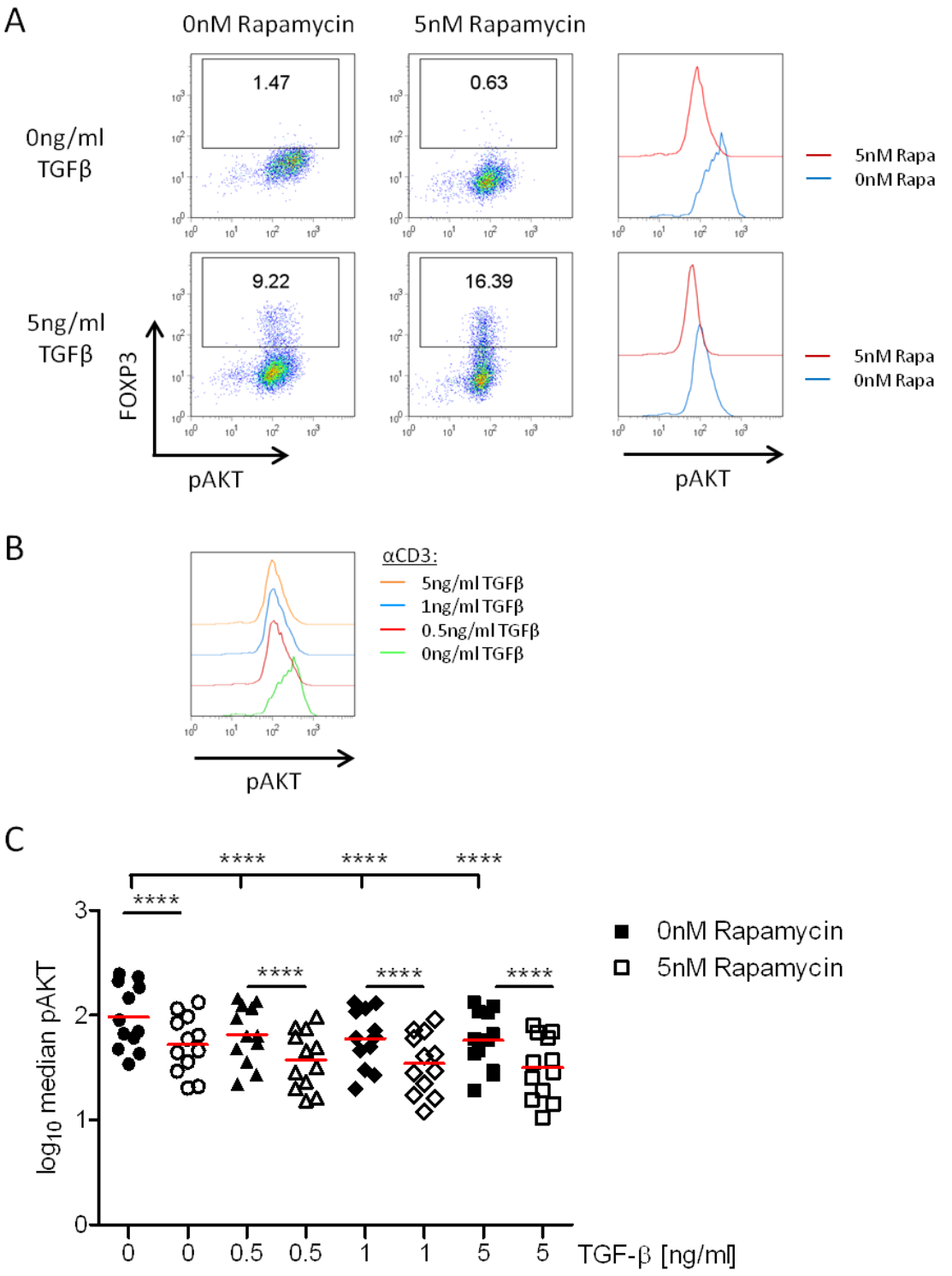


Figure 26. Rapamycin and TGFβ lower the phosphorylation levels of AKT at S473. EL4.B02 cells were stimulated at 10^4 cells/ml for 3 days with αCD3, the indicated TGFβ concentrations and with or without 5nM Rapamycin. (A and B) Representative FACS plots of FOXP3 expression and pAKT levels and pAKThistograms are shown. Dot plots and histograms show live cells. Dead cells were excluded by gating on 7-AAD low cells. (A) highlights the Rapamycin mediated downregulation of pAKT levels whereas (B) shows the TGFβ effect. (C) Summary of the percentage of levels of pAKT measured in the experiments described in (A). Graphs contain data of 12 independent experiments. The mean is indicated by a red bar. Statistical analysis was performed by comparing the levels of pAKT of cells stimulated without Rapamycin to those stimulated with Rapamycin (or +/- TGFβ) using repeated measure one-way ANOVA with Bonferroni's multiple comparison post test (****p<0.0001).

The latter result was rather unexpected since TGFβ is known to induce AKT phosphorylation at S473. This TGFβ mediated activation of mTORC2 and concomitant increase in pAKT S473 levels, was however demonstrated to be transient [208]. In the absence of any studies showing a negative effect of TGFβ on mTORC2 activity and in the light of studies demonstrating that PP2A, a phosphatase known to be activated by TGFβ [204], can mediate S473 dephosphorylation [209-211], it seemed unlikely that the reduced levels of pAKT by TGFβ were a result of mTORC2 inhibition. Similarly with respect to levels of phosphorylation of S6, the reduction of S473 phosphorylation of AKT could be completely blocked by the addition of the PP2A inhibitor okadaic acid (Figure 27). Although this effect did not reach statistical significance the trend points towards a TGFβ-mediated activation of PP2A resulting in decreased pAKT levels. In line with findings of Sarbassov et al. and irrespective of the effect of TGFβ, prolonged Rapamycin exposure clearly reduced the levels of S473 phosphorylation even in the presence of TGFβ [13].

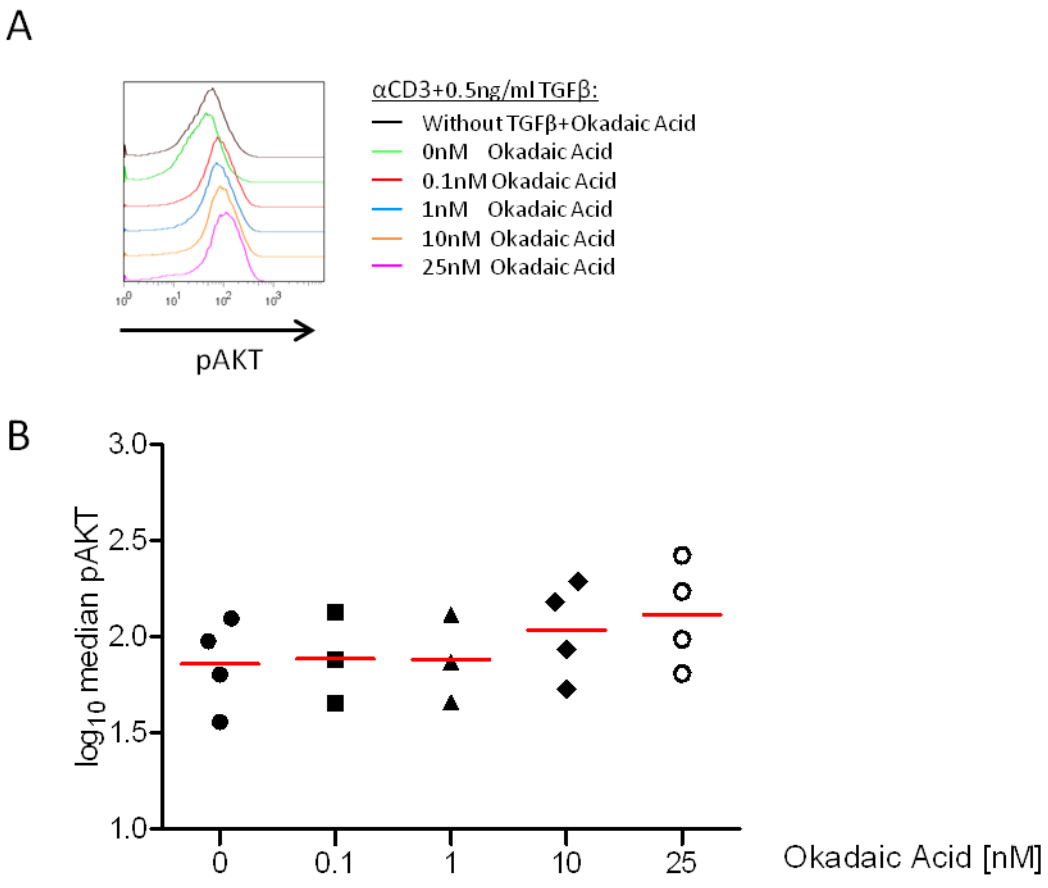


Figure 27. TGFβ reduces the levels of pAKT via activation of PP2A. (A) EL4.B02 cells were stimulated at 10^4 cells/well/ml for 3 days in the presence of plate bound αCD3 (KT3, 5µg/ml), with or without 0.5ng/ml TGFβ and the indicated concentrations of okadaic acid. Representative and pAKT histogram are shown. Histograms show live cells. Dead cells were excluded by gating on 7-AAD low cells. (B) Summary of experiments described in (A) (all stimulated with 0.5ng/ml TGFβ). Graph contains data of 4 independent experiments. The mean is indicated by a red bar.

Although mTORC1 is thought to be the AA sensitive mTOR complex [11], mTORC2 activity was measured in cells stimulated under limiting concentrations of EAA. pAKT levels were significantly lower under EAA starvation conditions compared to cells stimulated in medium containing 100% EAA (Figure 28, 0ng/ml TGFβ: $p<0.001$, 0.5 and 5ng/ml TGFβ: $p<0.01$), indicating that EAA starvation also reduces TORC2 activity.

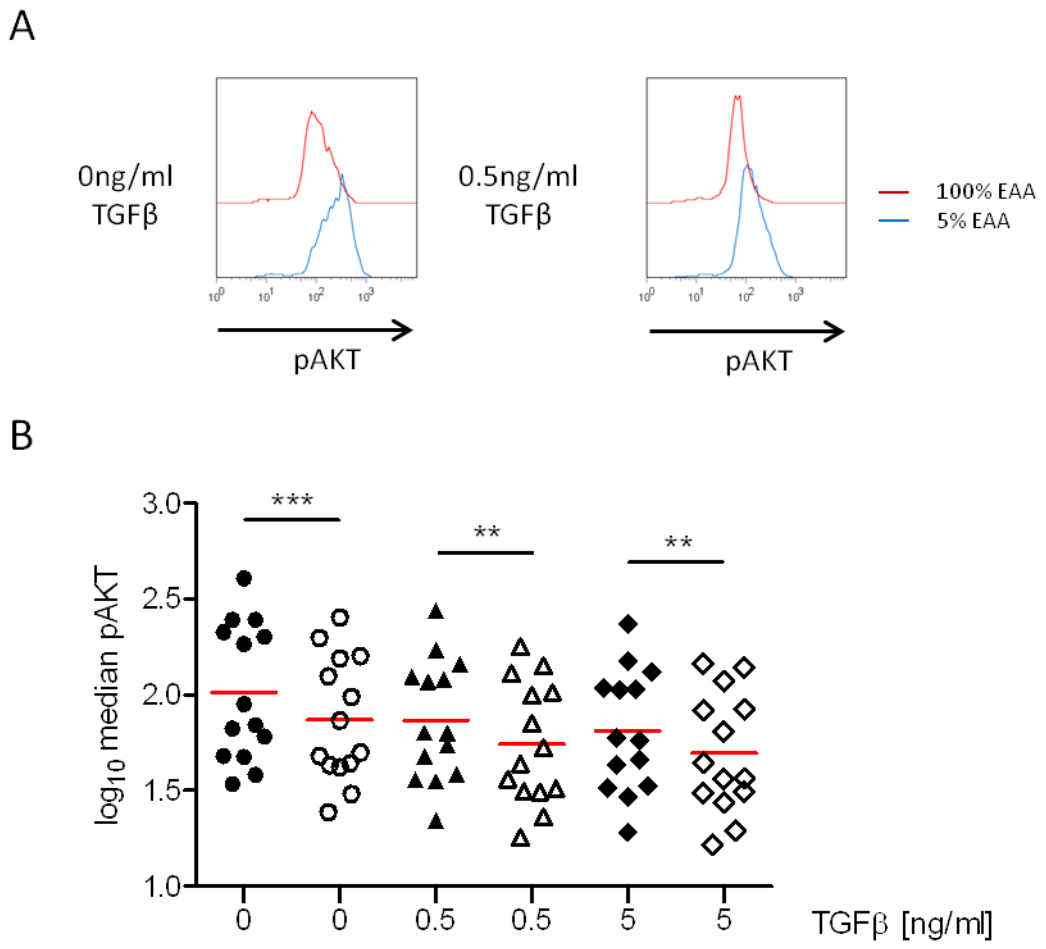


Figure 28. EAA starvation reduces the levels of pAKT. (A) EL4.B02 cells were stimulated at 10^4 cells/well/ml for 3 days in the presence of plate bound αCD3 (KT3, 5μg/ml), with or without 0.5ng/ml TGFβ and in medium containing either 100% or 5% EAA. Representative and pAKT histogram are shown. Histograms show live cells. Dead cells were excluded by gating on 7-AAD low cells. (B) Summary of experiments described in (A) (all stimulated with 0.5ng/ml TGFβ). Graph contains data of 4 independent experiments. The mean is indicated by a red bar. Statistical analysis was performed by comparing the levels of pAKT of cells stimulated in 100% EAA medium to those stimulated in 5% EAA medium using repeated measure one-way ANOVA with Bonferroni's multiple comparison post test (****p<0.0001).

A recent publication investigating the role of RAG GTPases in sensing AA and regulation of mTORC1 activity, demonstrated that mTORC2 activity is actually elevated by an AA starvation-like signal (RagA and C knockdown) [42], possibly by interfering with the negative feedback of S6K on mTORC2 activity. On the other hand Tato et al. provide clear evidence in a system based on AA withdrawal, that AA can activate mTORC2 resulting in elevated S473 AKT phosphorylation [212]. At least in the scenario in which

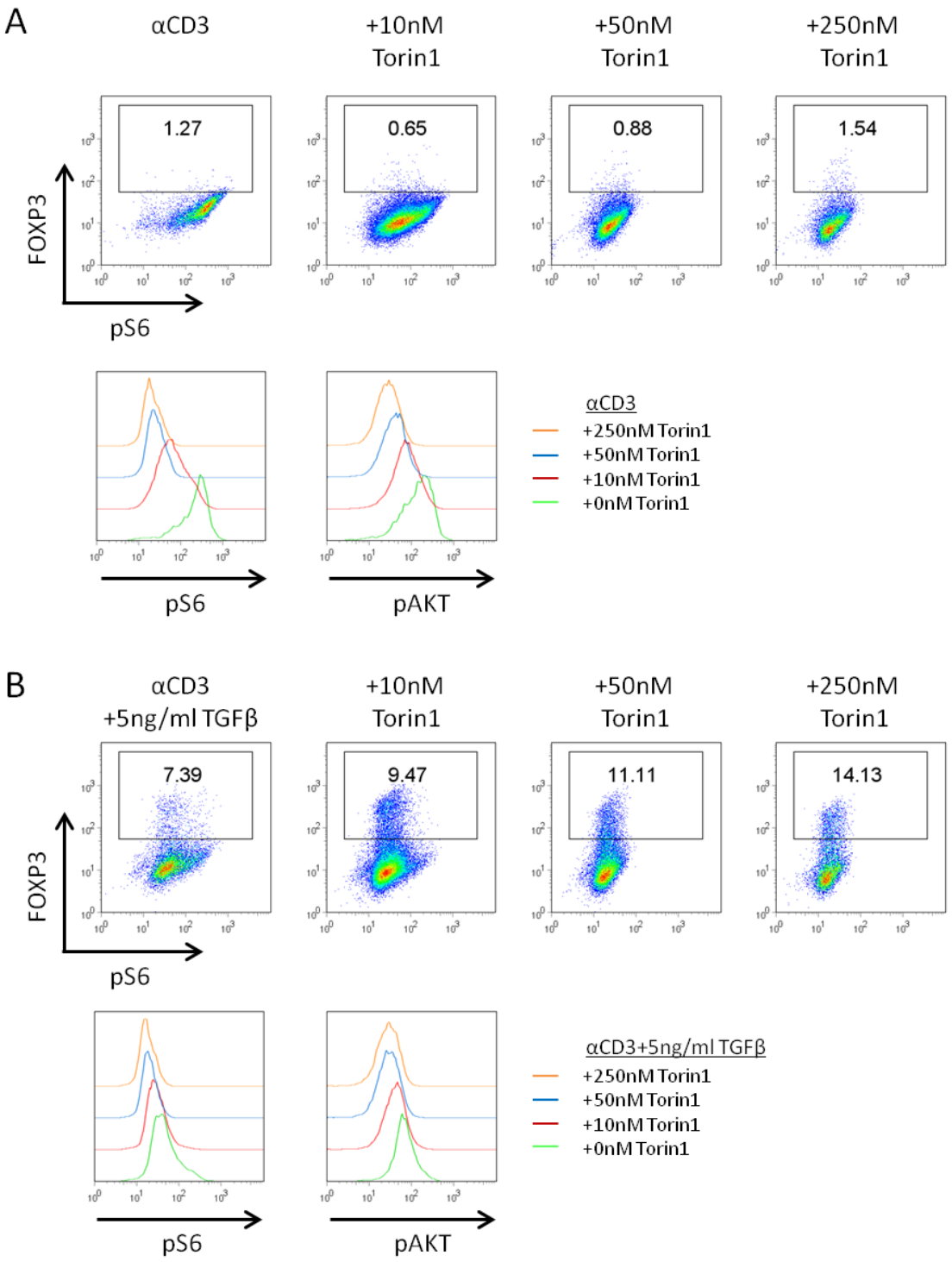
cells were stimulated in the absence of TGFβ, the results obtained from cells stimulated under limiting amounts of EAA point towards a role of EAA in regulating not only mTORC1 but also mTORC2 activity.

Nevertheless, the fact that Rapamycin and possibly EAA starvation both inhibited mTORC1 and 2 in EL4.B02 evoked the question of whether mTORC2 is either positively or negatively involved in regulating the expression of FOXP3. The discovery of a novel ATP-competitive inhibitor, Torin 1, that inhibits the kinase activity of mTOR in both complexes, created the opportunity to test another mTORC1/2 inhibitor with respect to its ability to enhance the induction of FOXP3 [14]. Besides the different mode of action (inhibition of kinase activity versus structural disruption of complexes by Rapamycin), Torin 1 was demonstrated to inhibit both complexes more completely revealing Rapamycin resistant mTOR functions [16].

In order to determine the optimal concentration of Torin 1 that inhibits mTORC1 and 2 in EL4.B02, increasing amounts of Torin 1 were added to cells stimulated at low cell density with αCD3 and TGFβ. As expected Torin 1 robustly and significantly inhibited both mTORC1 and mTORC2 at a concentration of 10nM and above (Figure 29 D and E). This decrease in mTORC1 and mTORC2 activity was accompanied by a significant increase in the proportion of FOXP3 expressing cells (50nM: $p<0.01$, 250nM: $p<0.05$). In the case of 250nM Torin1 the increase of $FOXP3^+$ cells was even observed in the absence of added TGFβ, although the MFI of FOXP3 was relatively low and the effect did not reach statistical significance. A similar effect was observed at 0.1, 0.25 and 0.5ng/ml TGFβ for both mTORC1 and 2 activity as well as FOXP3 (n=3, data not shown). The enhancement of the induction of FOXP3 by Torin 1 was comparable to that

observed when cells were stimulated with Rapamycin, indicating that Rapamycin insensitive mTOR functions were neither positively nor negatively involved in the induction.

A different ATP-competitive mTOR inhibitor, PP242, inhibited mTORC1 and 2 activity efficiently at high concentrations, however PP242 did not increase the proportion of $FOXP3^+$ cells that were induced (data not shown). Moreover, it also abolished the enhancement effect of Rapamycin on the expression of FOXP3. This rather surprising finding could be due to inhibition of other kinases whose signalling is relevant to the induction of FOXP3 resulting from the lower specificity of PP242 for the ATP-binding pocket of mTOR compared to Torin 1 [15].


A
αCD3
+10nM Torin1
+50nM Torin1
+250nM Torin1
1.27
0.65
0.88
1.54
FOXP3
pS6
pS6
pAKT
αCD3
+250nM Torin1
+50nM Torin1
+10nM Torin1
+0nM Torin1
B
αCD3 +5ng/ml TGFβ
+10nM Torin1
+50nM Torin1
+250nM Torin1
7.39
9.47
11.11
14.13
FOXP3
pS6
pS6
pAKT
αCD3+5ng/ml TGFβ
+250nM Torin1
+50nM Torin1
+10nM Torin1
+0nM Torin1

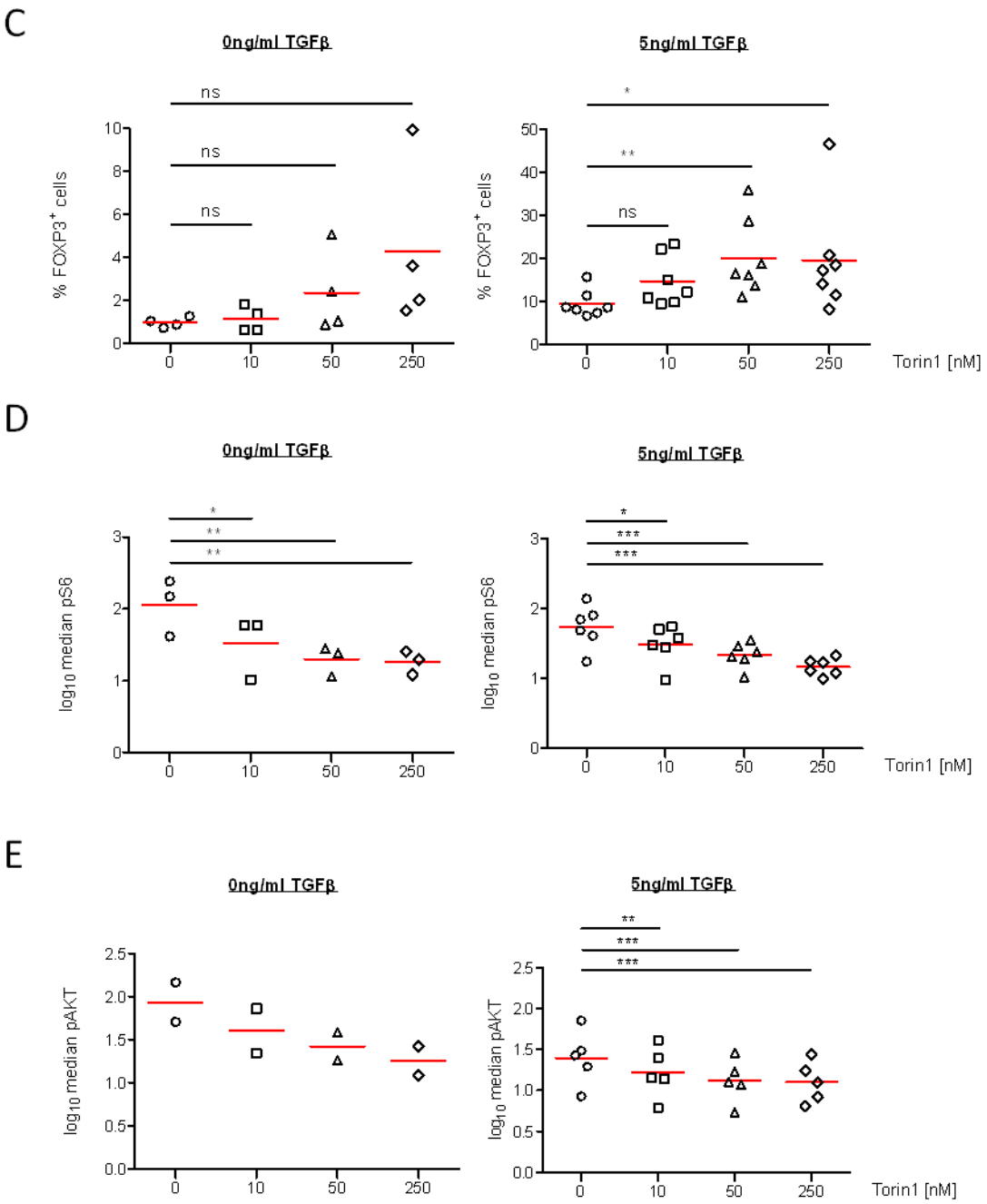


Figure 29. The ATP-competitive mTOR inhibitor Torin1 inhibits both TORC1 and 2 and enhances the induction of FOXP3. EL4.B02 cells were stimulated at 10^4 cells/ml for 3 days with αCD3, 0ng/ml (A (overleaf), C-E left panel) and 5ng/ml (B (overleaf), C-E right panel) and with the indicated concentrations of Torin1. (A and B) Representative FACS plots of FOXP3 expression and pS6 levels and pS6 and pAKT histograms are shown. Dot plots and histograms show live cells. Dead cells were excluded by gating on 7-AAD low cells. (C-E) Summary of the percentage of $FOXP3^+$ cells (C), the levels of pS6 (D) and pAKT (E) measured in the experiments described in (A and B). Graphs contain data of at least 4 (FOXP3), 3 (pS6) and 2 (pAKT) independent experiments. The mean is indicated by a red bar. Statistical analysis was performed by comparing the percentage of $FOXP3^+$ cells and the levels of pS6 and pAKT of cells stimulated without Torin1 to those stimulated with the indicated Torin1 concentrations using repeated measure one-way ANOVA with Bonferroni's multiple comparison post test (*p<0.05,, **p<0.01, ***p<0.001, ****p<0.0001).

In summary the analysis of mTORC2 activity in the different experimental conditions demonstrated that stimulation of EL4.B02 cells in the presence of the allosteric mTORC1 inhibitor Rapamycin or the ATP-competitive mTOR inhibitor Torin 1 or in EAA starvation conditions resulted in reduced mTORC2 activity, with the latter scenario needing further investigation to substantiate the preliminary findings. All the conditions mentioned above resulted in similar increases in the proportion of $FOXP3^+$ cells and marked mTORC1 inhibition. The fact that all experimental conditions resulted in a similar outcome with respect to FOXP3 and mTORC1/2 activity might indicate that common molecular mechanisms act downstream of the different stimuli. Neither of the experiments could however shed light on the role of the individual mTOR complexes in the regulation of FOXP3 expression. However, considering that Rapamycin affects mTORC2 activity only after prolonged exposure (>24h) [13] and the almost identical magnitude of the response induced in Rapamycin and Torin1 treated cells, it seems unlikely that mTORC2 inhibition has a negative effect on the induction of FOXP3.

4.2 | Kinetics of the enhancement of FOXP3 induction mediated by mTORC inhibition

4.2.1 | Rapamycin and Torin 1 display distinct kinetics of mTORC2 inhibition and enhanced FOXP3 induction

Despite being subject to extensive investigation, little is known about the kinetics of FOXP3 induction, particularly in the setting of an inhibited mTOR pathway. An analysis of the course of the induction over time might shed more light on the temporal requirements of mTOR associated signals underlying the induction of FOXP3. However, a detailed study of the temporal parameters with respect to TORC inhibition was hindered by the fact that an analysis of FOXP3 protein expression was difficult at early time points due to low expression of the transcription factor. Furthermore, conditions such as EAA starvation-induced mTOR inhibition were found to be greatly dependent on the state of the cells at the start of the stimulation. Since the depletion of EAA is likely to dependent on the proliferative potential of the cells, EAA depletion induced TORC inhibition was achieved at varying time points during the stimulation. Furthermore, although the analysis of mTORC2 activity in EAA starvation conditions indicated a trend towards inhibited mTORC2, the effect was less pronounced and needed further investigation. In order to circumvent these technical problems, the kinetic analysis of mTOR mediated FOXP3 induction was restricted to cells stimulated in the presence of mTOR inhibitors Rapamycin and Torin 1. Rather than measuring the activity of the two mTOR complexes and the induction of FOXP3 at different time points after the stimulation was set up, the cells were stimulated at low cell density

with the basic signals, αCD3 and TGFβ, for the usual 72h and the inhibitors added for various durations of the stimulation. In this way, the TCR and TGFβ signals were able to reveal their full effect on the induction of FOXP3 and the duration during which mTOR inhibition was allowed to facilitate the induction of FOXP3 was tightly controlled. This experimental set up was based on the hypothesis that both Rapamycin and Torin 1 inhibited the mTOR complexes almost instantly.

In order to test this hypothesis before proceeding with the actual experiment, a time course study in which cells were stimulated for short intervals in the presence or absence of the inhibitors was performed and the activity of mTORC1 and 2 assessed by FACS. The analysis revealed that Rapamycin and Torin 1 inhibited mTORC1 activity maximally in less than 2h, whereas the addition of TGFβ did not affect the levels of pS6 (Figure 30A and C, $p<0.0001$ for all time points and both drugs). In contrast mTORC2 activity was differentially inhibited by the two drugs. As in the case of mTORC1 activity, Torin1 inhibited mTORC2 maximally within 2h of the stimulation, however the effect did not reach statistical significance (Figure 30D). Rapamycin, on the other hand, only started to inhibit mTORC2 after 6h of stimulation (Figure 30B). Levels of pAKT similar to Torin 1 were not achieved by Rapamycin at any of the measured time points, although at 10h mTORC2 activity was starting to decline closer to that in the presence of Torin 1. These differences in the kinetics of mTORC2 inhibition by the two drugs provided a window of opportunity to test the differential contribution of the two mTOR complexes to the regulation of FOXP3 expression.

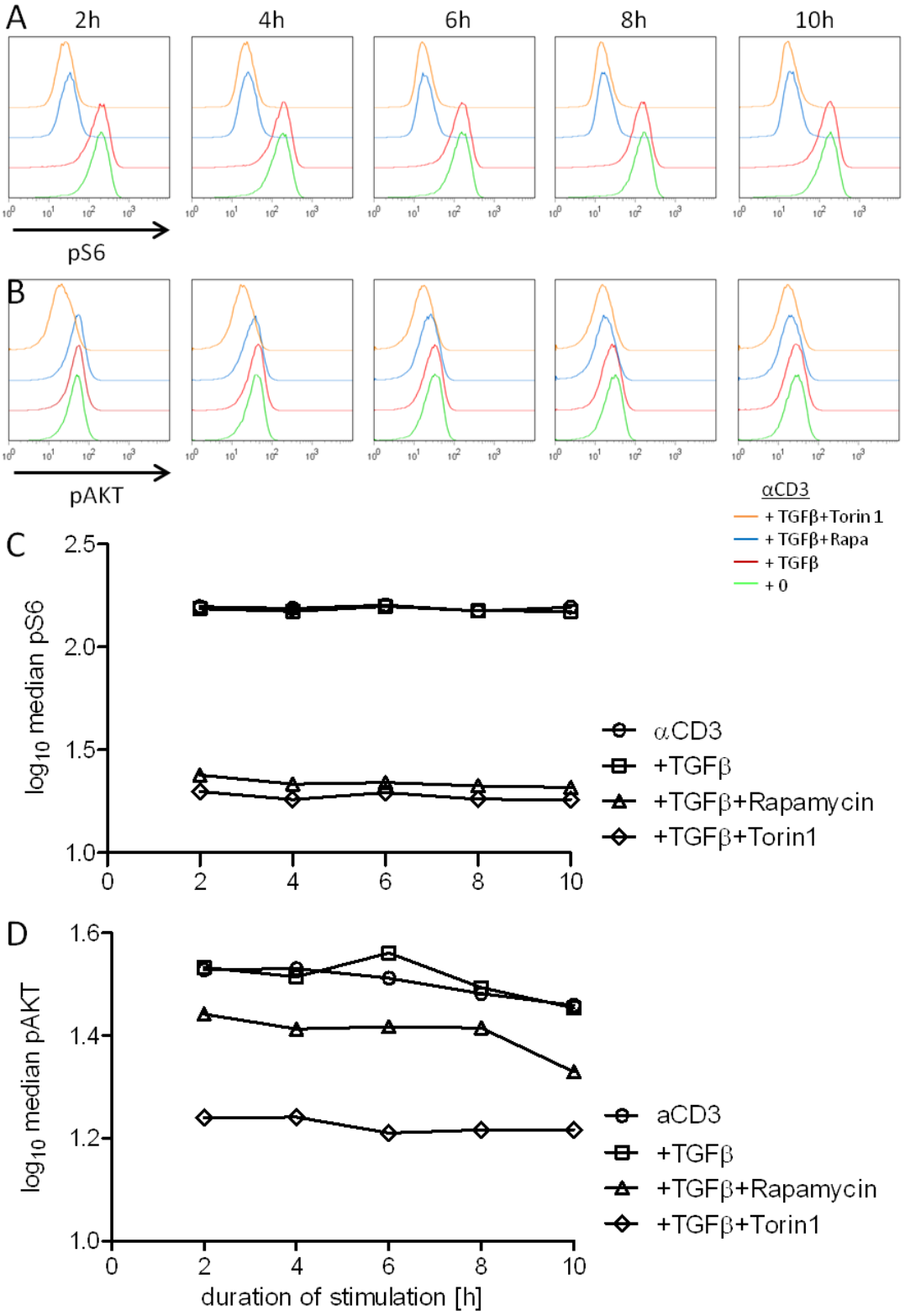


Figure 30. A time course analysis reveals differential kinetics of TORC2 inhibition by Rapamycin and Torin1. EL4.B02 cells were stimulated for 2-10h αCD3, 0ng/ml or 5ng/ml plus 5nM Rapamycin or 250nM Torin 1. (A and B) Representative FACS histograms of pS6 (A) and pAKT (B) levels are shown. Histograms show live cells. Dead cells were excluded by gating on 7-AAD low cells. (C and D) Summary of the levels of pS6 (C) and pAKT (D) measured in the experiments described in (A and B). Graphs contain data of 3 independent experiments. The mean is indicated by symbols.

Taking into account the above mentioned differences in inhibition of mTORC1 and 2 by Rapamycin and Torin 1, cells were stimulated with αCD3 and TGFβ for the usual 72h and the inhibitors added for various durations of the stimulation, thereby allowing an analysis of the differential contribution of the two complexes to the induction of FOXP3. If the inhibitors were added for the last few hours before the end of the stimulation, then only Torin1 but not Rapamycin would be expected to produce a significant inhibition of mTORC2. If mTORC2 inhibition contributed to the induction of FOXP3, Torin 1 inhibition should therefore increase the proportion of $FOXP3^+$ cells when present for shorter periods than Rapamycin.

The FACS analysis revealed that this was indeed the case (Figure 31). Whereas Rapamycin only significantly enhanced the induction when it was present for the last 24h (24 and 48h: $p<0.001$), Torin 1 increased the proportion of $FOXP3^+$ cells within 6h (6h: $p<0.05$, 24 and 48h: $p<0.01$). This finding indicates that inhibition of mTORC2 may play a crucial role in the regulation of FOXP3 expression. However, a role for mTORC1 inhibition-mediated FOXP3 induction could not be excluded. It is important to note that neither Rapamycin nor Torin1 addition, irrespective of how long the drugs were present during the stimulation, significantly increased the proportion of dead cells in the cultures (data not shown). Therefore a contribution of preferential survival effects of $FOXP3^+$ cells to the observed increase in the percentage of $FOXP3^+$ cells seemed negligible.

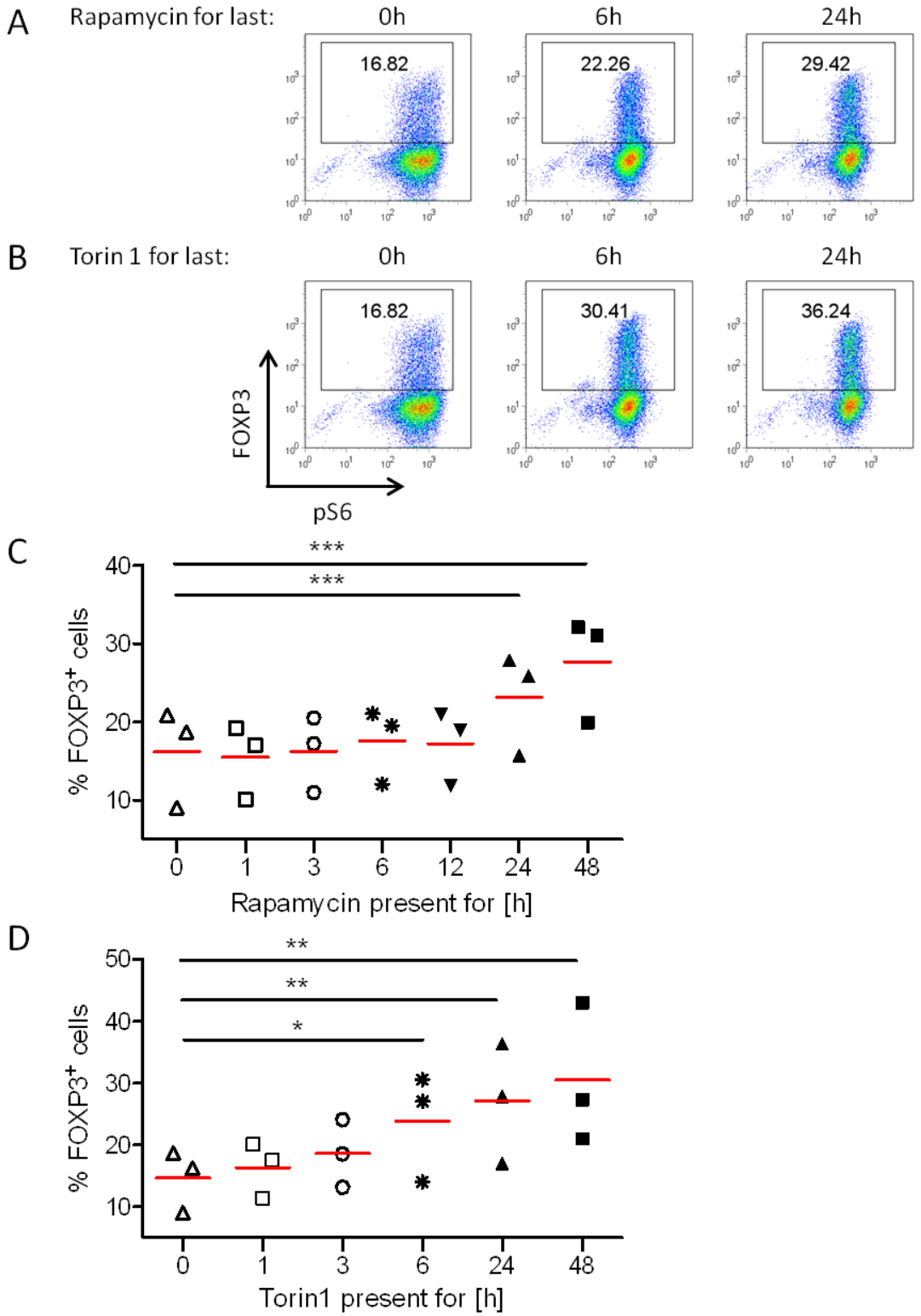


Figure 31. Torin 1 enhances FOXP3 expression with faster kinetics than Rapamycin. EL4.B02 cells were stimulated at 10^4 cells/ml for 3 days with αCD3, 0.5ng/ml TGFβ and with 5nM Rapamycin or 250nM Torin 1 for the indicated hours (counted from the end of the experiment). (A and B) Representative FACS plots of FOXP3 expression and pS6 levels in live cells (7-AAD low) after treatment with Rapamycin (A) and Torin 1 (B) are shown. (C and D) Summary of the percentage of $FOXP3^+$ cells measured in the experiments described in (A and B). Graphs contain data of at 3 independent experiments. The mean is indicated by a red bar. Statistical analysis was performed by comparing the percentage of $FOXP3^+$ cells obtained without inhibitor with that measured in the presence of Rapamycin or Torin1 using repeated measure one-way ANOVA with Bonferroni's multiple comparison post test (*p<0.05, **p<0.01, ***p<0.001).

4.3 | mTORC1 inhibition by Rapamycin contributes to the induction of FOXP3

The time course analysis of Rapamycin and Torin 1 mediated mTORC1 and 2 inhibition (Figure 30) not only enabled an analysis of the role of mTORC2 in the regulation of FOXP3 expression (Figure 31), but also revealed that Rapamycin left mTORC2 activity essentially intact during the first 4-6h. As mentioned before, due to the relatively slow upregulation of FOXP3 at protein level it was not technically feasible to assess the effect of Rapamycin at these early time points by FACS. Since the effect of Rapamycin and mTORC1 inhibition on *Foxp3* transcription should precede an upregulation at the protein level, the levels of *Foxp3* mRNA at these early time points were measured by qPCR.

The analysis demonstrated clearly that Rapamycin significantly enhanced the levels of *Foxp3* mRNA even at time points at which mTORC2 is still partially active (Figure 32, $p<0.001$). Therefore a role for mTORC1 inhibition in the regulation seemed plausible. In line with the evidence given in the last chapter, inhibition of mTORC1 and 2 by Torin 1 at the same time points further increased the amounts of *Foxp3* mRNA compared to the Rapamycin treated samples. However, the observed increase over Rapamycin treated samples did not reach statistical significance. Nevertheless this observation further underscored the role of mTORC2 inhibition in regulating FOXP3 expression.

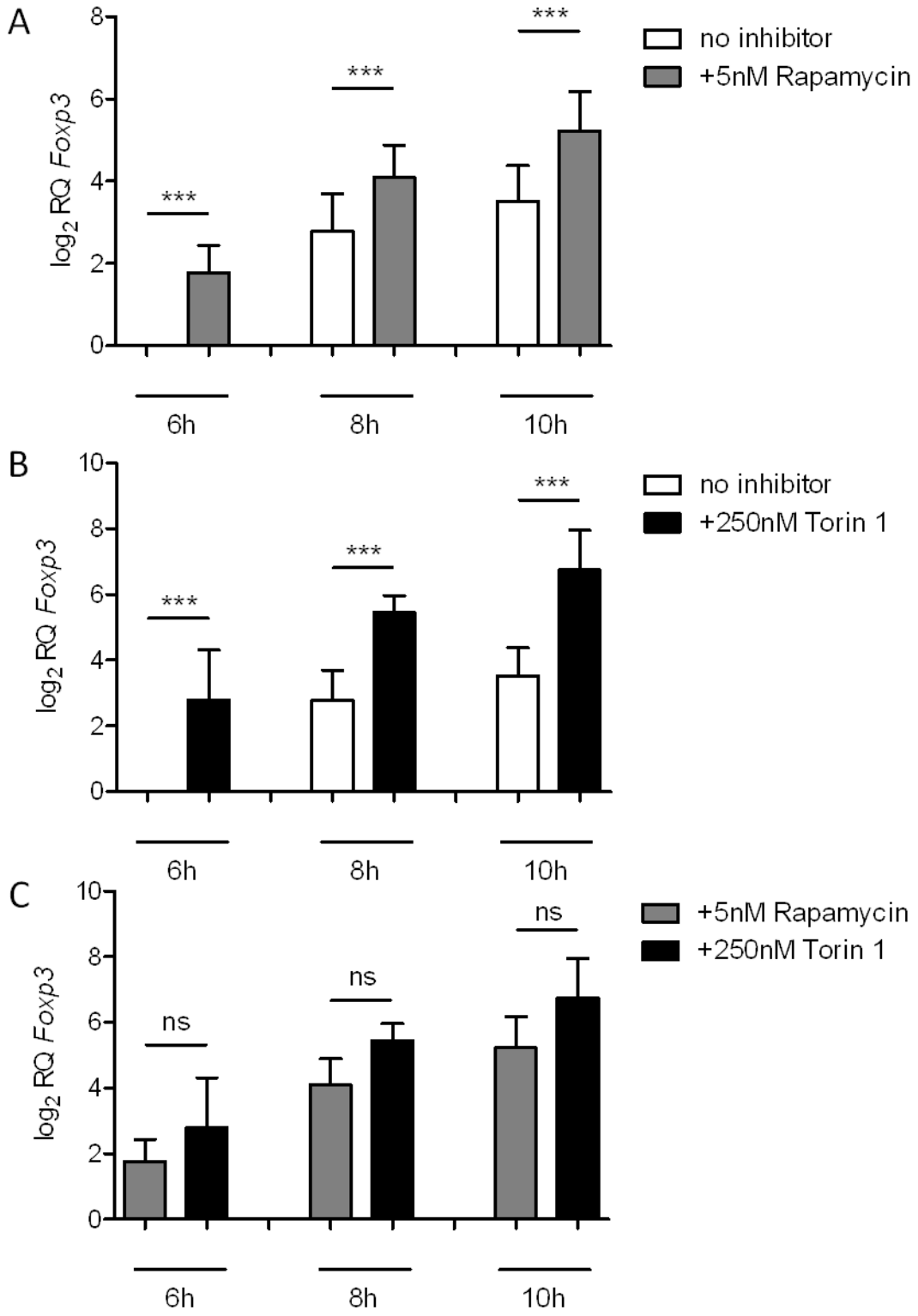


Figure 32. Rapamycin and Torin 1 enhance *Foxp3* transcription at early time points during the stimulation. Real-time PCR analysis *Foxp3* expression in cDNA samples prepared from EL4.B02 stimulated for 6, 8 and 10h with αCD3, 5ng/ml TGFβ with and without 5nM Rapamycin and 250nM Torin 1. Data was normalized to *Hprt1* cDNA levels and is presented relative to cells stimulated without inhibitor for 6h. Mean and standard deviation of 8 (A), 3 (B) and 3 (C) biological replicates is presented. Statistical analysis was performed to compare samples generated from cells stimulated without inhibitor compared to inhibitor treated cells (A and B) and Rapamycin and Torin 1 treated cells (C) using repeated measure one-way ANOVA with Bonferroni's multiple comparison post test (***p<0.001).

4.4 | Rapamycin titrations suggest roles for mTORC1 and mTORC2 mediated enhancement of FOXP3 induction

Based on the observation that Rapamycin mediated disruption of mTORC2 assembly inhibited mTORC2 functions in cell lines that show Rapamycin sensitive AKT phosphorylation [13], the hypothesis arose that by careful titration of the amount of Rapamycin added to the cultures one could achieve selective or preferential inhibition of mTORC1 whilst leaving mTORC2 activity unaffected.

As demonstrated earlier (Figure 23) low doses of Rapamycin significantly inhibited mTORC1 activity and consequently the phosphorylation of S6 (Figure 33: levels of pS6 and pAKT are shown relative to those measured without Rapamycin; 50 and 100pM: $p<0.05$, 150-1000pM: $p<0.001$). mTORC2 activity as measured by phosphorylation of AKT at S473 was only significantly reduced at Rapamycin concentrations of 500pM and above (500 and 1000pM: $p<0.05$), indicating a differential sensitivity of both complexes to the drug. Interestingly, a clear trend was observable with respect to the percentage of $FOXP3^+$ cells that were induced. Low doses of Rapamycin (50-100pM) enhanced the induction of FOXP3, although the effect did not reach statistical significance. This was probably due to variation in the overall percentage of cells responding to the basic stimuli αCD3 and TGFβ between the biological replicates. Nevertheless, a significantly enhanced proportion of $FOXP3^+$ cells was detected in the samples stimulated with 150pM Rapamycin upwards (150pM: $p<0.05$, 250-1000pM: $p<0.001$). It is important to note that at the lower end of this concentration range (150-250pM) only mTORC1 and not mTORC2 activity is significantly inhibited, providing further support for the

hypothesis that not only mTORC2 but also mTORC1 inhibition contributed to the enhanced induction of FOXP3.

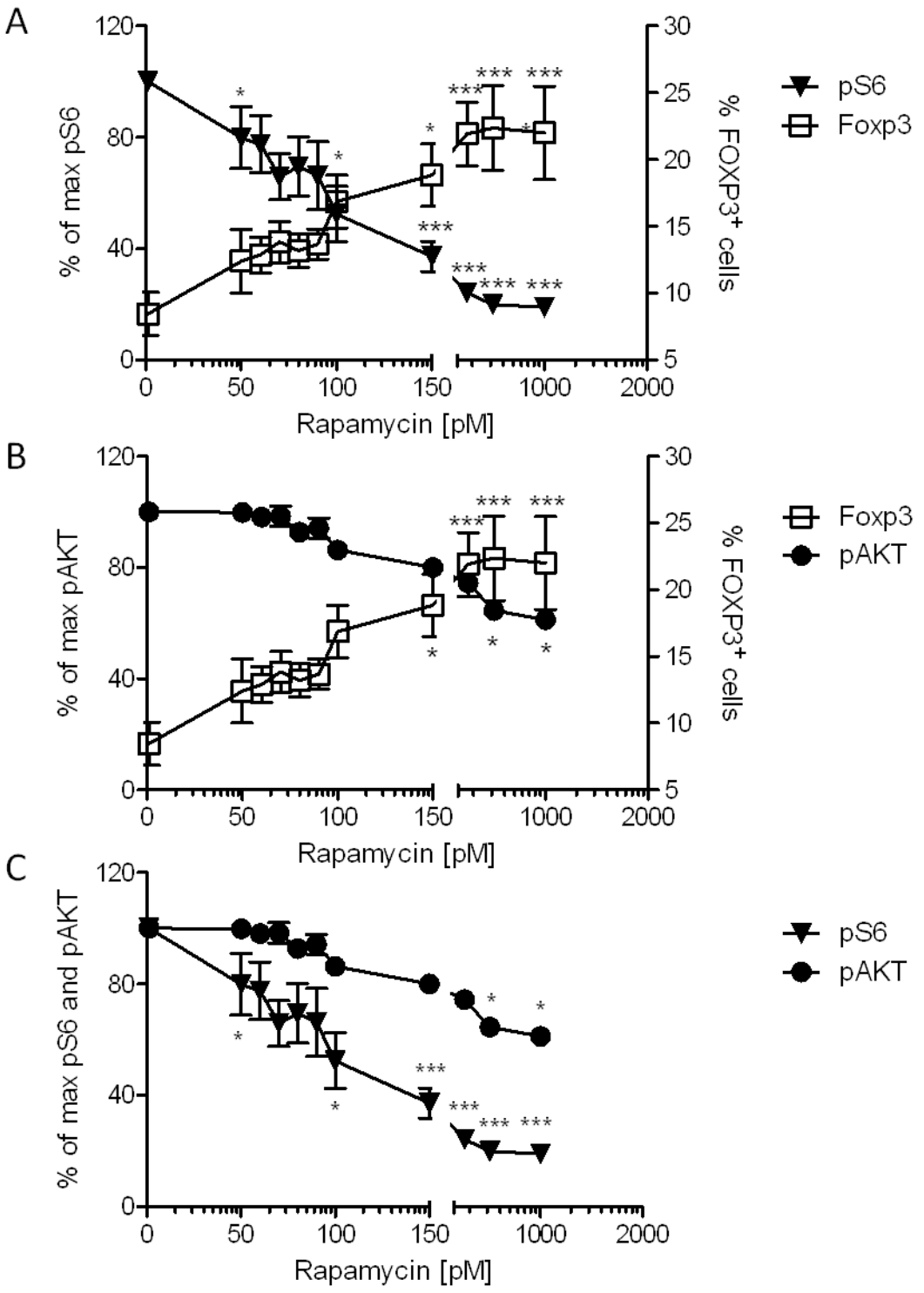


Figure 33. Titration of Rapamycin reveals differential sensitivity of mTORC1 and 2 to the drug and highlights a role for mTORC1 in regulating FOXP3 expression. EL4.B02 cells were stimulated at 10^4 cells/ml for 3 days with αCD3, 0.5ng/ml TGFβ and the indicated concentrations of Rapamycin. Median of pS6 and pAKT was normalized to the levels measured in the absence of Rapamycin. (A-C) Summary of the percentage of $FOXP3^+$ cells and the levels of pS6 and pAKT measured at the different Rapamycin concentrations. Graphs contain data of 4 independent experiments. The mean and the standard error are shown. Statistical analysis was performed by comparing the percentage of $FOXP3^+$ cells and the normalized levels of pS6 and pAKT detected at each Rapamycin concentration to those measured in the absence of Rapamycin using repeated measure one-way ANOVA with Bonferroni's multiple comparison post test (*p<0.05, ***p<0.001).

Chapter 5 | THE DOWNSTREAM TARGETS OF mTOR INVOLVED IN THE INDUCTION OF FOXP3

5.1 | Luciferase assays identify mTOR responsive regulatory elements in the *Foxp3* CNS1 and 2

Having established that inhibition of the mTOR pathway by Rapamycin, Torin 1 and EAA depletion can enhance the induction of FOXP3 in the lymphoma T-cell clone EL4.B02, the cell line system provided the basis for the investigation of the molecular events downstream of the two mTOR complexes leading to the expression of FOXP3.

The identification of 5 conserved non coding sequences (CNS) in the *Foxp3* locus enabled the characterization of the molecular mechanisms that drive the activity of the *Foxp3* promoter. *Foxp3* transcription seems to be tightly regulated by intronic and upsteam enhancer elements. Although the *Foxp3* promoter is engaged by transcription factors necessary for the induction of *Foxp3* upon stimulation with signals such as TGFβ, its full activation seems to be dependent on the formation of supramolecular complexes with proteins that are bound to the enhancer elements (Figure 34A). This interaction between promoter and enhancers was exemplified by Tone et al. who demonstrated that TGFβ induced SMAD3 activation increased *Foxp3* promoter driven luciferase activity only in the presence of CNS1 (containing the SMAD3 binding site) [160]. In contrast to TGFβ, an mTOR responsive element has not yet been defined. The only functional link between PI3K/mTOR inhibition and FOXP3 induction was shown by studies performed by Sauer et al. that detected an increase in permissive histone modifications at the *Foxp3* transcription start site as well as in the 5' untranslated region [124]. Considering the multitude of pathways and factors downstream of mTOR that could potentially act as relay between the mTOR complexes and the activation of

Foxp3 transcription, an identification of the factors involved in the induction using conventional biochemical methods seemed difficult and time consuming. Therefore an approach utilizing *Foxp3* promoter and enhancer driven luciferase constructs was chosen. Analysis of any identified sites could subsequently allow for an identification of mTOR responsive sequences and discovery of factors that are known to interact with these sites (Figure 34B).

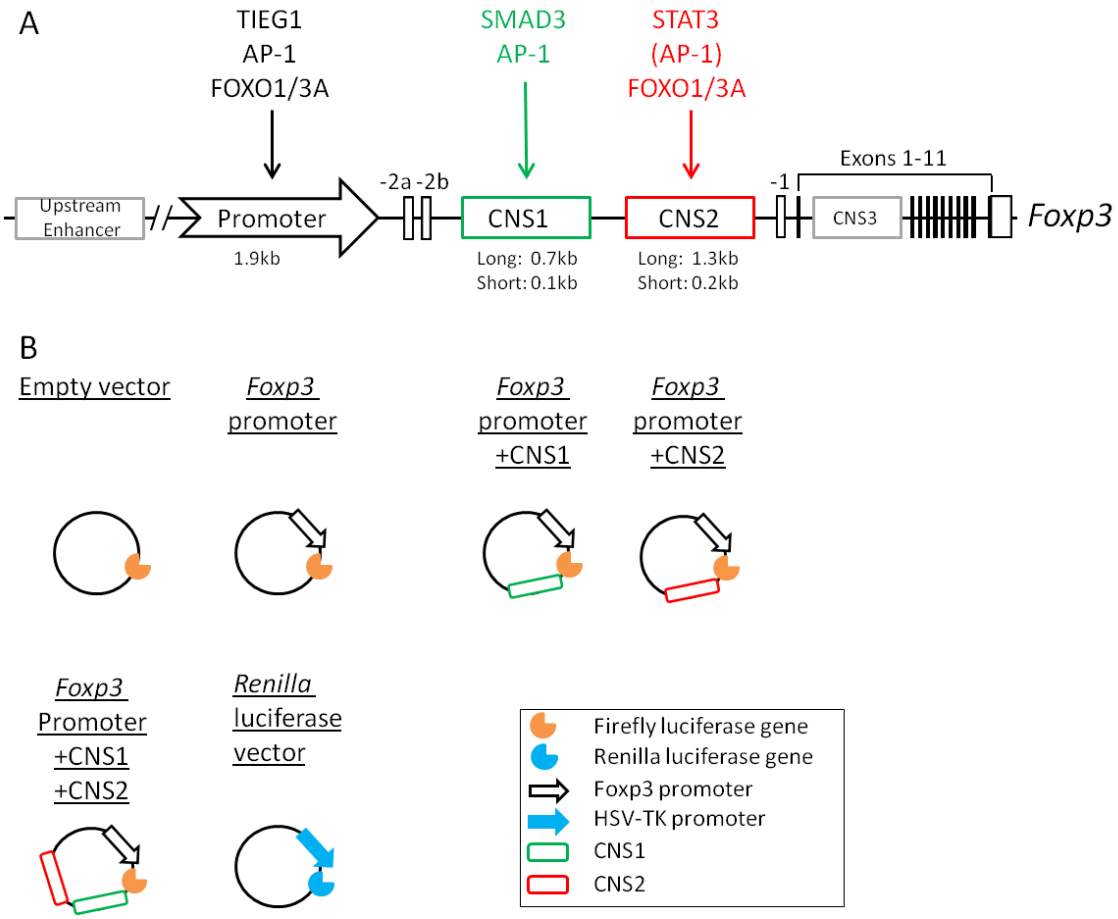


Figure 34. Schematic illustration of the *Foxp3* locus, the transcription factors that bind to the regulatory elements that were investigate and the *Foxp3* luciferase vectors. (A) Location and size of the regulatory regions within the *Foxp3* locus that control *Foxp3* gene expression as well as the location of the *Foxp3* exons are shown (CNS1 and CNS2: Long and short refers to length of the full size and core enhancer sequences used for the firefly luciferase reporter constructs shown in (B)). Above each regulatory element the transcription factors that bind to the respective regulatory element that were investigated are displayed. (B) Schematic illustration of the firefly and *Renilla* luciferase vectors containing the *Foxp3* promoter, CNS1 and/or CNS2.

The basic luciferase constructs containing *Foxp3* promoter and CNS1 and 2 that were used to investigate the effect of mTOR inhibition were based on Promega's pGL4 vector and were kindly provided by Tone et al. Vectors containing only the firefly luciferase gene without any regulatory elements such as promoters or enhancers were used as control vectors to determine background due to any leaky expression of the firelfy gene and to demonstrate that responses induced by the different stimuli were dependent on regulatory elements that have been inserted into these vectors. Each pGL4 firefly construct was cotransfected with a vector containing a thymidine kinase promoter driven Renilla luciferase gene that is constitutively expressed and should result in luciferase protein expression independent of any stimuli that were applied. Since firefly and renilla luciferase use different substrates, the luminescence produced by the enzymatic activity of the two luciferases can be measured in one sample using the Promega Dual Luciferase Reporter Assay. The constitutively expressed Renilla construct was used as a transfection normaliser between the different Firefly constructs. Stimuli dependent changes in the ratio of the two luciferases would therefore indicate transcriptional activation (higher firefly to renilla ratio) or inhibition (lower firefly to renilla ratio). The *Foxp3* promoter sequence in the firefly constructs extended from positions -1702 to +174, the long CNS1 sequence from positions +1988 to +2738 and the long CNS2 sequence from positions +4003 to +5353. The *Foxp3* promoter sequence was cloned directly upstream of the firefly luciferase gene, whereas the CNS1 and CNS2 sequences were inserted downstream of the gene. After transient cotransfection of the firefly and renilla reporter constructs and a stimulation for 16h under various conditions, the cells were lysed and the luciferase activity measured using an automated luminometer.

As expected, the analysis of cells transfected with the empty vector revealed that the expression of luciferase was only marginally affected by the various stimulation conditions. Nevertheless, it is important to note that the statistical analysis indicated that the addition of Rapamycin and Torin 1 significantly increased the ratio of firefly/renilla reporter activity (Figure 35A). The magnitude of the effect (average increase: 1.3 fold) was however very small. Compared to the untreated cells, no significant difference was detected when cells were stimulated with αCD3, TGFβ and Rapamycin or Torin 1. Considering the marginal size of the effect, the findings are still in line with the presumption that a construct without any genetic regulatory elements cannot properly regulate the expression of the firefly gene in response to external stimuli. This statement is further underlined by fact that the analysis of the second control construct that contains only the *Foxp3* promoter whose activity is supposed to be highly dependent on enhancers, does not show the same effect. In contrast, stimulation with αCD3 and αCD3+TGFβ significantly reduced the activity of firefly/renilla compared to untreated and αCD3 stimulated samples respectively (Figure 35B). In summary the reporter control plasmids indicated that the system was to a large extend independent of any stimulation induced changes in the ratio of firefly to renilla luminescence, signifying that the luciferase reporter assay was a valid system to probe mTOR inhibition effects on the transcriptional activation of the *Foxp3* locus.

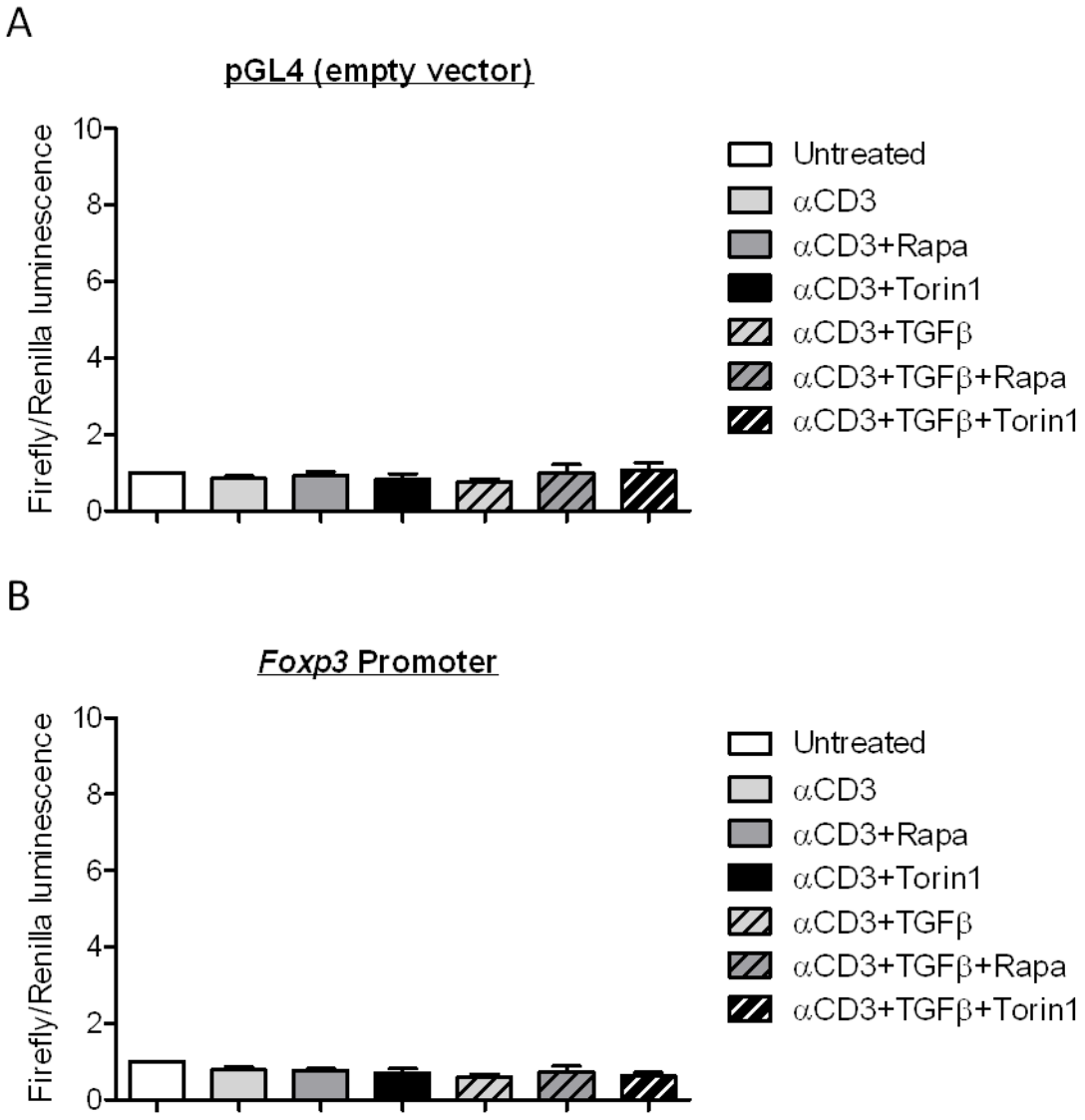


Figure 35. Luciferase control vectors do show any considerable responses upon stimulation. EL4.B02 cells were cotransfected with pTK Renilla luciferase and pGl4 or pGL4 *Foxp3* promoter constructs and stimulated for 16 hours with indicated stimuli (αCD3: as described before, 5ng/ml TGFβ, 5nM Rapamycin (Rapa) and 250nM Torin 1). Renilla and firefly luciferase was measured using the Promega Dual Luciferase Assay and an automated luminometer. The mean and standard deviation of the ratio of firefly to renilla luminescence measured in 4 independent experiments are shown. Means are normalized to untreated cells.

Stimulation of cells transfected with the *Foxp3* promoter+CNS1 (long) construct resulted in profound changes in the ratio of firefly to renilla luminescence. In line with the notion that the *Foxp3* promoter only displays significant activity in the presence of one of the enhancers, a significant increase in the luciferase ratio was measured when the cells were stimulated with αCD3+TGFβ compared to αCD3 stimulation only (Figure

36A, $p<0.05$). This enhanced expression was further increased by the addition of Rapamycin and Torin 1, with the latter inducing a highly significant increase in the ratio of the luciferase signals (Torin 1: $p<0.001$). This clearly indicated an activation of the artificial *Foxp3* locus by mTOR inhibition. The fact that Rapamycin increased the expression, although to a lesser extend, further supported this interpretation. Taking into account the previously demonstrated role for mTORC1 and 2 in regulating the expression of FOXP3 (results chapter 2), the reduced magnitude of the Rapamycin effect could be due to fact that the drug only inhibits mTORC2 activity at later time points during the stimulation, therefore resulting in a less pronounced effect.

The analysis of the *Foxp3* promoter+CNS2 (long) construct that contains a CD3 response element further validated the luciferase reporter assay as a system faithfully reflecting transcriptional regulation of the *Foxp3* locus (Figure 36B). As expected of a CD3 responsive enhancer element, the presence of CNS2 in the construct allowed for a significant CD3 dependent increase in firefly to renilla luminescence ($p<0.01$). Surprisingly, mTOR inhibition by Rapamycin and Torin 1 also significantly enhanced the firefly luciferase activity induced from the promoter CNS2 construct (Rapamycin: $p<0.01$, Torin 1: $p<0.001$). This effect was also detected in the presence of TGFβ, although the response was of a lower magnitude. Nevertheless Torin 1 significantly enhanced the reporter activity even in the presence of TGFβ ($p<0.01$). In line with the results obtained in experiments using the CNS1 containing construct, Torin1 seemed to have a larger effect than Rapamycin. These results indicated that either the *Foxp3* promoter or CNS1 and 2 contain mTOR responsive DNA sequences.

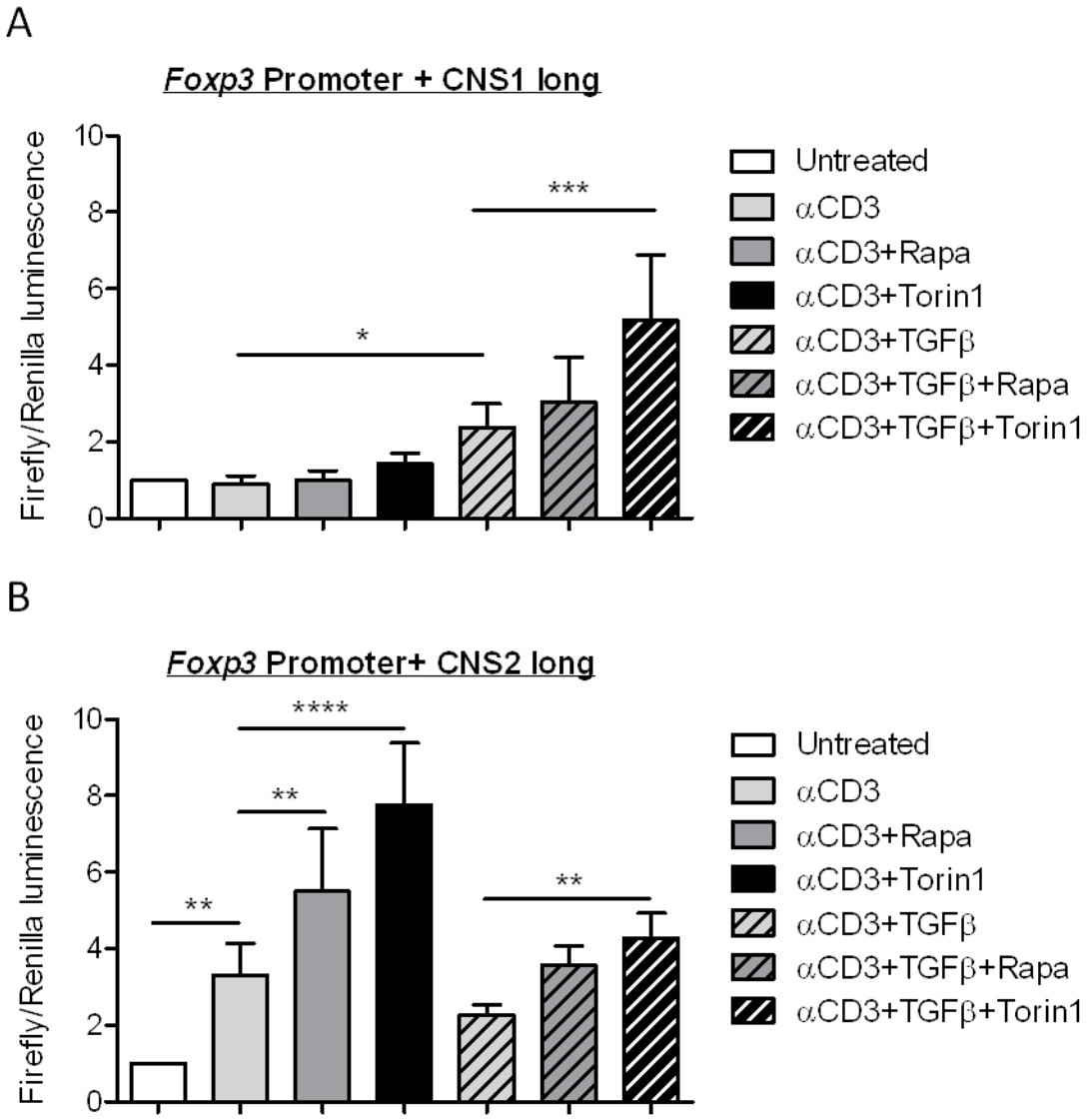


Figure 36. mTOR inhibition enhances TGFβ and αCD3 stimulation induced CNS1 and 2 activation. EL4.B02 cells were cotransfected with pTK Renilla luciferase and pGL4 *Foxp3* promoter+CNS1(long) (A) or pGL4 *Foxp3* promoter+CNS2(long) constructs (B) and stimulated for 16 hours with indicated stimuli (αCD3: as described before, 5ng/ml TGFβ, 5nM Rapamycin (Rapa) and 250nM Torin 1). Renilla and firefly luciferase was measured using the Promega Dual Luciferase Assay and an automated luminometer. The mean and standard deviation of the ratio of firefly to renilla luminescence measured in 4 independent experiments are shown. Means are normalized to untreated cells. Statistical analysis was performed by comparing the firefly/renilla luminescence ratio of the indicated samples using repeated measure one-way ANOVA with Bonferroni's multiple comparison post test (*p<0.05, **p<0.01, ***p<0.001, ****p<0.0001).

Since both enhancer sequences comprised fairly large stretches of DNA that are likely to contain putative binding sites for a multitude of transcription factors, subsequent experiments were performed using considerably shortened enhancer sequences. The

shortened CNS1 sequence ranged from positions +2079 to +2198 and the CNS2 sequence from positions +4287 to +4498 of the *Foxp3* locus.

Encouragingly, both shortened CNS1 and 2+promoter constructs retained their respective responsiveness to TGFβ and CD3 stimulation (Figure 37A and B). In fact the magnitude of the difference between the different stimulation conditions increased considerably, presumably due to the deletion of inhibitory sequences compared to the longer enhancer sequences (Tone et al. personal communications). Consistent with the results obtained with the longer enhancer sequences, mTOR inhibition by Rapamycin and Torin 1 increased the expression of the firefly reporter signal compared to the renilla signal, indicating that the mTOR response elements were still present in the constructs. Indeed, the Rapamycin induced enhancement of transcriptional activation of CNS1 (short)-containing constructs now reached statistical significance ($p<0.05$). Interestingly, the reduced magnitude in cells transfected with CNS2 constructs in the presence of TGFβ was still detectable, signifying that the putatative, inhibitory TGFβ responsive elements were still part of the shortened CNS2 sequence. Nevertheless, mTOR inhibition by Rapamycin and Torin 1 still retained a considerable effect even in the presence of TGFβ.

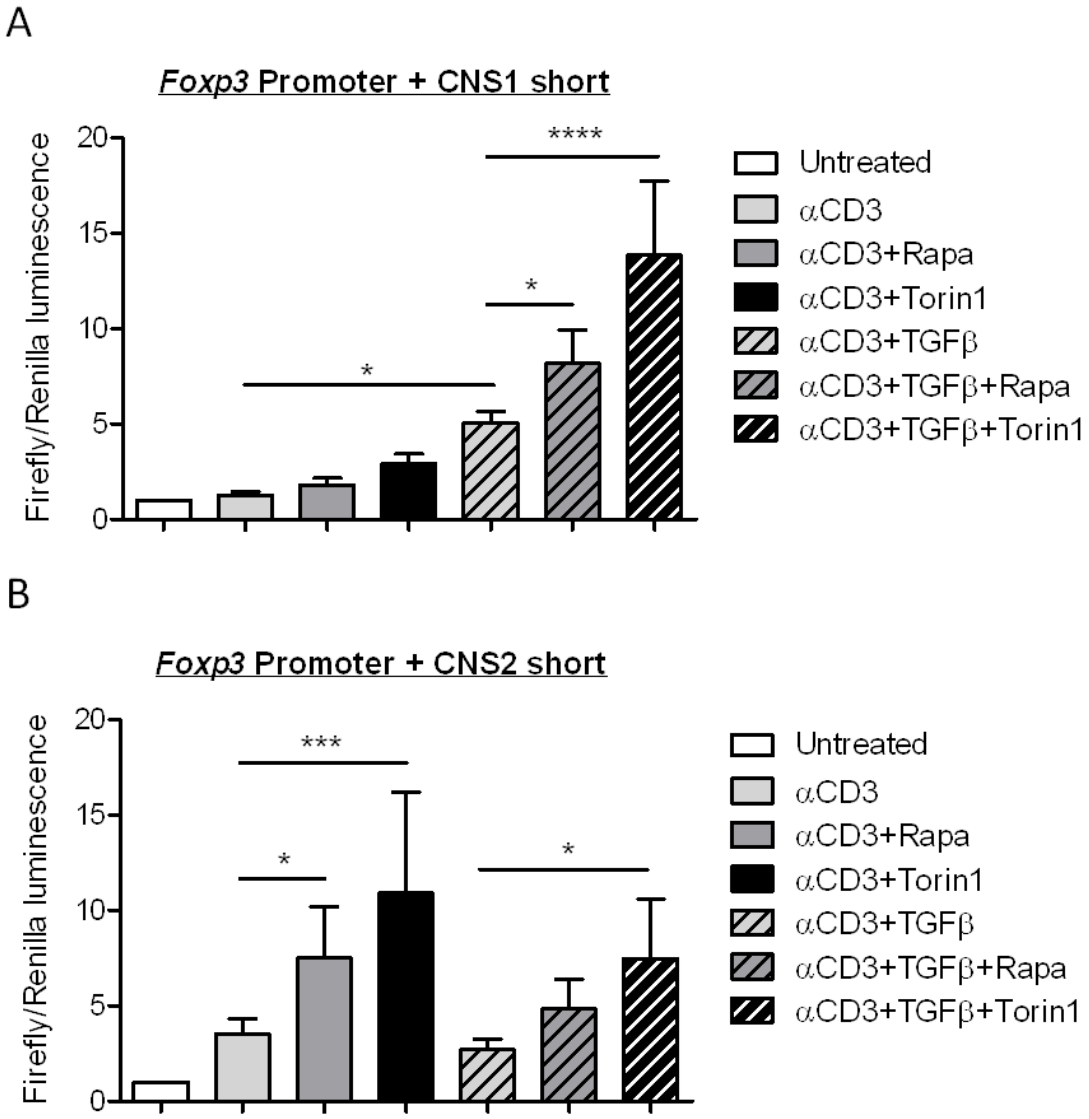


Figure 37. Significantly shortened CNS1 and 2 retain their TGFβ, CD3 and mTOR responsiveness. EL4.B02 cells were cotransfected with pTK Renilla luciferase and pGL4 *Foxp3* promoter+CNS1(short) (A) or pGL4 *Foxp3* promoter+CNS2(short) constructs (B) and stimulated for 16 hours with indicated stimuli (αCD3: as described before, 5ng/ml TGFβ, 5nM Rapamycin (Rapa) and 250nM Torin 1). Renilla and firefly luciferase was measured using the Promega Dual Luciferase Assay and an automated luminometer. The mean and standard deviation of the ratio of firefly to renilla luminescence measured in 4 independent experiments are shown. Means are normalized to untreated cells. Statistical analysis was performed by comparing the firefly/renilla luminescence ratio of the indicated samples using repeated measure one-way ANOVA with Bonferroni's multiple comparison post test (*p<0.05, ***p<0.001, ****p<0.0001).

In summary, the luciferase reporter assays demonstrated that the *Foxp3* promoter and/or both CNS1 and CNS2 sequences appear to contain mTOR responsive elements (besides the known TGFβ and CD3 responsive sequences). By reducing the stretch of CNS1 and CNS2 sequences to ~120bp and ~200bp respectively, whilst retaining CD3, TGFβ and mTOR responsiveness, the number of putatively involved transcription factor binding sites was substantially reduced. Additionally, the experiments confirmed data presented in the previous chapters that mTOR inhibition enhances the induction of FOXP3 by increasing *Foxp3* transcription.

5.2 | AP-1 does not seem to be involved in mTOR mediated induction of FOXP3

A combination of bioinformatic analysis, literature search and personal communication with our collaborators Tone et al. led to the hypothesis that mTOR inhibition might facilitate the induction of FOXP3 by regulating the activity of the transcription factor AP-1. Several AP-1 binding sites have been described in the human and mouse *Foxp3* locus, including the promoter, CNS1 [179] and CNS2 (personal communications with Tone et al.). Whereas the role of the AP-1 sites in the promoter and CNS2 have yet to be characterized, Xu et al. demonstrated that deletion of the CNS1 AP-1 site resulted in markedly reduced transcriptional activation [179], indicating a positive role of AP-1 in the regulation of FOXP3 expression. In line with their findings and reports in the literature that TGFβ and TCR signalling can induce AP-1 activation [179], addition of a JNK inhibitor prevented TGFβ and mTOR mediated FOXP3 induction (data not shown). The functional AP-1 transcription factor is a dimeric complex composed of JUN, FOS or ATF

family members [213]. In the case of FOXP3 expression it is believed that c-JUN activation is important for AP-1 mediate transcriptional activation [179]. In relation to this, Vartanian et al. demonstrated that Rapamycin mediated mTORC1 inhibition can only promote c-JUN homodimer formation by AIP4/ITCH mediated ubiquitination and subsequent proteosomal degradation of JUNB in the setting of quiescent AKT signalling. In their system this process converts the transcription repressing c-JUN/JUNB heterodimer into a transcription activating c-JUN homodimer, resulting in increased transcription of the target gene [214]. Taking into account the previous results demonstrating that Rapamycin mediated mTORC1 and 2 inhibition leads to reduced AKT S473 phosphorylation, indicative of reduced AKT activity, it seemed conceivable that mTOR inhibition could enhance the induction of FOXP3 by allowing JUNB degradation and c-JUN homodimer formation.

In order to assess whether JUNB degradation in the setting of inhibited mTORC1 and 2 complexes was occurring, EL4.B02 cells were stimulated for different durations (0-6h) with αCD3, TGFβ and Torin 1 and both protein amount and localization determined by performing western blots of crude cytoplasmic and nuclear fractions of the differentially treated lysates. Figure 38 illustrates that the 39kDa protein JUNB is mainly located in the cytoplasmic fraction irrespective of the stimulation. Furthermore, no decrease in the mounts of JUNB was detected at any of the time points in any of the stimulations. At least in the time frame that was analyzed, an mTOR inhibition induced, AIP4/ITCH mediated degradation of JUNB can therefore be ruled out.

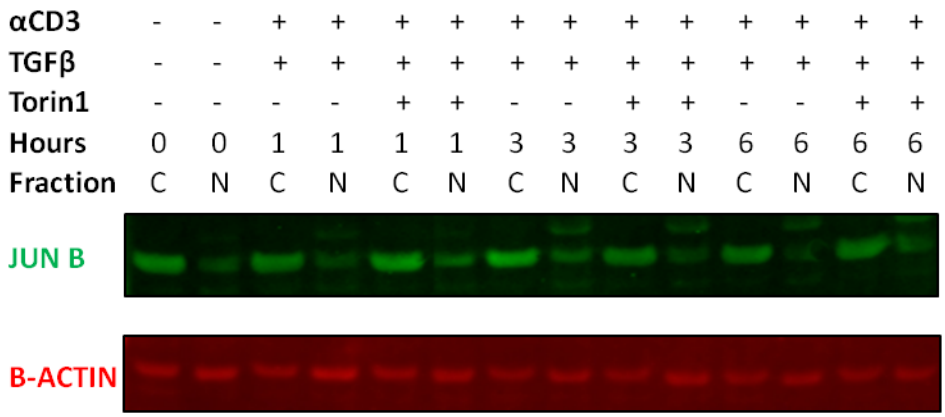


Figure 38. Stimulation with αCD3, TGFβ and Torin 1 does not result in reduced levels of JUN B. EL4.B02 cells were left unstimulated or stimulated for the indicated periods hours with indicated stimuli (αCD3: as described before, 5ng/ml TGFβ, 250nM Torin 1). Crude cytoplasmic (C) and nuclear fractions (N) were prepared. Western blot was probed with αJUN B and αβ-actin and appropriate fluorochrome conjugated secondary antibodies. PVDF membranes were scanned on an Odyssey Infrared Scanner.

Since mTOR inhibition could enhance AP-1 activity by a yet unidentified mechanism and in order to rule out that mTOR inhibition acts on AP-1 to induce FOXP3, two commercially available AP-1 luciferase reporter constructs were obtained. Both constructs, AP1 (1) and AP1(2), contained several repeats of two different typical AP-1 consensus sites upstream of a minimal TA promoter and the TATA box from the Herpes simplex virus thymidine kinase promoter. Whereas AP(1) is designed to monitor induction of AP-1 by SAPK/JNK signalling pathway, AP(2) can serves as a readout for PKC and related pathway mediated AP-1 activation.

Stimulation of cells transiently transfected with the empty vector control did not result in any considerable changes in the ratio of firefly to renilla luminescence at the two time points analyzed (Figure 39A, 24h data not shown). In contrast the AP(1) reporter showed highly significant increases ratio of the luminescence intensity of firefly versus renilla when the cells were stimulated with PMA/Ionomycin for 6h and 24h (Figure 39B, $p<0.001$, 24h data not shown). Furthermore αCD3 stimulation also resulted in a significant activation of the AP-1 reporter construct ($p<0.05$), indicating that CD3

engagement indeed stimulates AP-1 activity presumably through the JNK signalling pathway. Neither TGFβ nor mTOR inhibition by Rapamycin or Torin 1 further increased the activity of AP-1, indicating that mTOR inhibition does not enhance AP-1 activation. Similar results were obtained using the AP1(2) construct, confirming the PMA/Ionomycin induced significant activation of AP-1 (Figure 39C, 6h: $p<0.001$, 24h data not shown). Also the CD3 stimulatory effect was seen with the second construct, but did not reach statistical significance, potentially indicating that CD3 mediated AP-1 activation is mediated to a lesser degree by the PKC pathway. As in the case of the AP1(1) construct, mTOR inhibition did not increase the AP-1 activation measured by the assay any further. Therefore mTOR inhibition mediated AP-1 activation is not likely to contribute to the increased induction of FOXP3 observed in the presence of mTOR inhibitors.

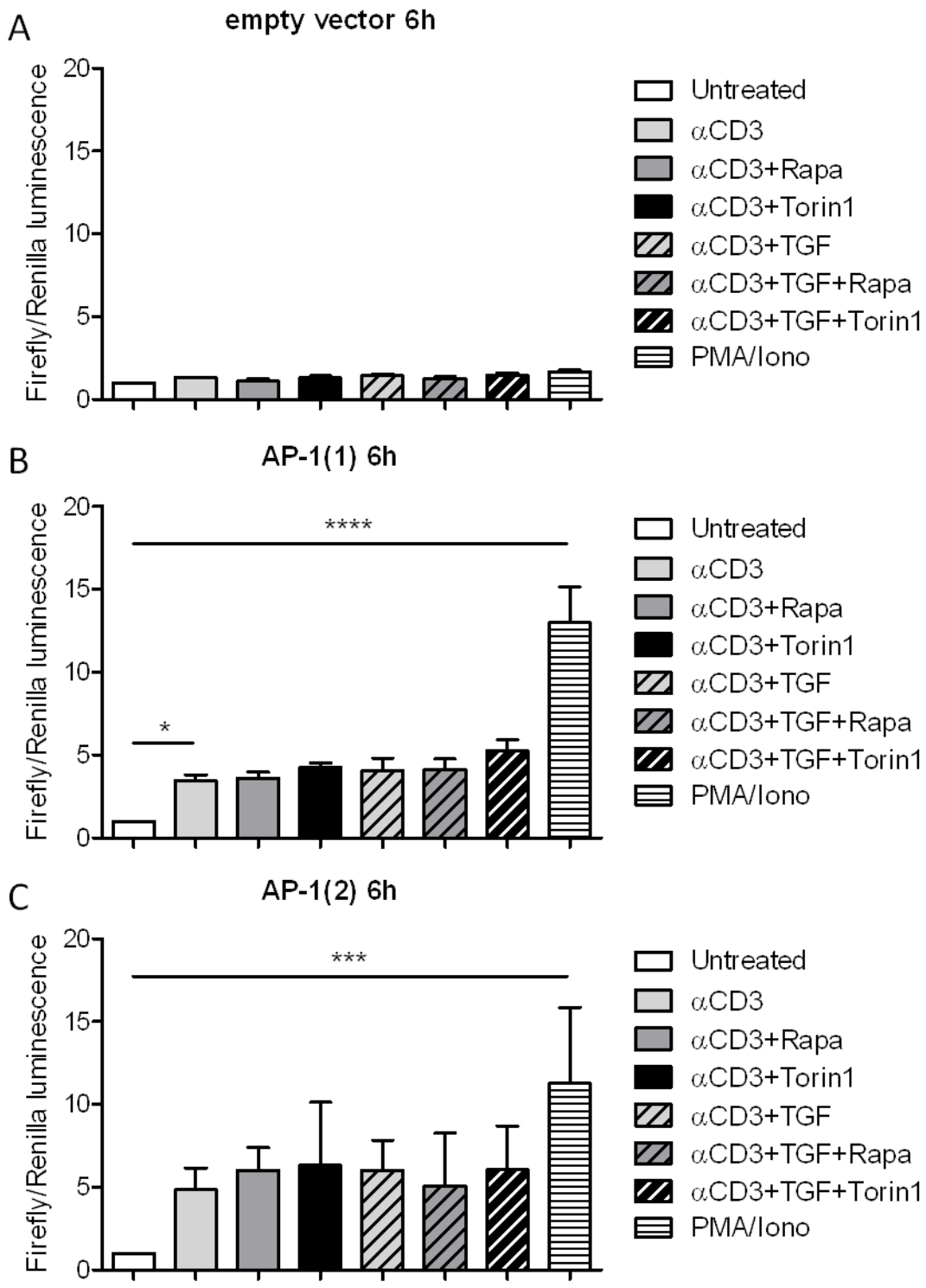


Figure 39. mTOR inhibition does not enhance AP-1 activation. EL4.B02 cells were cotransfected with pTK Renilla luciferase and empty firefly luciferase vector (A), pAP-1(1) (B) or pAP-1(2)constructs (C) and stimulated for 6 hours with indicated stimuli (as described in other luciferase assays, 50ng/ml PMA+500ng/ml Ionomycin). The mean and standard deviation of the ratio of firefly to renilla luminescence measured in at least 3 independent experiments are shown. Means are normalized to untreated cells. Statistical analysis was performed by comparing the firefly/renilla luminescence ratio of the indicated samples using one-way ANOVA with Bonferroni's multiple comparison post test (*p<0.05, ***p<0.001, ****p<0.0001).

5.3 | TIEG1 constitutively localizes to the nucleus and seems to bind to *Foxp3* promoter sequences but neither is affected by mTOR inhibition

Since the luciferase experiments demonstrated an enhancement of activity by mTOR inhibition for both CNS1 and CNS2 containing constructs, the possibility was considered that mTOR inhibition was acting on the *Foxp3* promoter rather than acting on both CNS1 and CNS2 enhancer elements. This hypothesis seemed plausible since the response magnitude of both CNS1 and CNS2 constructs, albeit to different stimuli (TGFβ and CD3), was similarly enhanced by mTOR inhibition.

A number of transcription factors including STAT5, RUNX, c-rel and NFAT have been demonstrated to bind and activate the *Foxp3* promoter [215]. The TGF-β-inducible early gene 1 (TIEG1) is yet another transcription factor known to take part in the activation of F*oxp3* transcription. Venuprasad et al. demonstrated that naïve *Itch*$^{-/-}$ T-cells display impaired TGFβ mediated FOXP3 induction, due to insufficient ubiquitinylation of TIEG1 resulting in decreased *Foxp3* promoter binding and transactivation [170, 216]. Considering the previously mentioned mechanism of mTORC2/AKT inhibition mediated AIP4/ITCH activation [214], it seemed conceivable that mTORC2 inhibition mediated AKT deactivation could result in TIEG1 activation via ITCH-dependent ubiquitinylation.

In order to determine whether TIEG1 induction and/or translocation to the nucleus in response to αCD3 and TGFβ stimulation was affected by mTOR inhibition by Rapamycin or Torin 1, B02 cells were left unstimulated or stimulated with combinations of αCD3, TGFβ and Rapamycin or Torin 1 for different durations (Torin 1: 1-10h, Rapamycin: 8-16h, due to delayed mTORC2 inhibition). Surprisingly, TIEG1 was expressed and

showed nuclear translocation even in the absence of any stimulation (Figure 40A). Furthermore Torin 1 did not induce an increase in nuclear TIEG1 content in the first 6 hours of stimulation. Since the kinetics of induction and translocation might be slower than originally anticipated, lysates of cells stimulated for prolonged periods were analyzed, however, still no effect was detectable (Figure 40B). As for Torin 1, no effect on expression or translocation could be detected in cells stimulated in the presence of Rapamycin, therefore it seemed unlikely that mTOR inhibition regulates TIEG1 expression and nuclear translocation (data not shown).

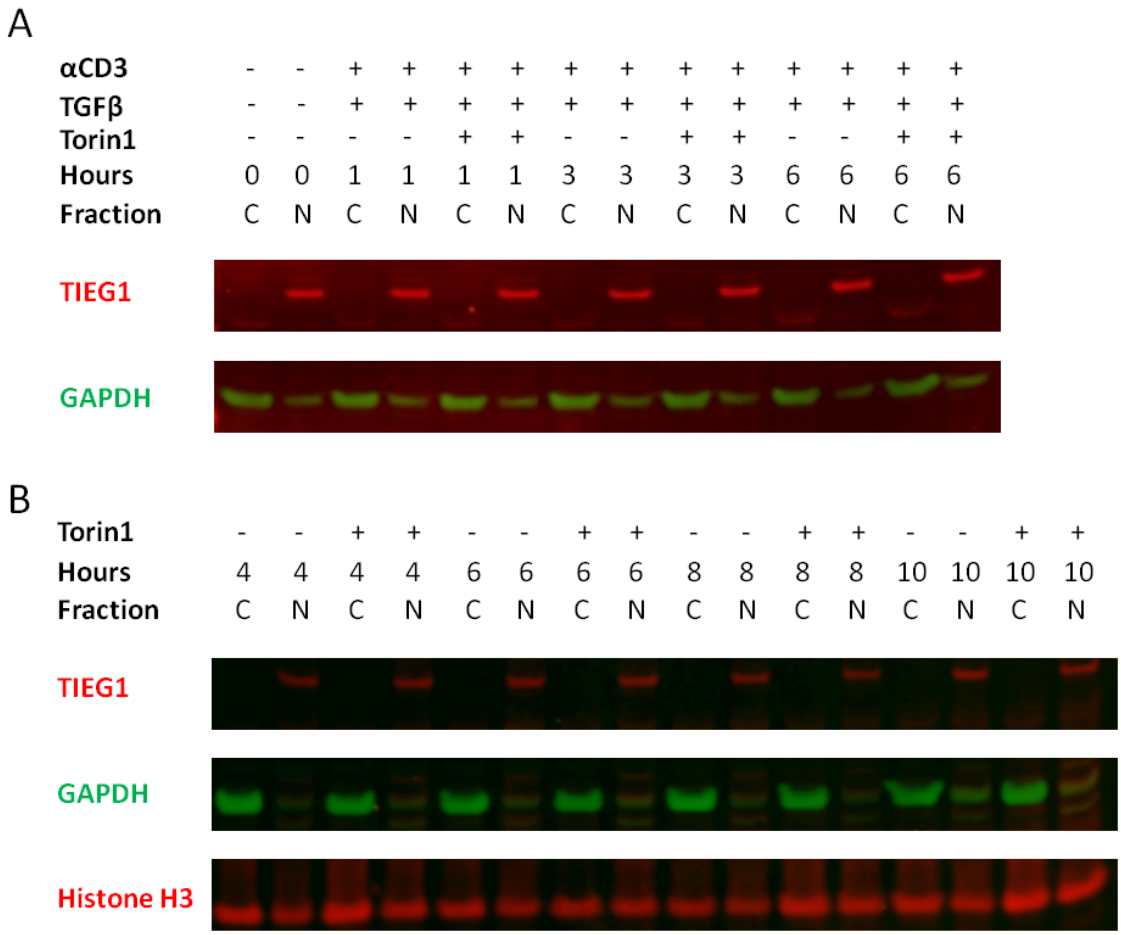


Figure 40. TIEG1 is constitutively expressed and translocated to the nucleus. EL4.B02 cells were left unstimulated or stimulated for the indicated hours with indicated stimuli (αCD3: as described before, 5ng/ml TGFβ, 250nM Torin 1). Crude cytoplasmic (C) and nuclear fractions (N) were prepared. Western blot was probed with αTIEG1, αGAPDH (both (A) and (B)), αHistone H3 (B) and appropriate fluorochrome conjugated secondary antibodies. PVDF membranes were scanned on an Odyssey Infrared Scanner.

Nonetheless, these results did not rule out that TIEG1 activity was modulated by mTOR, i.e. via ITCH mediated ubiquitinylation. Since the analysis of ubiquitinylation of endogenous proteins is difficult and usually requires overexpression of tagged proteins and the addition of proteasome inhibitors, an electrophoretic mobility shift assay (EMSA) that analyses the DNA-binding capacity of TIEG 1 was performed. Venusprad et al. demonstrated TIEG1 binding to a double stranded 42bp oligo containing Foxp3 promoter sequences (-142 to -100) using EMSA and supershift induced by αTIEG1 antibodies. Despite extensive optimization of the buffer conditions as well as careful titration of the amount of nuclear extracts, oligo and superhsift antibody (2 antibodies tested), a TIEG1 supershift was not achieved (data not shown). Unfortunately, it was impossible in the absence of any descriptions of buffer conditions by Venusprad et al. to try to mimic the conditions used in their experiments. Since the demonstration of specificity of binding events in EMSA reactions is crucial, competitor (identical to test oligo but unlabelled and used in excess), scrambled (identical base pair composition in randomized order) and TIEG1 consensus oligos (5 repeats of TIEG1 consensus site GGTGTG) were used in order to test whether certain bands were specific for TIEG1 binding events. Rather than using radioactively labelled oligos, fluorescently labelled oligos were chosen because they are reported to possess superior sensitivity (test oligo: red, competitor oligos: green).

Time course analysis revealed no significant differences between cells stimulated for 0.5-6 hours (data not shown). The analysis of the EMSA indicated that TIEG1 did indeed bind to the *Foxp3* promoter oligo (Figure 41). Whereas no shift of the free double stranded oligo was detected in the absence of any nuclear extracts (lanes 1-3), at least four bands were detected in all lanes containing test oligo only (lanes 4-6). No

difference in the intensity of any of the bands was detected, indicating that the stimulation did not affect any of the binding events. Importantly, the intensity of the free stranded oligo decreased as a consequence of the binding of nuclear proteins to the oligo (weaker signal in bottom band compared to lane 1-3). Addition of excess competitor oligo (lane 7-9) increased the levels of free test oligo to levels seen in the absence of nuclear extracts. The excess competitor oligo almost completely abolished binding events of the test oligo (faint bands 2 and 4), and shows a similar band pattern but expectedly more intense signal in the green channel. In contrast the addition of excess scrambled oligo hardly interfered with any of the binding events of the test oligo, indicating that most of the bands represent specific interactions of proteins with the oligo. This notion is supported by the fact that the scrambled oligo displayed a different band pattern than the *Foxp3* promoter test oligo (with the exception of band 3, lane 10-12). Further evidence that at least bands 1 and 3 might contain TIEG1 protein could be extrapolated from the band pattern observed with TIEG1 consensus oligo (lane 13-15). Since the consensus oligo with its TIEG1 site repeats should pull most of the TIEG1 protein out of the nuclear extracts, the disappearance of bands in the test oligo should indicate TIEG1 containing DNA-protein complexes. Therefore bands 1 and 3 seemed to be composed of TIEG1 protein. The different sizes of the complexes could be due to dimer formation or interaction with other factors resulting in a greater molecular weight. However, in the light of the lack of an αTIEG1 induced supershift this interpretation remains speculative. In order to confirm the presence of TIEG1 the identified DNA-protein complexes could be excised from the gel and analyzed by mass spectrometry. Along the same lines, an oligo mediated pulldown followed by mass spectrometry mediated identification of bound proteins might help

to determine whether TIEG1 or other proteins bind to the *Foxp3* promoter sequences. Irrespective of these findings, it seemed that TIEG1 expression, cellular localization or activity was not affected by mTOR inhibition.

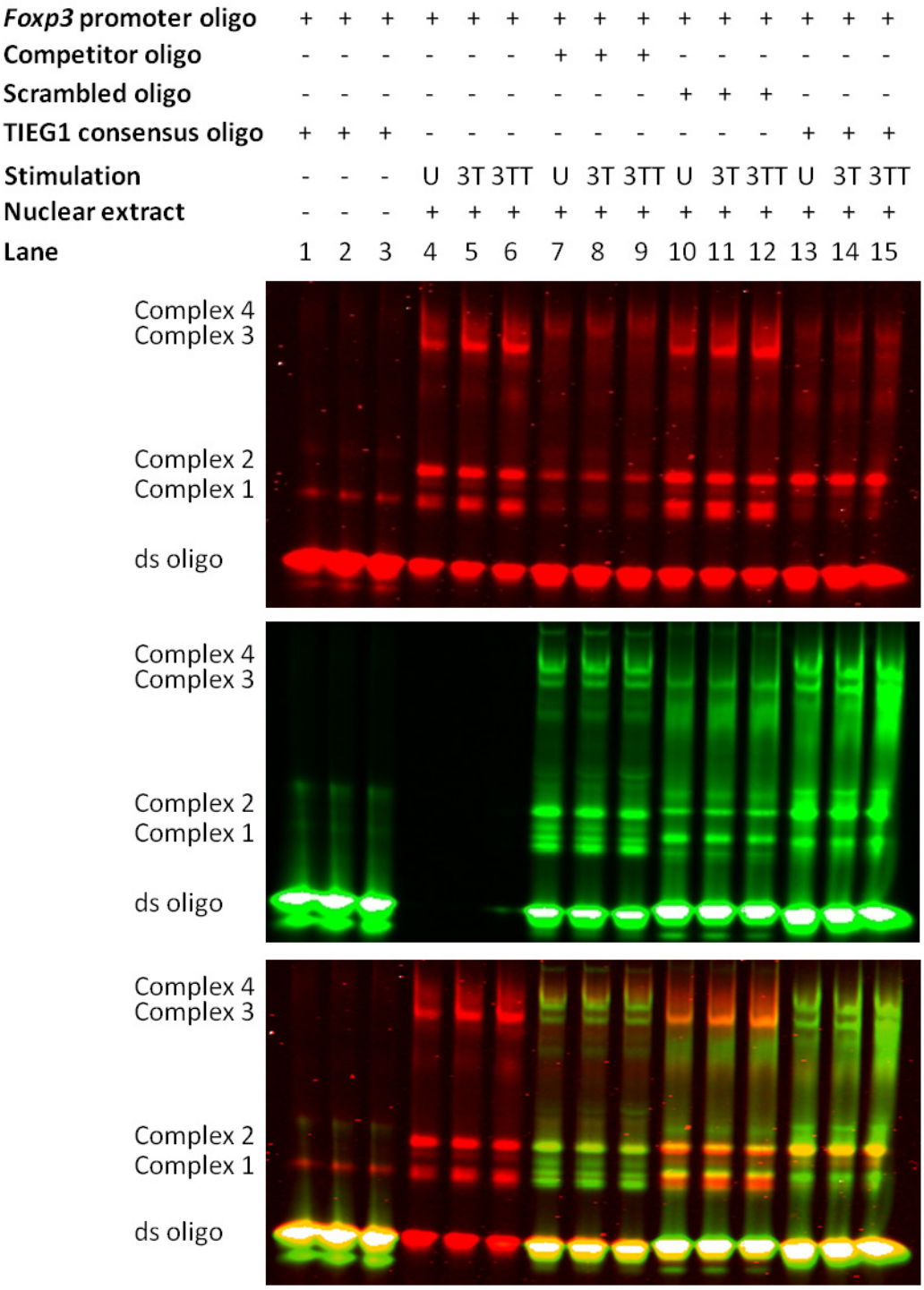


Figure 41. TIEG1 binds to Foxp3 promoter oligos but the binding is not affected by mTOR inhibition. EL4.B02 cells were left unstimulated (U) or stimulated for 6h αCD3+1ng/ml TGFβ without (3T) or with 250nM Torin 1 (3TT) for 6 hours. Crude nuclear extracts were prepared and 5µg of each stimulation incubated with the different oligos for 30min. Competitor, scrambled and TIEG1 consensus oligo (green) were added in 80-fold excess compared to *Foxp3* oligo (red). Samples were subjected to electrophoresis on a 4-16% Bis-tris native gel and imaged using the Odyssey Infrared Scanner. Top image shows band pattern detected in red channel (*Foxp3* oligo only). Middle image shows the competitor, scrambled and TIEG1 consensus oligo in green channel. Bottom image shows the overlay of both red and green channels.

5.4 | SMAD3 phosphorylation at S423/425 is not regulated by mTOR inhibition

Although regulation of factors binding to the *Foxp3* promoter by mTOR represented a plausible explanation of why both CNS1 and CNS2 constructs showed similar responses to mTOR inhibition, it also seemed conceivable that mTOR inhibition was acting on a set of factors that regulate CNS1 and CNS2 activity independently. Since CNS1 is known to be essential for TGFβ mediated iTreg differentiation due to the activity of SMAD3 in activating the enhancer [160], SMAD3 phosphorylation was analyzed in the setting of an inhibited mTOR pathway. The analysis of western blot for SMAD3 phosphorylated at S423/425, a site that is believed to result in transcriptional activation of SMAD3, revealed that pSMAD3 could only be detected in the nucleus of cells stimulated with αCD3 and TGFβ (Figure 42). Simultaneous inhibition of mTOR by Torin1 for 1, 3 or 6h did not affect the level of pSMAD3. Thus, the increased activity of CNS1 containing luciferase constructs by mTOR inhibition was unlikely to be controlled by enhanced SMAD3 activity, although an effect at later time points or on other activating SMAD3 phosphorylation sites could not be ruled out.

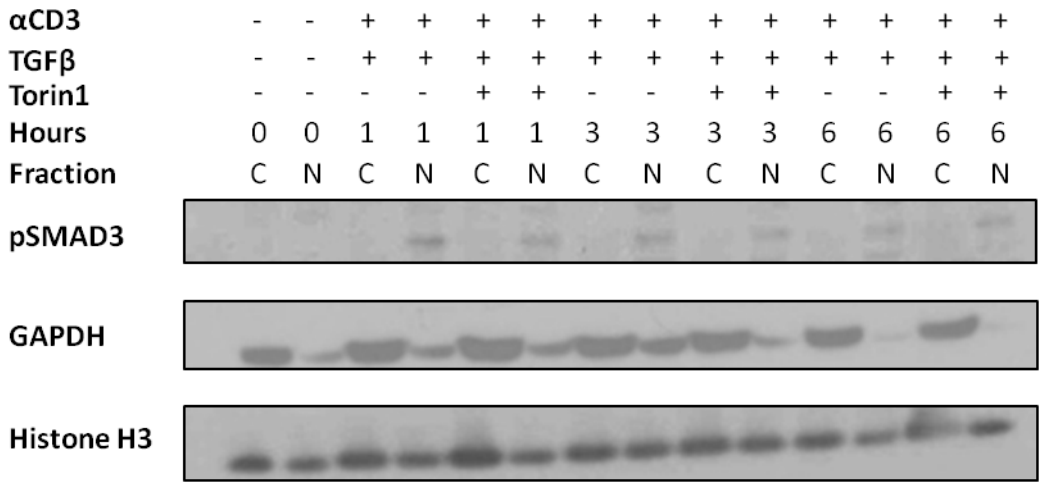


Figure 42. SMAD3 phosphorylation is induced upon stimulation in the nuclear fraction but is unaffected by mTOR inhibition. EL4.B02 cells were left unstimulated or stimulated for the indicated hours with indicated stimuli (αCD3: as described before, 5ng/ml TGFβ, 250nM Torin 1). Crude cytoplasmic (C) and nuclear fractions (N) were prepared. Western blot was probed with αpSMAD3-S423/425, αGAPDH, αHistone H3 and appropriate HRP-conjugated secondary antibodies.

5.5 | The contribution of FOXO1 and FOXO3A to the induction of FOXP3 under mTOR inhibition conditions remains questionable

The forkhead transcription factors, FOXO1 and FOXO3A, are known to be tightly regulated by PI3K/AKT pathway and have been demonstrated to be essential for the induction of FOXP3 and iTreg differentiation [167-169]. Interestingly, Quyang et al. showed using ChIP ananlysis that both FOXO1 and FOXO3A bind the *Foxp3* promoter and CNS2. Considering the intimate link between PI3K/AKT signalling and the mTOR pathway, with AKT acting both upstream of mTORC1 and downstream of mTORC2, mTOR could regulate FOXP3 expression via the FOXO proteins. The activity of FOXO1 and FOXO3A is regulated at several levels but the regulation by AKT mediated phosphorylation that results in the retention of the transcription factors in the cytoplasm, is thought to be an

important mechanism. Therefore is seemed conceivable that mTORC2 inhibition could regulate FOXO translocation by reducing AKT activity.

In order to investigate whether FOXO1, FOXO3A or both are involved in the mTOR mediated FOXP3 induction, the localisation of the two transcription factors was analyzed by immunostaining and confocal fluorescence microscopy. In cells stimulated at low cell density for 24h with αCD3 and 0.5ng/ml TGFβ, FOXO3A was clearly located within the small rim of cytoplasm around the nucleus (Figure 43, top row). Addition of the PI3K inhibitor LY294002, a well established signal inducing FOXO translocation to the nucleus, resulted in translocation in only a small population of cells (Figure 43, middle row, red arrows: nuclear, white arrow: cytoplasmic). A similar but less impressive effect was seen when cells were stimulated in the presence of Rapamycin (Figure 43, bottom row, red arrows: nuclear, white arrow: cytoplasmic).

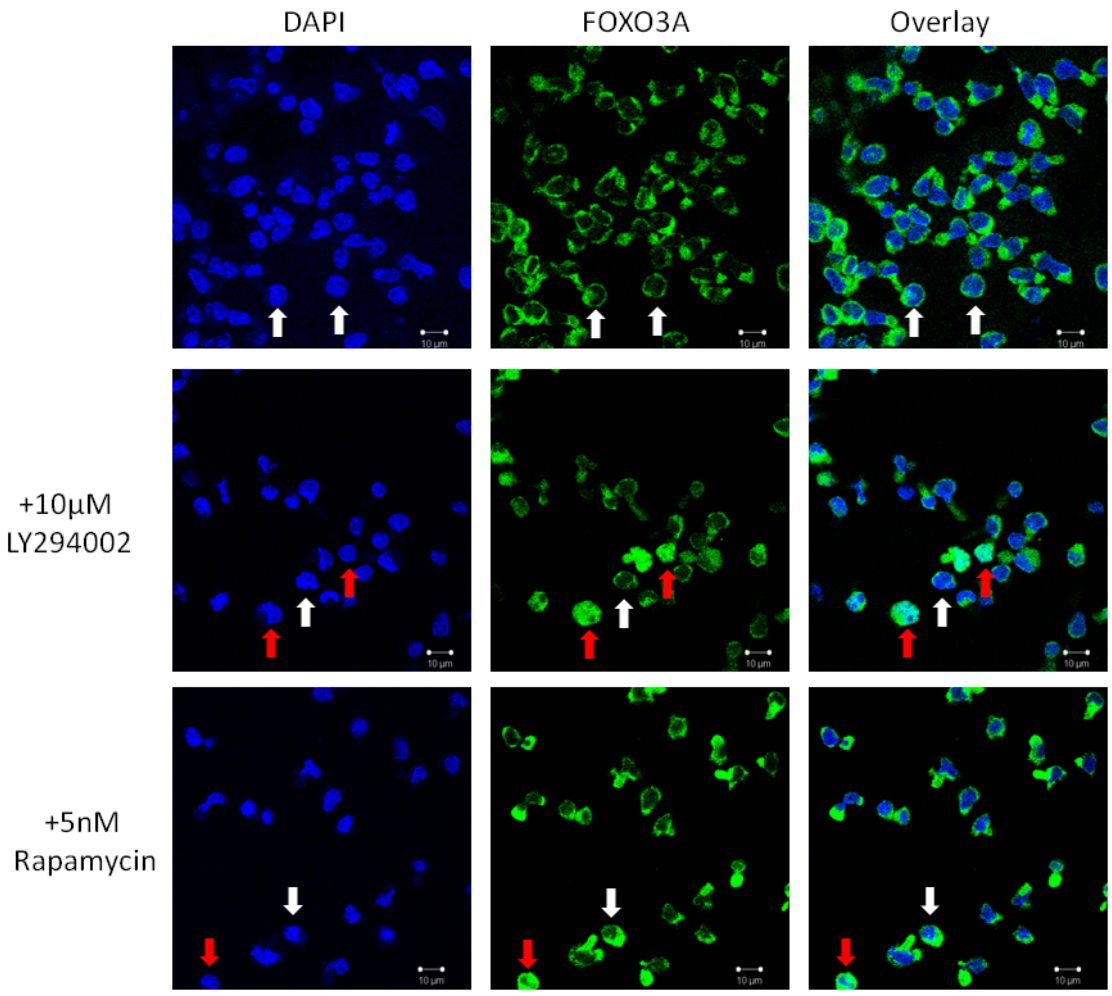


Figure 43. Only few cells translocate FOXO3A to the nucleus in response to PI3K or mTOR inhibition. EL4.B02 cells were left stimulated for 24 hours with αCD3 and 0.5ng/ml TGFβ plus the indicated drugs and stained with DAPI and αFOXO3A plus Alexa488 conjugated secondary antibody. White arrows indicate cells in which FOXO is located in the cytoplasm. Red arrows indicate cells in which FOXO3A is located in the nucleus.

Since the translocation event was not particularly frequent even in the presence of PI3K inhibitor LY294002, cells were stimulated for 48 hours in the hope that the effect might be more pronounced at later time points. Analysis of cells stimulated in the absence of Rapamycin confirmed that both FOXO3A and FOXO1 were exclusively localized in the cytoplasm (Figure 44, 1st and 3rd row respectively). In the case of FOXO1 no nuclear translocation was detected even in the presence of Rapamycin, whereas a small number of cells seemed to have reacted to the Rapamycin stimulus by translocation of FOXO3A. However, the abundance of cells showing this translocation

was very low. Even if only the cells that went on to express FOXP3 translocated FOXO3A to the nucleus, a larger proportion of cells would have been expected to express nuclear FOXO3A. Considering the low frequency of translocation events the attempts to investigate the involvement were temporarily ceased. However in the light of the acquisition of an Imagestream instrument by the department that allows confocal like analysis whilst extending the number of analyzed cells to a statistically robust number, the involvement of FOXO proteins in the mTOR mediated induction of FOXP3 will be revisited. This new technology will also allow for a more detailed analysis of the kinetics of FOXO regulation, which was very laborious using traditional confocal microscopy. On the basis of the data shown here, a conclusive interpretation is not possible.

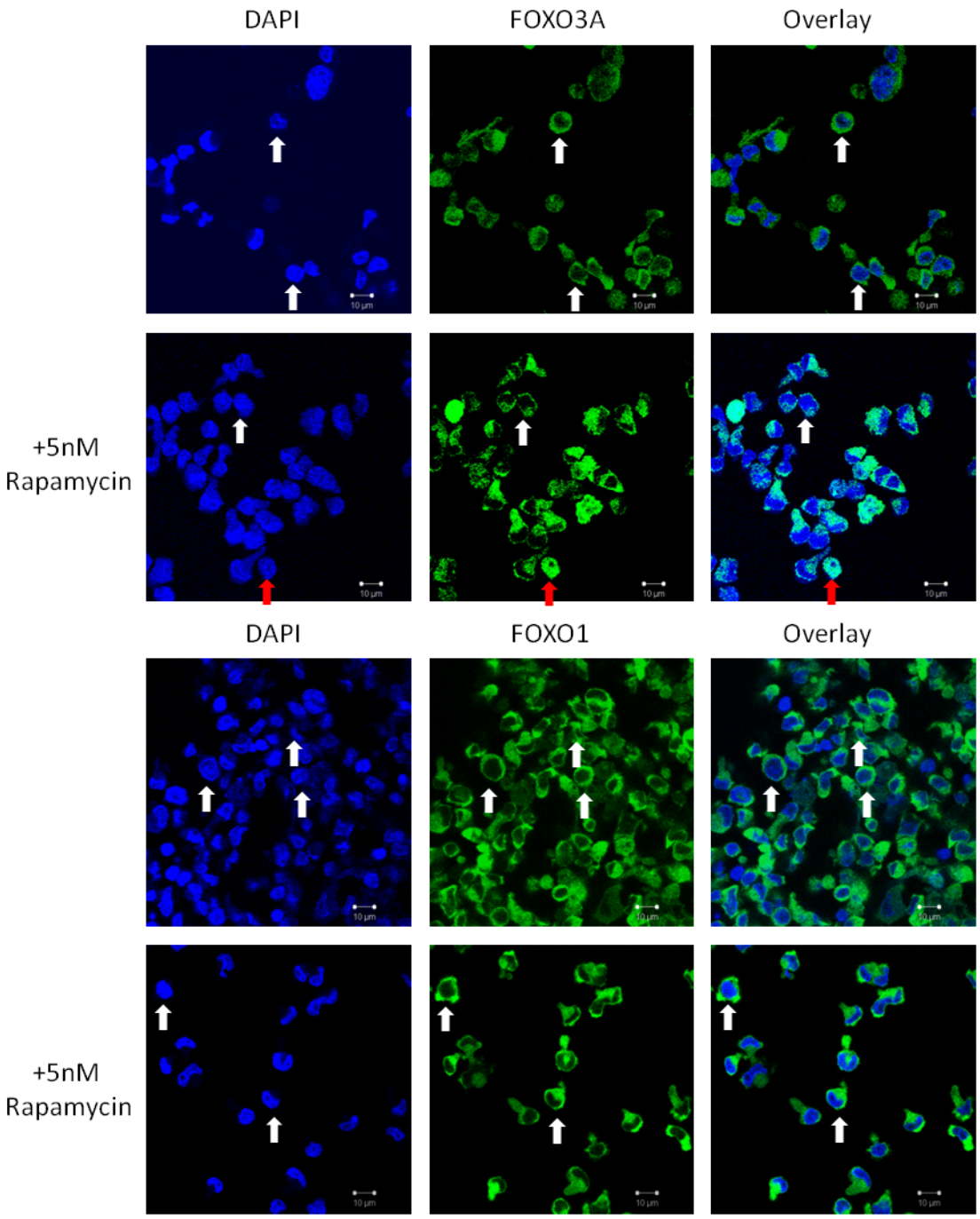


Figure 44. FOXO1 is consistently located in the cytoplasm and only few cells translocate FOXO3A to the nucleus in response to mTOR inhibition. EL4.B02 cells were left stimulated for 48 hours with αCD3 and 0.5ng/ml TGFβ with or without 5nM Rapamycin and stained with DAPI and αFOXO3A or αFOXO1 plus Alexa488 conjugated secondary antibody. White arrows indicate cells in which FOXO3A/FOXO1 is located in the cytoplasm. Red arrows indicate cells in which FOXO3A is located in the nucleus.

5.6 | The serine/threonine phosphatase PP2A does not seem to be involved in the mTOR inhibition mediated induction of FOXP3

Experiments utilizing the PP2A inhibitor okadaic acid demonstrated that PP2A seemed to be activated by TGFβ resulting in reduced phosphorylation levels of the mTORC1 (Figure 17: pS6) and mTORC2 (Figure 27: pAKT) readouts. Since active mTOR signalling has been described to inhibit PP2A activation, it appeared plausible that TGFβ and mTOR inhibition could synergize to enhance FOXP3 induction by activating PP2A.

Addition of increasing amounts of okadaic acid to cells stimulated at low density with αCD3 and TGFβ, did not increase the percentage of $FOXP3^+$ cells that were induced, indicating that TGFβ induced activation of PP2A did not contribute to the induction of FOXP3 by TGFβ (Figure 45). In line with the notion that in the presence of Rapamycin pS6 and pAKT levels should not be affected by PP2A inhibition due to the blockade of mTOR kinase activity, no significant increase in either the mTORC1 and mTORC2 activity readout was measured when okadaic acid was added to cells stimulated with αCD3, TGFβ and Rapamycin (Figure 46). Furthermore PP2A inhibition by okadaic acid did not block the enhancement effect of Rapamycin on the induction of FOXP3, thereby illustrating that mTOR inhibition mediated PP2A activation did not seem to contribute to the induction (Figure 47).

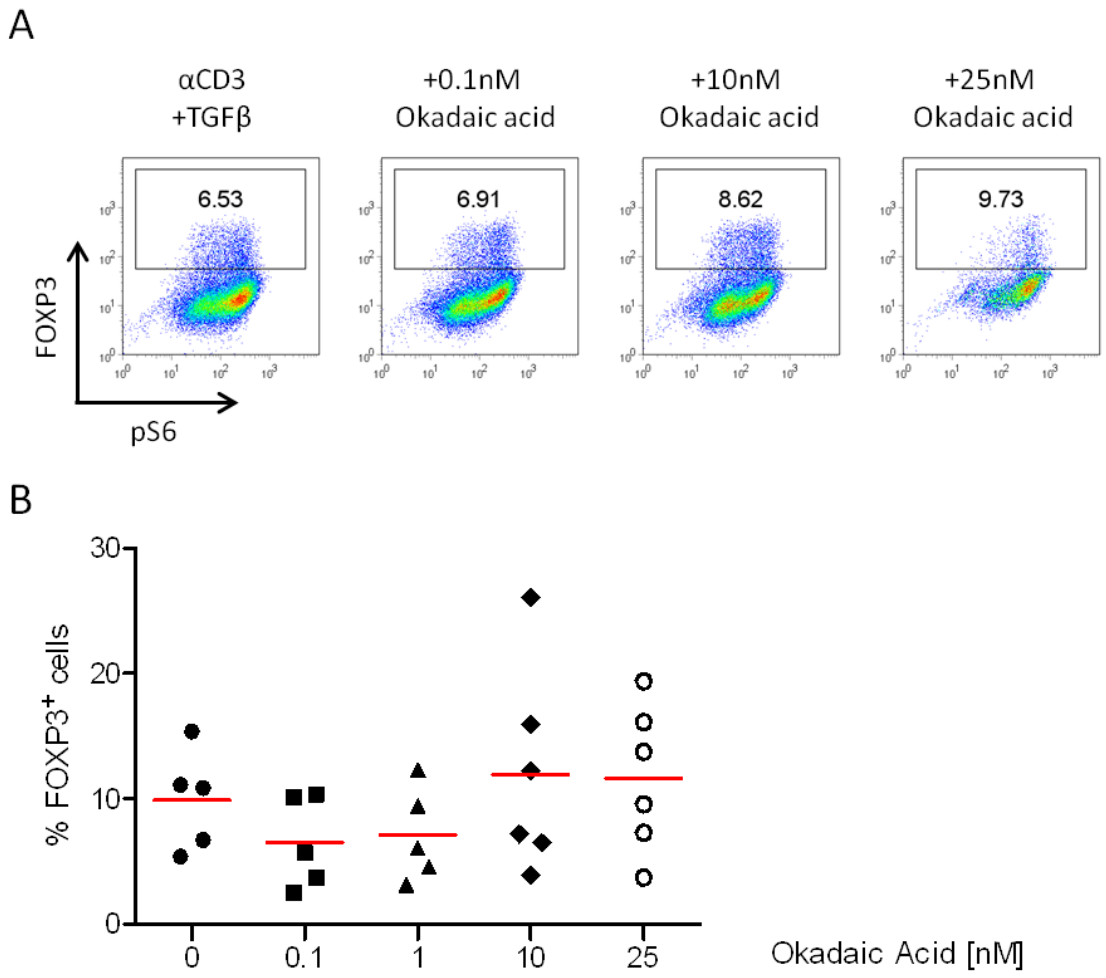


Figure 45. PP2A inhibition does not enhance αCD3 and TGFβ inducted FOXP3 expression. EL4.B02 cells were stimulated at 10^4 cells/ml for 3 days with αCD3, TGFβ and the indicated concentrations of PP2A inhibitor okadaic acid. (A) Representative FACS plots of FOXP3 expression and pS6 levels in live cells (7-AAD low) are shown. (B) Summary of the percentage of $FOXP3^+$ cells measured in the experiments described. Graphs contain data of at least 5 independent experiments. The mean is indicated by a red bar. Statistical analysis was performed by comparing the percentage of $FOXP3^+$ cells obtained without inhibitor with that measured in the presence of the increasing concentrations of okadaic acid using one-way ANOVA with Bonferroni's multiple comparison post test.

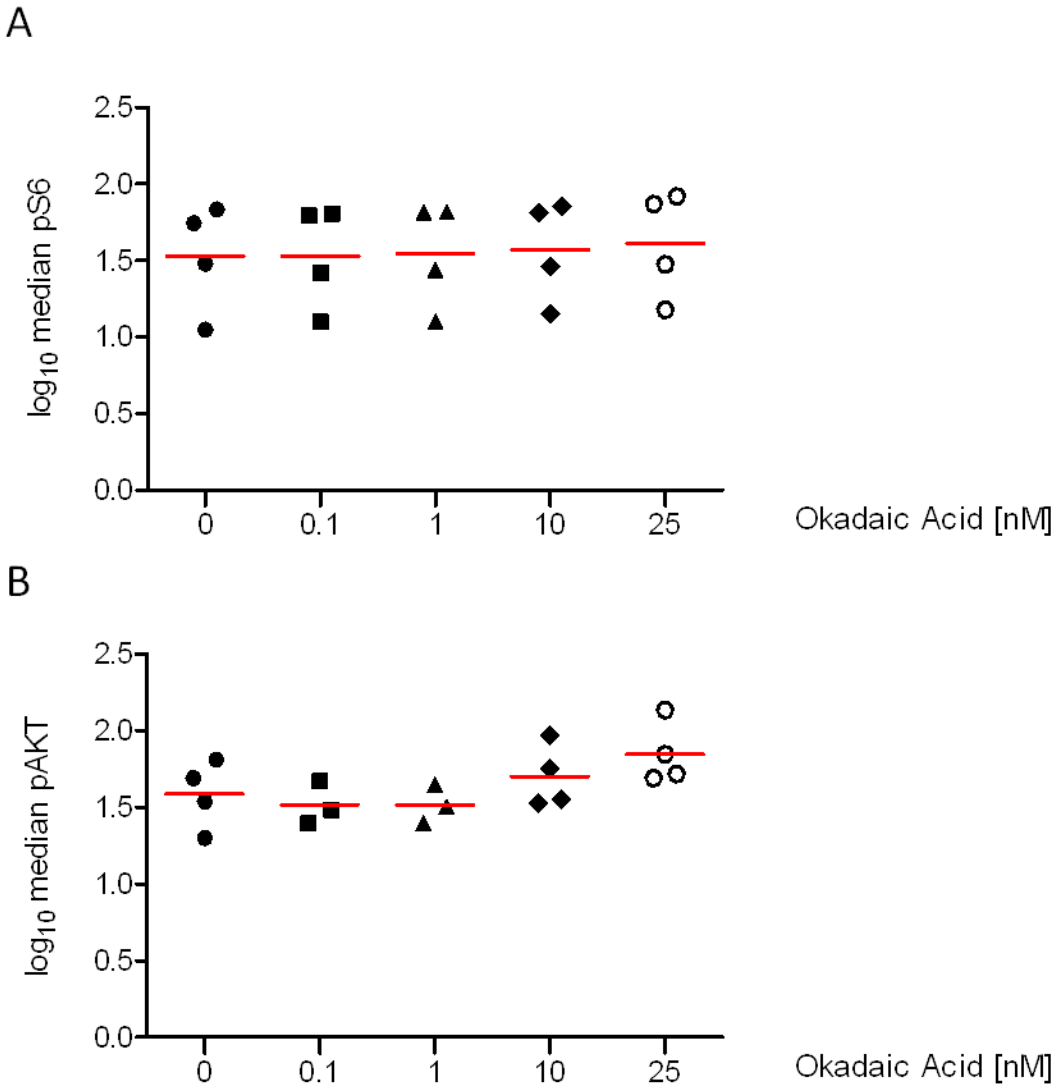


Figure 46. PP2A inhibition does not significantly increase the levels of pS6 and pAKT. EL4.B02 cells were stimulated at 10^4 cells/ml for 3 days with αCD3, TGFβ, 5nM Rapamycin and the indicated concentrations of PP2A inhibitor okadaic acid. (A) Summary of the median of pS6 measured in the experiments described. Graphs contain data of 4 independent experiments. The mean is indicated by a red bar. (B) Summary of the median of pAKT measured in the experiments described. Graphs contain data of at least 3 independent experiments. The mean is indicated by a red bar. Statistical analysis was performed by comparing the percentage of $FOXP3^+$ cells obtained without inhibitor with that measured in the presence of the increasing concentrations of okadaic acid using one-way ANOVA with Bonferroni's multiple comparison post test.

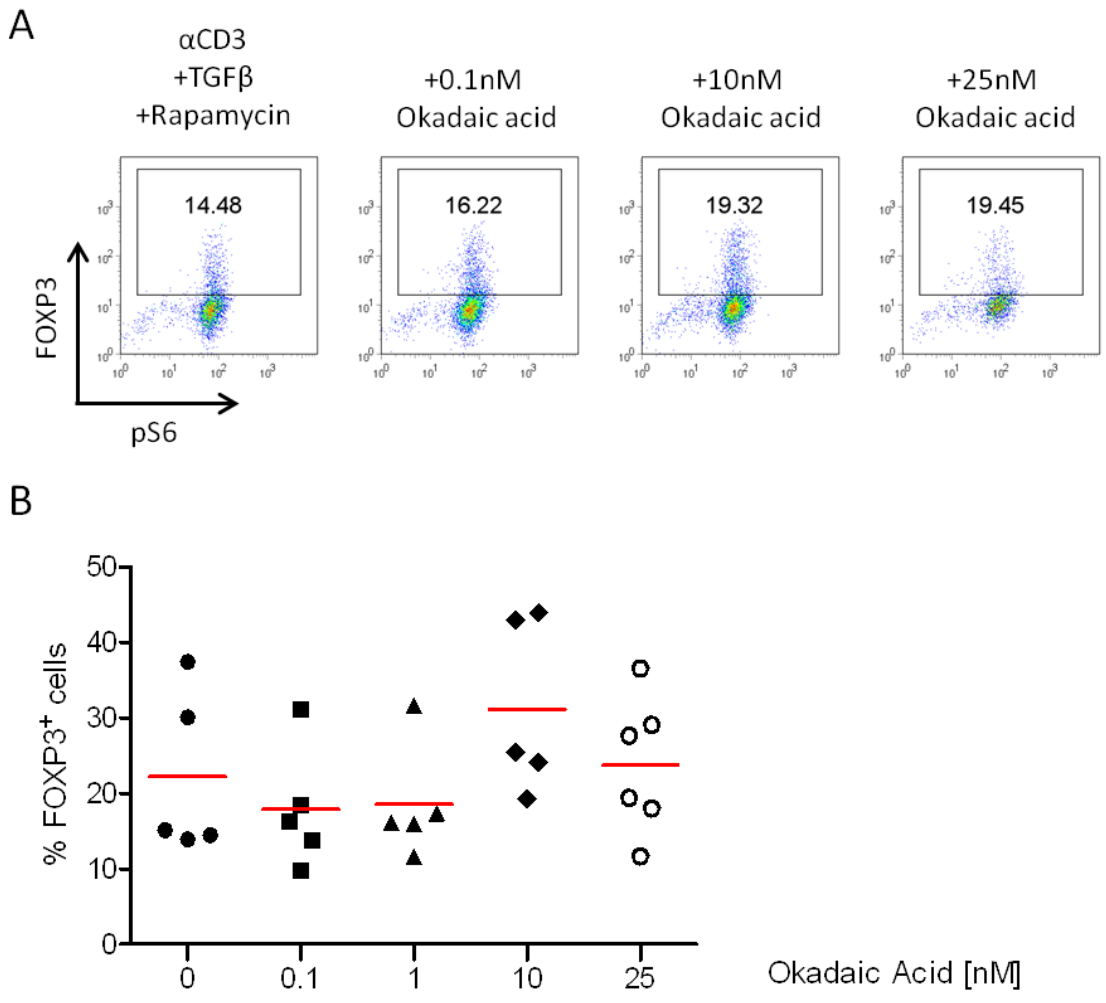


Figure 47. PP2A does not seem to be involved in the Rapamycin mediated enhancement of FOXP3 induction. EL4.B02 cells were stimulated at 10^4 cells/ml for 3 days with αCD3, TGFβ, Rapamycin and the indicated concentrations of PP2A inhibitor okadaic acid. (A) Representative FACS plots of FOXP3 expression and pS6 levels in live cells (7-AAD low) are shown. (B) Summary of the percentage of $FOXP3^+$ cells measured in the experiments described. Graphs contain data of 5 independent experiments. The mean is indicated by a red bar. Statistical analysis was performed by comparing the percentage of $FOXP3^+$ cells obtained without inhibitor with that measured in the presence of the increasing concentrations of okadaic acid using one-way ANOVA with Bonferroni's multiple comparison post test.

5.7 | In the presence of TCR stimulation EL4.B02 constitutively phosphorylates STAT3

Initiated by reports of Xu et al. that the parental cell line EL4 expresses constitutively phosphorylated STAT3, the role of STAT3 in the mTOR mediated induction of FOXP3 was investigated. Since cytokines such as IL-27, IL-23 and IL-6 that are known to activate STAT3, have been demonstrated to inhibit TGFβ mediated FOXP3 induction [174-178, 217], it seemed conceivable that mTOR inhibition could regulate the induction of FOXP3 by negatively regulating STAT3 activation. The molecular mechanism underlying STAT3 mediated FOXP3 repression was described by Xu and colleagues who showed that STAT3 binding to *Foxp3* CNS2 interferes with SMAD3 binding to the CNS1, thereby inhibiting transcriptional activation of the *Foxp3* locus. This mechanism involving CNS2 mediated inhibition of CNS1 could also explain the finding that mTOR inhibition activated both CNS1 and CNS2 containing luciferase constructs to a similar extent (Figure 36 and 37). It is important to note that besides negatively regulating iTreg differentiation, IL-6 induced STAT3 activation was demonstrated to facilitate the differentiation of naive $CD4^+$ T-cells towards the inflammatory Th17 cell subset by binding and activating the *Il-17a and Il-17f* promoters [218]. Therefore mTOR inhibition induced STAT3 inactivation could provide a mechanism that regulates both Th17 and iTreg induction, thereby controlling the balance between inflammatory Th17 and regulatory T cell differentiation.

FACS analysis of cells stimulated with αCD3 antibody confirmed the findings of Xu et al. that EL4.B02, similarly to the parental EL4 cell line, constitutively phosphorylates STAT3 at both Y705 and S727 sites (Figure 48A). The former site is thought to be essential for

STAT3 dimerization and the latter to enhance transcriptional activity [219], indicating that STAT3 proteins in stimulated B02 cells should be fully competent to act as transcriptional regulators. In order to test whether the phosphorylated STAT3 molecules are transcriptional active, the expression of a well characterized STAT3 target gene needed to be analyzed. Considering the T-cell origin of the EL4.B02 clone, *Il-17a* represented an obvious STAT3 target gene. The FACS analysis of EL4.B02 cells stimulated with αCD3, indeed demonstrated that a large proportion of cells expressed high levels of IL-17A upon TCR stimulation (Figure 48B).

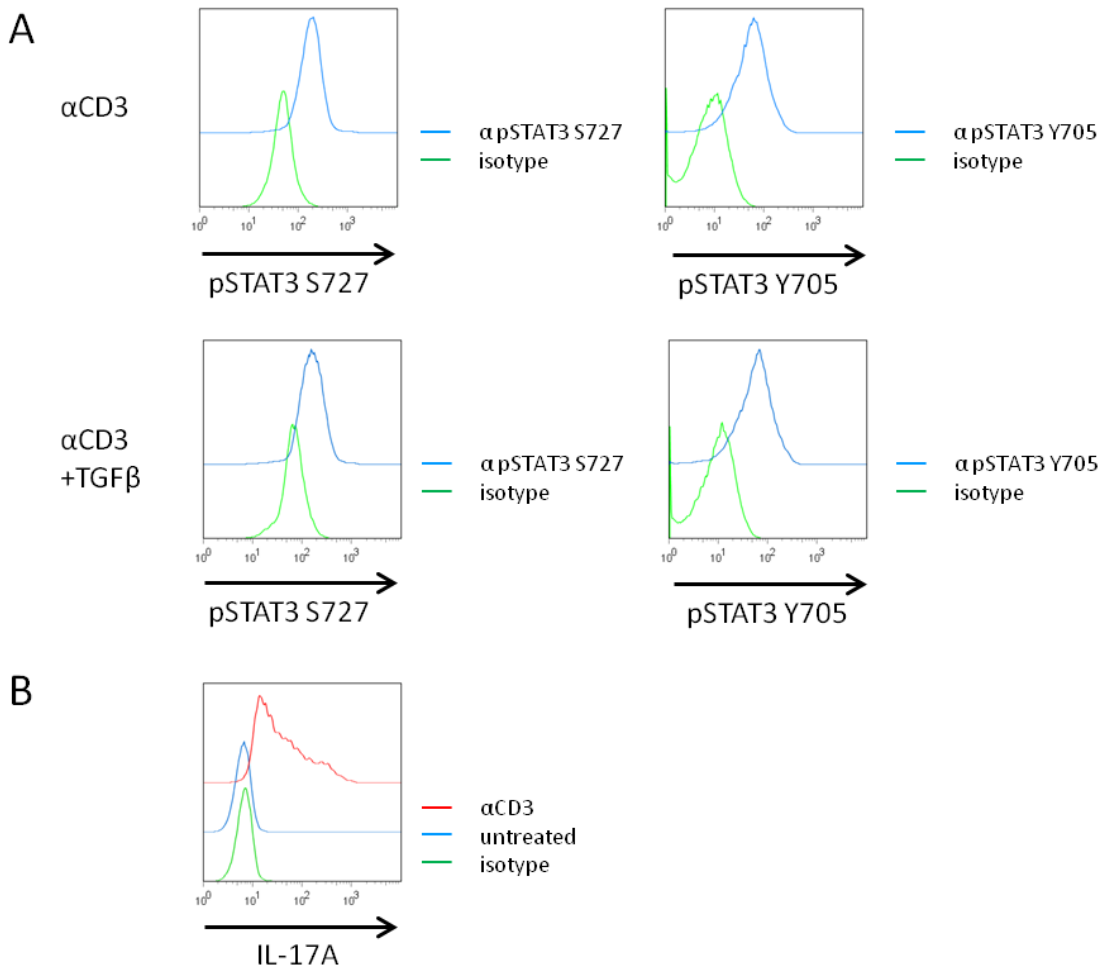


Figure 48. αCD3 stimulated EL4.B02 constitutively phoshporylates STAT3 and expresses high levels of IL-17A. EL4.B02 cells were stimulated at 10^4 cells/ml for 3 days with αCD3 with and without TGFβ (A) Representative FACS plots of pSTAT S727 and Y705 (A) and IL-17A in live cells (7-AAD low) are shown.

5.7.1 | STAT3 phosphorylation and IL-17A expression in EL4.B02 is independent of exogenous IL-6

In order to test whether the addition of exogenous can enhance the phosphorylation of STAT3 or the induction of IL-17A, cells were stimulated for 1 hour with or without 100ng/ml IL-6. The analysis of pSTAT3 levels (Figure 49A) revealed that both S727 and Y705 phosphorylation sites were not affected by the addition of exogenous IL-6. Similarly, the stimulation of cells for 72 hours with αCD3 and with or without IL-6 did not result in increased pSTAT3 levels in the presence of IL-6 (Figure 49B). In line with these results, addition of IL-6 did not increase the proportion of IL-17A expressing cells in cells stimulated with αCD3 and increasing concentrations of IL-6 (Figure 49C, left column).

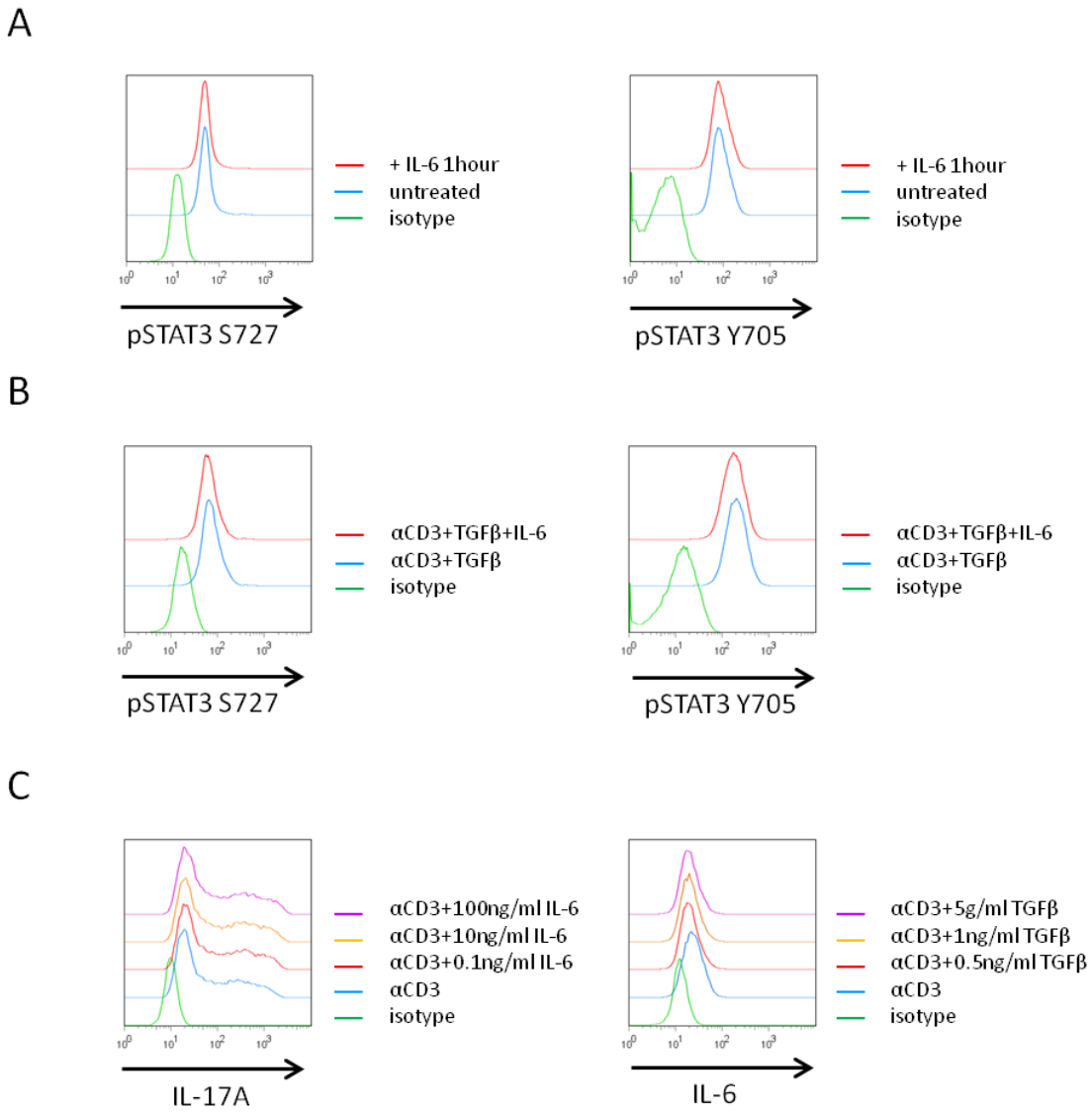


Figure 49. Exogenous IL-6 or TGFβ do not increase STAT3 phosphorylation levels or IL-17A expression.
Representative FACS plots of pSTAT3 S727 and Y705 (A and B) and IL-17A exression in live cells (7-AAD low) are shown. (A) EL4.B02 cells were either left untreated or stimulated at 10^5 cells/ml for 1 hour with 100ng/ml IL-6. (B) EL4. B02 cells were stimulated at 10^4 cells/ml for 3 days with αCD3, 5ng/ml TGFβ and with or without 100ng/ml IL-6. (C) EL4.B02 cells were stimulated at 10^4 cells/ml for 3 days with αCD3 and the indicated concentrations of IL-6 or the indicated concentrations of TGFβ.

Since the constitutive phosphorylation of STAT3 in stimulated B02 cells could result from the production of IL-6 by the cells themselves, the expression of IL-6 was analyzed by intracellular FACS analysis. Indeed, in unstimulated cells (data not shown) as well as in cells stimulated with αCD3 and various concentrations of TGFβ expression of IL-6 was detectable, albeit the levels were very low (Figure 49C, right column). Whether

these low levels of endogenous IL-6 were sufficient to maximally stimulate STAT3 phosphorylation at S727 and Y705 remains to be determined, i.e. by neutralization of the cytokine with an appropriate neutralizing αIL-6 antibody. Irrespective of whether endogenous IL-6 or mutations resulting in constitutive activation of the STAT3 signalling pathway, an event known to contribute to the transformation of cells [220], is responsible for the expression of IL-17A after TCR stimulation, the experiments established that the EL4.B02 clone represents a good model to investigate role of mTOR inhibition in the regulation of STAT3 phosphorylation, IL-17A expression and FOXP3 induction.

5.7.2 | The expression of *Il-17a* mRNA is increased by TGFβ, whereas IL-17A protein expression is largely independent of TGFβ

Earlier experiments have demonstrated that the induction of FOXP3 is highly dependent on TGFβ in the stimulated cultures (Figure 9). Although differentiation of Th17 cells also requires the presence TGFβ, high concentrations of TGFβ have been demonstrated to inhibit the expression of IL-17A and favour the differentiation of $FOXP3^+$ iTreg [221]. Because a simultaneous analysis of the effect of mTOR inhibition on IL-17A and FOXP3 would only be feasible if IL-17A expression can be induced in the presence of sufficient TGFβ to induce FOXP3 in EL4.B02 cells, cells were stimulated in the presence of different concentrations of TGFβ and their IL-17A and FOXP3 expression analyzed. The experiments illustrated in figure 50A and B showed that the induction of IL-17A protein, in contrast to that of FOXP3, was independent of exogenous TGFβ. The analysis of *Il-17a* mRNA levels in a time course experiment,

however revealed that addition of intermediate concentrations of TGFβ did enhance the induction of *Il-17a* (Figure 50C, 12 and 36h: $p<0.05$, 24 and 48h: $p<0.01$). The enhancement is only about 2-fold for *Il-17a* message across all time points, which may not directly correlate with protein expression, particularly as this is primarily observed as an increase in the proportion of IL-17A$^+$ cells.

Irrespective of the apparent discrepancy of the TGFβ induced *Il-17a* mRNA and IL-17A protein expression, the fact that IL-17A was induced at high levels in the presence of TGFβ allowed an analysis of effect of mTOR inhibition on IL-17A and FOXP3 induction.

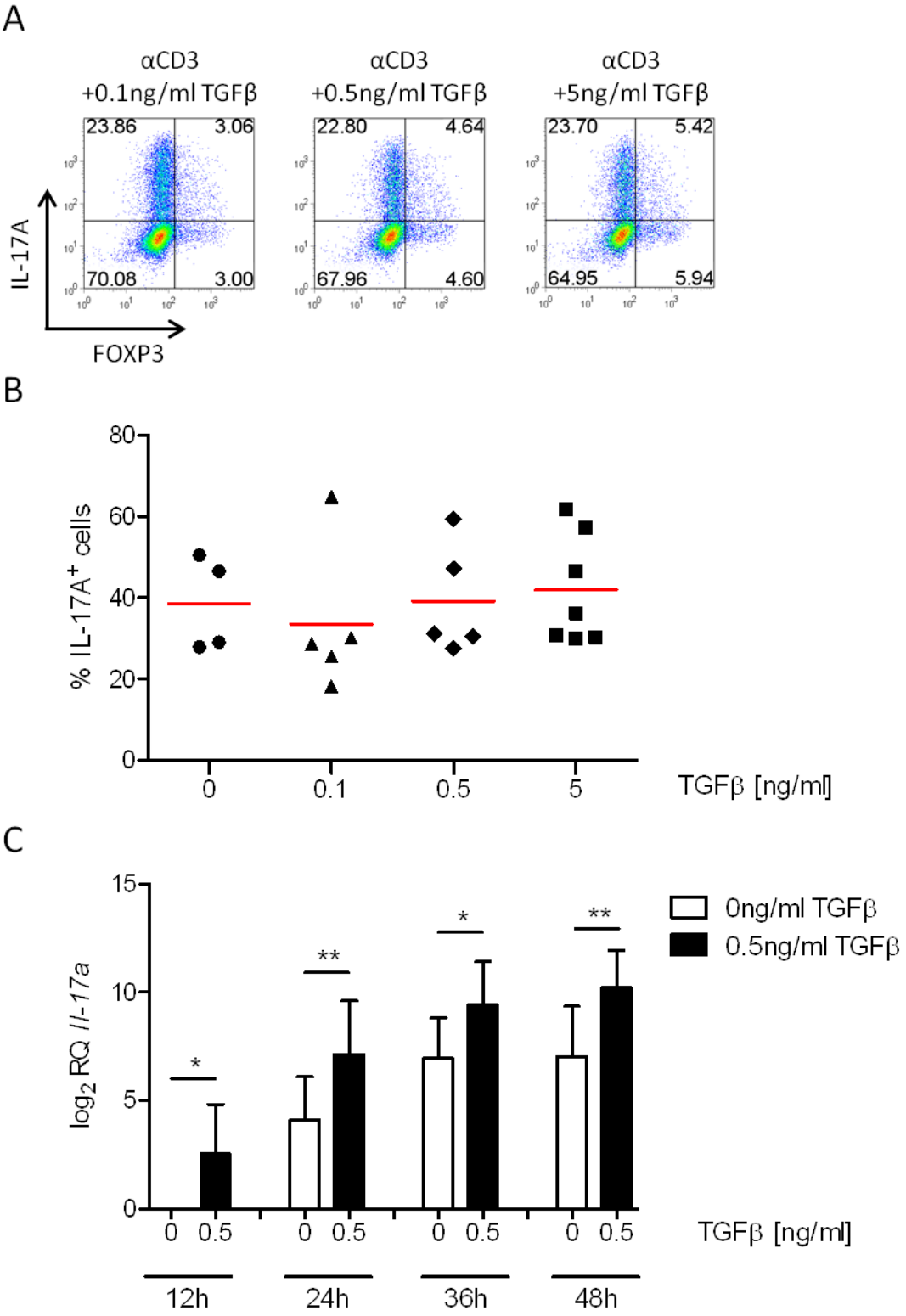


Figure 50. IL-17A protein expression but *Il-17a* mRNA levels is independent of TGFβ. (A and B) EL4.B02 cells were stimulated at 10^4cells/ml for 3 days with αCD3 and the indicated TGFβ concentrations. (A) Representative FACS plots of FOXP3 and IL-17A expression in live cells (7-AAD low) are shown. (B) Summary of the % IL-17A$^+$ cells measured at day 3. Graphs contain data of at least 4 independent experiments. The mean is indicated by a red bar. (C) Real-time PCR analysis *Il-17a* expression in cDNA samples prepared from EL4.B02 stimulated at low density. Data was normalized to *Hprt1* and is presented relative to cells stimulated at 10^4 cells/ml with αCD3 for 12 hours. Mean and standard deviation of 4 biological replicates is presented. Statistical analysis was performed by comparing the percentage of IL-17A$^+$ cells (B) or *Il-17a* levels (C) in the absence of TGFβ to the values with TGFβ using one-way ANOVA with Bonferroni's multiple comparison post test (*p<0.05, **p<0.01).

5.7.3 | mTOR inhibition by Rapamycin reduces the levels of pSTAT3 and reduces the proportion of IL-17A$^+$ cells

Evidence for a role of mTOR in the regulation of STAT phosphorylation is presented by studies demonstrating that immunoprecipitated mTOR can phosphorylated S727 *in vitro*, that this phosphorylation event is Rapamycin sensitive and depends on the presence of AA [222, 223]. In the case of Y705 phosphorylation of STAT3, however, a direct phosphorylation by the serine/threonine kinase mTOR seemed unlikely and it is probably mediated via an mTOR downstream target. Studies utilizing T-cell specific mTOR knock-out mice, however, have demonstrated that, in the absence of mTOR Y705 phosphorylation of STAT3 is markedly reduced [136].

In order to determine whether Rapamycin affects the phosphorylation of STAT3, cells were stimulated with αCD3 and various concentrations of TGFβ in the presence or absence of Rapamycin. The FACS analysis of pSTAT3 S727 revealed that although Rapamycin consistently reduced the levels of the phosphorylation events at the serine site, the effect did not reach statistical significance (Figure 51A and C, $p>0.05$). In the case of phosphorylation events at Y705 of STAT3, however, Rapamycin caused a significant reduction in the levels of pSTAT3 compared to those detected in absence of Rapamycin (Figure 51B and D, 0-1ng/ml TGFβ: $p<0.01$, 5ng/ml: $p<0.001$). This inhibition of tyrosine phosphorylation of STAT3 was detected at all TGFβ concentrations.

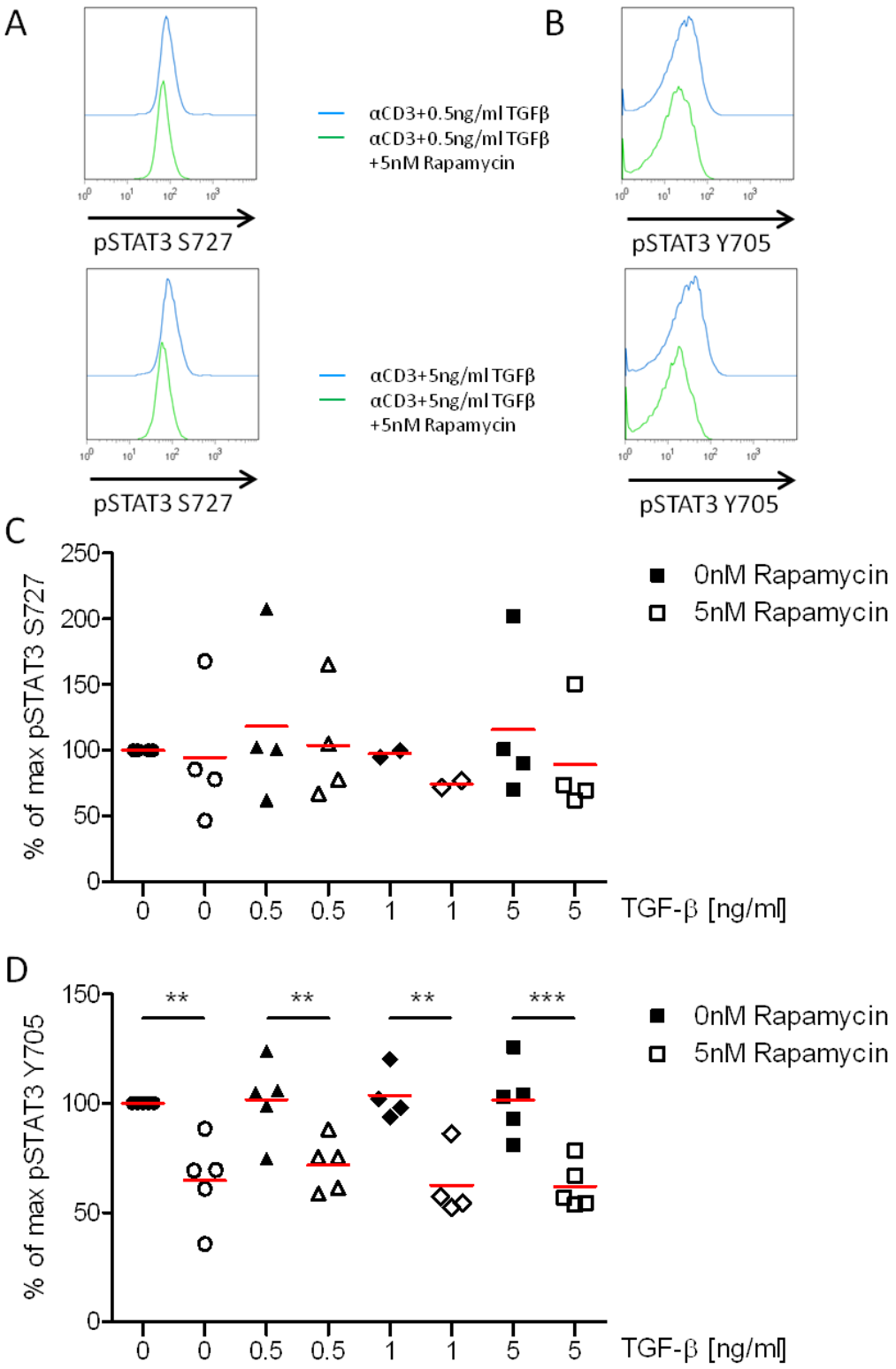


Figure 51. Rapamycin reduces the levels of STAT3 phosphorylation. EL4.B02 cells were stimulated at 10^4 cells/ml for 3 days with αCD3, the indicated TGFβ concentrations and with or without 5nM Rapamycin. Representative histograms of pSTAT S727 (A) and Y705 (B) are shown. (B and C) pSTAT3 levels at 0ng/ml TGFβ and in the absence of Rapamycin were set to 100%. (C) Summary of the normalized pSTAT3 S727 levels measured at day 3. Graphs contain data of at least 2 independent experiments. The mean is indicated by a red bar. (D) Summary of the normalized pSTAT3 Y705 levels measured at day 3. Graphs contain data of at least 4 independent experiments. The mean is indicated by a red bar. Statistical analysis was performed by comparing the normalized pSTAT3 at the different TGFβ concentrations to the values obtained at the same TGFβ concentration with Rapamycin using one-way ANOVA with Bonferroni's multiple comparison post test (**p<0.01, ***p<0.001).

The validity of this finding was confirmed by western blot analysis of cell lysates from primary $CD4^+FOXP3^-$ T-cells stimulated with αCD3, αCD28, IL-2, TGFβ and IL-6 or Rapamycin (Figure 52). Whereas the addition of IL-6 resulted in marked increase in Y705 phosphorylation, S727 phosphorylation levels were surprisingly not affected. Rapamycin on the other hand reduced both Y705 and S727 phosphorylation induced by αCD3, αCD28, IL-2, TGFβ stimulation, highlighting that Rapamycin mediated mTOR inhibition also affects STAT3 phosphorylation in primary $CD4^+$ T-cells.

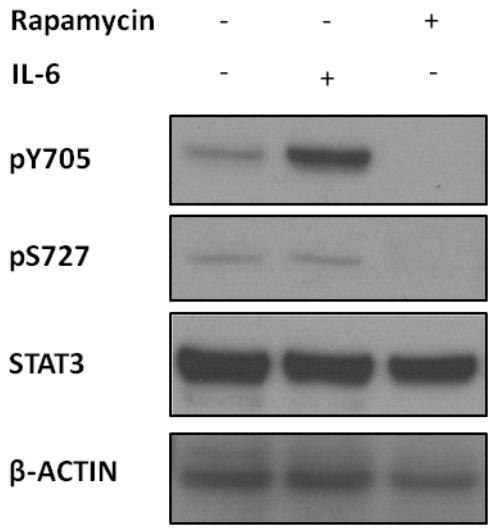


Figure 52. Rapamycin inhibits stimulation induced phosphorylation of STAT3 in mouse $CD4^+FOXP3^-$ T cells. $CD4^+FOXP3^-$ splenic T-cells sorted from hCD2 FOXP3 KI mice were stimulated at 10^5 cells/ml with plate-bound αCD3, αCD28 (1µg/ml), IL-2 (50U/ml) and 0.5ng/ml TGFβ for 3 days. Whole cell lysates were subjected to SDS-page and western blotting. PVDF membrane was probed with αpSTAT3-Y705, αpSTAT3-S727, αSTAT3, αβ-ACTIN and appropriate HRP-conjugated secondary antibodies.

Considering the importance of STAT3 activation in the induction of *Il-17a* and in line with reduced levels of STAT3 phosphorylation, stimulation of cells in the presence of Rapamycin significantly reduced the proportion of $IL\text{-}17A^+$ cells that were induced during the 72 hour stimulation period (Figure 53A and B). This effect was evident at all TGFβ concentrations that were tested, but was more pronounced at higher concentrations of TGFβ (Figure 53B, 0 and 0.1ng/ml: $p<0.05$, 0.5ng/ml: $p<0.001$ and

5ng/ml: p<0.0001). A marked, but less severe, reduction in the proportion of IL-17A secreting cells was also detected when mTOR was inhibited by EAA depletion (data not shown). Therefore mTOR inhibition by Rapamycin or EAA starvation not only seemed to enhance the induction of the Treg marker FOXP3 but also limit the expression of the Th17 signature cytokine IL-17A, presumably through inactivation of STAT3 signalling.

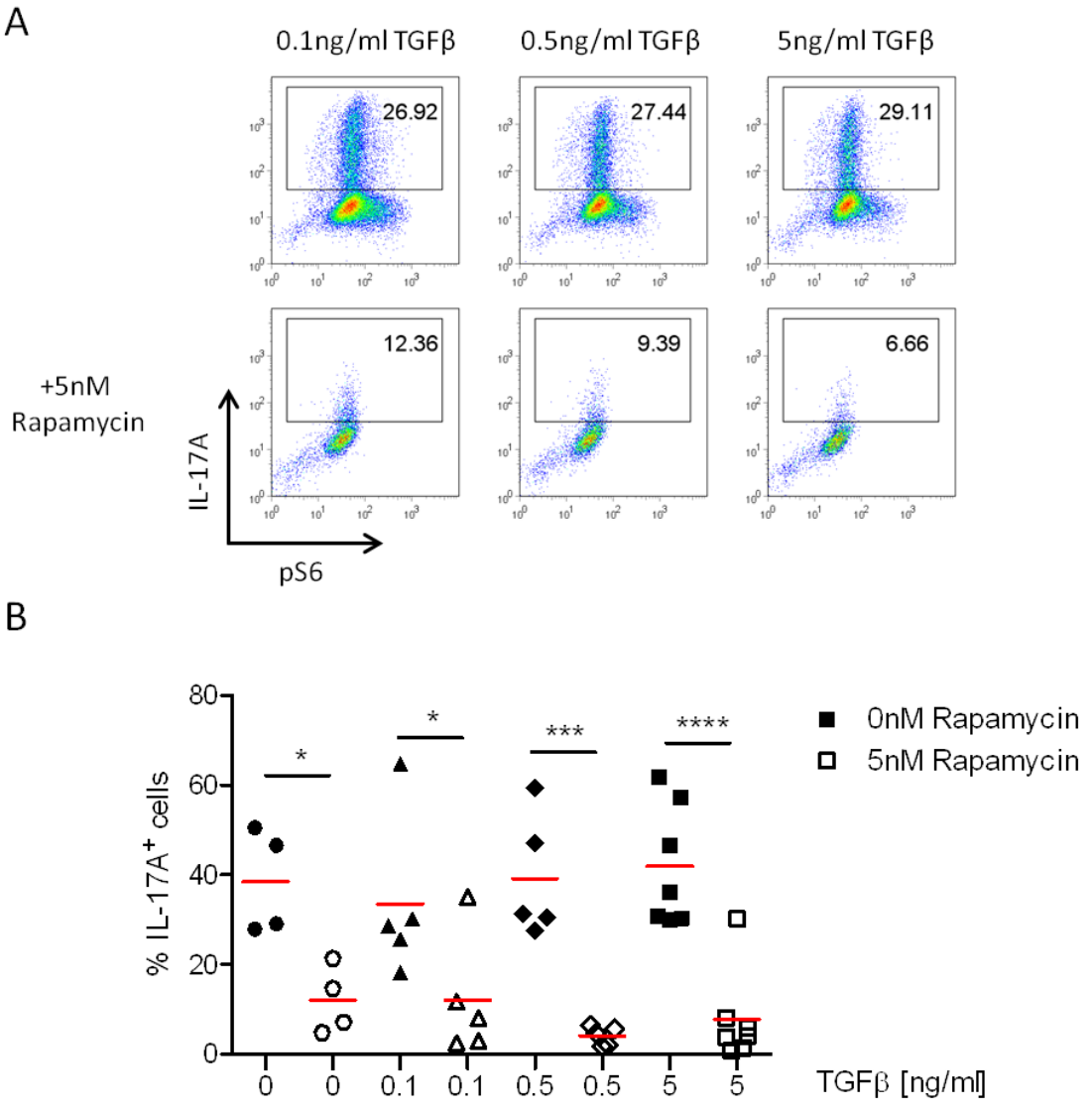


Figure 53. Rapamycin reduced the expression of IL-17A. EL4.B02 cells were stimulated at 10^4 cells/ml for 3 days with αCD3, the indicated concentrations of TGFβ with and without 5nM Rapamyin. (A) Representative FACS plots of IL-17A expression and pS6 levels in live cells (7-AAD low) are shown. (B) Summary of the percentage of IL-17A$^+$ cells measured in the experiments described. Graphs contain data of at least 4 independent experiments. The mean is indicated by a red bar. Statistical analysis was performed by comparing the percentage of IL-17A$^+$ cells obtained at each TGFβ concentration without Rapamycin with that measured in the presence of Rapamycin using one-way ANOVA with Bonferroni's multiple comparison post test (*p<0.05, ***p<0.001, ****p<0.0001).

5.7.4 | Both Rapamycin and Torin 1 reduce the proportion of IL-17A$^+$ cells in a concentration dependent manner

In order to gain insights into whether mTORC1 or mTORC2 or both regulated IL-17A expression, the amount of Rapamycin added to stimulated cultures was carefully titrated. The analysis revealed a similar effect on IL-17A expression as the one observed in the case of FOXP3 induction (Figure 33). As seen for the proportion of FOXP3$^+$ cells, the percentage of IL17A$^+$ cells induced was significantly reduced at the very low concentrations of Rapamycin that only affect mTORC1 but not mTORC2 activity (Figure 54A and B, IL-17A: 50nM: $p<0.01$, 60nM and above: $p<0.001$). This indicates a role for mTORC1 in regulating IL-17A in addition to FOXP3 expression. Based on these results it is, however, difficult to determine whether the mTORC2 inhibition only detectable at higher concentrations of Rapamycin also contributed to the reduced induction of IL-17A. A similar trend across all TGFβ concentrations tested (0.1, 0.25 and 5ng/ml) was seen for all parameters that were measured. The fact that the proportion of IL-17A$^+$ cells across the different concentrations of Rapamycin almost mirrored the proportion of FOXP3$^+$ cells indicated that a similar mechanism regulating the expression of both genes might be at work. These experiments further highlighted the powerful and opposing effects of mTOR inhibition in regulating the balance of Treg and Th17 differentiation.

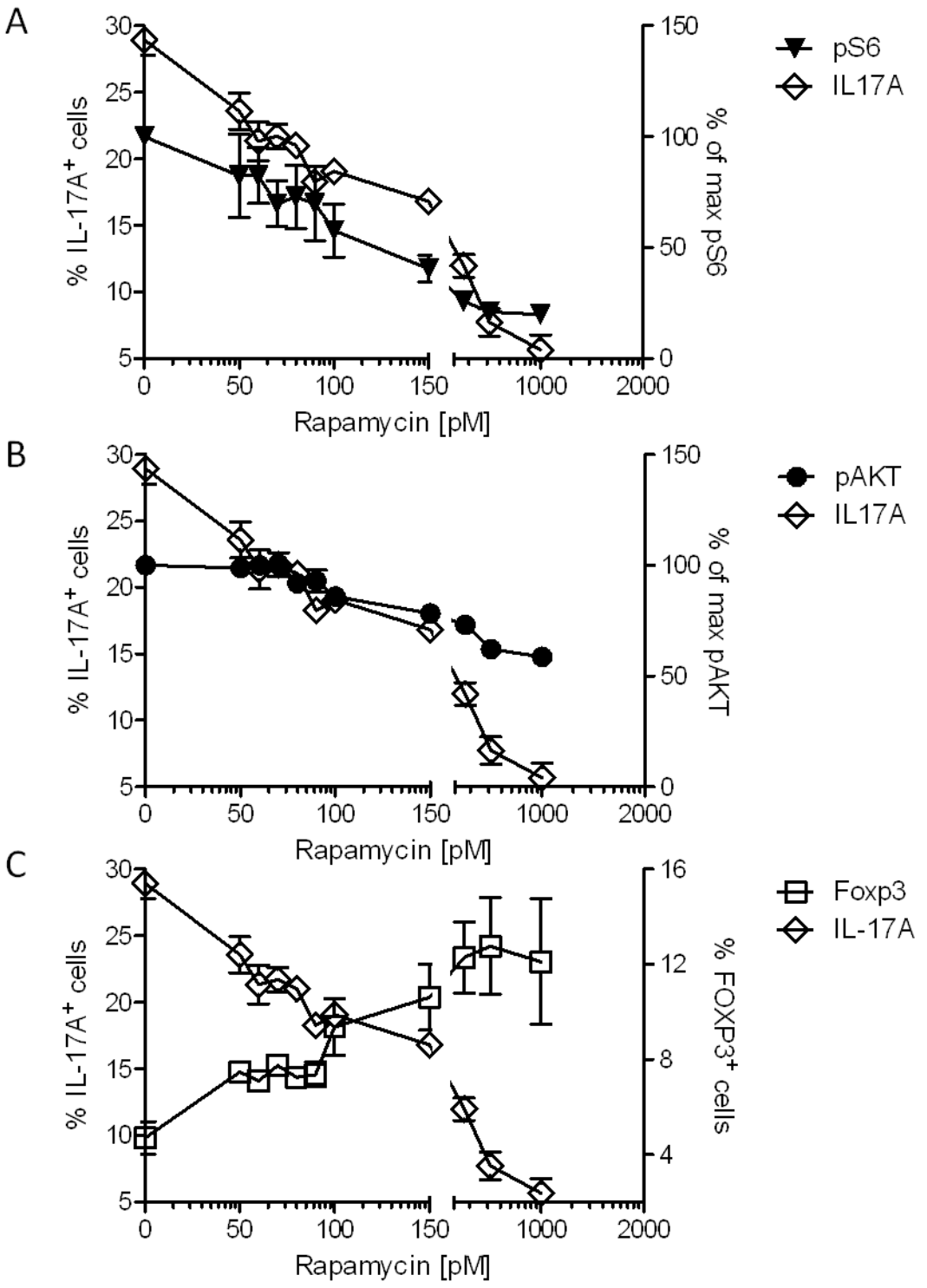


Figure 54. Titration of Rapamycin indicates a role for mTORC1 in regulating IL-17A expression. EL4.B02 cells were stimulated at 10^4 cells/ml for 3 days with αCD3, 0.5ng/ml TGFβ and the indicated concentrations of Rapamycin. Median of pS6 and pAKT was normalized to the levels measured in the absence of Rapamycin. (A-C) Summary of the percentage of IL-17A$^+$ and FOXP3$^+$ cells and the levels of pS6 and pAKT measured at the different Rapamycin concentrations. Graphs contain data of at least 2 independent experiments. The mean and the standard error are shown. Statistical analysis was performed by comparing the percentage of IL-17A$^+$ and FOXP3$^+$ cells and the normalized levels of pS6 and pAKT detected at each Rapamycin concentration to those measured in the absence of Rapamycin using one-way ANOVA with Bonferroni's multiple comparison post test.

In order to further consolidate the findings that the kinase activity of mTOR was required for the induction of IL-17A, cells were stimulated in the presence of increasing concentrations of the ATP-competitive mTOR inhibitor Torin 1 (Figure 55). Similar to the findings obtained in Rapamycin treated cells, increasing amounts of Torin1, irrespective of the concentration of TGFβ, significantly inhibited IL-17A induction in a dose dependent manner (Figure 55C). Interestingly the effect of very low concentrations of Torin1 was more pronounced at higher concentrations of TGFβ (1 and 10nM Torin 1, Figure 55B versus 55C). In line with findings that mTOR inhibition by Rapamycin inhibited STAT3 phosphorylation, Torin 1 also reduced the levels of pSTAT3 (data not shown), which raised the question how mTOR regulates the phosphorylation of STAT3.

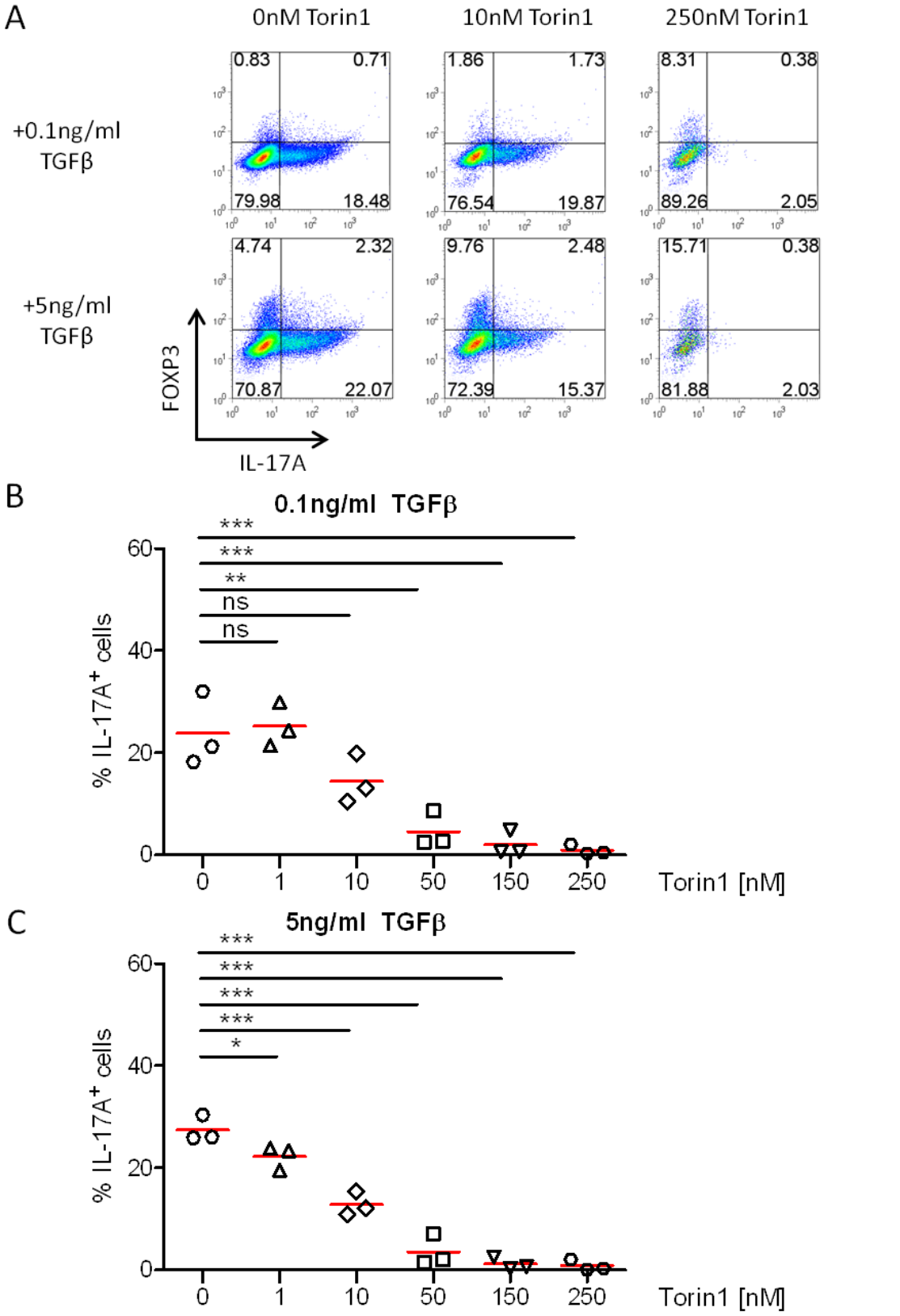


Figure 55. Torin 1 inhibits IL-17A in a concentration dependent manner. EL4.B02 cells were stimulated at 10^4 cells/ml for 3 days with αCD3, the indicated concentrations of TGFβ and Torin1. (A) Representative FACS plots of IL-17A and FOXP3 expression are shown. Summary of the percentage of IL-17A$^+$ cells detected at 0.1 (B) and 5ng/ml TGFβ (C). Both graphs (B and C) contain data of 3 independent experiments. The mean is indicated by a red bar. Statistical analysis compares the percentage of IL-17A$^+$ cells w/o Torin1 versus the percentage in the presence of Torin1 using one-way ANOVA with Bonferroni's multiple comparison post test (*p<0.05, **p<0.01, ***p<0.001).

5.7.5 | Mechanism of mTOR mediated reduction of STAT3 phosphorylation: Rapamycin and EAA depletion upregulate *Socs1* and *3* expression and reduce IL-6 production

STAT phosphorylation is regulated by a wide variety of mechanism including phosphatases, receptor associated kinase activity and a family of proteins called suppressors of cytokine signalling (SOCS) [224-226]. Since a panel of serine/threonine and tyrosine phosphatase inhibitors did not show any significant effect on STAT3 phosphorylation levels (data not shown), further experiments focused on the role of SOCS proteins in the mTOR mediated reduction of STAT3 phosphorylation. SOCS proteins provide a negative feedback mechanism for cytokine and growth factor induced STAT signalling, since their expression is induced by STAT activation and they subsequently inhibit further STAT activation. This inhibition can be accomplished by a range of different mechanism including inhibition of receptor associated kinases or targeting of these kinases for proteosomal degradation [226]. Out of the 7 SOCS proteins that have been identified, SOCS1 and SOCS3 have been demonstrated to inhibit STAT3 activation mediated by IL-6 [218, 227-229], whereas SOCS5 regulates STAT6 activation [226]. Therefore the effect of mTOR inhibition induced by Rapamycin or EAA depletion on the expression of SOCS1 and 3 was analyzed by qPCR.

The analysis revealed that TGFβ enhanced the induction of *Socs3* but not *Socs1* mRNA levels in a statistically significant manner at all time points (Figure 56A and B, *Socs3*: 12 and 24 hours: $p<0.01$, 36 and 48h: $p<0.05$). However, a trend towards stronger expression of *Socs1* in the presence of TGFβ was detected.

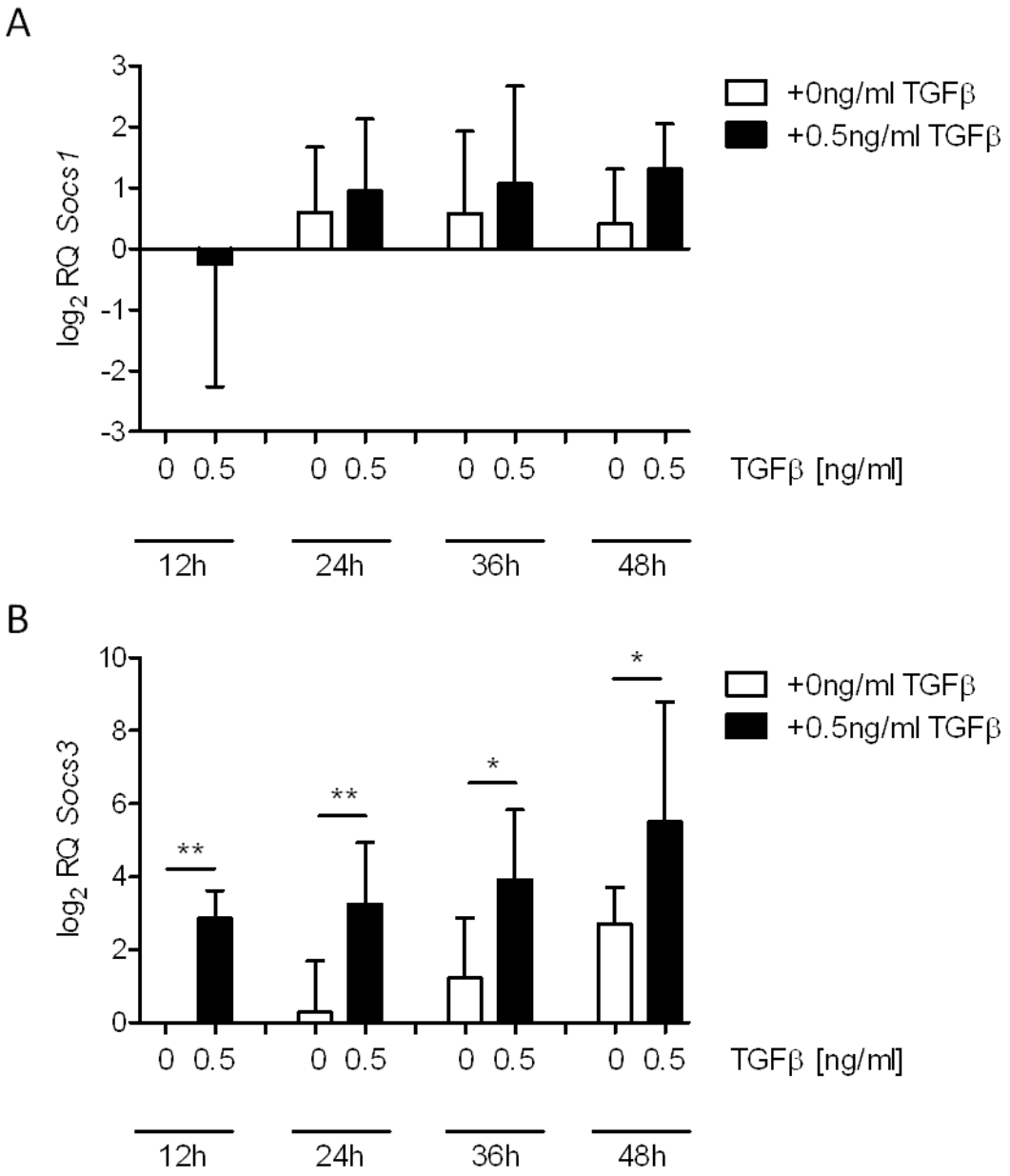


Figure 56. TGFβ increases the expression of *Socs1* and *Socs3*. (A) Real-time PCR analysis *Socs1* (A) and *Socs3* (B) expression in cDNA samples prepared from EL4.B02 stimulated with αCD3 at low cell density for the indicated durations and TGFβ concentrations. Data was normalized to *Hprt1* cDNA levels and is presented relative to cells stimulated at low density with αCD3 for 12 hours. Mean and standard deviation of 4 biological replicates is presented. Statistical analysis was performed to compare the expression in the presence and absence of TGFβ at each time point using repeated measure one-way ANOVA with Bonferroni's multiple comparison post test (*p<0.05, **p<0.01).

A similar trend for enhanced *Socs1* expression is seen in the presence of Rapamycin, which significantly increased *Socs1* mRNA levels at 36h (Figure 57A, $p<0.01$). Rapamycin seemed to increase the levels of *Socs3* expression, however no statistically significant effect was achieved (Figure 57B, $p>0.05$).

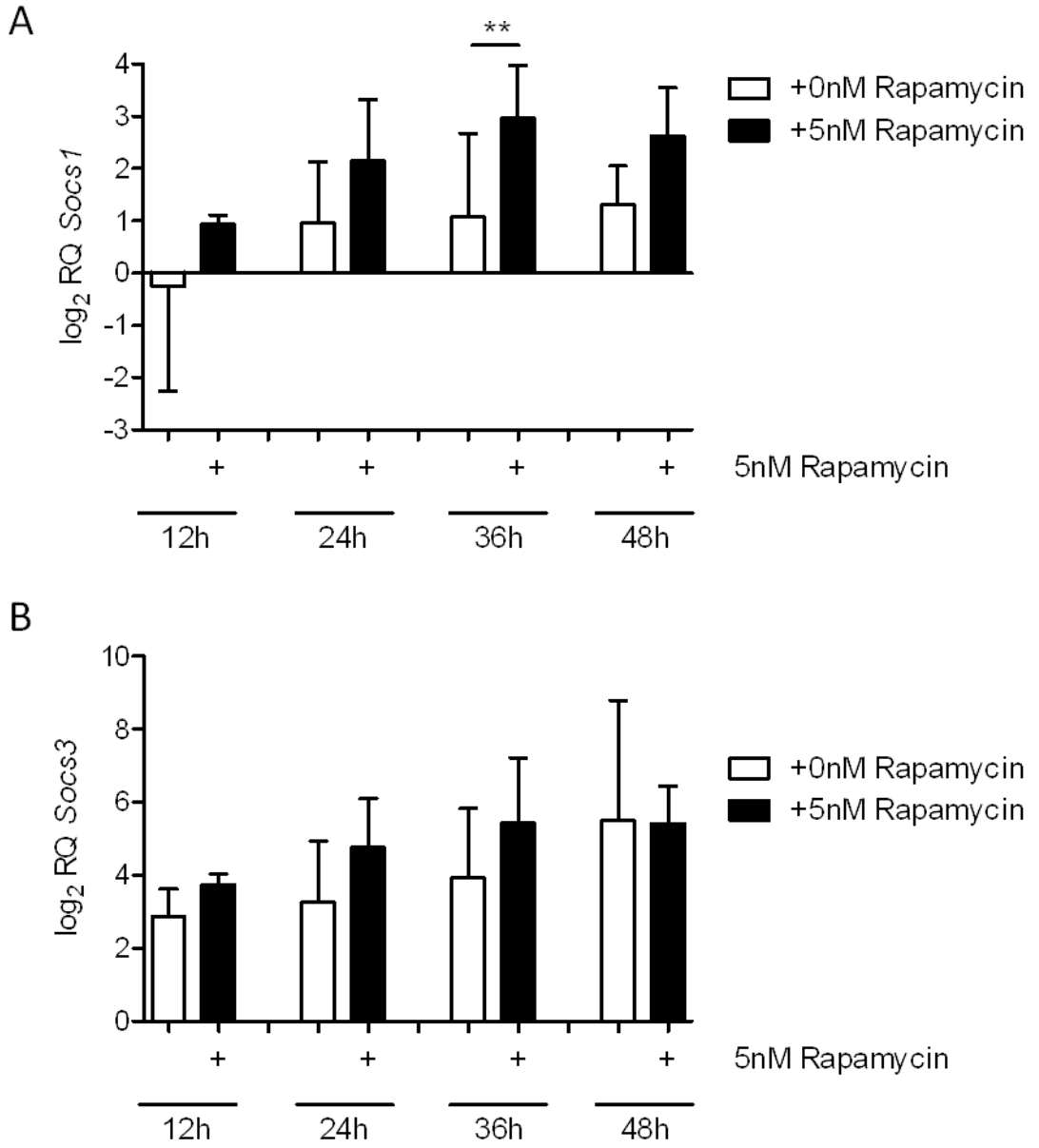


Figure 57. Rapamycin enhances the expression of *Socs1* and *Socs3*. Real-time PCR analysis *Socs1* (A) and *Socs3* (B) expression in cDNA samples prepared from EL4.B02 stimulated at low cell density with αCD3, 0.5ng/ml TGFβ and 5nM Rapamycin where indicated (for the indicated durations). Data was normalized to *Hprt1* cDNA levels and is presented relative to cells stimulated at low density with αCD3 for 12 hours. Mean and standard deviation of 4 biological replicates is presented. Statistical analysis was performed to compare the expression in the presence and absence of Rapamycin at each time point using repeated measure one-way ANOVA with Bonferroni's multiple comparison post test (**p<0.01).

In line with the trend observed in Rapamycin treated samples, mTOR inhibition mediated by EAA starvation also enhanced the expression of *Socs1* mRNA levels (Figure 58A). Stimulation of cells under limiting amounts of EAA resulted in consistently higher expression of *Socs1* than that measured in samples generated from cells stimulated in normal medium. In line with the observation that TGFβ enhanced the expression in normal medium (Figure 56A), TGFβ treated cells stimulated in 5% EAA medium also expressed higher levels of *Socs1* transcripts than those cells stimulated in the absence of TGFβ. A similar trend was observed for *Socs3* mRNA levels when transcript expression in cells stimulated in normal medium and medium containing 5% EAA were compared (Figure 58B).

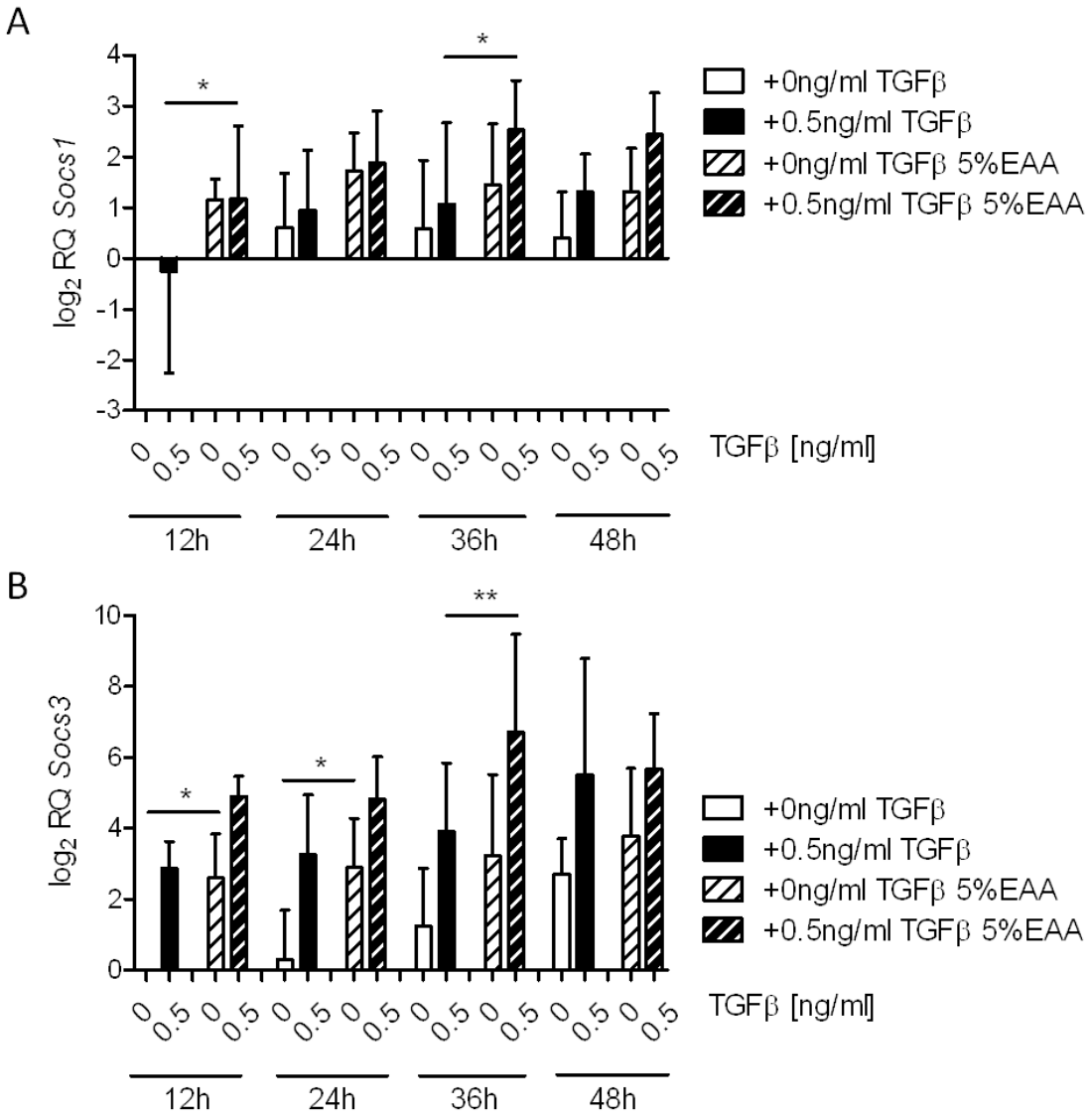


Figure 58. EAA starvation enhanced the expression of *Socs1* and *Socs3*. Real-time PCR analysis *Socs1* (A) and *Socs3* (B) expression in cDNA samples prepared from EL4.B02 stimulated at low cell density with αCD3, 0 or 0.5ng/ml TGFβ and in medium containing 100% or 5% EAA of normal EAA levels (for the indicated durations). Data was normalized to *Hprt1* cDNA levels and is presented relative to cells stimulated at low density with αCD3 for 12 hours. Mean and standard deviation of 4 biological replicates is presented. Statistical analysis was performed to compare the expression in cells stimulated in medium containing 100% EAA to that in cells stimulated in medium containing 5% EAA levels at each time point using repeated measure one-way ANOVA with Bonferroni's multiple comparison post test (*p<0.05, **p<0.01).

In summary both *Socs1* and *Socs3* expression seemed to be at least to some extent upregulated by TGFβ and mTOR inhibition induced by Rapamycin or EAA depletion. The upregulation of these factors that are known to antagonize STAT3 activation could at least in part explain the reduced levels of pSTAT3 that was detected in cells treated

with Rapamycin. It cannot however not be ruled out that other factors contributed to the reduction of STAT3 phosphorylation under mTOR inhibition. Evidence of at least one other component that could contribute to the reduced levels of pSTAT3 came from the analysis of IL-6 expression by Rapamycin treated cells. Compared to cells stimulated in the absence of Rapamycin, the drug seemed to reduce the amounts of IL-6 that were secreted by the cells, which could in turn result in reduced pSTAT3 levels. Support for the role of SOCS3 mediated inhibition of STAT3 phosphorylation and Th17 differentiation comes from studies performed by Delgoffe et al. which demonstrate that $CD4^+$ T-cells with disrupted mTORC1 signalling express higher levels of *Socs3* mRNA and SOCS3 protein, resulting in a marked reduction in IL-17 production [139]. The effects seen in T-cells with disrupted mTORC1 are remarkably similar to those induced by Rapamycin and EAA starvation in EL4.B02 cells, thereby further validating the EL4.B02 system as a model for Treg/Th17 differentiation.

5.7.6 | An analysis of STAT3 knock-down and overexpression of STAT3 mutants fails to establish the role of STAT3 in the regulation of FOXP3

In order to investigate the functional link between mTOR inhibition mediated STAT3 inactivation and the enhancement of FOXP3 induction, EL4.B02 cells were transfected with 5 different Mission™ lentiviral vectors containing different shRNA sequences that target STAT3. A scrambled non-transcript targeting shRNA vector was transfected as a control. After puromycin resistant cells started to emerge in the cultures, STAT3 levels were quantified by qPCR to determine the efficiency of the STAT3 knock-down by the

different shRNA sequences (Figure 59). As expected, not all the STAT3 containing shRNA constructs efficiently reduced the levels of STAT3 transcripts. However, one of the tested constructs, shRNA 53, reduced the levels of STAT3 by ~60% compared to the scrambled control.

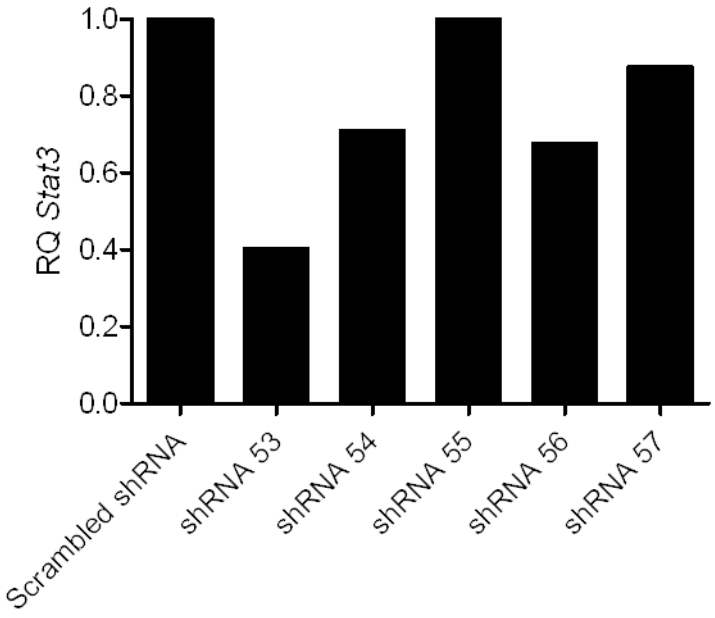


Figure 59. *Stat3* targeting shRNA 53 knocks down *Stat3* expression efficiently. El4.B02 cells were transfected and puromycin selected for different Misson™ shRNA constructs targeting *Stat3*. Real-time PCR analysis of *Stat3* expression of cDNA samples prepared from the indicated stable transfectants. *Stat3* expression was normalized to *Hprt* cDNA and is shown relative to scrambled control transfectants. Graph shows the mean of three technical replicates.

Since this level of expression was still considered to be too high for an effective analysis of the effect of STAT3 on the expression of FOXP3, the shRNA 53 construct was transfected into fresh EL4.B02 cells. Rather than performing the selection in one big culture, the transfected cells were split up evenly into 48 wells in order to establish distinct knock-down lines. All of the 48 lines were subsequently selected for transfected cells by puromycin addition and several days later screened for *Stat3*

knock-down efficiency by qPCR (Figure 60). Evidently the procedure established distinct knock-down lines with different degrees' of STAT3 knock-down. Knock down lines with increased knock-down efficiency compared to the first attempt (<60% KD, indicated by a star) were established, indicating that by limiting the number of competing cells per culture the chances for the outgrowth of knock-down resistant cells was reduced.

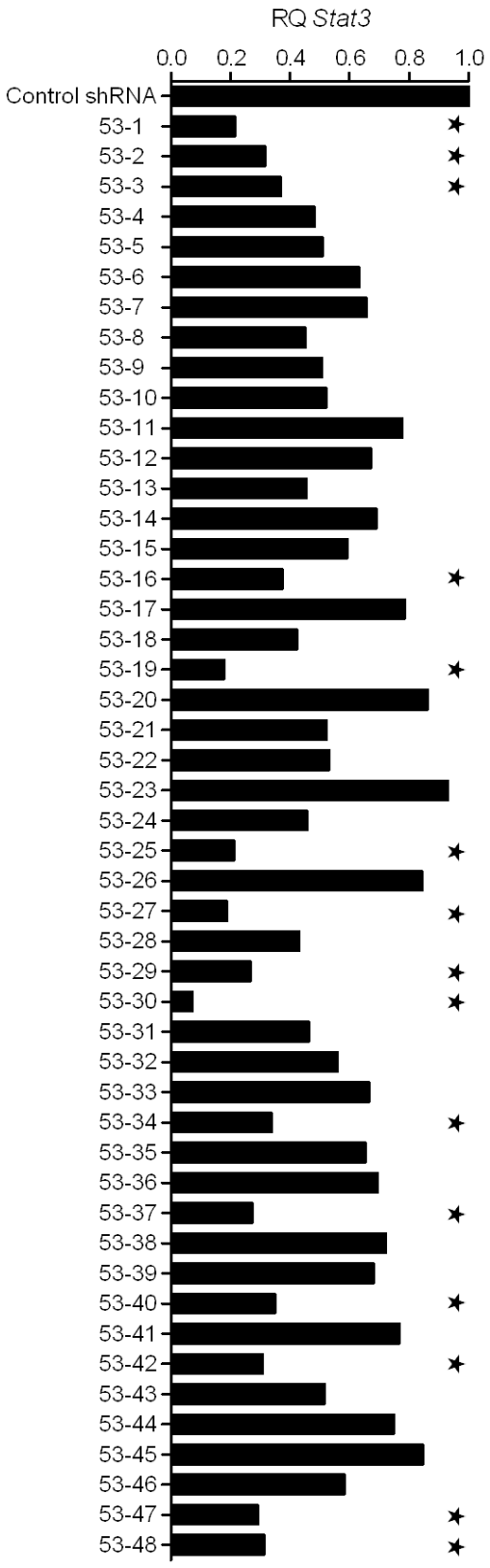


Figure 60. Screening of 48 sh53 *Stat3* targeting lines identifies several lines with increased *Stat3* knock-down efficiency. El4.B02 cells were transfected and puromycin selected for *Stat3* targeting Misson™ shRNA construct sh53. Selection in separate cultures yielded 48 sh53 line (sh53-1 – 48) Real-time PCR analysis of *Stat3* expression of cDNA samples prepared from the indicated sh53 line. *Stat3* expression was normalized to *Hprt* cDNA and is shown relative to scrambled control transfectants. Graph shows the mean of three technical replicates. Stars indicate lines with increased Knock-down efficiency compared to the original sh53 knock down line (Figure 53).

Subsequently, selected STAT3 KD-lines were tested for their ability to induce IL-17A and FOXP3 in the presence and absence of Rapamycin. According to the hypothesis that Rapamycin regulates FOXP3 and IL-17A expression by reducing STAT3 activation, STAT3 KD-lines compared to control cells should induce a higher proportion of $FOXP3^+$ and lower proportion of $IL\text{-}17A^+$ cells in the absence of Rapamycin and should exhibit a smaller effect of Rapamycin on FOXP3 and IL-17A expression.

Surprisingly, stimulation of most of the tested STAT3 KD-lines with αCD3 and TGFβ at low cell density revealed that the cells had lost their ability to induce any significant amounts of FOXP3 and IL-17A (Figure 61). This loss of responsiveness to the FOXP3 and IL-17A inducing signals was less pronounced when the cells were stimulated at high cell densities, although the induced expression of FOXP3 and IL-17A was still weak compared to that seen in non-transfected B02 cells. This loss in responsiveness made an interpretation of the effect of STAT3 KD difficult, especially as Rapamycin addition to cells stimulated at low and high density resulted in a very high percentage of dead cells (data not shown). The fact that even the cells transfected with scrambled shRNA constructs showed a reduced inducibility of both FOXP3 and IL-17A pointed towards a transfection or selection effect as the cause rather than the STAT3 KD itself. Interestingly, however whereas Rapamycin did not exhibit an enhancement effect on FOXP3 at high density before (Figure 10) addition of Rapamycin addition to high density stimulations of STAT3 KD-lines enhanced the induction of FOXP3 in most cases. However, high density stimulation conditions were not considered to be a well controlled setting due to “system intrinsic” mTORC1 inhibition and the putative production of a FOXP3 inducing factor that were described in earlier chapters.

Therefore the attempts to investigate the role mTOR regulated STAT3 activation by STAT3 knock-down were abandoned.

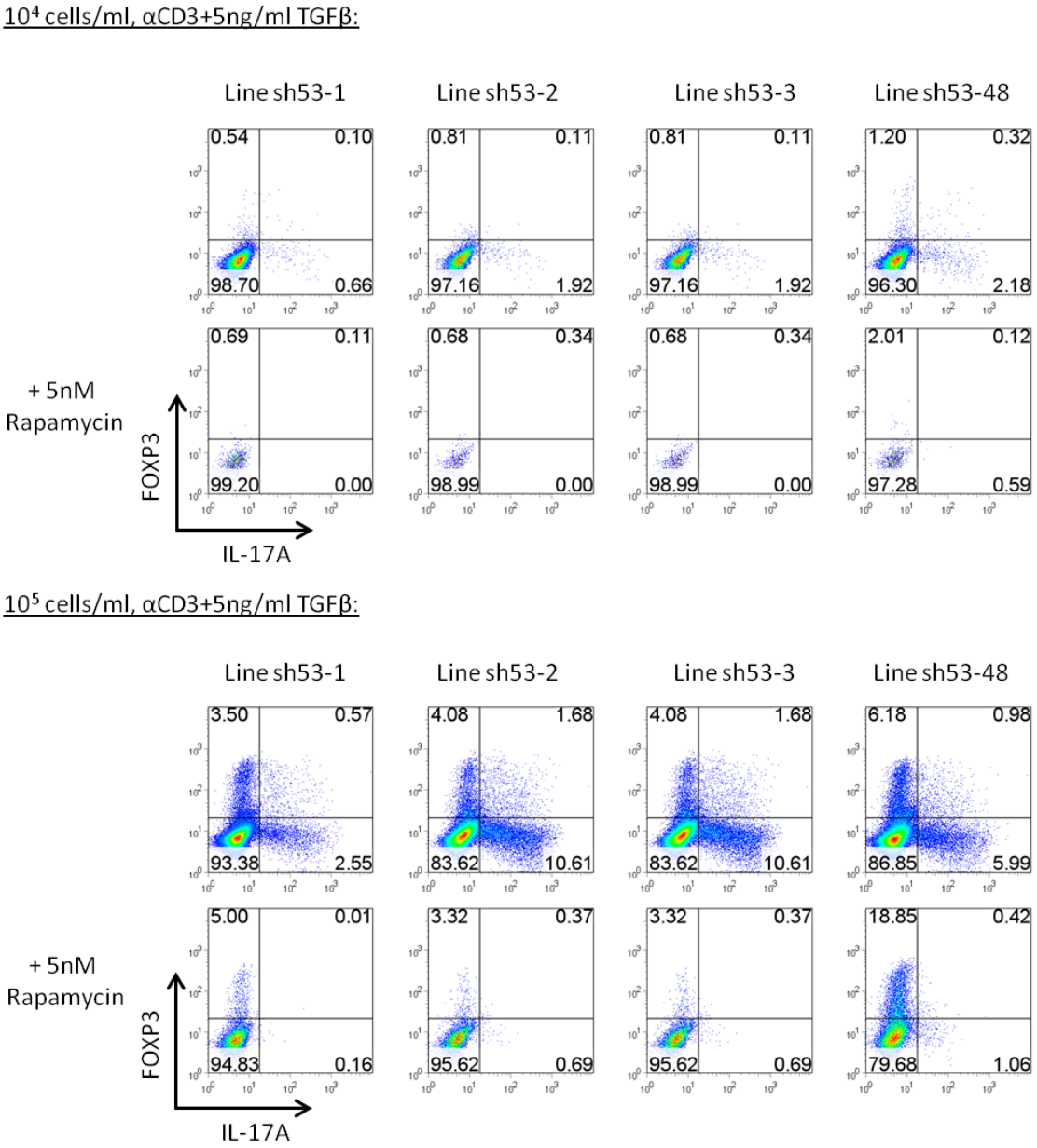


Figure 61. Low cell density stimulation of sh53 *Stat3* knock down lines reveals unresponsiveness to stimuli inducing IL-17A and FOXP3 expression, which is partially restored at high cell density. EL4.B02 sh53 lines were stimulated for 3days at 10^4 and 10^5 cells/ml with αCD3, 5ng/ml TGFβ and 5nM Rapamycin as indicated. Representative FACS plots of IL-17A and FOXP3 expression in live cells (7-AAD low) are shown.

Since the STAT knock-down approach was abandoned due to technical difficulties, the role of mTOR mediated STAT3 activation was addressed by over-expressing dominant positive and negative STAT3 mutants. Several mutants of STAT3 have been described in the literature, including several non phosphorylatable molecules (mutation of phosphosites on S/T to A and Y to F) [230-233], constitutive dimers (introduction of two cysteins that form a disulfide bond that facilitate dimerization) [234] and DNA binding mutants [233]. In order to make these constructs, STAT3α was cloned from cDNA samples prepared from EL4.B02 cells and mutated by one or several rounds of site directed mutagenesis. The mutants were then subcloned in several steps into the pEF1α-FLAG-IRES-EGFP vector, so that the expression of STAT3 proteins was driven by the EF1α promoter, resulted in coexpression of EGFP and expressed STAT3 proteins which were FLAG tagged. Additionally the neomycin/kanamycin resistance gene encoded on the vector should allow for stable transfectants using the drug G418, rather than the puromycin that had to be used for the shRNA containing vectors. The hope was that G418 selection might circumvent putative puromycin induced unresponsiveness of the cells.

After an initial transfection of EL4.B02 cells and G418 mediated selection of transfectants over several weeks, cells were FACS sorted for EGFP expression to further enrich for cells expressing the construct. FACS analysis showed that both STAT3 WT and constitutive STAT3 dimer constructs were efficiently expressed as measured by EGFP expression (Figure 62A). However, it was also noticed that the Fixation/Permeabilization buffer used for all staining (eBioscience) quenched the GFP fluorescence, a phenomenon also reported by other groups [235, 236]. Despite testing several different fixation and permeabilization protocols that didn't quench the EGFP

fluorescence, a protocol that would allow simultaneous FOXP3 staining could not be achieved (data not shown). Therefore cells stimulated and stained for FOXP3 could not be analyzed for their EGFP expression.

Stimulation of cells at low and high cell density with αCD3 and TGFβ with and without Rapamycin, disappointingly demonstrated that the transfectants similarly to cells containing the shRNA constructs, seemed to have lost responsiveness in terms of inducibility of FOXP3 and IL-17A (Figure 62B). In line with findings made in the knock-down lines, stimulation at higher densities overcame this unresponsiveness at least partially, however since a clear analysis of the contribution of the mTOR pathway due to “system intrinsic” mTOR inhibition was not feasible under these conditions, the established STAT3 WT and dimer construct expressing cell lines did not provide a good system to study the role of STAT3 in mTOR regulated FOXP3 and IL-17A expression. Additional attempts using the same and different STAT3 mutant constructs yielded similar results or the selection of stably expressing lines did not work (data not shown).

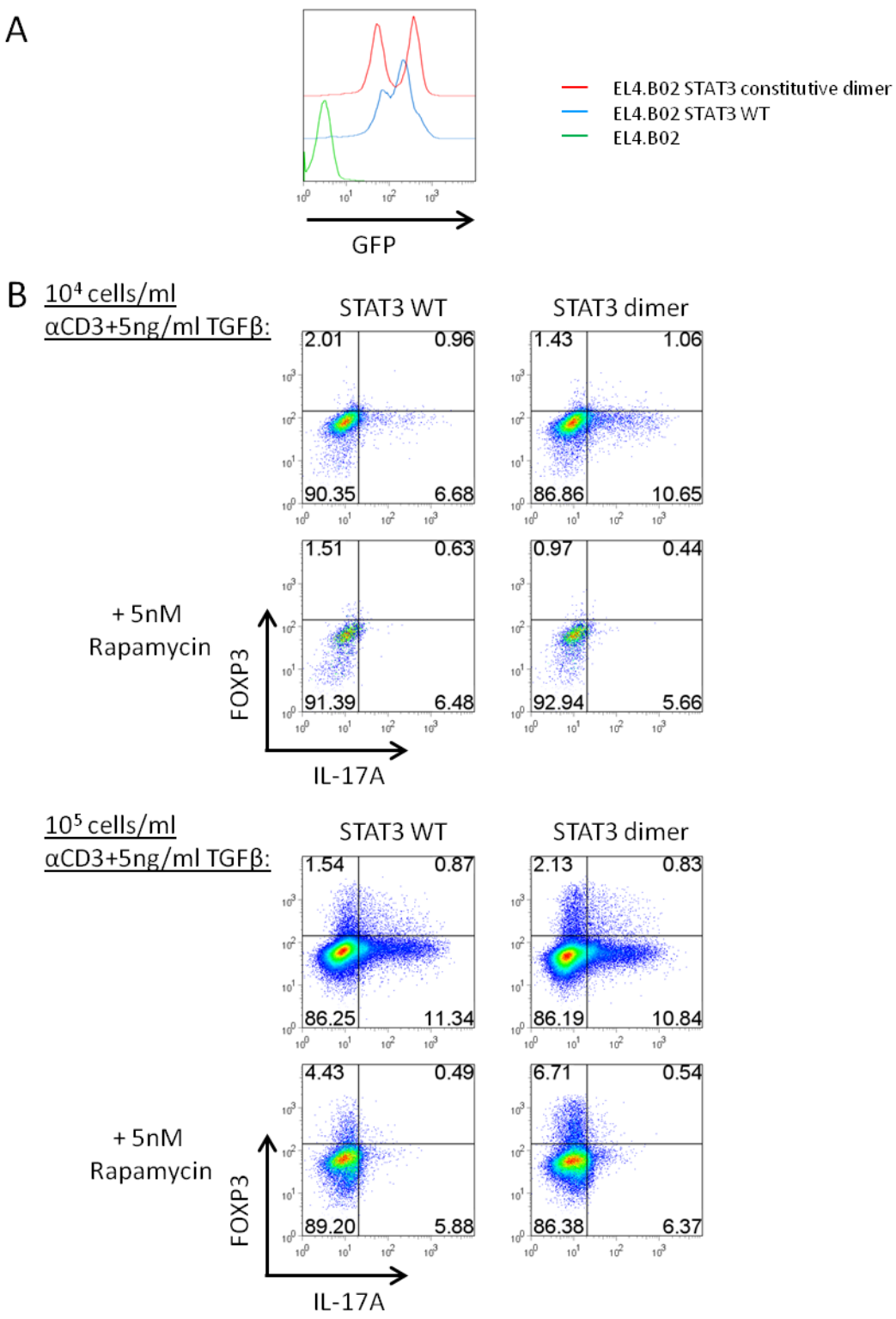


Figure 62. Constitutively active STAT3 dimers do not seem to affect the expression of FOXP3. EL4.B02 STAT3 WT and STAT3 constitutive dimer expressing cell lines were established. (A) FACS plots of GFP expression in transfected EL4.B02 cells. (B) Transfectans were stimulated for 3 days at 10^4 and 10^5 cells/ml with αCD3, 5ng/ml TGFβ and 5nM Rapamycin as indicated. Representative FACS plots of IL-17A and FOXP3 expression in live cells (7-AAD low) are shown.

In summary, although STAT3 expression was significantly knocked down by a shRNA construct targeting the 5'UTR of STAT3, the effect of STAT3 could not be analyzed due to drastically reduced inducibility of the cell line in terms of FOXP3 and IL-17A. The original plan to express dominant positive and negative STAT3 mutants in the knock-down background therefore had to be abandoned. Unfortunately, when the expression of the STAT3 mutants in EL4.B02 was, in at least in two cases, successfully achieved, the selected cells again exhibited reduced FOXP3 inducibility. The fact that a well controlled investigation of the role of mTOR inhibition could not be pursued under these conditions due to "system intrinsic" mTOR inhibition, led to the cessation of the experiments. Nevertheless, the lack of any significant effect of STAT3 knock-down or over-expression of a dominant positive STAT3 protein on the expression of FOXP3 even at high densities raised doubts whether mTOR inhibition mediated STAT3 inactivation is involved in the regulation of FOXP3. However, it was not tested whether the constitutive dimer really represents a constitutively active STAT3 dimer. It is conceivable that the phosphorylation of STAT3 is involved in the transcriptional activation besides its role in faciliting dimerization.

These experiments revealed one of the major limitations of the EL4.B02 cell line system in that the transfection efficiency using various techniques was low and selection resulted in largely unresponsive cells. In fact the supposed amenability of cell lines to transfection and therefore genetic manipulation was one of the major incentives for why mTOR inhibition was studied in EL4 cells.

5.7.7 | Mutation of the STAT3 binding site in CNS2 of double enhancer constructs raises doubts over the involvement of STAT3 in the mTOR mediated induction of FOXP3

Since the analysis of STAT3 knock-down and mutant STAT3 overexpressing cells did not shed any more light on the importance of mTOR inhibition mediated STAT3 inactivation for the induction of FOXP3, a strategy based on an approach of Xu et al. was employed. In their studies Xu and colleagues demonstrated that luciferase constructs containing the *Foxp3* promoter, CNS1 and CNS2 exhibited a decreased activity when stimulated with αCD3 with and without TGFβ compared to constructs containing only the *Foxp3* promoter and CNS1. They further indicated that the constitutively activated STAT3 in the EL4 cell line was causing CNS2 in the double enhancer constructs to act as a silencer, since deletion of the STAT3 binding site alleviated the silencing effect and converted CNS2 into an enhancer element [179].

Based on the *Foxp3* luciferase vectors described earlier, constructs containing the *Foxp3* promoter as well as CNS1 and 2 were cloned. In contrast to the Xu et al. vectors in which CNS1 and 2 are located immediately downstream of the *Foxp3* promoter, the two CNS sequences had to be cloned downstream of the luciferase gene due to the availability of suitable restriction sites and the insertion of CNS1 downstream of the luciferase gene (constructs: *Foxp3* promoter - luciferase - CNS1 - CNS2 rather than Xu's *Foxp3* promoter - CNS1 - CNS2 - luciferase). Since enhancer elements are thought to be able to act on the promoter activity even if separated by large stretches of DNA this difference was thought not to affect the function of the constructs in relation to those

of Xu et al. In fact our constructs mimic the *Foxp3* locus more accurately since CNS1 is situated ~2kb downstream of the *Foxp3* promoter.

In order to test whether the double enhancer constructs retain their TGFβ (CNS1), CD3 (CNS2) and mTOR inhibition (CNS1 and 2) responsiveness, cells transfected with the constructs were stimulated with various combinations of the different stimuli. The analysis of the results obtained from the luciferase assay revealed that indeed the double enhancer constructs, irrespective of whether short or long enhancer sequences were used, responded to all stimuli that the individual enhancers had shown earlier (Figure 63).

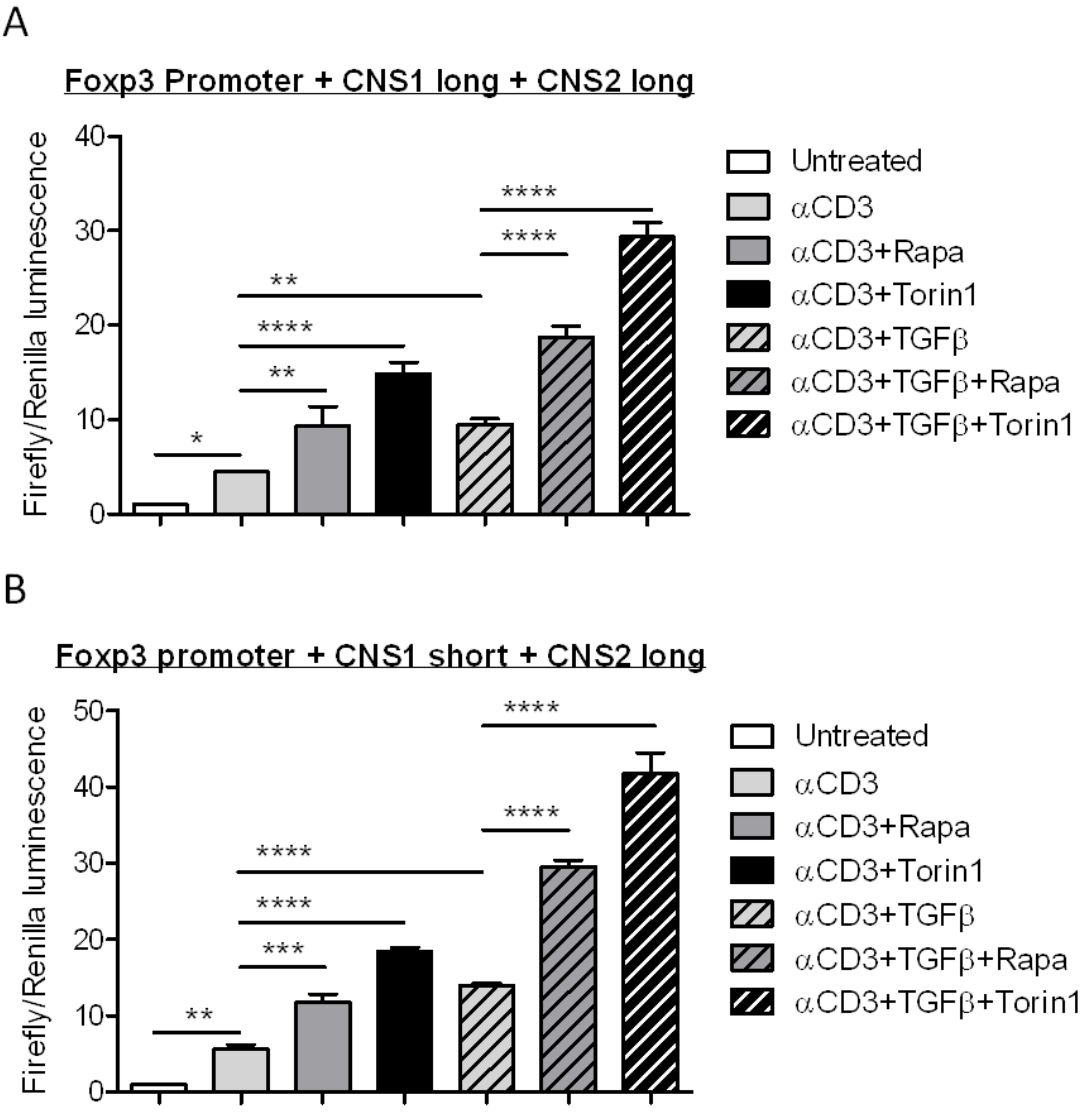


Figure 63. Double enhancer constructs retain the responsiveness of the individual enhancer by responding to their TGFβ, CD3 and mTOR inhibition. EL4.B02 cells were cotransfected with pTK Renilla luciferase and pGL4 *Foxp3* promoter+CNS1(long)+CNS2(long) (A) or pGL4 *Foxp3* promoter+CNS1(short)+CNS2(long) constructs (B) and stimulated for 16 hours with indicated stimuli (αCD3: as described before, 5ng/ml TGFβ, 5nM Rapamycin (Rapa) and 250nM Torin 1). Renilla and firefly luciferase was measured using the Promega Dual Luciferase Assay and an automated luminometer. The mean and standard deviation of the ratio of firefly to renilla luminescence measured in 3 independent experiments are shown. Means are normalized to untreated cells. Statistical analysis was performed by comparing the firefly/renilla luminescence ratio of the indicated samples using repeated measure one-way ANOVA with Bonferroni's multiple comparison post test (*p<0.05, **p<0.01, ***p<0.001, ****p<0.0001).

Surprisingly, the initial analysis of the experiments did not indicate the silencing effect of CNS2 on CNS1 activity that was described by Xu et al.. This initial contradiction was however resolved when the data of both CNS1 and CNS1 and 2 constructs was normalized to the αCD3 stimulated cells rather than unstimulated cells. Since, for

reasons that could not be determined the CNS1 containing luciferase constructs only very weakly respond to CD3 engagement compared to the response described by Tone et al. and Xu et al., the inclusion of CNS2 in the double enhancer constructs added a functional CD3 response element that made it seem like the double enhancer construct showed enhanced activity compared to only CNS1 containing constructs (Figure 64A). Normalization to CD3 stimulated cells revealed a negative effect of CNS2 insertion into CNS1 constructs in the presence of TGFβ, in line with the mechanism of STAT3 mediated inhibition of SMAD3 binding to CNS1 proposed by Xu et al. (Figure 64B).

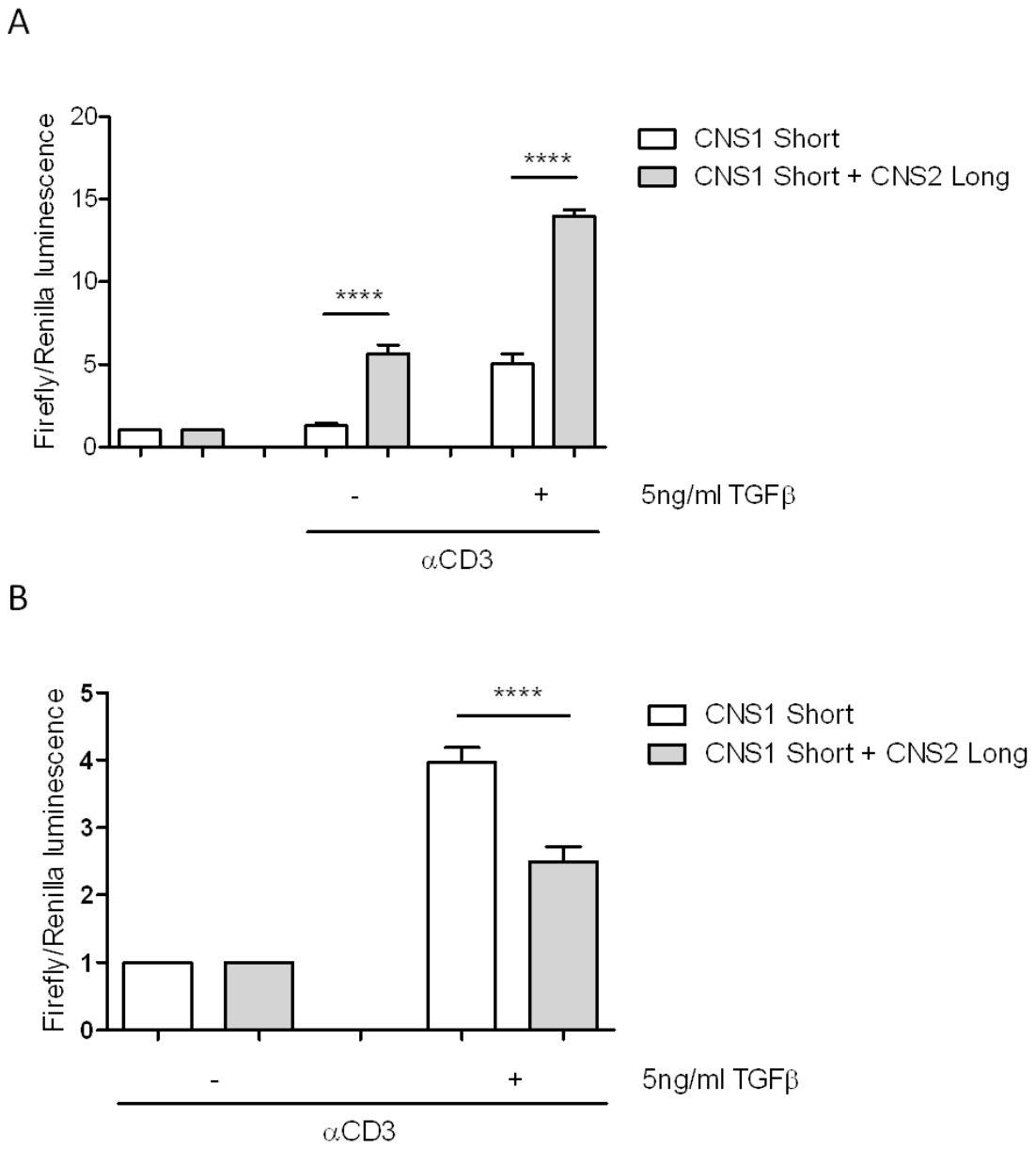


Figure 64. The activity of the *Foxp3* promoter+CNS1 seems to be reduced in the presence of CNS2 and TGFβ. EL4.B02 cells were cotransfected with pTK Renilla luciferase and pGL4 *Foxp3* promoter+CNS1(short) or pGL4 *Foxp3* promoter+CNS1(short)+CNS2(long) constructs and stimulated for 16 hours with indicated stimuli (αCD3: as described before, 5ng/ml TGFβ). Renilla and firefly luciferase was measured using the Promega Dual Luciferase Assay and an automated luminometer. The mean and standard deviation of the ratio of firefly to renilla luminescence measured in at least 3 independent experiments are shown. Means are normalized to untreated cells(A) and αCD3 stimulated cells (B). Statistical analysis was performed by comparing the firefly/renilla luminescence ratio of the indicated samples using one-way ANOVA with Bonferroni's multiple comparison post test (****p<0.0001).

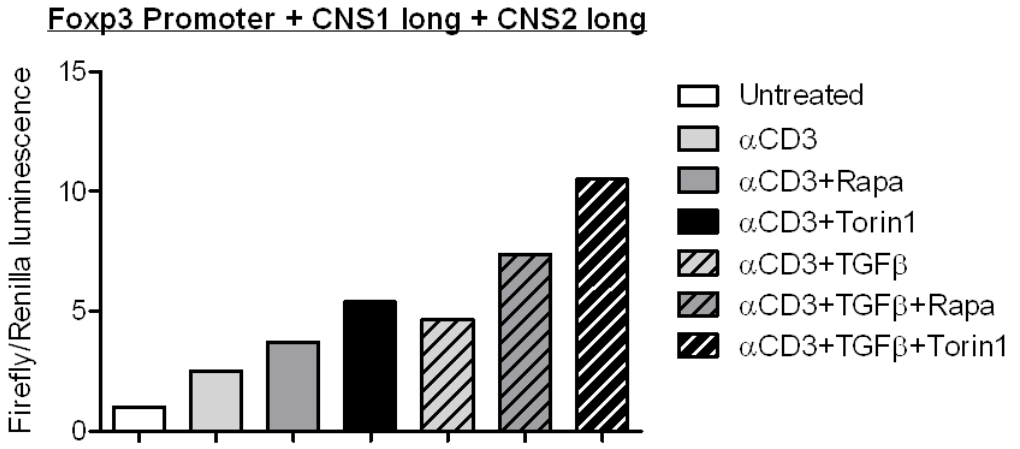
In order to investigate the involvement of the STAT3 binding site in the mTOR inhibition mediated increase in luciferase acitivity/FOXP3 induction, the first 4bp of the 9bp STAT3 binding site in CNS2 were mutated both in CNS2 and in CNS1 and 2 double

enhancer constructs (STAT3 binding site: TTCTCGGAA, mutated: ggtaCGGAA). Mutation of the STAT3 binding site was preferred over a deletion since less deleterious effects on transcription factors that bind adjacent sequences were assumed to occur in this scenario. Han et al. demonstrated that the indicated mutation resulted in reduced STAT3 driven luciferase activity in their experimental system [237].

Surprisingly and in contrast to the reports of Xu et al., the mutation of the STAT3 binding site in CNS2 in double enhancer constructs did not enhance the luciferase activity compared to constructs with an intact STAT3 binding site (Figure 65). Furthermore the mTOR inhibition mediated enhancement of luciferase activity was still detectable. A similar trend was also observed for the constructs containing only CNS2 with or without mutated STAT3 binding site. This could either indicate that the mutation did not abolish STAT3 binding and thereby mTOR inhibition by Rapamycin and Torin 1 were still effective or that STAT3 binding was indeed blocked but is not involved in the mTOR mediated induction of FOXP3. Unfortunately Xu et al. did not show the effect of stimulation on CNS2 constructs, nor an absence of an effect of STAT3 deletion on CNS2, which would be expected according to their hypothesis. Considering that TGFβ reduced the activity of CNS2 constructs (Figure 36B), the observed reduction in double enhancer constructs could be attributed to this TGFβ effect (Figure 64B). Furthermore, Xu et al. observed an effect of STAT3 binding site deletion even in the absence of TGFβ, which should not be detected without SMAD3 activation (according to their hypothesis of STAT3 mediated interference with SMAD3 binding), although baseline SMAD3 activation might occur even in the absence of any exogenous TGFβ. However, it also seems conceivable that differences in the promoter, CNS1 and CNS2 sequences or the different approach of blocking STAT3 binding

(deletion versus mutation) might have caused the different results. This question could only be answered if more similar constructs are used. Due to time constraints this experiment could however not be performed. In the light of these findings and the lack of effects in STAT3 knock-down and STAT3 mutant overexpression experiments, a role for mTOR mediated FOXP3 induction via STAT3 inactivation seemed unlikely. The experiments using double enhancer constructs enforced however the hypothesis that mTOR inhibition might act on a transcription factor that binds to the *Foxp3* promoter since the mTOR inhibition effect on luciferase activity seen in single enhancer constructs (CNS1: enhancement of TGFβ induced activation, CNS2: enhancement of CD3 induced activation) was not increased in double enhancer constructs.

A



B

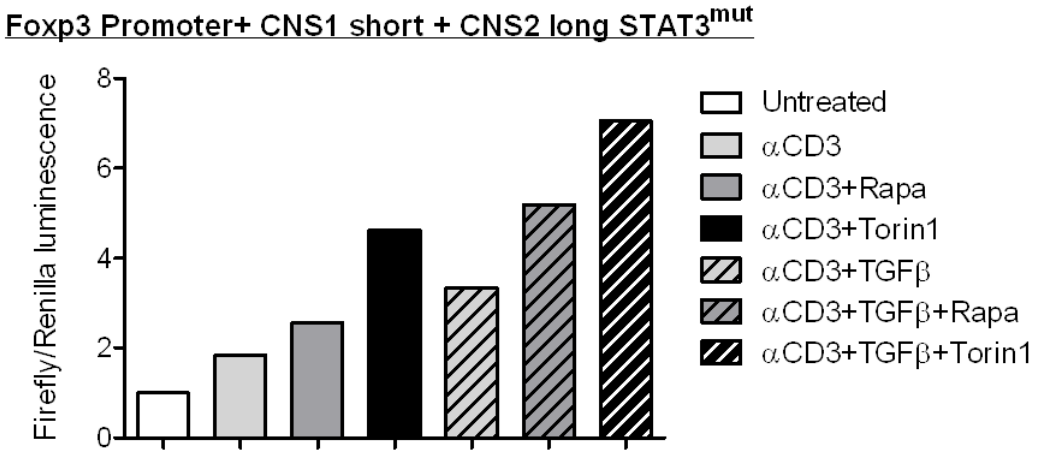


Figure 65. Mutation of the STAT3 binding site in CNS2 does not enhance the activity of double enhancer constructs. EL4.B02 cells were cotransfected with pTK Renilla luciferase and pGL4 *Foxp3* promoter+CNS1(short)+CNS2(long) (A) or pGL4 *Foxp3* promoter+CNS1(short)+CNS2(long) STAT3^{mut} constructs (B) and stimulated for 16 hours with indicated stimuli (αCD3: as described before, 5ng/ml TGFβ, 5nM Rapamycin (Rapa) and 250nM Torin 1). Renilla and firefly luciferase was measured using the Promega Dual Luciferase Assay and an automated luminometer. The ratio of firefly to renilla luminescence measured in 1 experiment is shown. Ratios are normalized to untreated cells.

5.7.8 | mTOR inhibition by Rapamycin and EAA depletion do not reduce the levels of *Il-17a* mRNA early in the stimulation, but at later time points

In the hope that an analysis of the kinetics of the STAT3 dependent expression of *Il-17a* at the transcription level would shed more light on whether STAT3 could be involved in the regulation of *Foxp3* expression, the levels of *Il-17a* transcripts were analyzed by qPCR. Based on the observation that Rapamycin and Torin 1 consistently enhanced *Foxp3* transcription starting at very early time points (~6h, Figure 32) and the hypothesis that mTOR inhibition mediated STAT3 deactivation enhances *Foxp3*, the *Il-17a* expression should exhibit the opposite effect.

The analysis of *Il-17a* transcript levels in cells stimulated for short periods (2-10h, data not shown) in the presence of Rapamycin or Torin 1 demonstrated a small and transient decrease in *Il-17a* message with both inhibitors. This was not observed at the intermediate time points (Figure 66A, 12-48h), in contrast to what was observed for *Foxp3* mRNA levels (Figure 25). Starvation of cells of EAA also did not decrease *Il-17a* transcription at the intermediate time points (Figure 66B). In contrast EAA starvation consistently increased the expression of *Il-17a*.

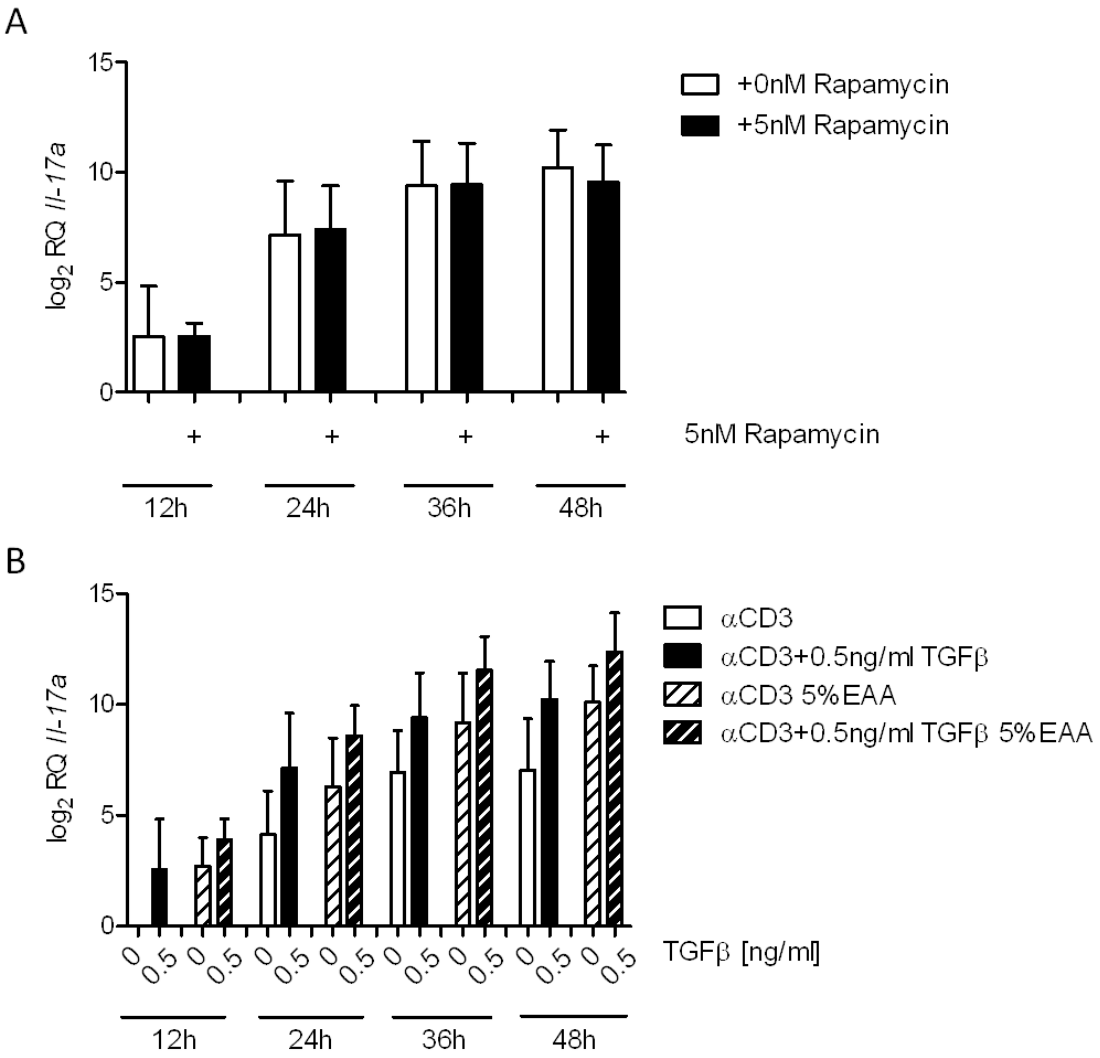


Figure 66. mTOR inhibition by Rapamycin or EAA starvation does not inhibit *Il-17a* expression at intermediate time points. (A) Real-time PCR analysis *Il-17a* epression in cDNA samples prepared from EL4.B02 stimulated at low cell density with αCD3, 0 or 0.5ng/ml TGFβ and 5nM Rapamycin where indicated (for the indicated durations). Data was normalized to *Hprt1* cDNA levels and is presented relative to cells stimulated at low density with αCD3 for 12 hours. Mean and standard deviation of 4 biological replicates is presented. (B) Real-time PCR analysis *Il-17a* expression in cDNA samples prepared from EL4.B02 stimulated at low cell density with αCD3, 0 or 0.5ng/ml TGFβ and in medium containing 100% or 5% EAA of normal EAA levels (for the indicated durations). Data was normalized to *Hprt1* cDNA levels and is presented relative to cells stimulated at low density with αCD3 for 12 hours. Mean and standard deviation of 4 biological replicates is presented.

5.7.9 | PMA partially circumvents Rapamycin mediated reduction of IL-17A and the enhancement of FOXP3 induction

Considering that Rapamycin decreased IL-17A protein expression strongly at 72 hours, a slow decrease in *Il-17a* transcription by Rapamycin was likely to occur (>48 hours). This slow effect of Rapamycin would be consistent with the fact that considerable increases in *Socs1* and *3* transcripts were only observed at later time points (Figure 57) and the observation that the Rapamycin mediated STAT3 inactivation did not occur within the first hours of the addition of the drug (data not shown).

In line with the notion that Rapamycin decreases *Il-17a* mRNA levels later in the stimulation, reduced levels of *Il-17a* mRNA levels were detected at 60h (data not shown) and 72h (Figure 67A). At this time point Rapamycin not only significantly reduced *Il-17a* mRNA levels but also expectedly increased *Foxp3* transcript levels (Figure 67B).

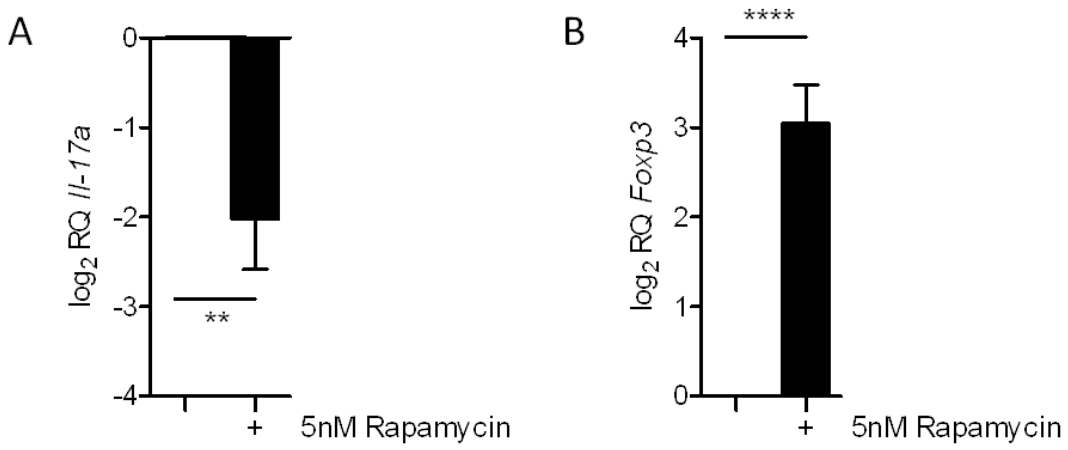


Figure 67. Rapamycin inhibits *Il-17a* expression at late time points and enhances *Foxp3* expression. Real-time PCR analysis *Il-17a* (A) and *Foxp3* (B) expression in cDNA samples prepared from EL4.B02 stimulated at low cell density for 3 days with αCD3, 0.5ng/ml TGFβ and 5nM Rapamycin as indicated. Data was normalized to *Hprt1* cDNA levels and is presented relative to cells stimulated at low density with αCD3 and 0.5ng/ml TGFβ for 3 days. Mean and standard deviation of 5 biological replicates is presented. Statistical analysis was performed to compare the expression in cells stimulated without Rapamycin to that in cells stimulated in the presence of the inhibitor using repeated measure one-way ANOVA with Bonferroni's multiple comparison post test (**p<0.05, ** **p<0.0001).

Restimulation of cells with phorbol esters and ionophores such as phorbol myristate acetate (PMA) and ionomycin is common practice when cytokine production of lymphocytes is analyzed *in vitro* and *ex vivo*. By activating PKC and Ca^{2+} signalling pathways, PMA and ionomycin are thought to reveal the cytokine profile that a given cell is capable of producing based on its differentiation state. Importantly, the brief stimulation with PMA/Ionomycin (4-6h) is thought to merely provide an activation signal that would allow for an analysis of cytokine production of a given cell rather than inducing cytokine expression *de novo*.

In initial experiments PMA/Ionomycin was added to EL4.B02 cells stimulated with αCD3 for the last 4h of the 3 day stimulation period, since it was not known at the time whether CD3 engagement alone was sufficient to be able to detect cytokine release by the cells. These experiments revealed an interesting phenomenon with respect to Rapamycin mediated inhibition of IL-17A production. Whereas Rapamycin significantly decreased the proportion of IL-17A producing cells and enhanced the proportion of $FOXP3^+$ cells (Figure 24, 53 and 68), addition of PMA/Ionomycin almost completely blocked this effect. Similar results were obtained under EAA starvation conditions. In order to assess whether this was due to *de novo* induction of *Il-17a* expression or solely a result of increased translation of preexisting *Il-17a* mRNA, cells were stimulated with αCD3 and TGFβ with and without Rapamycin, PMA and ionomycin and expression of *Foxp3*, *Il-17a* and *Rorc* were analyzed by qPCR. Surprisingly, PMA stimulation not only significantly inhibited *Foxp3* transcription but also enhanced *Il-17a* and *Rorc* mRNA levels, indicating that the observed effect of PMA/ionomycin on IL-17A protein was due to PMA induced transcription of the *Il-17a* gene (Figure 68). A role for STAT3 and HIF1α activation in this process was ruled out by comparing the level of pSTAT3 and HIF1α by

FACS (data not shown). However since PMA is known to activate a variety of PKCs including PKC-θ which is known to act downstream of mTORC2, it may be that PMA mediated activation of PKC-θ circumvents Rapamycin induced mTORC2 inhibition thereby releasing *Il-17a* expression from the Rapamycin mediated inhibition of *IL-17a* expression (possibly by enhancing transcription of the Th17 lineage determining factor RORC). Irrespective of the precise mechanism underlying this effect, these results indicate that analysis of cytokine production *in vitro* or *ex vivo* by PMA/ionomycin stimulation is likely to mask effects of mTOR inhibition on IL-17A expression. However, further experiments will have to be conducted to address the role of PKC signalling in the regulation of *Il-17a* and *Foxp3* expression in greater detail.

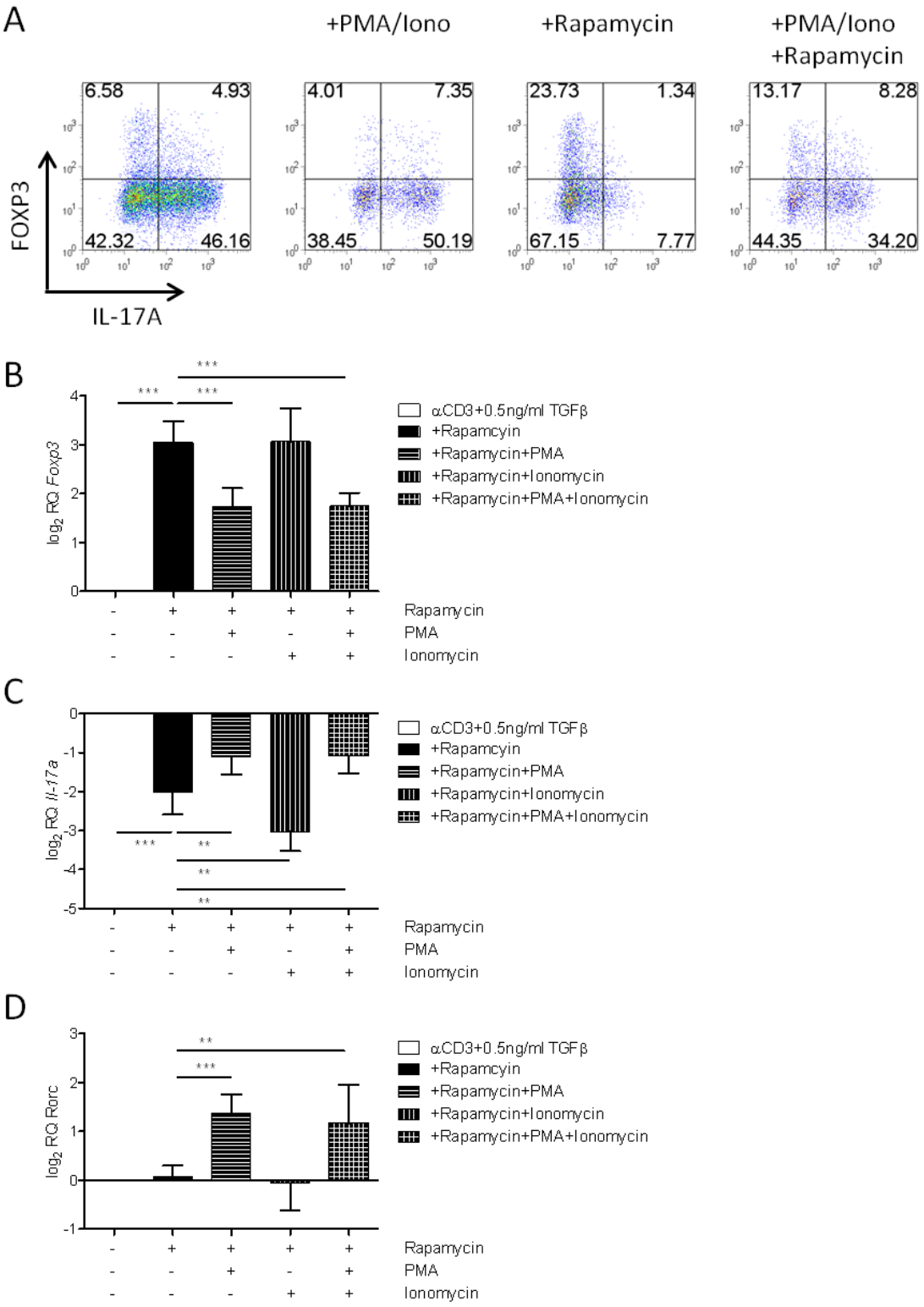


Figure 68. PMA partially blocks both the Rapamycin induced reduction of *Il-17a* expression and the enhancement of *Foxp3* induction. EL4.B02 cells were stimulated at 10^4 cells/ml for 3 days with αCD3, 0.5 (B-D) or 5ng/ml (A) TGFβ, plus minus 5nM Rapamycin. 50ng/ml PMA and 500ng/ml Ionomycin was added for the last 4h of the stimulation as indicated. (A) Representative FACS plots of IL-17A and FOXP3 expression are shown. Real time PCR analysis of *Foxp3*, *Il-17a* and *Rorc* expression in cDNA samples prepared from EL4.B02 stimulated as described above and indicated. Data was normalized to *Hprt1* cDNA levels and is presented relative to cells stimulated at low density with αCD3+0.5ng/ml TGFβ for 3 days. Mean and standard deviation of 5 biological replicates is presented. Statistical analysis was performed using repeated measure one-way ANOVA with Bonferroni's multiple comparison post test (**p<0.01, ***p<0.001, ****p<0.0001).

Chapter 6 | A PHOSPHO-PROTEOMICS SCREEN TO IDENTIFY DOWNSTREAM TARGETS OF mTOR INVOLVED IN THE INDUCTION OF FOXP3

Despite extensive efforts to indentify the downstream targets of mTOR involved in the regulation of FOXP3 expression, the luciferase based “bottom up” approach failed to pin down promising candidates. Since immediate targets of the mTOR kinase will likely be regulated by phosphorylation at serine and threonine residues, a mass spectrometry based phospho-proteomics approach was chosen to screen for targets downstream of the two mTOR complexes.

Insights gained from previously described experiments on the characteristics of the EL4.B02 system, the role of the two mTOR complexes in the regulation of FOXP3 expression as well as the kinetics of mTORC1 and 2 inhibition by Rapamycin and Torin 1 provided the basis for the design of the phospho-proteomics approach. The basic parameters for the stimulation used in the proteomics experiments were established early on by revealing a high dependency for induction of FOXP3 on TGFβ and CD3 signalling (Figure 9). Additional experiments have demonstrated that stimulation at high cell densities for short periods was both technically feasible and resulted in enhanced induction of *Foxp3* mRNA in the presence of both Rapamycin and Torin 1 as early as 6 hours into the stimulation (Figure 32). Therefore an mTOR mediated signalling event is likely to occur within those first 6 hours. This does not of course, rule out that events which occur at later time points contribute to the enhanced induction of FOXP3. Both Rapamycin titrations and time course analysis illustrated that inhibition of both complexes seemed to contribute independently to the induction of FOXP3 (Figure 31 and 33). Furthermore, time course studies analyzing the activity of the two mTOR complexes in the presence of Rapamycin and Torin 1 demonstrated that the former almost exclusively inhibited mTORC1 in the first hours of stimulation whereas the latter inhibited both complexes almost instantly (Figure 30). Based on these data

the cells to be analyzed were stimulated for 2 hours with αCD3 and TGFβ with or without Rapamycin or Torin 1.

In order to allow quantitation of phosphorylation events affected by Rapamycin or Torin 1 and to prevent the introduction of processing mediated artefacts, an approach based on stable isotope labelling by amino acids in cell culture (SILAC) was chosen [238-241]. In this technique cell lines are cultured in medium lacking the essential amino acids lysine and arginine but supplemented instead with non-radioactive, isotopically labelled forms of these amino acids. The cells cultured in these media incorporate labelled amino acids into all newly synthesized proteins over the course of several divisions. By using amino acids of different molecular weight ("light" (normal AA), "intermediate" and "heavy" AA) proteins and peptides derived from three differentially labelled cell lines can be distinguished by mass spectrometry based on the mass difference detected for a given peptide sequence. Furthermore differences in peptide abundance ratio from the "light", "intermediate" and "heavy" cell lines can be quantified. The introduction of artefacts that result from the differential handling of the three populations of labelled proteins is minimized since the ability of the mass spectrometer to distinguish the differentially labelled proteins permits pooling of proteins in one sample. In the experiments described in this chapter the triple SILAC labelling was utilized to distinguish and quantify the changes in the phosphorylation events that were induced in EL4.B02 cells stimulated with αCD3, TGFβ and IL-2 following the addition of Rapamycin or Torin 1.

Although over 500 kinases are known to facilitate phosphorylation of proteins and tens of thousands of phosphorylation sites have been identified in the human proteome [242-246], phosphorylated proteins are still relatively infrequent compared to their

unphosphorylated counterparts and non-phosphorylated proteins. Even though a given phospho-protein often contains multiple phosphorylation sites across its AA sequence the relative abundance decreases even further when phospho-proteins are analyzed at the peptide level as is required for mass spectrometry mediated analysis. Since a multiply phosphorylated protein will yield some phospho-peptides and a multitude of non-phosphorylated peptides, the relative abundance of phospho-peptides is extremely low in a peptide mixture derived from a whole cell lysate. Given that the most frequent peptides will be preferentially identified even with an instrument of high sensitivity such as a mass spectrometer, only the most abundant phospho-peptides will be indentified and quantified. Therefore a successful phospho-proteomics approach must comprise a phospho-protein/peptide enrichment step in order to yield a respectable number of identified phosphorylated sites. Immunoprecipitation of tyrosine-phosphorylated proteins has been successfully employed to enrich for tyrosine-phosphorylated proteins [247-250]. In principal immunoprecipitation could also provide a means to enrich for proteins phosphorylated on serine and threonine residues [251], however the fact that antibodies against serine and threonine phosphorylated sites exhibit a higher degree of specificity towards the adjacent AA this approach would require a cocktail of different antibodies. The emergence of enrichment techniques such as immobilized metal ion affinity chromatography (IMAC) or titanium dioxide (TiO_2) chromatography that demonstrate high affinity towards phospho-amino acids enabled efficient enrichment of phospho-proteins and -peptides [252-257]. Both methods, IMAC and TiO_2 chromatography, are relatively simple, fast and do not require any expensive equipment and have therefore been used extensively in phospho-proteomics studies [244, 245, 258-263]. Since phospho-peptide enriched fractions

still represent a relatively complex mixture further pre-fractionation techniques such as strong cation exchange (SCX) chromatography were combined with the phospho-peptide enrichment protocols in order to facilitate better identification of phospho-sites in global phosphorylation analysis [264]. During SCX chromatography peptides are fractionated according to their solution charge state at low pH. Most tryptic peptides have a solution charge state of +2 due to argine or lysine residues at the one end of the peptide and the free amine group at the other end. Basic AA within the peptide sequence that are protonated at low pH will further increase the total charge by +1 whereas phosphate groups of phospho-tyrosine, -serine or -threonine residues will lower the solution charge of a peptide by -1. Therefore most phospho-petides will have solution charge state of +1. In contrast to peptides generated from proteins digested with the lysyl endopeptidase C (LysC), used in the first phospho-proteomics experiment, tend to have higher solution charges. This is because the protease only cleaves after lysines and therefore produces longer peptides which increases the likelihood that additional positively charged AA are part of the peptide sequence.

Until Dephoure et al. established a simple, solid phase extraction column based SCX protocol an expensive HPLC system was necessary to perform fractionation of peptides by solution charge [191]. The phospho-proteomics experiments illustrated in figure 69 followed the basic protocol of Dephoure et al. with minor alterations. Furthermore TiO_2 rather than IMAC mediated phospho-peptide enrichment was used since this technique had been successfully employed in the department previously.

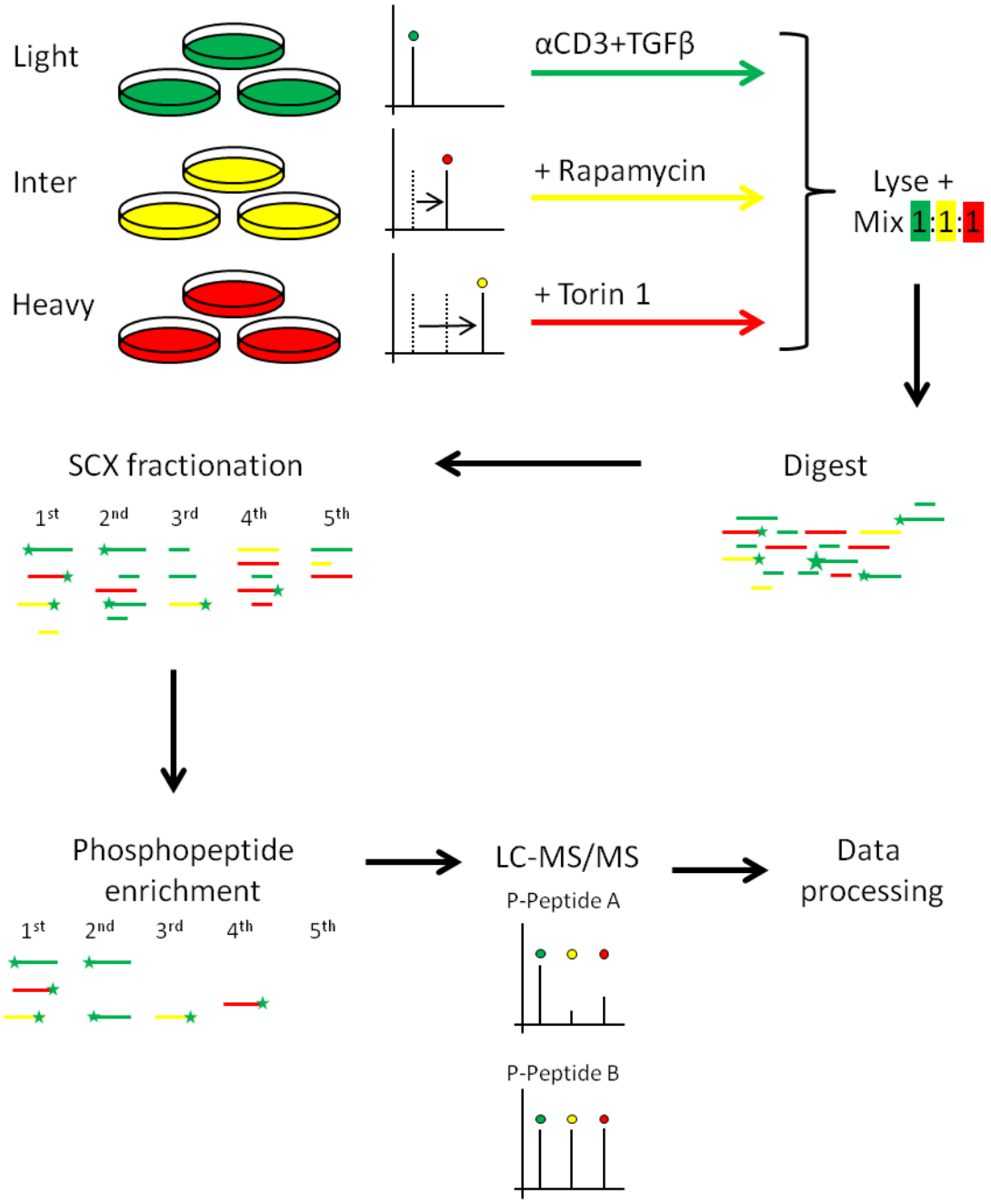


Figure 69. Workflow of the phosphoproteomics experiments. SILAC labelled EL4.B02 cells were stimulated for 2 hours with αCD3, 5ng/ml TGFβ and 250U/ml IL-2 (not indicated) in the presence or absence of 5nM Rapamycin or 250nM Torin 1. Either cells or lysates were mixed at one to one to one ratio and digest with LysC/trypsin. SCX-fractionation of the peptide mixture separates the peptides according to their solution charge and whereas TiO_2 enriches for phospho-peptides. LC-MS/MS identifies and quantifies the peptides along with their isotope labels and modifications.

6.1 | EL4.B02 cells readily grow in SILAC labelling medium and retain their FOXP3 inducibility

Since some cells lines divide very slowly or even die in the SILAC medium (for example due to the slightly different composition of the media or the supplementation of dialysed FCS instead of normal FCS), the growth of the cells was monitored carefully after the medium exchange. After an initial lag phase in which the cells exhibited decreased proliferation an almost normal growth rate was reached. After 7 days of culture and at least 10 cell divisions stocks of “light”, “intermediate” and “heavy” cells were frozen.

It was important to check whether the cells retained their FOXP3 inducibilty and were still responsive to Rapamycin mediated mTOR inhibition. “Heavy” SILAC labelled EL4.B02 cells were stimulated with αCD3, TGFβ, IL-2 and with or without Rapamycin for 3 days. Although the proportion of cells responding was slightly decreased compared to unlabelled cells, Rapamycin efficiently enhanced the induction of FOXP3 (Figure 70).

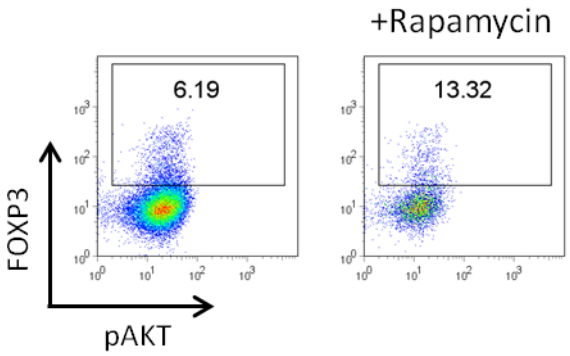


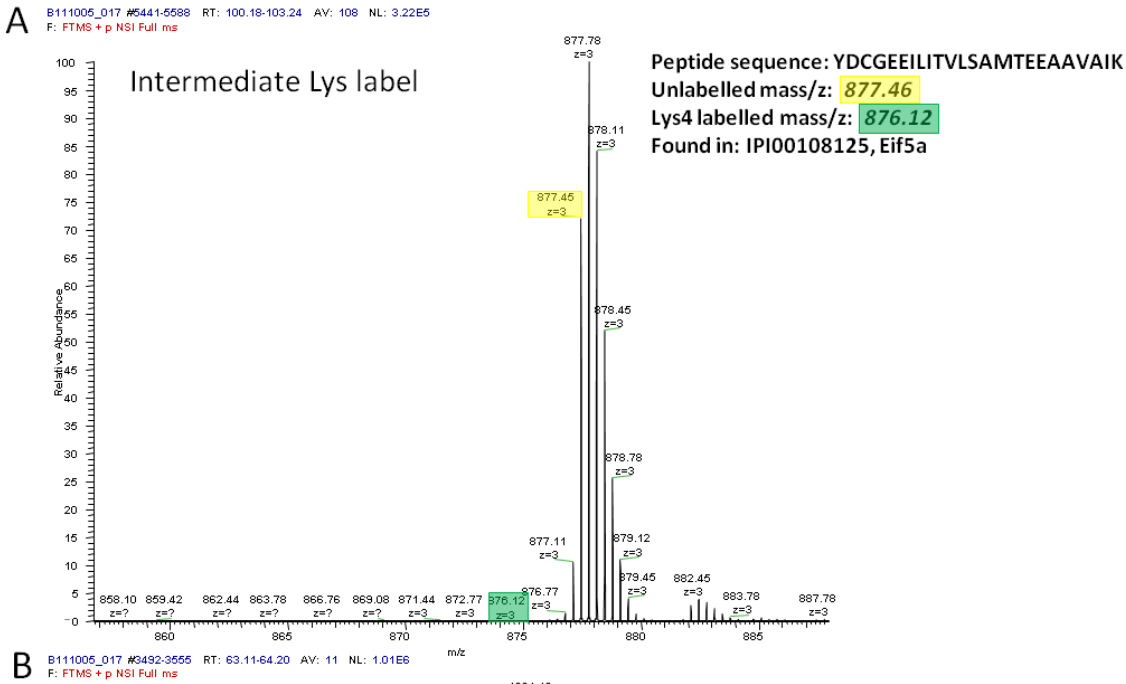
Figure 70. Heavy SILAC labelled EL4.B02 cells retain their responsiveness with respect to mTOR inhibition mediated FOXP3 induction. EL4.B02 cells were stimulated at 10^4 cells/ml with αCD3, 5ng/ml TGFβ and 250U/ml IL-2 in the presence or absence of 5nM Rapamycin. Dot plots indicating the percentage of $FOXP3^+$ cells and the levels of pAKT are shown.

6.2 | Selected proteins in intermediate and heavy SILAC EL4.B02 cells show more than 95% incorporation of the isotopically labelled AAs

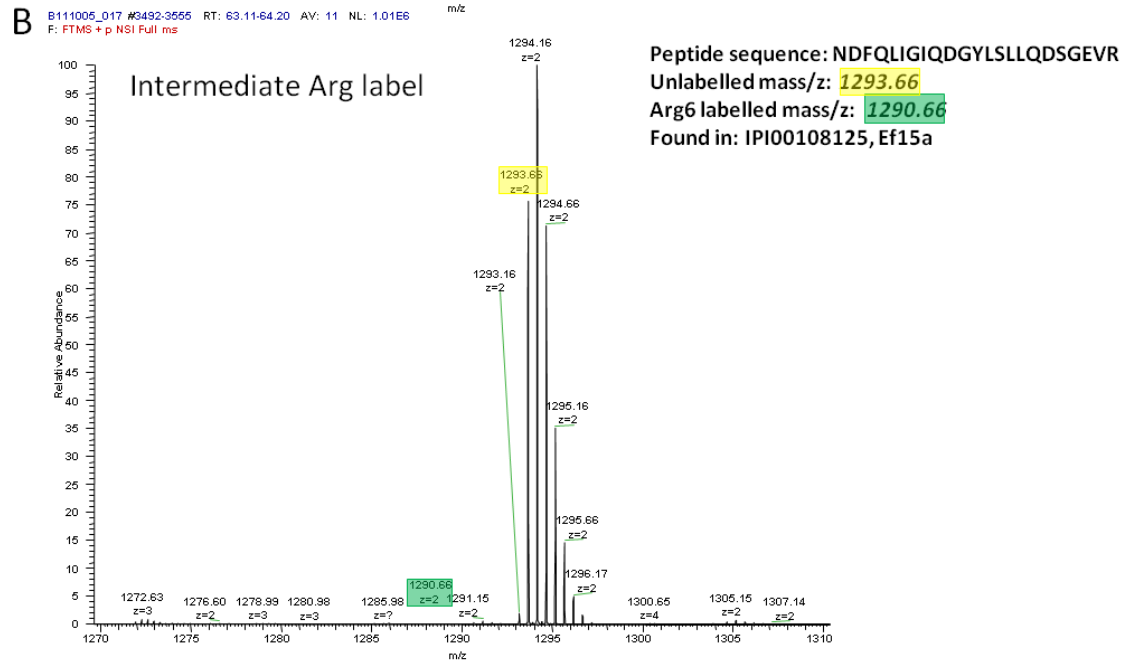
The thorough labelling of cellular proteins with the isotopically labelled AAs is a prerequisite for an accurate quantitation of changes in the phosphorylation state of proteins. Therefore EL4.B02 cells labelled with “light”, “intermediate” and “heavy” AAs were lysed and subjected to SDS-PAGE. Random bands of each label were cut out, digested with trypsin and analyzed by LC-MS/MS mass spectrometry. As illustrated in figure 71, the mass spectra for a four selected peptides indicated homogenous incorporation of the different labels.

Furthermore it was important to establish that lysates derived from the differentially labelled cells can be accurately mixed at a ratio of 1:1:1. Only if equal amounts of each set of labelled proteins are pooled into one sample, can an accurate quantitation of changes in the labelled proteins be achieved. Similarly to the analysis of label incorporation the 1:1:1 mixture was separated by SDS-PAGE, trypsin digested and analyzed by LC-MS/MS mass spectrometry. The analysis revealed that equal amounts of each lysates were mixed, since the peaks for the selected peptides exhibit similar intensities (Figure 72).

A


B111005_017 #5441-5588 RT: 100.18-103.24 AV: 108 NL: 3.22E5
F: FTMS + p NSI Full ms
Intermediate Lys label
Peptide sequence: YDCGEEILITVLSAMTEEAAVAIK
Unlabelled mass/z: 877.46
Lys4 labelled mass/z: 876.12
Found in: IPI00108125, Eif5a
Relative Abundance
m/z

B


B111005_017 #3492-3555 RT: 63.11-64.20 AV: 11 NL: 1.01E6
F: FTMS + p NSI Full ms
Intermediate Arg label
Peptide sequence: NDFQLIGIQDGYLSLLQDSGEVR
Unlabelled mass/z: 1293.66
Arg6 labelled mass/z: 1290.66
Found in: IPI00108125, Ef15a
Relative Abundance
m/z

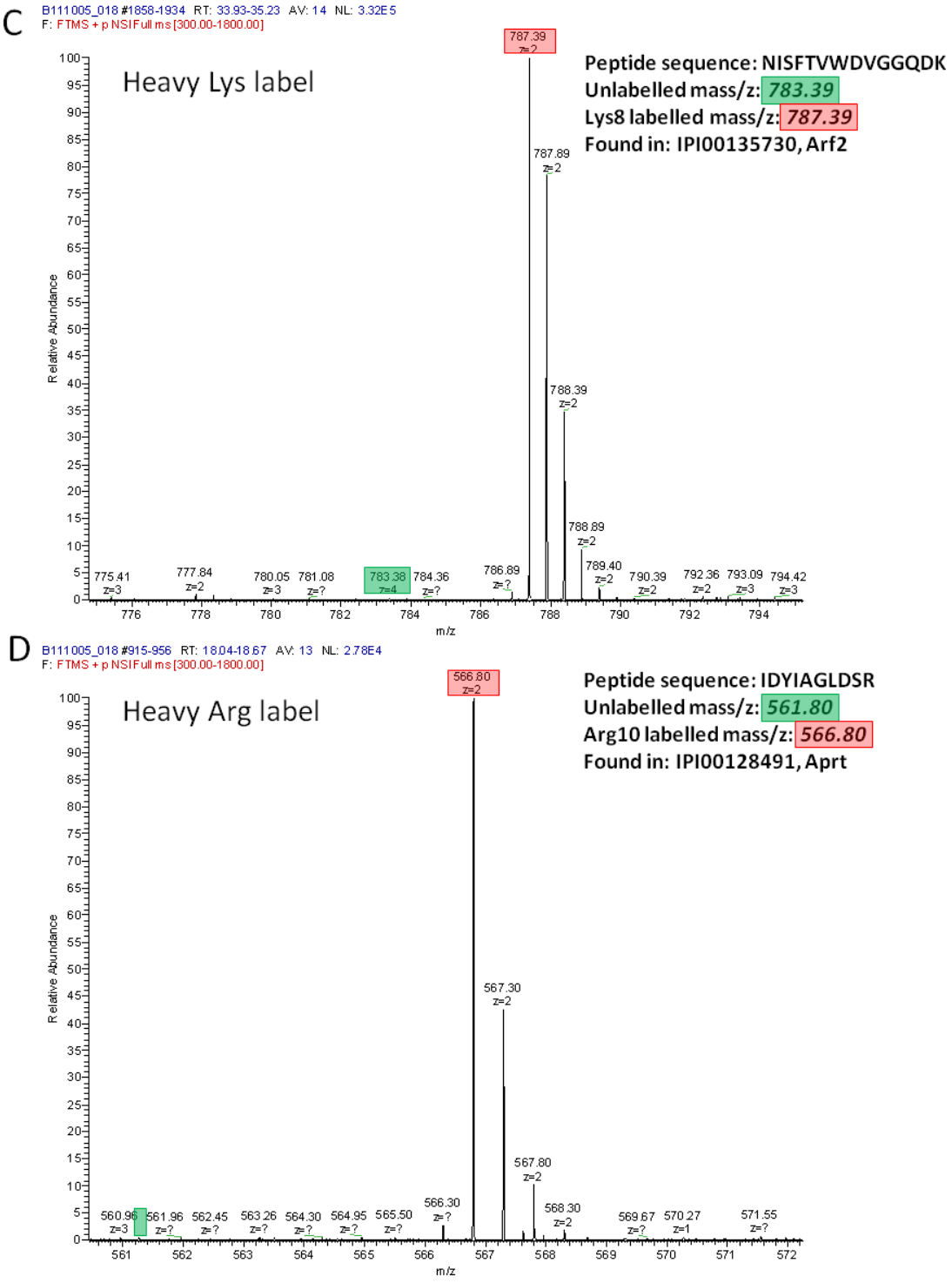


Figure 71. Massspectra of peptides derived from intermediate and heavy SILAC labelled EL4.B02 cells. SILAC labelled cells were lysed and lysates subjected to SDS-PAGE, tryptic digest and LC-MS/MS analysis. (A, overleaf) Representative peptide with incorporated intermediate weight Lysine. (B, overleaf). Representative peptide with incorporated intermediate weight Arginine. (C) Representative peptide with incorporated heavy weight Lysine. (D) Representative peptide with incorporated heavy weight Arginine.

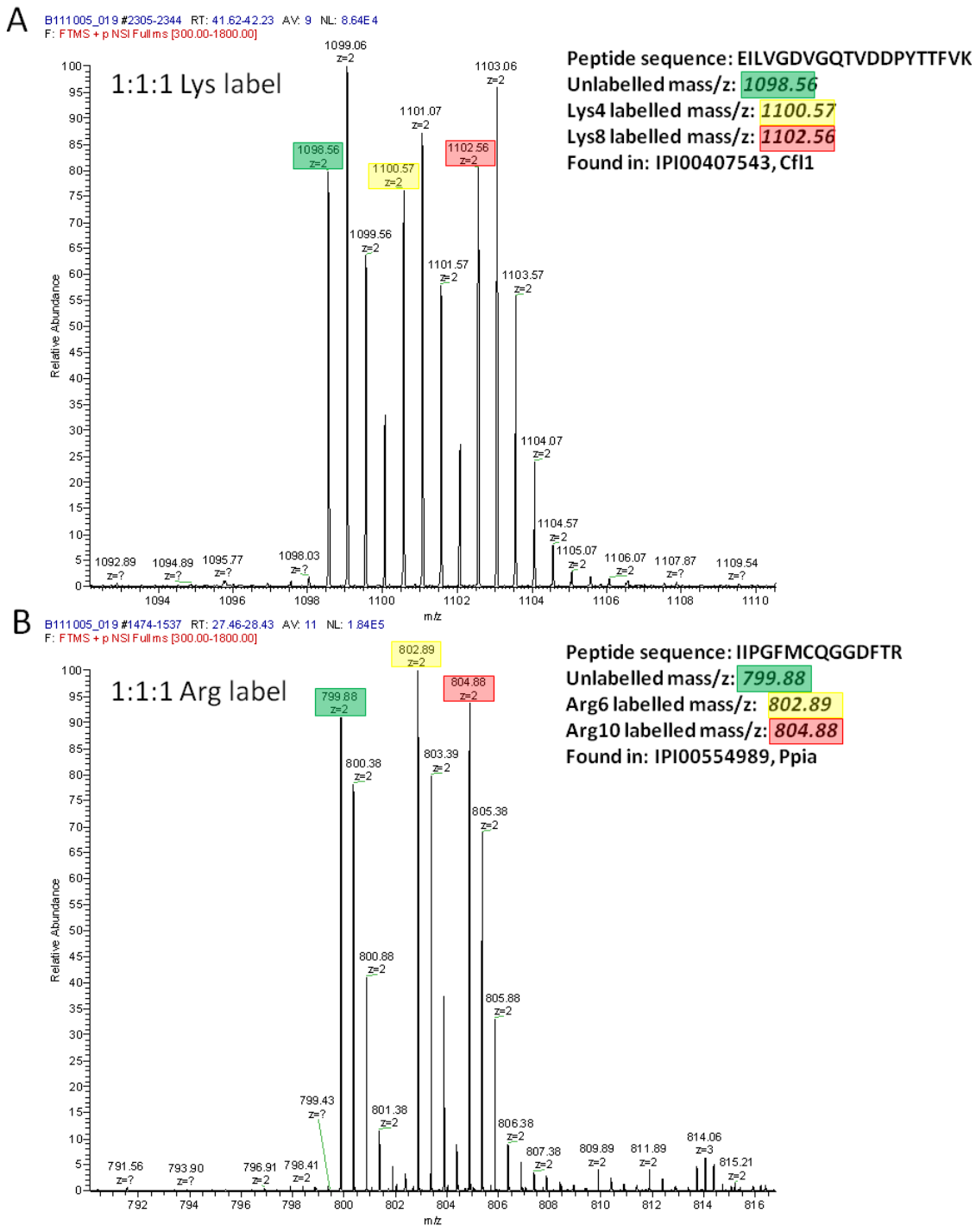


Figure 72. Massspectra of peptides derived from 1:1:1 (light:intermediate:heavy) mix of SILAC labelled cells. SILAC labelled cells were lysed and mixed at 1:1:1 ratio. Lysate mixture was subjected to SDS-PAGE, tryptic digest and LC-MS/MS analysis. (A) Representative peptide showing similar intensities of light, intermediate and heavy Lysine label. (B) Representative peptide showing similar intensities of light, intermediate and heavy Arginine label.

6.3 | The first phospho-proteomics experiments

6.3.1 | SCX fractionation separates peptides based on their solution charge state

As mentioned earlier phospho-peptide enrichment should be preceded by a SCX fractionation step that separates the peptides by solution charge and further reduces the complexity of the sample. The analysis of the solution charge of peptides in the 6 SCX, TiO_2 enriched fractions that were generated from LysC digested peptides in the first experiment revealed that the protocol based on Dephoure et al. did indeed clearly separate peptides according to their charge (Figure 73A (all peptides) and B (phospho-peptides only)). Predictably, the contribution of lower charged peptides to the overall number of peptides in each fraction was higher when non phospho-peptides were excluded from the analysis since the phosphate groups in the phospho-peptides reduced the charge of a given peptide (compare figure 73B versus 73A). As expected from LysC digested peptides the majority of peptides had a solution charge of +2, an effect that was even more pronounced when only phospho-peptides were analyzed (Figure 73C and D). Additionally the distribution of peptides over the different charge states seemed to be shifted to lower charges when non-phospho-peptides were excluded from the analysis (-1, due to the negative charge of the phosphate groups). Furthermore, the first 3 fractions that contained the lower solution charge peptides also contained the highest number of peptides (Figure 73E and F). This effect was again more pronounced when only phospho-peptides were analyzed.

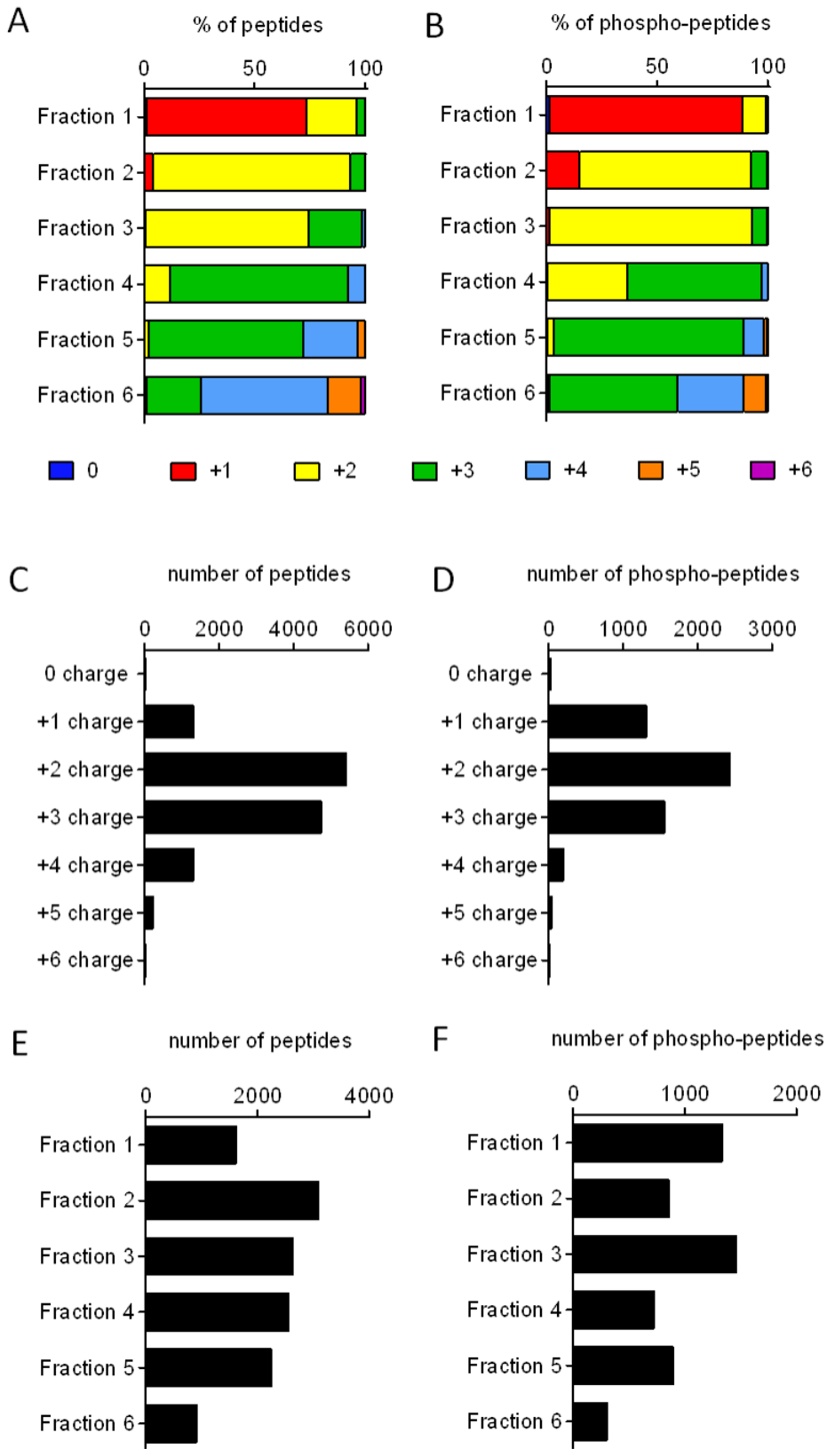


Figure 73. SCX-fractionation separates peptides according to their solution charge. Top panel (A,C,D) and bottom panel (B,D and F) show results for all peptides or phospho-peptides respectively. (A and B) The proportion of (phospho-)peptides with solution charges of 0 to +6 within the different SCX fractions. (C and D) The absolute number of (phospho-)peptides with solution charges of 0 to +6. (E and F) The absolute number of (phospho-)peptides identified in the SCX fractions.

6.3.2 | TiO_2 results in moderate enrichment of phospho-peptides

The analysis of the efficiency of the TiO_2 mediated phospho-peptide enrichment revealed that only a moderate enrichment was achieved (average enrichment over all fractions: 42.6%). Very good enrichment should have resulted in more than 70% phospho-peptides of all the peptides that were identified. This could indicate that the conditions during incubation of the peptide mixture with the TiO_2 were not appropriate to block non-specific binding or that the subsequent washing steps were not stringent enough. Nevertheless, these results provided a good starting point for further optimisation of the protocol.

A detailed analysis demonstrated that the enrichment only achieved high efficiencies in the 1st fraction or solution charge states of 0 and +1 and was low in the subsequent fractions and solution charge states (Figure 74A and B). This could on one hand, be explained by the fact that this fraction was already enriched for phospho-peptides due to the SCX fractionation or on the other hand, that the lower number of peptides in this fraction (Figure 73E and F) resulted in less non-specific binding. The latter explanation seemed to be unlikely since the 6th fraction contained even fewer peptides than the 1st fraction, however the enrichment efficiency was considerably lower.

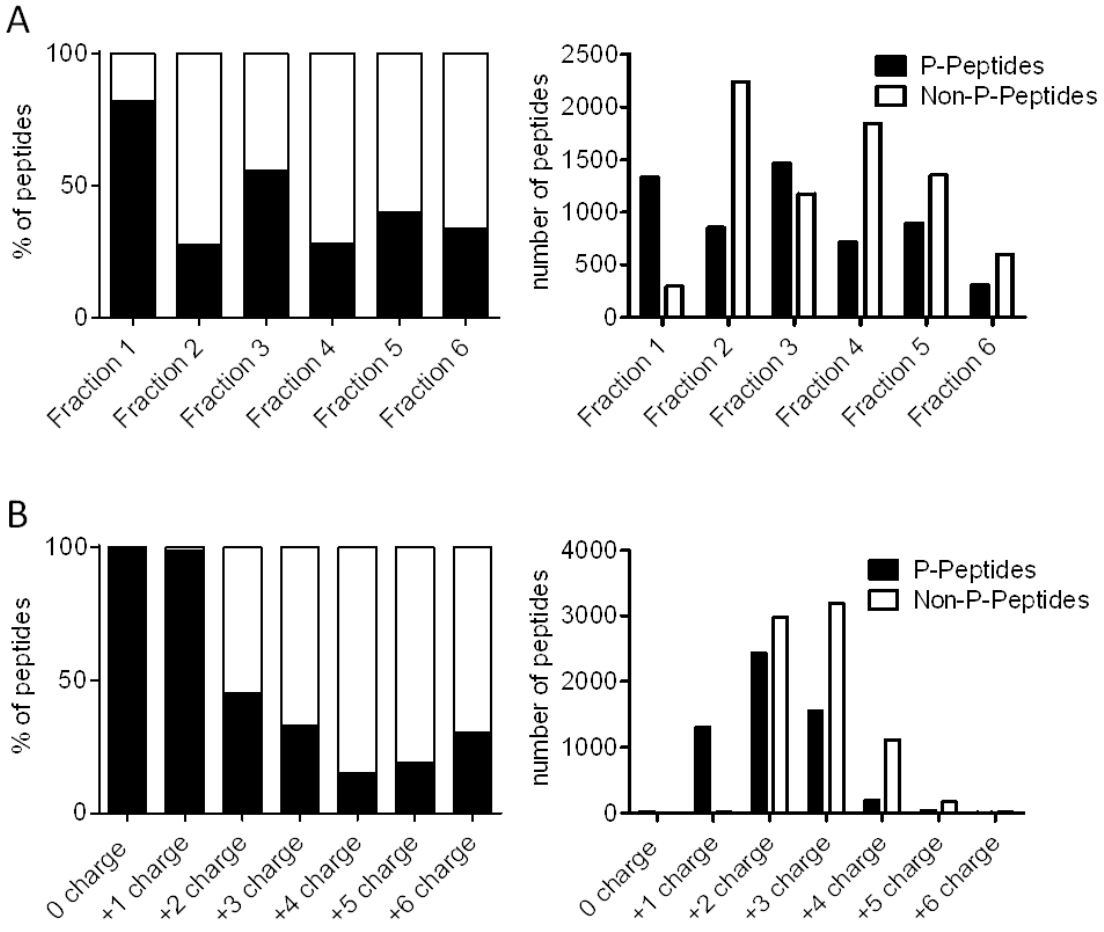


Figure 74. Titanium dioxide incubation moderately enriches for phospho-peptides. (A) The proportion and absolute number of phospho-peptides (black) and non-phospho-peptides (white) found in the six SCX fractions are displayed. (B) The proportion and absolute number of phospho-peptides (black) and non-phospho-peptides (white) with the indicated solution charge.

6.3.4 | TiO_2 enriches preferentially for monophosphorylated peptides

Since TiO_2 is known to preferentially enrich for peptides with one rather than multiple phosphorylations due to the extremely high affinity of the resin for phosphate groups [265], the degree of phosphorylation of the identified peptides was analyzed. Indeed, the total number of monophosphorylated peptides was by far larger than that of peptides with multiple phosphorylation sites (Figure 75A). Expectedly, the proportion of peptides with multiple phophorylations was highest in the peptides with solution charges of 0 and +1 (Figure 75B). Considering the small number of peptides with multiple phosphorylation sites, these charge states contributed little to the overall number of phospho-peptides (Figure 75C).

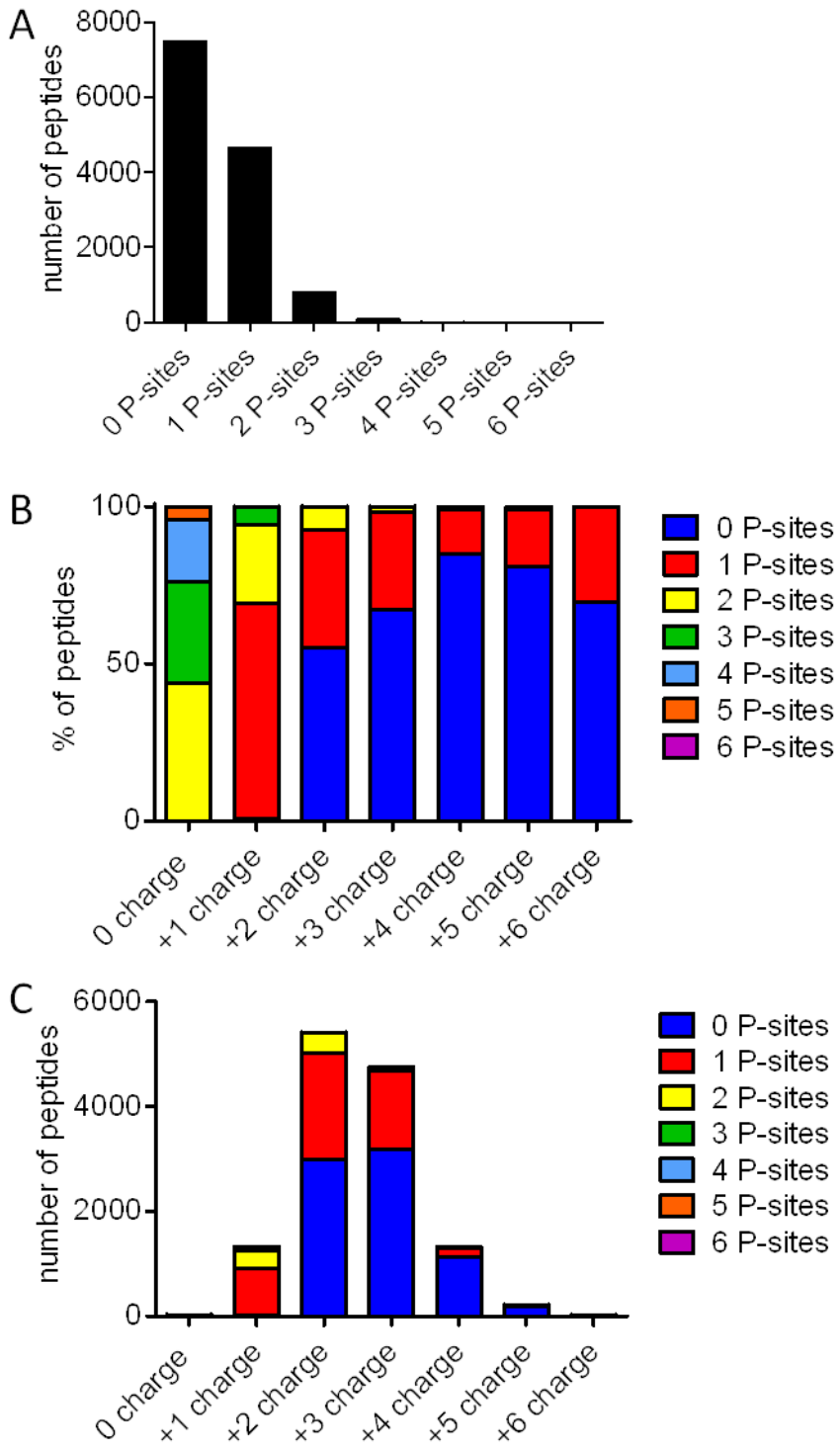


Figure 75. Titanium dioxide preferentially enriches for monophosphorylated peptides. (A) The absolute number of peptides with 0 to 6 phospho-sites are displayed. (B) The proportion and (C) absolute number of peptides with 0 to 6 phospho-sites and their respective solution charge.

6.3.5 | Analysis of proteins with sites differentially regulated by Rapamycin and Torin 1

The analysis of phospho-sites and the corresponding proteins revealed a number of caveats with the software tools used for the analysis. These problems remain unresolved to date and, at least in part, interfered with an unambiguous, conclusive and comprehensive analysis of the datasets.

In order to focus on phospho-peptides that included phospho-sites with considerable changes in their phosphorylation levels in response to Rapamycin or Torin 1 treatment, the MaxQuant output files (version 1.2.2.5, Ensembl genome assembly NCBIM37 release 67) were loaded into the Proxeon Protein Center software. However, Protein Center does not yet contain functions that allow filtering of the data at the peptide or phospho-site level. As this is a prerequisite for a proper analysis of phospho-proteomics datasets, analyses such as the calculation of fold-change cut-offs and the filtering of the datasets had to be performed in Microsoft Excel. Modified and filtered text-files generated in Excel were then loaded into Protein Center and analyzed with respect to signalling pathway enrichment and gene ontology. Due to the laborious nature of this procedure, the data presented here does not represent a comprehensive analysis and is likely to just scratch the surface of the information in the datasets. Since neither Excel nor Protein Center allowed for an exclusion of peptides that did not uniquely identify a given protein (peptide sequences found in several isoforms of a protein or in (closely) related proteins), the data presented here also has to be interpreted with caution with respect to the identified proteins. The inability to exclude peptides that do not uniquely identify proteins plus the fact that splice variants of a given protein are

listed as separate proteins, frequently resulted in larger numbers of identified proteins than peptides.

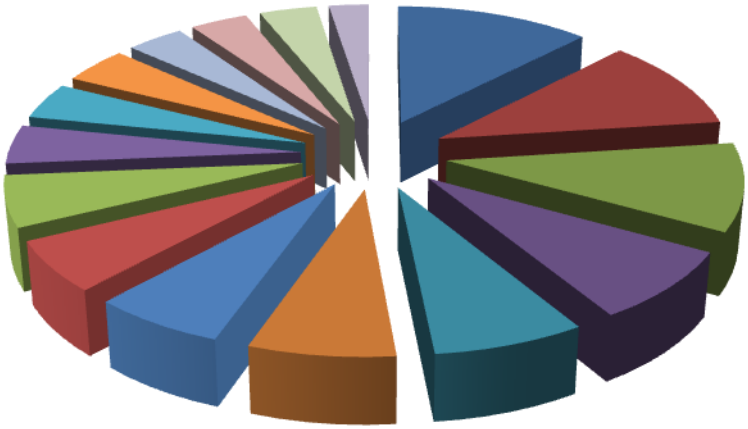
In addition to settings applied in Maxquant which aim to restrict the analysis on accurately identified peptides, phospho-sites and proteins (FDR smaller than 0.01 for all) additional cut-offs were defined. Only peptides with Andromeda score greater than 20 (Andromeda score: arbitrary unit/score indicating the similarity of the theoretical MS/MS spectra of a given peptide and the measured MS/MS spectra) and phospho-sites that could be localized with a probability greater than 0.5 (probability with which MaxQuant can assign the detected phosphorylation to a particular serine, threonine or tyrosine residue) were included in the analysis. In order to define a significance cut-off for changes in the ratio between the differentially treated cells, i.e. “light” versus “intermediate” (no inhibitor/Rapamycin) label and “light” versus “heavy” label (no inhibitor/Torin 1), the absolute z-score was calculated. The formula for the calculation was the following:

$$\text{Absolute z-score} = \frac{(\log_2 \text{ of ratio} - \text{median of all } \log_2 \text{ ratios})}{(\text{median } |\log_2 \text{ ratio} - \text{median of all } \log_2 \text{ ratios}| * 1.4826)}$$

Similarly to analysis performed by Hsu et al., values beyond 2.5 and -2.5 were considered significant changes [266].

The experiment identified 3586 unique phospho-peptides with an Andromeda score above 20 in 3597 proteins. At the phospho-site level 2343 sites were detected with a score greater than 20 and a localization probability of greater than 0.5. The 2343 sites were assigned to 3134 proteins. The analysis for KEGG Pathway enrichment revealed

that a variety of signalling pathways, including the mTOR pathway, were over-represented in the dataset (Figure 76). The 13 proteins annotated as components of the mTOR signalling pathway included mTOR complex components such as RAPTOR, RICTOR and PRAS40 as well as upstream and downstream targets of the two mTOR complexes such as AKT2, EIF4E2, TSC2 and S6K1. The identification of phospho-proteins of the mTOR pathway was essential for the analysis since it provided a quality control for the experiment and raised the chances that mTOR targets involved in the regulation of FOXP3 could be identified. Gene ontology analysis highlighted that a multitude of molecular functions (277) were overrepresented in the dataset. Encouragingly, these included molecular functions such as “chromatin binding” (GO:0003682, Count: 128), “transcription factor binding” (GO:0008134, Count: 108) and “DNA binding” (GO:0003677, Count: 483), supporting the aim of the approach in screening for proteins involved in transcriptional regulation. Amongst the phospho-proteins annotated as “DNA binding”, transcription factors known to regulate T-cell differentiation, such as ATF2, BCL6, FOXO1, IRF3 and SP-1, as well as proteins involved in the regulation of epigenetic modifications, such as DNMT1, DNMT3A and HDAC7, were identified.



KEGG Pathway	Count	FDR p-value
RNA transport (mmu03013)	44	6.09E-15
Tumor viruses and cancer (mmu05203)	38	4.00E-08
Spliceosome (mmu03040)	36	3.03E-13
Epstein-Barr virus infection (mmu05169)	29	5.19E-04
Alcoholism (mmu05034)	26	1.71E-05
Cell cycle (mmu04110)	25	4.40E-06
Herpes simplex infection (mmu05168)	23	2.48E-02
mRNA surveillance pathway (mmu03015)	21	2.90E-06
Ribosome (mmu03010)	21	3.57E-06
Ribosome biogenesis in eukaryotes (mmu03008)	16	5.25E-04
Systemic lupus erythematosus (mmu05322)	15	9.17E-03
Oocyte meiosis (mmu04114)	15	3.13E-02
mTOR signaling pathway (mmu04150)	13	2.27E-03
Fc gamma R-mediated phagocytosis (mmu04666)	13	2.48E-02
Progesterone-mediated oocyte maturation (mmu04914)	13	2.48E-02
DNA replication (mmu03030)	9	3.44E-03

Figure 76. KEGG-pathway enrichment of 1st phospho-proteomics data set. All KEGG pathways with significant enrichment as determined by the analysis of the MaxQuant out-put files in Proxeon Protein Center are shown. A false discovery rate (FDR) of 0.05 was set for the analysis. "Count" indicates the number of proteins present in the dataset for the indicated KEGG-pathway.

The use of the z-score cut-off of +/-2.5 showed that the vast majority of phospho-sites did not seem to be regulated by mTOR inhibition mediated by Rapamycin or Torin 1 (Figure 77, median $\log_2$(Rapamycin/no inhibitor): -0.01588, median $\log_2$(Torin 1/no inhibitor): -0.03959).

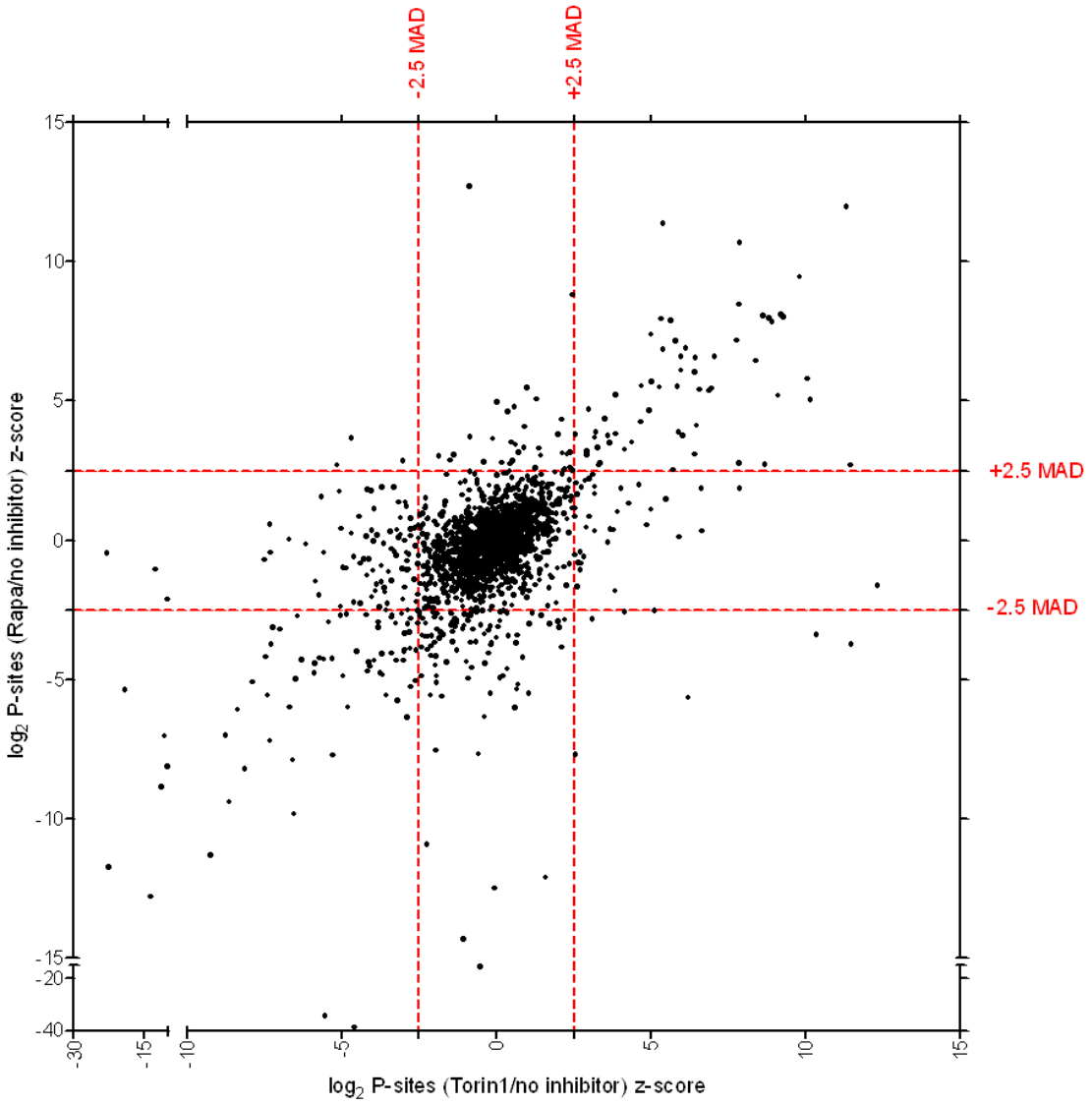


Figure 77. mTOR inhibition reduces and increases the levels of phosphorylation at a large number of phospho-sites. The absolute z-score values of the ratio of differentially treated cells for each phosphorylation site detected (individual dots) is indicated in the graph. Z-scores above +2.5 and below -2.5 were considered as significantly up- and down-regulated.

194 phospho-sites in 382 proteins were negatively regulated by Rapamycin. These sites included 5 known mTOR pathway proteins such as S6K1, RICTOR and EIF4EBP1. The identification of these sites confirmed that Rapamycin reduced the kinase activity of mTOR towards well established downstream targets. Besides the mTOR pathway, proteins in “Ribosome” and “RNA transport” pathways were also significantly enriched (mTOR: FDR p=0.00577, Ribosome: FDR p= 0.0000354, RNA transport: FDR p=0.00703). Gene ontology analysis revealed that numerous molecular functions are overrepresented in the phospho-proteins negatively regulated by Rapamycin.

The “DNA binding” category included transcriptional regulators DNMT3A and NFATc2, whose phosphorylations at S102 and S328 respectively were negatively regulated by Rapamycin. The function of these phosphorylation sites for the activity of these two proteins is currently unknown, however both DNMT3A and NFAT proteins have been implicated in the regulation of *Foxp3* expression. Whereas DNMT3A transfection inhibited the activity of *Foxp3* enhancer containing luciferase constructs, NFAT was demonstrated to bind and cooperate with SMAD3 in the induction of FOXP3 [160, 171]. Interestingly, the activity and nuclear localization of NFAT was demonstrated to be dependent on several dephosphorylation events [267], raising the possibility that the mTOR inhibition-mediated dephosphorylation at S328 might contribute to the activation of NFAT. Consistent with a role of mTOR in regulating NFATc2 phosphorylation at S328, this site was also negatively regulated by Torin 1, however the z-score (-2.48) was just above the cut-off of -2.5. Similarly, S102 DNMT3A was also negatively regulated by Torin 1. However, the involvement of these changes in the mTOR inhibition-mediated enhancement of FOXP3 induction remains speculative.Additional experiments are needed to validate the effect on NFATc2 and

DNMT3A phosphorylation and demonstrate a role in the regulation of FOXP3 expression.

Another phospho-protein of interest with respect to the regulation of FOXP3 expression that was negatively regulated by both Rapamycin and Torin 1 is the SUMO E3 ligase PIAS1 (S483 and S485). PIAS$^{-/-}$ mice have increased number of natural Treg as well as an increased propensity to differentiate into FOXP3^{+} iTreg *in vitro*. PIAS1 is thought to exert its effect on FOXP3 expression by recruiting DNA methyltransferases, such as DNMT3A, to the *Foxp3* promoter and thereby inhibit FOXP3 expression [268]. It seems therefore possible that mTOR inhibition enhances FOXP3 expression by negatively regulating both PIAS1 and DNMT3A activity, resulting in reduced promoter methylation. Experiments using bisulfide conversion of methylated DNA or ChIP against methylated cytidine could be used as a starting point to investigate the methylation status of the *Foxp3* promoter under mTOR inhibition conditions. Generally though, more extensive “data mining” is necessary to filter out other candidates within the phospho-proteins negatively regulated by Rapamycin that could be involved in the regulation of FOXP3 expression by mTOR.

81 phospho-sites (in 135 proteins) of the 194 sites negatively regulated by Rapamycin were also downregulated by Torin 1, indicating that the two inhibitors had both overlapping and independent effects. This was at least to some extend expected due to the different mode of inhibition (Rapamycin: allosteric, Torin 1: ATP-competitive) and the differential targeting of the two mTOR complexes by the two drugs within the experimental conditions (Rapamycin: mostly mTORC1, Torin 1: mTORC1 and mTORC2).

Torin 1 inhibited the phosphorylation of 327 proteins at 179 unique phospho-sites. KEGG pathway analysis demonstrated that this set of proteins was enriched for

proteins associated with the mTOR pathway (FDR p=0.0000201). The 7 proteins annotated as being associated with mTOR signalling that were detected included 3 proteins also identified as negatively regulated by Rapamycin (S6K1, EIF4B, EIF4EBP1). Additionally Torin 1 inhibited the phosphorylation of the mTOR signalling pathway components PRAS40, RAPTOR, AKT2 and ULK1. The latter is known to be involved in autophagy, a cellular function known to be controlled by mTOR signalling [269].

Somewhat surprisingly mTOR inhibition by Rapamycin and Torin 1 also increased the levels of phosphorylation at a large number of sites (phospho-sites/proteins: 97/230 and 109/232 respectively). mTOR inhibition could cause these increases by alleviating the inhibitory effect of mTOR activity on downstream kinases or by reducing the activation of downstream phosphatases. Due to time constraints, the analysis of potentially interesting phospho-proteins that are positively regulated by mTOR inhibition is, as most of the in depth analysis, at very early stage. Therefore again only a few selected candidates will be discussed.

An analysis based on the gene ontology of phospho-proteins positively regulated by Rapamycin indicated an enrichment of proteins with “nucleic acid binding” functions. One of the proteins with increased phosphorylation levels was ARID4B, that is a subunit of the histone deacetylase-dependant SIN3A transcriptional corepressor complex. 4 different serine phospho-sites in ARID4B were deteceted, namely S431, S482, S675 and S756. However, only one, S756, was positively regulated by Rapamycin treatment. Interestingly, mice with a haploinsufficiency of ARID4B on an ARID4A deficient background ($ARID4B^{+/-}$ $ARID4A^{-/-}$), but not $ARID4A^{-/-}$ mice, exhibit decreased expression of *Foxp3* mRNA in bone marrow, pointing towards a positive role of ARID4B in the regulation of FOXP3 expression [270]. As with many of the phosphorylation sites

identified in this experiment, a precise role for the S756 phosphorylation in ARID4B function is unknown. Interestingly, the same site was not regulated by Torin 1 treatment indicating that the effect of Rapamycin on ARID4B phosphorylation might be mTOR-independent, i.e. the interaction of Rapamycin with its molecular target FKBP12 could affect other molecular targets. Further experiments will have to address whether ARID4B is involved in the regulation of FOXP3 expression, particularly in the setting of an inhibited mTOR pathway.

Another candidate whose phosphorylation status is differentially regulated by Rapamycin and Torin 1, one which could be involved in the regulation of FOXP3 expression by mTOR is the histone-lysine-N-methyltransferase EZH2. EZH2 was recently demonstrated to be involved in the epigenetic silencing of the *Foxp3* promoter through tri-methylation of Histone H3 K27 [271]. The phospho-proteomics screen revealed that the threonine sites 416 and 487 were unaffected by Rapamyin or Torin 1 treatment, whereas serine 380 was differentially regulated by the two drugs. Rapamycin inhibited the phosphorylation whilst Torin 1 enhanced the phosphorylation at the latter site. This discrepancy could be explained by the fact that under the conditions used Rapamycin only inhibited mTORC1, whereas Torin 1 inhibited both complexes. The increase in the phosphorylation detected in Rapamycin treated compared to uninhibited cells could be caused by hyper-activation of mTORC2 that is frequently observed in cells exposed to Rapamycin [272].

In summary the analysis revealed several potentially interesting proteins whose phosphorylation status seems to be regulated by mTOR inhibition and whose function could be linked to the regulation of FOXP3 expression based on evidence in the literature. The involvement of these proteins in the activation of *Foxp3* transcription

and the mechanism of how mTOR regulates the activity of these downstream targets (potentially via intermediates) will have to be addressed by further validation experiments. Additionally a more in depth analysis is likely to reveal additional putative regulators of FOXP3 expression. Nonetheless the analysis showed that the phospho-proteomics approach seemed feasible, although adaptations in the fractionation and enrichment protocols should further improve the quality and quantity of phospho-peptide, phospho-site and phospho-protein identifications.

6.4 | The second, adapted phospho-proteomics experiment shows enhanced phospho-peptide enrichement, a greater number of identified phospho-peptides and phospho-sites, but little overlap with the 1st experiment

Based on the results obtained from the first phospho-proteomics experiment, the protocol was adjusted with the aim to further reduce the complexity of the individual samples. One of the adaptations was to prepare cytoplasmic and nuclear extracts, so that the likelihood for identifications of transcriptional regulators controlled by mTOR was increased. As part of the SCX fractionation additional salt steps at the lower range (2, 5, 15mM) should facilitate the spread of peptides with lower solution charge states over more fractions, thereby reducing the complexity of the samples and aiding identification of less abundant peptides. Moreover the enrichment protocol was adapted so that the unspecific binding of non-phosphorylated peptides to the TiO_2-spheres should be reduced and a greater enrichment for phospho-peptides should be

achieved. In the following sections, which will illustrate the advances made by the new protocol with respect to fractionation and phospho-peptide enrichment, mainly the results obtained from cytoplasmic fractions are shown, since the nuclear fractions produced very similar results.

6.4.1 | The adapted SCX-protocol fractionates peptides with lower solution charge over an increased number of fractions

Similarly to the first experiments the adapted SCX-fractionation protocol separated peptides according to their solution charge. The analysis revealed that the inclusion of additional salt steps resulted in a wider distribution of peptides (with respect to number of fractions) with low solution charge (Figure 78A). It is important to note that the solution charges of the identified peptides in the second experiment were lower compared to the first experiment, since the tryptic digest generated shorter peptides (compared to the LysC digest) which have a reduced likelihood to contain additional positively charged lysine or arginine residues in the peptide sequence. Whereas in the first experiment the majority of peptides had a solution charge of +2, peptides identified in the second experiment predominantly carried a charge of +1 (Figure 78B and C, versus figure 73C and D). Predictably, this shift towards lower solution charges was even more pronounced when non-phospho-peptides were excluded from the analysis (Figure 78B versus C).

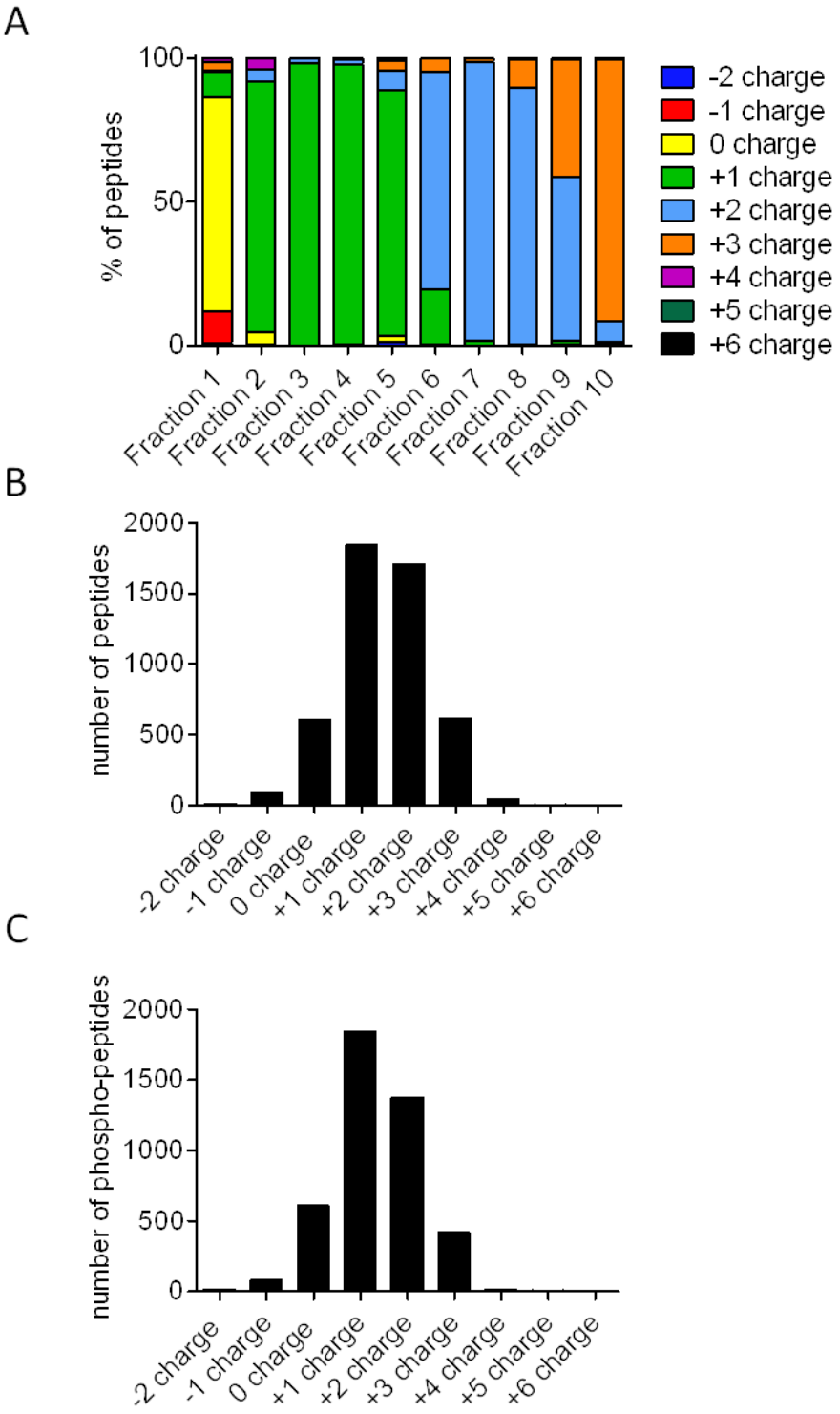


Figure 78. The adapted SCX-protocol fractionates peptides with lower solution charge over an increased number of fractions. Representative data obtained from cytoplasmic extracts are shown (nuclear extracts produced similar results). (A) The proportion of (phospho-)peptides with solution charges of -2 to +6 within the different SCX fractions. (B and C) The absolute number of all peptides (B) and phospho-peptides (C) with solution charges of -2 to +6.

6.4.2 | The adapted TiO_2-protocol enriches for phospho-peptides with very high efficiency

Surprisingly, the increased number of fractions, which was supposed to reduce complexity of the samples and thereby facilitate the identification, did not yield a greater number of peptide IDs (Figure 79A). This indicates that sample complexity might not be the limiting factor in determining large number of IDs from a given sample. However, the number of phospho-peptides was significantly increased by the alterations of the experimental protocol. Whether this increase was due to the adapted SCX-fractionation or increased efficiency of the TiO_2-mediated enrichment of phospho-peptides, remains to be determined. Compared to the 42% enrichment achieved by the original protocol, the enrichment by adapted protocol was significantly increased. 91.2% of the peptides that were identified contained one or more phosphate groups. This improvement is likely to be due to increased stringency (saturated glutamic acid) during the binding of peptides to the TiO_2-beads. With the exception of two fractions all samples showed an enrichment of greater than 70% (Figure 79B). The proportion of phospho-peptides was also analyzed with respect to the solution charge of the individual peptides. As observed in the first experiment the enrichment was best at lower solutions charges (Figure 79C). However, only 49 peptides with a solution charge greater than +3 were analyzed.

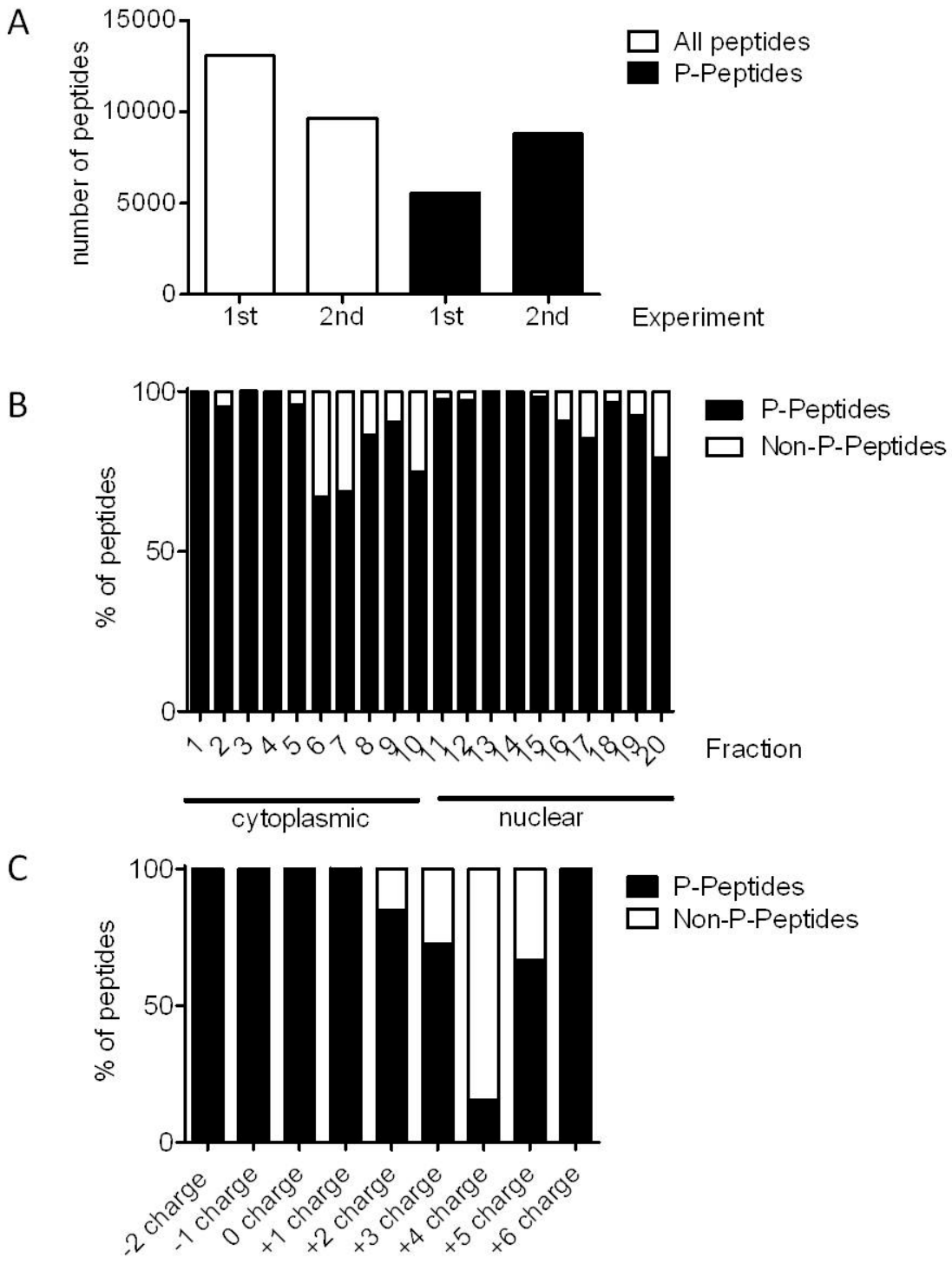


Figure 79. The adapted TiO_2-protocol enriches for phospho-peptides with very high efficiency. (A) The absolute number of peptides (white) and phospho-peptides (black) detected in the two phospho-proteomics experiments that were performed. (B) The proportion phospho-peptides (black) and non-phospho-peptides (white) found in the 20 SCX fractions (cytoplasmic extract: fraction 1-10, nuclear extracts: fraction 11-20) are displayed. (C) The proportion of phospho-petides (black) and non-phospho-peptides (white) with solution charge of -2 to +6.

6.4.3 | The adapted TiO_2-protocoll shows increased efficiency to enrich for peptides with multiple phosphorylations

The analysis of the degree of phosphorylation of the identified peptides revealed that the modified TiO_2-enrichment was not only highly efficient for monophosphorylated peptides, but that also a greater number of peptides with multiple phosphorylation sites identified compared to the first experiment (Figure 80A). An almost even number of mono- and double-phosphorylated peptides were identified. Furthermore, a significant increase in the number of phospho-peptides with three phosphorylation sites was detected. As expected, the proportion of peptides with multiple phophorylations was highest in peptides with low solution charges (Figure 80B). With increasing solution charge, the contribution of peptide with multiple phosphorylation sites decreased. Starting at a solution charge of +4 the proportion for multi-phosphopeptides was negligible. Considering the small number of peptides with solution charges above +3, the number of peptides with multiple phosphorylation sites was far greater than in the previous experiment (Figure 80C versus figure 75C).

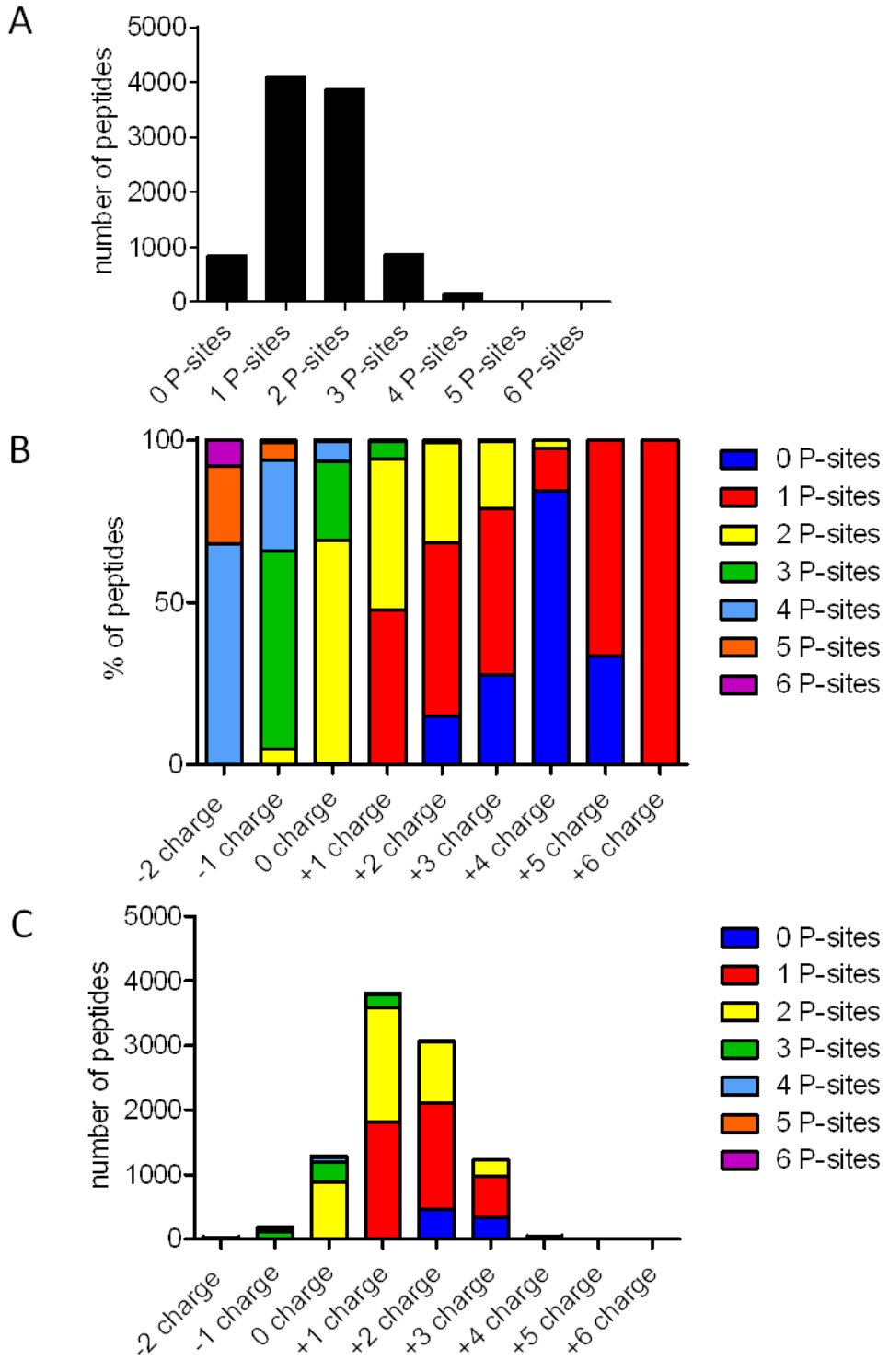


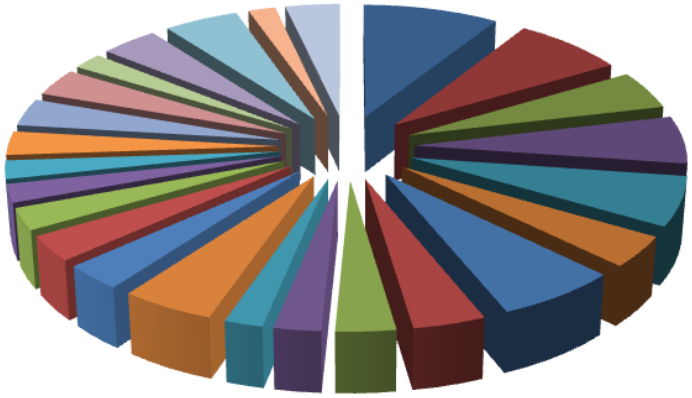
Figure 80. The adapted TiO_2-protocoll shows increased efficiency to enrich for peptides with multiple phosphorylations. (A) The absolute number of peptides with 0 to 6 phospho-sites are displayed. (B) The proportion and (C) absolute number of peptides with 0 to 6 phospho-sites and their respective solution charge.

6.4.5 | The adapted phospho-proteomics protocol identifies an increased number of phospho-peptides, phospho-sites and phospho-proteins

The main aim of the adapted protocol was to increase the number of detected phospho-peptides, phospho-sites and phospho-proteins in order to raise the probability to indentify downstream targets of mTOR involved in the regulation of FOXP3. An increased number of phospho-proteins with molecular functions such as “DNA binding”, “Chromatin binding” and “Nucleic acid binding” as well as an enrichment of signalling pathways relevant to the stimulation (TCR, TGFβ) would further increase the likelihood of discovering how mTOR inhibition enhances the TCR plus TGFβ induced FOXP3 expression.

The analysis followed the same strategy as described for the first experiment i.e. Andromeda score greater than 20, localization probability greater than 0.5 and absolute z-score +/- 2.5. The experiment identified 4570 unique phospho-peptides (3661 proteins) with an Andromeda score above 20, which represents an increase in identifications of ~25% compared to the first experiment. At phospho-site level, the adaptations to the experimental protocol showed an even bigger effect. 3442 phospho-sites compared to the 2343 sites in the first experiment were detected with a score greater than 20 and a localization probability of greater than 0.5 (almost 50% increase). The 3442 sites were assigned to 3218 proteins. The analysis for KEGG Pathway enrichment revealed that a variety of signalling pathways, including the mTOR and the TCR signalling pathway, were overrepresented in the dataset (Figure 81). A total of 14 proteins annotated as components of the mTOR signalling pathway including mTOR

complex components such as RAPTOR, RICTOR and PRAS40 as well as upstream and downstream targets of the two mTOR complexes such as AKT2 and 3, EIF4B, TSC2, and S6K1 (Figure 82A). The 15 proteins annotated as components of the TCR signalling pathway include, amongst others, members of the Calcium signalling pathway (PLCγ1), the MAPK signalling pathway (SOS and RAF1), proteins involved in the regulation of the actin cytoskeleton (NCK2 and PAK2) and the transcriptional regulator NFATc2 (Figure 82B). Other pathways with significant overrepresentation included “RNA transport”, “Spliceosome”, “Ribosome biogenesis in eukaryotes” and “Transcriptional misregulation in cancer” (Figure 81).



KEGG Pathway	Count	FDR p-value
RNA transport (mmu03013)	40	3.22E-12
Spliceosome (mmu03040)	33	3.90E-11
Ribosome biogenesis in eukaryotes (mmu03008)	21	5.21E-07
Cell cycle (mmu04110)	26	1.08E-06
Transcriptional misregulation in cancer (mmu05202)	27	8.06E-05
ErbB signaling pathway (mmu04012)	17	3.42E-04
Epstein-Barr virus infection (mmu05169)	29	4.02E-04
Prostate cancer (mmu05215)	17	4.63E-04
mTOR signaling pathway (mmu04150)	14	4.63E-04
Lysine degradation (mmu00310)	11	2.02E-03
DNA replication (mmu03030)	9	2.71E-03
Protein processing in endoplasmic reticulum (mmu04141)	22	6.42E-03
mRNA surveillance pathway (mmu03015)	14	8.49E-03
Ribosome (mmu03010)	14	9.94E-03
Chronic myeloid leukemia (mmu05220)	12	9.97E-03
Non-small cell lung cancer (mmu05223)	10	1.03E-02
Acute myeloid leukemia (mmu05221)	10	1.12E-02
Progesterone-mediated oocyte maturation (mmu04914)	13	1.54E-02
T cell receptor signaling pathway (mmu04660)	15	1.54E-02
Oocyte meiosis (mmu04114)	15	1.92E-02
Endometrial cancer (mmu05213)	9	2.07E-02
Ubiquitin mediated proteolysis (mmu04120)	17	2.36E-02
Herpes simplex infection (mmu05168)	22	2.36E-02
Basal transcription factors (mmu03022)	8	2.36E-02
Insulin signaling pathway (mmu04910)	16	4.38E-02

Figure 81. KEGG-pathway enrichment of 2nd phospho-proteomics data set. All KEGG pathways with significant enrichment as determined by the analysis of the MaxQuant out-put files in Proxeon Protein Center. A false discovery rate (FDR) of 0.05 was set for the analysis. "Count" indicates the number of proteins present in the dataset for the indicated KEGG-pathway.

A **mTOR signalling pathway proteins**

Gene	Description
Akt3	Isoform 1 of RAC-gamma serine/threonine-protein kinase
Braf	Isoform 1 of Serine/threonine-protein kinase B-raf
Pdpk1	3-phosphoinositide-dependent protein kinase 1 isoform B
Eif4ebp1	Eukaryotic translation initiation factor 4E-binding protein 1
Rps6kb1	Isoform Alpha I of Ribosomal protein S6 kinase beta-1
Tsc2	tuberin isoform 2
Rictor	Isoform 1 of Rapamycin-insensitive companion of mTOR
Eif4b	Eukaryotic translation initiation factor 4B
Rps6	40S ribosomal protein S6
Akt2	RAC-beta serine/threonine-protein kinase
Rptor	regulatory-associated protein of mTOR
Rps6ka3	Ribosomal protein S6 kinase alpha-3
Akt1s1	Proline-rich AKT1 substrate 1
Ulk1	serine/threonine-protein kinase ULK1

B **TCR signalling pathway proteins**

Gene	Description
Akt3	Isoform 1 of RAC-gamma serine/threonine-protein kinase
Nfatc2	nuclear factor of activated T-cells, cytoplasmic 2 isoform b
Ptpn6	Isoform 2 of Tyrosine-protein phosphatase non-receptor type 6
Pdcd1	Programmed cell death protein 1
Lat	Linker for activation of T-cells family member 1
Raf1	Isoform 1 of RAF proto-oncogene serine/threonine-protein kinase
Sos1	Son of sevenless homolog 1
Nck2	non-catalytic region of tyrosine kinase adaptor protein 2
Akt2	RAC-beta serine/threonine-protein kinase
Pak6	Serine/threonine-protein kinase PAK 6
Gsk3b	Glycogen synthase kinase-3 beta
Plcg1	1-phosphatidylinositol-4,5-bisphosphate phosphodiesterase gamma-1
Map3k8	Mitogen-activated protein kinase kinase kinase 8
Pak2	Serine/threonine-protein kinase PAK 2
Ptprc	Isoform 1 of Receptor-type tyrosine-protein phosphatase C

Figure 82. Proteins annotated as components of the mTOR (A) and TCR (B) signalling pathway. All mTOR (A) and TCR(B) signalling pathway components as determined by KEGG pathway analysis in Proxeon Protein Center are shown. A false discovery rate (FDR) of 0.05 was set for the analysis.

Gene ontology analysis highlighted that a multitude of molecular functions (222) were overrepresented in the dataset. Encouragingly, these included molecular functions such as “chromatin binding” (GO:0003682, Count: 139), “nucleic acid binding transcription factor activity” (GO:0001071, count: 211) and “DNA binding” (GO:0003677, Count: 570). Most of these categories showed an increased number of identified proteins compared to the first experiment indicating that the fractionation into cytoplasmic and nuclear extracts had the desired effect. In line with this, a greater number of transcription factors known to be involved in the differentiation of T-cells including ATF2 and 7, BCL6, FOXO1 and 3, GATA3, KLF10, NFATc2, RORγ, RUNX1, SP1 as well as several proteins involved in epigenetic regulation of gene transcription were identified.

The use of the z-score cut-off of +/-2.5 showed that the vast majority of phospho-sites did not seem to be regulated by mTOR inhibition mediated by Rapamycin or Torin 1 (Figure 83, median $\log_2$(no inhibitor/Rapamycin): 0.01564, median $\log_2$(Torin 1/no inhibitor/Torin 1): 0.04194). 126 phospho-sites in 198 proteins were negatively regulated by Rapamycin. These sites included 3 known mTOR pathway proteins: EIF4B, RICTOR and RPS6. In line with the fact that Torin 1 inhibits mTORC2 function in addition to mTORC1, the drug reduced the phosphorylation levels at more sites than Rapamycin. 281 phospho-sites in 467 proteins were negatively regulated by Torin 1. KEGG pathway analysis revealed that “mTOR signalling”, “RNA transport” and “Lysine degradation” pathways were enriched in this data subset (FDR p=0.00696, FDR p=0.000444 and FDR p= 0.000342 respectively). In addition to the Rapamycin regulated sites in EIF4B and RPS6, Torin 1 also reduced the phosphorylation of RAPTOR, PRAS40

and EIF4EBP1, indicating that these phosphorylation events might be regulated by the mTORC2 complex or its downstream targets.

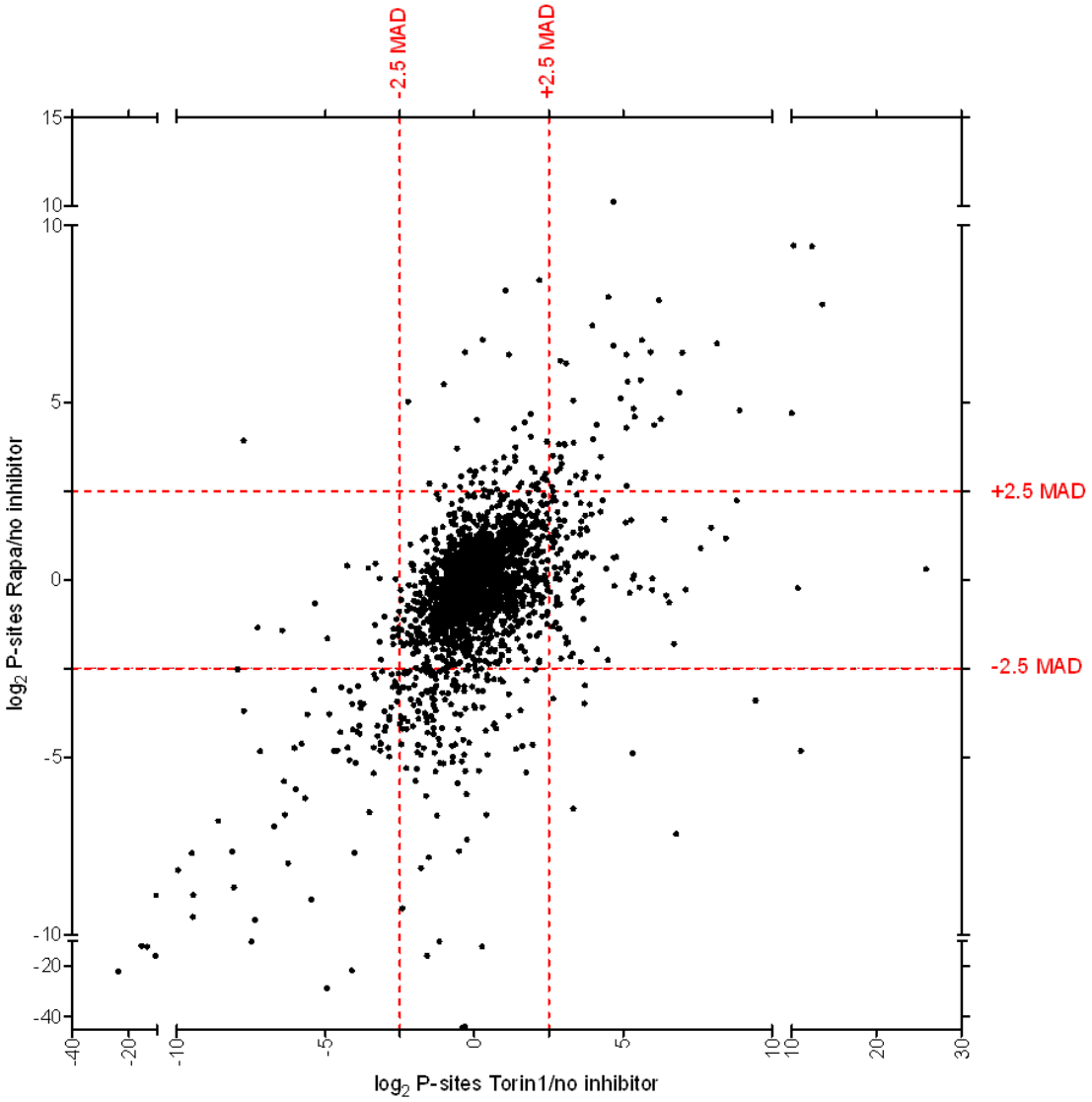


Figure 83. mTOR inhibition reduces and increases the levels of phosphorylation at a large number of phospho-sites. The absolute z-score values of the ratio of differentially treated cells for each phosphorylation site detected (individual dots) is indicated in the graph. Z-scores above +2.5 and below -2.5 were considered as significantly up- and down-regulated

The previously negatively regulated phospho-site S102 in DNMT3A, did not show any changes upon Rapamycin or Torin 1 treatment in the second experiment. The sites in NFATc2, PIAS and EZH2 as well as the positively regulated site in ARID4B that were also discussed as potentially interesting with respect to the regulation of FOXP3 expression,

were also not identified in this experiment, which at least raises some doubts whether they are truly regulated by mTOR signalling. However, the fact that the latter four phospho-sites were not detected at all, might also be caused by the adapted, more stringent binding conditions that were used in the TiO_2 enrichment protocol. It is possible that such alterations can render some phospho-peptides undetectable, presumably through insufficient affinity of the phospho-peptides to the TiO_2 spheres under these binding conditions. In line with the hypothesis that changes in the experimental protocol affected the phospho-peptides and phospho-proteins that were identified, only 2069 of the 5171 proteins (40%) identified in the two experiments are shared between both datasets (Figure 84). At the peptide level, only 691 (9.2%) of peptides can be found in both datasets, indicating that technical adaptations might have affected the composition of the peptides that were present in the samples submitted for analysis. In addition to the alterations in the methodology, the relatively small overlap is, at least in part, caused by the relatively small coverage of the cellular peptide/protein pool that the experiments managed to achieve. An increased coverage is therefore likely to increase the robustness of the data.

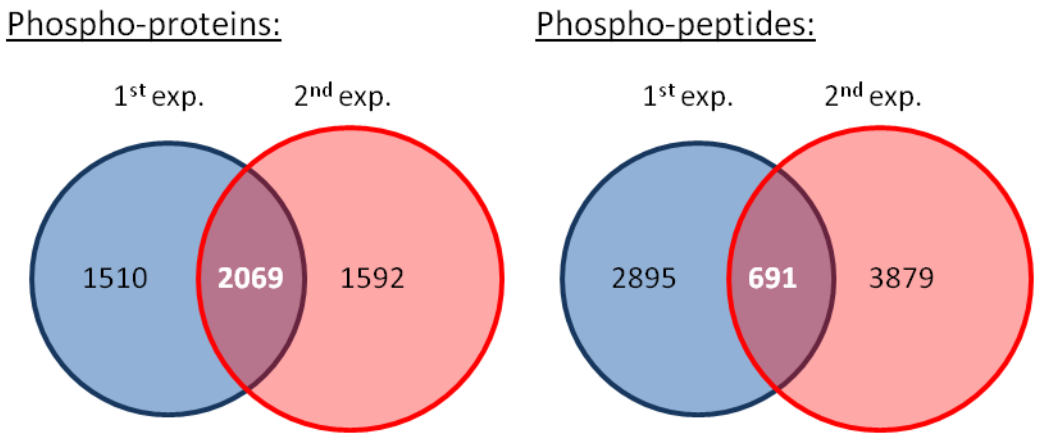


Figure 84. Common and distinct phospho-proteins and phospho-peptides were detected in the two phospho-proteomics experiments. Venn diagrams displaying the phospho-proteins and phospho-peptides shared (overlap) between the two phospho-proteomics experiments. The was generated from MaxQuant output files analyzed in Proxeon Protein Center.

Despite being unable to confirm the regulation of the candidates from the first experiments, the adapted approach revealed that a site in FOXO3A, a protein that has been demonstrated to regulate FOXP3 by several groups [167-169, 273], is differentially regulated when mTOR is inhibited. Torin 1 treatment resulted in reduced phosphorylation levels of FOXO3A at S279 and S283, whereas the inhibition by Rapamycin did not quite reach the cut-off (z-score= -2.47) used to define it as responsive to the drug. This observation could imply that the phosphorylation of FOXO3A is dependent on mTORC2 activity, which seems plausible considering that two of the most important kinases, AKT and PKC, which are known to regulate FOXO3A phosphorylation [63, 273], are targets of mTORC2 [11, 140]. The activity of FOXO transcription factors is thought to be regulated by multiple mechanisms including phosphorylation events, which sequester the transcription factors in the cytoplasm through the association with 14-3-3 proteins [63]. Therefore a mechanism by which mTORC2 inhibition reduced AKT and PKC activity, resulting in reduced FOXO3A phosphorylation and enhanced nuclear translocation and FOXP3 induction seems conceivable. However, the role of the S279 and S283 phosphoryolation sites in the regulation of FOXO3A translocation is not known to date. Therefore an involvement of the sites in the mTOR-mediated enhancement of FOXP3 expression needs to be tested in further experiments.

In summary the phospho-proteomics experiments have indicated several cellular targets that mTOR inhibition could act on to regulated the expression of FOXP3. However, further experiments using identical protocols will have to confirm that the phosphorylation events in these candidate proteins are consistently responsive to

mTOR inhibition. The adaptations made to the protocol, particularly those to the TiO_2 mediated phospho-peptide enrichment, have significantly improved the number of phospho-peptides and phospho-sites that were identified. However, the relatively small overlap in the detected phospho-proteins between the two experiments, indicates that the binding conditions greatly influence which peptides will be enriched and therefore which proteins will be identified. The even smaller overlap at the peptide level is additionally reduced by the fact that two different proteases were used in the two experiments to generate peptide mixtures (Lys C versus LysC+trypsin). In order to increase the range of peptides and proteins that can be identified, several rounds of enrichments with increasing stringency (increasing proportion of saturated glutamic acid) could be performed. Furthermore, although the SCX fractionation based on the protocol described by Dephoure et al. seemed to consistently fractionate the peptides according to their solution charge state, the use of an HPLC-system for the fractionation should increase the number of identified peptides even further, since a better fractionation can be achieved with such a system.

Equally important to the improvement of technical aspects of the experiments is a more in-depth analysis of the data. Time constraints as well as the lack of suitable software or the help of a bioinformatition made it difficult to analyze the data beyond the level presented here. During the analysis process, for example, it became apparent that MaxQuant, the software used for quantitation of peptides and phospho-sites, could not process peptides that were present in one label i.e. stimulation without mTOR inhibitor, and absent in another, i.e. stimulation with Rapamycin. Therefore the most responsive phospho-peptides, which are likely to contain proteins of interest, were “lost” from further analysis. This could be circumvented by the use of different

quantitation software or by spiking each sample with a defined amount, i.e. 10% of overall protein, of each labelled lysate (here: “Light”, “intermediate” and “heavy” no inhibitor lysates). In the latter case the quantitation performed in MaxQuant would need to be corrected for the inclusion of the spiked samples.

Although mTOR pathway and TCR signalling pathways were overrepresented in some of the datasets, no proteins involved in TGFβ signalling were indentified. Since the induction of FOXP3 in EL4.B02 mediated by mTOR inhibition was dependent on the presence of TGFβ, it is likely that mTOR acts on a signal induced by TGFβ. The lack of identifications of these TGFβ-signalling components could be due to the relatively long duration of the stimulation used for the experiment (2 hours.) An analysis of the phospho-proteome at earlier time points (αCD3+mTOR inhibitors for 2h+TGFβ for the last 15-30min) might allow for an analysis of the effect of mTOR inhibition on TGFβ signalling.

Although definite conclusions are still pending, the experiments demonstrated that the phospho-proteomics approach can be a valuable technique to screen for mTOR targets involved in the regulation of FOXP3 expression, especially when the technical difficulties in the experimental protocol and the data analysis are resolved.

Chapter 7 | GENERAL DISCUSSION

Over the last decade evidence has accumulated for a crucial role of FOXP3$^+$ Treg in the maintenance of immune homeostasis as well as impacting disease settings such as cancer and autoimmunity [274, 275]. Considering the importance of the transcription factor FOXP3 in Treg differentiation and function along with the therapeutic potential associated with the targeted manipulation of FOXP3 expression, it does not come as a surprise that regulation of the *Foxp3* locus has been subject to intensive research in the last years. Despite major advances, the signals regulating the expression of FOXP3, as well as the molecular events underlying this process, are far from being understood. Although advances, including knock-out and knock-in animals of genes of interest, have significantly increased the understanding of the signalling mechanisms controlling FOXP3 expression, a cell line model mimicking the behaviour of T-cells with respect to FOXP3 induction would represent an invaluable resource for the investigation of these complex biochemical events. Due to the sparseness of signalling components compared to the other elements of the cellular machinery, large quantities of cells are often required for analysis, such needs being easily accommodated by such a cell line.

In this thesis, the clone EL4.B02, which was isolated from the mouse lymphoma T-cell line EL4 by limiting dilution cloning, was established and characterized. In comparison to the parental EL4 line, EL4.B02 exhibits a considerably increased propensity to induce FOXP3 protein expression, which can be measured by antibody-staining, in response to a multitude of signals known to induce it in naive primary CD4$^+$ T-cells. This increased responsiveness provided the basis for the investigation of the role of the mTOR signalling pathway in the regulation of FOXP3 expression.

The EL4.B02 induce substantial amounts of FOXP3 when stimulated with plate-bound monoclonal antibody targeting the CD3ε component of the TCR signalling complex only in the presence of TGFβ. Titrations of both anti-CD3 antibody (data not shown) and TGFβ (Figure 9 and 14) demonstrated that the signal strength required for optimal induction is comparable to that seen in primary T-cells [148, 149, 152]. This concentration dependency of both signals indicates that the cellular signalling network is organized in a way that results in a threshold for both minimal and maximal FOXP3 induction. Although evidence is accumulating that the spatial and temporal assembly of the TCR signalosome as well as positive and negative feedback loops regulate the threshold required for optimal T-cell activation, the precise mechanisms of how the threshold is set and how other signals such as CD28 signalling contribute to the activation events, remain elusive [276, 277]. In this context it is important to note that the role of CD28 signalling in the regulation of FOXP3 expression remains somewhat controversial. Whereas some researchers report a direct role in the induction of FOXP3 by activating downstream transcription factors such as RelA, others indicate that the effect of CD28 is indirect by enhancing IL-2 production required for FOXP3 expression [153, 278]. The induction of FOXP3 in EL4.B02 seemed to be independent of both CD28 and IL-2 signalling (data not shown). Neither CD28 engagement nor IL-2 addition or IL-2 neutralization showed a significant effect on the proportion of cells expressing FOXP3 that are induced. This might be explained by the fact that some features of EL4.B02 (cell division, cell size, preactivated PI3K-AKT-mTOR pathway) more closely resemble the phenotype of a T-cell blast rather than a naïve T-cell. Therefore it seems conceivable that the lack of responsiveness with respect to CD28 and IL-2 stimulation might be due to the constitutive “activation-like” phenotype of the cells, rendering

additional costimulatory signals via CD28 obsolete. It is however important to note that the expression of FOXP3 in EL4.B02 was strictly dependent on TCR stimulation.

It is becoming increasingly clear that the strength of TCR engagement crucially shapes the differentiation of $CD4^+$ T-cell subsets, such as Th1, Th2 and Th17 cells [279-281]. Whereas Th17 lineage commitment seems to require low-strength T-cell activation [281], Gottschalk et al. demonstrated that both weak and strong TCR agonists can induce FOXP3 expression, albeit at different concentrations (strong agonist: low dose, weak agonist: high dose). However, only in the former case was the induced FOXP3 stably expressed. The authors further showed that the role of TGFβ in the induction is, at least in part, to reduce the sensitivity of the TCR to high-affinity ligation, which broadens and raises the range of antigens compatible with FOXP3 induction [98]. The observation that high concentrations of TGFβ not only enhance the induction of FOXP3, but also inhibit the differentiation of Th17 cells [221], could be partially due to the reduced sensitivity of the TCR signal, resulting in a desensitization for low strength activation that favours Th17 differentiation.

Reduced induction of Th17 differentiation in high concentrations of TGFβ is, in addition, regulated by the interaction of FOXP3 with RORγT as well as with RUNX1, resulting in functional inhibition of RORγT and reduced *Il-17a* transcription [221, 282, 283]. A negative effect of high concentrations of TGFβ on IL-17A expression was, however, not observed in EL4.B02 cells. The previously described effect of FOXP3 on RORγT function was mostly observed in cells over-expressing FOXP3, which might result in a more robust effect, particularly because in these systems FOXP3 is present before IL-17A is

induced [282, 283]. In EL4 cells RORγT is constitutively expressed [282] and significant levels of FOXP3 are only induced at later time points in the stimulation conditions, therefore enabling unimpaired IL-17A expression. However, in the presence of mTOR inhibitors in which IL-17A expression is negatively affected and FOXP3 induction is enhanced, this interaction between FOXP3 and RORγT/RUNX1 might contribute to the reduced levels of IL-17A detected at later time points. Potential mechanisms that mTOR uses to control IL-17A transcription will be addressed in more detail later in the discussion.

The observation that stimulation of EL4.B02 at high cell densities resulted in a time-dependent drop in mTORC1 activity which coincided with an increased proportion of cells expressing FOXP3 (Figure 11), raised the hypothesis that depletion of the culture medium of nutrients could result in an mTOR inhibition-mediated enhancement of FOXP3 induction. The fact that cell density titrations showed that this "system intrinsic" mTOR inhibition could be prevented at 10-fold lower cell density and that fewer cells induced FOXP3 at this density (Figure 12), provided further support for this hypothesis. An effect of cell to cell contact was ruled out, since conditioned medium also enhanced the induction at low density (Figure 15) and transwell experiments demonstrated that the induction at low density could only be enhanced when a large number of cells was added to the transwell (Figure 16). Neither of the experiments could, however, rule out that the induction at high density was facilitated by an endogenous factor that enhanced FOXP3 expression and only achieved effective levels at high cell density. Evidence supporting the hypothesis that a soluble factor, at least in part, contributed to the enhanced induction of FOXP3 at high cell densities is illustrated by the fact that *Foxp3* mRNA levels are high, compared to low cell density stimulations, even at time

points at which mTOR is not yet inhibited by medium depletion (Figure 14A). The involvement of two potential factors, IL-2 (data not shown) and TGFβ, was ruled out since neutralization did not significantly affect the induction of FOXP3 (Figure 14B). The "system intrinsic" mTORC1 inhibition as well as the concomitant enhancement effect in high density versus low density stimulation was also observed in culture of primary $CD4^+$ T-cells (data not shown), indicating that this effect is not a unique and deceiving feature of the EL4 system. Further support for the effects of high cell density, comes from studies performed by Bernardo et al. [284]. The authors demonstrate that the proportion of $FOXP3^+$ cells among dividing cells is significantly larger when cells are stimulated at high densities compared to low cell densities. It is important to note that in their system this expression of FOXP3 does not confer a suppressive activity to the cells [284]. This lack of suppressive activity might be a peculiarity of human $CD4^+$ T-cells, because experiments in our laboratory, using high density stimulations of mouse $CD4^+$ T-cells, generate $FOXP3^+$ Treg with potent inhibitory activity *in vitro* and *in vivo* (data not shown). The discovery of this "system intrinsic" (presumably medium depletion induced) mTORC1 inhibition might have a significant impact on the interpretation of previously published data. Due to the lack of detailed descriptions of the stimulation conditions with respect to the cell density used in published work, it is in many cases difficult to assess whether this "system intrinsic" mTORC1 inhibition might have occurred in cultures that were used to generate $FOXP3^+$ Treg for *in vitro* and *in vivo* studies. Cell titration experiments using primary $CD4^+$ T-cells showed that after a 5 day culture the cells showed pS6 levels indicative of mTORC1 inhibition, even at cell densities of 10^5 cells/ml (data not shown). Considering that in the first and still frequently used protocol that described FOXP3 induction *in vitro* [152], stimulations for

up to 10 days at densities of up to $2x10^6$ cells/ml were used, it seems very likely that "system intrinsic" mTORC1 inhibition occurred. It should therefore be considered that in several studies, $FOXP3^+$ Treg were not generated using only TCR, TGFβ and IL-2 stimulation, but were also exposed to mTOR inhibition, which might influence the results with respect to signalling and function of any induced Treg.

In addition to the pronounced effect of cell density on the induction of FOXP3 during the stimulation of EL4.B02 cells, cell density during the maintenance and culture was also found to have a major impact on the responsiveness of the cells. If cells exceeded a density of more than $2x10^5$ cells/ml for prolonged periods without exchange of the culture medium, a significant reduction in the responsiveness with respect to the induction FOXP3 was observed (data not shown). Not only was the overall inducibility reduced, but the responsiveness to mTOR inhibition mediated by mTOR inhibitors or nutrient depletion (overgrowth and EAA depletion) was affected. The latter effect could be due to the fact that overgrowth of the culture results in prolonged nutrient-depletion induced mTORC1 inhibition, which could select for the outgrowth of cells that are less responsive to mTOR signalling. The overgrowth of the cells in culture could also reduce the expression levels or cause down-modulation of receptors relevant to the induction of FOXP3, such as the TCR or the TGFβ-receptor. Therefore it is important to maintain the EL4.B02 culture below the indicated densities to avoid the loss of inducibility.

Although cell density titration and transwell experiments, as well as experiments using conditioned medium, indicated that depletion of the stimulation medium of nutrients

might underlie the observed mTORC1 inhibition, the experimental setup could not pin down a particular nutrient that was causative for the inhibition. The mTOR pathway has evolved to regulate cellular responses to a variety of nutritional cues, such as energy and amino acid availability. In response to lack of any of these nutrients mTOR signalling is inhibited and downstream effector functions are tuned in order to adjust the cellular metabolism accordingly [11, 12]. Our laboratory has recently demonstrated that in $CD4^+$ T-cells inhibition of the mTOR pathway by starvation of essential amino acids (EAA) synergizes with TGFβ in the induction of FOXP3 [127]. Therefore it seems likely that the mTORC1 inhibition induced at high cell densities in normal culture medium resulted, at least in part, from the depletion of EAA.

In order to more directly test whether EAA depletion can inhibit mTORC1 in EL4.B02 cells and whether this inhibition enhanced the induction of FOXP3, cells were stimulated under limiting concentrations of EAA (5%). In line with the findings made in primary cells, the cells showed significantly reduced pS6 levels as well as increased FOXP3 expression as determined by FACS and by qPCR (Figures 17, 20 and 21). In line with the notion that a larger number of cells deplete EAA more rapidly, the proportion of induced of $FOXP3^+$ cells was greater at higher cell densities (Figure 22). The fact that even at high cell densities the induction was enhanced in medium containing limiting amounts of EAA, is likely to be due to the prolonged period that the cells experience mTORC1 inhibition. This extended period of mTORC1 inhibition could serve to increase the duration and probability that this inhibition signal could act on, and synergize with, TCR- and TGFβ-mediated signals. Complete elimination of EAA from the cultures, however, did not enhance the induction of FOXP3, although mTORC1 was inhibited (data not shown). This highlights that some EAA signalling is required before depletion

induced inhibition can facilitate the induction. The mechanism that EAA induced mTOR inhibition utilizes to enhance the induction, and why small quantities of EAA are required for the enhanced induction to occur, needs to be addressed in due course. Although some increase in cell death was observed under EAA deprivation conditions, a preferential survival effect does not seem to be the sole reason why $FOXP3^+$ cells accumulate, since both RT-PCR experiments as well as preliminary experiments using *Foxp3* luciferase constructs indicate an induction of *Foxp3* transcription (data not shown). A contribution of increased survival of $FOXP3^+$ cells over $FOXP3^-$ cells, as reported for Rapamycin treated cultures [133, 285], cannot be ruled out. In addition to its effect on the survival of $FOXP3^+$ T-cells, Rapamycin was demonstrated to allow preferential expansion of $FOXP3^+$ Treg over $FOXP3^-$ cells [130]. A similar mode of action of EAA starvation can be excluded, since no differences in the proliferation rates between CFSE labelled $FOXP3^+$ and $FOXP3^-$ cells was observed (data not shown). Despite the lack of a conclusive result with respect to the mechanism, by using a system devoid of APCs, we demonstrated for the first time that the EAA starvation induced mTOR inhibition acts on the T-cell itself to enhance the induction of FOXP3.

In line with the proposed, T-cell intrinsic role, heart allografts introduced into mice with $CD3^+$ T-cell specific deletion of the amino acid transporter CD98hc ($CD98hc^{-/-}$) indefinitely accepted their grafts and showed increased proportions of splenic $FOXP3^+$ cells. This increase in $FOXP3^+$ Treg is likely to be due to the reduced mTOR activity detected in $CD98hc^{-/-}$ $CD4^+$ T-cells [286]. Although the tryptophan depleting enzyme IDO expressed by APCs has been implicated in the inhibition of T-cell proliferation and in the expansion of Treg, only little attention has been paid to the contribution of mTOR signalling in these processes [287-293]. Whilst the negative effect of IDO on T-cell

proliferation was alleviated by addition of excess tryptophan [291-293], an effect on Treg expansion was not tested. Instead of tryptophan depletion as a mechanism, Chen et al. implicate kynurenine, the immediate product of tryptophan metabolised by IDO, in the expansion of FOXP3$^+$ Treg [287]. The interpretation of these experiments is, however, complicated by the presence of DCs in the co-culture system, making it difficult to assess whether kynurenine or IDO function to modulate DC or T-cell behaviour.

The role of mTOR in the regulation of FOXP3 expression in EL4.B02 was confirmed by demonstrating that the allosteric mTORC1 inhibitor Rapamycin enhanced the induction of FOXP3 to a similar extent as "system intrinsic" and EAA depletion-mediated mTOR inhibition. It is important to note that the enhancement was only detectable when cells were stimulated at low cell density, so that "system intrinsic" mTOR inhibition could be avoided (Figure 10, 23-25). The "system intrinsic" inhibition at high densities that presumably rendered Rapamycin mediated inhibition obsolete, could also be avoided by shortening the stimulation period and analysing the levels of *Foxp3* transcripts at early time points (Figure 32). Rapamycin significantly increased the proportion of induced FOXP3$^+$ cells and inhibited mTORC1 activity at concentrations as low as 50pM (Figure 23). This effect seemed to be dependent on the presence of TGFβ, although a trend towards higher percentages of FOXP3$^+$ cells was consistently observed in the absence of TGFβ (Figure 24). This strict dependency on TGFβ contrasts with the studies of Sauer et al. and Delgoffe et al. who observed an increased proportion of FOXP3$^+$ cells even in the absence of TGFβ, albeit using distinct stimulation conditions to the ones used in this thesis [124, 136]. The former interrogated the role of premature termination of TCR signalling (resulting in decreased mTOR activity) and contrasted the observed

effect on FOXP3 expression to that observed with prolonged TCR signalling and Rapamycin mediated inhibition. The enhanced induction resulting from premature termination was further enhanced by PI3K/mTOR inhibition and by TGFβ. However, the experimental setup does not indicate whether the increased proportion of $FOXP3^+$ cells resulting from premature removal of the TCR signal (reduced mTOR acitivity) or Rapamycin addition (mTOR inhibition) is a result of a *de novo* induction of FOXP3 or a preferential survival of $FOXP3^+$ cells as has been observed by other groups [133, 285]. Similarly, the fact that TGFβ addition to Rapamycin treated cells further increases the proportion of $FOXP3^+$ cells could be due to an enhanced induction or an increased stability of FOXP3 expression, since TGFβ signalling was demonstrated to be important for maintenance of $FOXP3^+$ Treg [150, 154]. The interpretation of the experiments performed by Delgoffe et al. is complicated since the starting T-cell population used in their assays contained $FOXP3^+$ T-cells. Although no expansion of $FOXP3^+$ cells was observed in wildtype cells, it seems difficult to rule out that the expansion of pre-existing $FOXP3^+$ (natural) Treg, or $CD25^+FOXP3^-$ cells already committed to Treg differentiation, contributed to the increased proportion of $FOXP3^+$ cells in $mTOR^{-/-}$ cells (especially since the expansion of $FOXP3^+$ Treg was encouraged by resting the cultures and by supplementation with IL-2 and IL-7).

The relative paucity of the requirement for exogenous TGFβ for the induction of FOXP3 in $mTOR^{-/-}$ cells compared to EL4.B02 cells, on the other hand could be due to the different degree of mTOR inhibition that is achieved by pharmacological inhibition and genetic deletion. However, Delgoffe et al. indicate that at least some endogenously produced TGFβ was required, since neutralization of TGFβ reduced the proportion of $FOXP3^+$ cells that are detected [136]. A similar observation was made by Gabrysova et al.,

who also showed that the Rapamycin-mediated enhancement of FOXP3 expression was dependent on endogenous TGFβ [135]. In line with the dependence on small amounts of TGFβ, mTOR knock-out T-cells exhibit both increased baseline and TGFβ induced SMAD3 phosphorylation (S423/425), indicating a TGFβ-hyper-sensitive phenotype [136]. Therefore inhibition of mTOR could act to release the "molecular break" (suppression of SMAD3 phosphorylation by mTOR) on FOXP3 expression by allowing stronger SMAD3 activation. In the absence of any experiments analyzing *Foxp3* transcription (Real-time PCR or luciferase assays) or experiments highlighting the functional involvement of increased SMAD3 phosphorylation (SMAD3 knock-down or mutant SMAD3 over-expression), the involvement of hyper-activated SMAD3 in the mTOR inhibition-mediated enhancement of FOXP3 expression remains speculative. A contribution of hyper-activated SMAD3 is put further in doubt since neither experiments performed by Sauer et al., nor those shown in this thesis, could confirm that SMAD3 is indeed hyper-phosphorylated when mTOR is pharmacologically inhibited (Figure 42) [124]. This could, however, be due to the previously mentioned differences in the experimental system (pharmacological inhibition versus genetic deletion). Evidence that Rapamycin can regulate the activation of SMAD3 comes from experiments that demonstrate that the drug can facilitate SMAD3 phosphorylation by sequestering the inhibitory FKBP12 away from the TGFβ type I receptor [294, 295]. This mechanism though, cannot be engaged in the experiments of Delgoffe et al. since genetic deletion of mTOR and not Rapamycin was used to simulate mTOR inhibition. A more plausible explanation for the observed hyper-activation of SMAD3 in $mTOR^{-/-}$ cells is presented by Song et al. who demonstrate that the mTORC2 target AKT prevents SMAD3 phosphorylation [296]. Further experiments validating the hyper-

activation of SMAD3 under mTOR inhibition conditions, and experiments focussing on the functional involvement of enhanced SMAD3 activation will have to demonstrate that this is a physiologically significant mechanism mTOR utilizes to enhance the induction of FOXP3.

A multitude of observations, including the fact that Rapamycin can also inhibit mTORC2 activity[13] and that a constitutively active form of AKT inhibits the TGFβ-dependent induction of FOXP3 [126], raised the question: which of the two mTOR complexes is involved in the regulation of FOXP3 expression. Having established that EAA starvation as well as the treatment of cells with Rapamycin and Torin 1 results in reduced activity of mTORC2, the role of mTORC1 and 2 activity in the regulation of FOXP3 expression was tested in a series of inhibitor titration and time course experiments (Chapter 4). The latter demonstrated that Rapamycin and Torin 1 display similar kinetics with respect to the inhibition of mTORC1, but differential kinetics of mTORC2 inhibition. Whereas Torin 1 inhibited mTORC2 within 2 hours, Rapamycin only started to reduce mTORC2 activity after prolonged exposure (>6 hours). The differential kinetics of mTORC2 inhibition therefore created the opportunity to test the involvement of mTORC1 and 2 activities in the regulation of FOXP3 induction.

A role for mTORC1 in the expression of FOXP3 was demonstrated by experiments that showed that *Foxp3* mRNA levels were increased in cells stimulated with Rapamycin for a time frame in which mTORC2 inhibition by the drug was marginal (Figures 30 and 32). Additional support for the involvement of mTORC1 was provided by Rapamycin titrations that indicated that concentrations of the drug, which essentially only inhibited mTORC1 activity, enhanced the induction of FOXP3 considerably. The evidence from the literature supporting the mTORC1 inhibition-mediated FOXP3

induction is scarce. Most publications that state that mTORC1 inhibition (or mTOR inhibition) is involved in the regulation of FOXP3 induction, interpreted their data based on the assumption that Rapamycin is a mTORC1 inhibitor and did not asses the activity of either one of the mTOR complexes or only that of mTORC1 [124, 126, 127, 135]. Delgoffe et al. used $RHEB^{-/-}$ cells to investigate the role of mTORC1 signalling in the regulation of FOXP3 expression. In contrast to the $mTOR^{-/-}$ T-cells, the inherent propensity to differentiate into $FOXP3^{+}$ Treg of $CD4^{+}$ T-cells from $RHEB^{-/-}$ mice is less pronounced. Strikingly, the small effect observed in the absence of TGFβ is not present when TGFβ is added to the cultures. These observations led the authors to conclude that mTORC2 inhibition is necessary for the enhancement of FOXP3 induction to occur [136]. However, this interpretation might underestimate the role of mTORC1 and overestimate the role of mTORC2 inhibition, since the $RHEB^{-/-}$ T-cells exhibit substantial hyper-activation of mTORC2 signalling [136]. If mTORC2 inhibition contributes to the enhanced induction of FOXP3, as demonstrated in this thesis as well as by Lee et al and by Delgoffe et al, the hyper-activation of mTORC2 in $RHEB^{-/-}$ cells (mTORC1 inhibition surrogate) might mask an effect of mTORC1 in the control of FOXP3 expression [139, 140]. In line with a contribution of mTORC1 inhibition, the addition of Rapamycin amounts that predominantly inhibit mTORC1 and not mTORC2 to wildtype cells enhanced the induction of FOXP3 whereas the drug does not affect the expression in $RHEB^{-/-}$ cells [139]. Furthermore, in the light of RHEB-independent activation of mTORC1, i.e. by phospholipase D1, $RHEB^{-/-}$ T-cells might not fully recapitulate mTORC1 inhibition [297].

A role of mTORC2 in the regulation of FOXP3 expression was, on the other hand, demonstrated by the fact that higher concentrations of Rapamycin enhanced the

induction of FOXP3 beyond the levels observed at concentrations that predominantly inhibited mTORC1. At these higher concentrations Rapamycin started to noticeably reduce mTORC2 activity, in addition to further mTORC1 inhibition (Figure 33). Further support for a role of mTORC2 in the regulation of FOXP3 was illustrated by the fact that the ATP-competitive mTOR inhibitor Torin 1 had to be present for shorter durations during the stimulation than Rapamycin to result in a significant enhancement of FOXP3 induction (Figure 31). Furthermore, although not reaching statistical significance, Torin 1 mediated-inhibition consistently increased the levels of *Foxp3* mRNA compared to Rapamycin treated cells when samples from short-term stimulations were analysed (Figure 32). The notion that mTORC2 inhibition is involved in the regulation of FOXP3 expression is confirmed by a number of studies. Firstly, Haxhinasto et al. demonstrated that the negative effect of a constitutively active version of AKT on the induction of FOXP3 is only partially reversible using Rapamycin, a observation that is in line with the fact that AKT signalling is both upstream of mTORC1 (inhibited by Rapamycin) and downstream of mTORC2 (not inhibited by Rapamycin, partial effect) [126]. Furthermore, Lee et al. showed that T-cells with disrupted mTORC2 signalling due to the genetic deletion of the mTORC2 component RICTOR, exhibit an increased propensity to differentiate into $FOXP3^+$ Treg in the presence of TGFβ. It is, however, important to note that the effect described by Lee et al. was confined to conditions favourable to FOXP3 induction, which needs to be distinguished to default differentiation of $mTOR^{-/-}$ cells into $FOXP3^+$ Treg under all Th polarising conditions [136, 140].

None of the three studies identified a downstream target that is involved in the mTOR mediated regulation of FOXP3, although the FOXO family of transcription factors seem to be likely targets. Both FOXO1 and FOXO3A are known to be involved in the TGFβ-

mediated FOXP3 induction [167-169] and a role of the mTORC2 downstream target AKT in the control of FOXO protein translocation is well established [63]. Recently, Ma et al. identified PKC-θ as a crucial regulator of FOXO1 and FOXO3A activity via AKT . PKC-$\theta^{-/-}$ T-cells as well as treatment of wildtype cells with PKC-θ inhibitor exhibit enhanced FOXP3 induction, whereas PKC activation with PMA reduced the expression of FOXP3 [273]. The latter findings are in line with the negative effect of short term PMA stimulation on the levels of *Foxp3* transcripts in the presence Rapamycin (Figure 68). The fact that PMA stimulation could, however, only partially reverse the positive effect of Rapamycin addition on *Foxp3* mRNA levels could indicate that PKC-θ is not the sole target of mTOR involved in the regulation of FOXP3. It also cannot be ruled out that the incomplete reversal of the Rapamycin effect is due to the short duration of the PMA stimulation which doesn't allow Rapamycin induced transcripts (putative via PKCθ) to be degraded quickly enough. In agreement with the latter hypothesis, PMA/Ionomycin stimulation in the presence of TGFβ and Rapamycin or stimulation with PMA/Ionomycin at high cell densities did not result in a similar enhancement of FOXP3 induction as was seen when cells were stimulated with αCD3 antibody (data not shown). With respect to percentage and MFI, the expression of FOXP3 induced by PMA/Ionomycin stimulation was consistently lower than with αCD3 stimulation, raising some doubts to whether PMA/ionomycin stimulation induces all the signals required for a proper induction of FOXP3. Further experiments, i.e. using PKC-θ inhibitors, will have to investigate the role of PKC-θ in the mTOR regulated FOXP3 induction, especially since Ma et al. failed to conclusively link the PKC-θ/AKT/FOXO axis to the mTOR pathway. Encouragingly, the second phospho-proteomics approach identified the S279 and S283 phospho-sites in FOXO3A as responsive to Torin1 treatment. In line

with the fact that FOXO3A phosphorylation is thought to be downstream of mTORC2, the site was not significantly regulated by Rapamycin. The observation made by other groups that the TGFβ-mediated FOXP3 induction is highly dependent on FOXO1 and FOXO3A activation [167-169], could be potentially be due to the TGFβ-mediated activation of PP2A resulting in reduced activation of AKT (S473) and increased FOXO translocation. It cannot be ruled out though that reliance on FOXO proteins is caused by the cooperation of the FOXOs with TGFβ-induced transcription factors, i.e. through the formation of a molecular complex at the CNS regions of the *Foxp3* locus, or other yet unidentified mechanisms.

In summary the data shown in this thesis regarding the differential contribution of the mTOR complexes indicates that the inhibition of both complexes may contribute independently but additively to the enhancement of FOXP3 induction. This interpretation contrasts with the conclusion of Delgoffe et al. who emphasize that simultaneous inhibition of both complexes is required for the induction of FOXP3 [139]. This discrepancy in the interpretation might be explained by the differences in the experimental system used to study the role of the two complexes, especially since pharmacological and genetic deletion-mediated inhibitions are compared in the two studies. Furthermore, in contrast to the experiments illustrated here, Delgoffe et al. investigated the mTOR-mediated induction of FOXP3 in the absence of TGFβ. It may be that inhibition of both complexes is required for the maximal hyper-sensitization to TGFβ, although no significant effect of mTOR inhibition was detected in EL4.B02 cells in the absence of added TGFβ. The concept that mTOR inhibition increases the sensitivity for TGFβ represents an appealing hypothesis, since it would facilitate the generation of $FOXP3^+$ Treg in a microenvironment that contains TGFβ concentrations that are

otherwise insufficient to induce significant number of Treg. Irrespective of the irrefutable function of adoptively transferred FOXP3$^+$ Treg in suppressing immune responses, the fact that *in vitro* the cells are commonly differentiated in the presence of a high concentration of TGFβ has been subject to extensive criticism and raised doubts about whether FOXP3$^+$ iTreg are induced *in vivo,* and consequently whether they contribute to immune homeostasis. Recent studies utilizing *Foxp3* CNS1 knock-out mice, which cannot generate iTreg, have, however, erased these doubts by demonstrating that iTreg have a key role in preventing Th2-driven pathologies at mucosal sites such as allergic inflammation in the gut and asthma [298]. This role of iTreg in the suppression of hypersensitive, autoreactive immune responses was further expanded by experiments suggesting that during evolution the CNS1-driven iTreg differentiation emerged in placental animals to control maternal-fetal tolerance [299]. Similarly, FOXP3 itself seems to have undergone extensive selection as part of the evolution of mammals, which enabled the transcription factor to interact and influence a wide array of interaction partners [300]. In the context of maternal-fetal tolerance the function of the tryptophan consuming enzyme IDO, which is amongst others expressed in the maternal uterine mucosa and the fetal syncytiotrophoblast, has been demonstrated to be essential to prevent the loss of allogeneic foetuses [301]. In addition to IDO, high levels of arginase activity were detected in the placenta, resulting the local depletion of L-arginine in the microenvironment, as well as downmodulation of the CD3ζ chain and T-cell hypo-responsiveness [302]. Furthermore a considerable expansion of the FOXP3$^+$ Treg compartment has been observed during pregnancy [301]. It may be that IDO and arginase expression might, at least in part, serve to expand FOXP3$^+$ Treg numbers via tryptophan and arginine depletion-mediated mTOR inhibition. Since a

foetus can be considered as an allograft and therefore bears some resemblance to the skin allograft models developed in our laboratory, an IDO and arginase-mediated enrichment of FOXP3^{+} Treg, similar to the EAA depletion-induced FOXP3^{+} Treg generation established by Cobbold et al., seems conceivable [127].

The establishment of the EL4.B02 cell line that responds to mTOR inhibition and other signals known to induce FOXP3 in T cells, enabled the interrogation of factors downstream of mTOR that maybe involved in the regulation of FOXP3 (Chapters 5 and 6). Although these experiments ruled out potential candidates (SMAD3, AP-1, TIEG1) or failed to demonstrate convincingly that FOXO1, FOXO3A and STAT3 are involved in the mTOR-mediated regulation of FOXP3 expression, they managed to identify *Foxp3* CNS regions responsive to mTOR inhibition. Even though these CNS regions, in particular the large *Foxp3* promoter region, are likely to contain hundreds of putative transcription factor binding sites, the list of potential candidates has been significantly reduced. Both promoter+CNS1 and promoter+CNS2 luciferase constructs responded to mTOR inhibition mediated by Rapamycin or Torin 1, indicating that mTOR regulates transcriptional regulators that bind to both CNS1 and CNS2 or to the *Foxp3* promoter included in both constructs (Figures 36 and 37) . Evidence for the latter scenario comes from the analysis of CNS1+CNS2 double enhancer constructs, which retained the TGFβ (CNS1) and αCD3 responsiveness (CNS2) as well as the mTOR responsiveness of the single enhancer constructs. In contrast to the additive effects of CD3 and TGFβ-receptor engagement on the activity of the double enhancer luciferase construct, the effect of mTOR inhibition did not change in magnitude (Figure 63). This could be explained by the activation of a transcription factor that engages the *Foxp3* promoter

and enhances transcriptional activity of the artificial *Foxp3* locus in cooperation with both CNS1 and CNS2. Additional experiments investigating the composition of transcription complexes that occupy CNS regions in response to mTOR inhibition, for example, by using oligo-pull-down experiments followed by mass spectrometry-mediated identification of bound proteins, will have to be conducted to shed more light on the identity of mTOR regulated proteins involved in FOXP3 transcription.

Even though the target of mTOR that regulates FOXP3 expression was not identified, the EL4.B02 system provided the means to reveal how mTOR might regulate the differentiation of Th17 cells. Due to the constitutive phosphorylation of STAT3 at both S727 and Y705 (Figures 48 and 49) as well as the constitutive expression of the transcription factor RORγT [282], EL4.B02 has the inherent propensity to differentiate towards an IL-17A secreting, Th17-like phenotype when stimulated through the TCR (Figure 50). The inhibition of the mTOR pathway by Rapamycin or Torin 1 inhibited IL-17A induction in a dose-dependent manner and reduced the levels of pY705 STAT3 (Figures 51-55). Considering the well-established link between *Il-17a* transcription and STAT3 activity [176, 178], mTOR inhibition is likely to impose its effect through the inactivation of STAT3, although other mechanism such as the FOXP3-mediated impairment of RORγT function cannot be excluded [221, 282, 283]. The fact that EAA depletion-mediated mTOR inhibition has a similar effect on the levels of IL-17A protein (data not shown) indicates that this represents a mechanism employed by several modes of mTOR inhibition. Although mTOR was demonstrated to directly phosphorylate STAT3 at S727 [222, 223], a direct effect of the inhibition of the serine/threonine kinase on phospho-tyrosine residues in STAT3 seemed unlikely. Sauer et al. identified *Socs1* and *Socs3* as mRNAs that are significantly upregulated in FOXP3$^+$

cells generated under mTOR inhibition [124]. Both SOCS1 and SOCS3 are members of the suppressor of cytokine signalling family and were demonstrated to be prevent tyrosine phosphorylation of STAT3 [218, 227-229]. Therefore an induction of SOCS1 and/or SOCS3 expression by mTOR inhibition could be responsible for the reduced levels of pY705 STAT3. Indeed, both Rapamycin and EAA depletion-mediated mTOR inhibition consistently increased the levels of *Socs1* and *Socs3* mRNA. In the case of SOCS3, these results were confirmed by studies of Delgoffe et al. that demonstrated that *Socs3* expression is positively regulated by mTORC1 inhibition ($RHEB^{-/-}$ T-cells). Therefore a model in which mTORC1 inhibition-induced *Socs* expression inhibits the tyrosine-phosphorylation of STAT3, resulting in reduced IL-17A expression, seems conceivable. Since STAT3 activation and binding to CNS2 was recently demonstrated to negatively regulate the expression of FOXP3 by interfering with the association of SMAD3 with CNS1 [179], this mechanism of STAT3 inactivation by mTORC1 inhibition could also explain the increased expression of FOXP3. Because the interpretation of experiments addressing this hypothesis using STAT3 knock-down and mutant STAT3 over-expression was difficult due to technical problems, a similar approach to that described by Xu et al. was pursued. However, the mutation of the STAT3 binding site in CNS2 resulted in neither an enhanced activity of double enhancer constructs, nor the cancellation of the mTOR inhibition-mediated increase in luciferase expression (Figure 65). The fact that the mutation of the site did not enhance the activity as did the deletion of the STAT3 site in the study by Xu et al., indicates that the base pair mutations might be insufficient to prevent STAT3 binding. Further experiments, i.e. using luciferase constructs containing deletions of the STAT3 binding site or ChIP experiments, will have to examine whether mTORC1 might regulate the expression of FOXP3 via STAT3

inactivation. A model that implicates mTORC1 inhibition-mediated STAT3 inactivation and mTORC2 inhibition-mediated FOXO activation could explain the observation that inhibition of both complexes independently and additively facilitate the induction of FOXP3.

As with the long standing success of research with T-cell lines such as Jurkat cells that have proven useful tools in deciphering early TCR signalling events [200], the EL4.B02 cell line established and characterized in this thesis could represent a valuable resource to investigate mechanisms involved in the induction of regulation as well as downstream effects of FOXP3 expression. The conditions delineated in this thesis with regards to signals that induce FOXP3 expression should provide a starting point for further investigations. Although the limitations of use of transformed cell lines and *in vitro* experiments with respect to the physiological relevance have to be acknowledged, the experiments illustrated here show that EL4.B02 represents a valid model system for the investigation of FOXP3 induction. Many of the findings made in primary $CD4^+$ T-cells in relation to the induction of FOXP3 in general and mTOR signalling in particular can be reproduced in the system. In addition to those features closely resembling primary $CD4^+$ T-cells that establish EL4.B02 as a valid model system, a cell line offers a multitude of properties that make it an attractive system to work with. One of the characteristics which was exploited in this thesis, is the amenability to SILAC labelling used for quantitative mass spectrometry-based proteomics research. The labelling of primary cells is difficult due to their limited proliferation capacity, a feature that is required to ensure complete incorporation of isotopically labelled amino acids. Although the phospho-proteomics approach has not yet consistently identified mTOR

targets that could be involved in the regulation of FOXP3, a number of phospho-sites in proteins known to control the expression of FOXP3 were demonstrated to be responsive to mTOR inhibition. The experiments performed so far demonstrated that the mass spectrometry-based screen is technically feasible, but optimization of both stimulation conditions and technical aspects such as the SCX-fractionation, the TiO_2-mediated phospho-peptide enrichment and the data analysis, are necessary in order to confirm some of the candidate proteins as well as identify additional ones. The emergence of novel techniques enabling genetic manipulation of cells, such as the transfection of zinc-finger nucleases to allow for site specific knock-out and knock-in [303] as well as highly efficient transfection using silicon nanowires [304], should enable the targeted investigation of the role of specific proteins of interest. The problems associated with stable expression of proteins as well as the shRNA mediated knock-down described in this thesis should be easily overcome in this way. Nevertheless, transient transfections of EL4.B02 are technically feasible and have allowed the use of luciferase assays to interrogate the transcriptional regulation of *Foxp3* by mTOR signalling. Furthermore, classical approaches used to study TCR signalling in Jurkat cells such as the random mutagenesis using radiation or chemicals to create mutants with desired phenotypes [200], could be employed. Since at least some aspects of the epigenetic regulation of FOXP3 were demonstrated to be intact in the parental EL4 cell line [160], it seems feasible to investigate these mechanism in greater detail in the EL4.B02 cell line. Furthermore studies could be extended beyond the regulation of FOXP3 expression, by investigating downstream targets of FOXP3 involved in the suppressive activity of $FOXP3^+$ Treg. For example, large quantities of SILAC labelled cells could be easily provided in order to investigate the FOXP3-dependent proteome. In

summary the EL4.B02 line could serve to facilitate FOXP3 relevant research at multiple levels and thereby help to expand the knowledge of how FOXP3-dependent regulation could be therapeutically exploited.

References

1. Thomson, A.W., Turnquist, H.R. & Raimondi, G. Immunoregulatory functions of mTOR inhibition. *Nat Rev Immunol* **9**, 324-337 (2009).
2. Heitman, J., Movva, N.R. & Hall, M.N. Targets for cell cycle arrest by the immunosuppressant rapamycin in yeast. *Science* **253**, 905-909 (1991).
3. Cafferkey, R. *et al.* Dominant Missense Mutations in a Novel Yeast Protein Related to Mammalian Phosphatidylinositol 3-Kinase and Vps34 Abrogate Rapamycin Cytotoxicity. *Molecular and Cellular Biology* **13**, 6012-6023 (1993).
4. Kunz, J. *et al.* Target of Rapamycin in Yeast, Tor2, Is an Essential Phosphatidylinositol Kinase Homolog Required for G(1) Progression. *Cell* **73**, 585-596 (1993).
5. Sabatini, D.M., Erdjumentbromage, H., Lui, M., Tempst, P. & Snyder, S.H. Raft1 - a Mammalian Protein That Binds to Fkbp12 in a Rapamycin-Dependent Fashion and Is Homologous to Yeast Tors. *Cell* **78**, 35-43 (1994).
6. Sabers, C.J. *et al.* Isolation of a Protein Target of the Fkbp12-Rapamycin Complex in Mammalian-Cells. *Journal of Biological Chemistry* **270**, 815-822 (1995).
7. Brown, E.J. *et al.* A Mammalian Protein Targeted by G1-Arresting Rapamycin-Receptor Complex. *Nature* **369**, 756-758 (1994).
8. Jacinto, E. What controls TOR? *Iubmb Life* **60**, 483-496 (2008).
9. Peterson, R.T., Beal, P.A., Comb, M.J. & Schreiber, S.L. FKBP12-rapamycin-associated protein (FRAP) autophosphorylates at serine 2481 under translationally repressive conditions. *Journal of Biological Chemistry* **275**, 7416-7423 (2000).
10. Takahashi, T. *et al.* Carboxyl-terminal region conserved among phosphoinositide-kinase-related kinases is indispensable for mTOR function in vivo and in vitro. *Genes to Cells* **5**, 765-775 (2000).
11. Laplante, M. & Sabatini, D.M. mTOR signaling at a glance. *J Cell Sci* **122**, 3589-3594 (2009).
12. Laplante, M. & Sabatini, D.M. mTOR Signaling in Growth Control and Disease. *Cell* **149**, 274-293 (2012).
13. Sarbassov, D.D. *et al.* Prolonged rapamycin treatment inhibits mTORC2 assembly and Akt/PKB. *Mol Cell* **22**, 159-168 (2006).
14. Liu, Q. *et al.* Discovery of 1-(4-(4-propionylpiperazin-1-yl)-3-(trifluoromethyl)phenyl)-9-(quinolin-3-yl)benz o[h][1,6]naphthyridin-2(1H)-one as a highly potent, selective mammalian target of rapamycin (mTOR) inhibitor for the treatment of cancer. *J Med Chem* **53**, 7146-7155 (2010).
15. Liu, Q. *et al.* Kinome-wide selectivity profiling of ATP-competitive mammalian target of rapamycin (mTOR) inhibitors and characterization of their binding kinetics. *J Biol Chem* **287**, 9742-9752.
16. Thoreen, C.C. *et al.* An ATP-competitive mammalian target of rapamycin inhibitor reveals rapamycin-resistant functions of mTORC1. *J Biol Chem* **284**, 8023-8032 (2009).
17. Apsel, B. *et al.* Targeted polypharmacology: discovery of dual inhibitors of tyrosine and phosphoinositide kinases. *Nature Chemical Biology* **4**, 691-699 (2008).
18. Feldman, M.E. *et al.* Active-Site Inhibitors of mTOR Target Rapamycin-Resistant Outputs of mTORC1 and mTORC2. *Plos Biology* **7**, 371-383 (2009).
19. Sancak, Y. *et al.* PRAS40 is an insulin-regulated inhibitor of the mTORC1 protein kinase. *Molecular Cell* **25**, 903-915 (2007).
20. Thedieck, K. *et al.* PRAS40 and PRR5-Like Protein Are New mTOR Interactors that Regulate Apoptosis. *PLoS One* **2** (2007).
21. Vander Haar, E., Lee, S.I., Bandhakavi, S., Griffin, T.J. & Kim, D.H. Insulin signalling to mTOR mediated by the Akt/PKB substrate PRAS40. *Nat Cell Biol* **9**, 316-323 (2007).

22. Abraham, R.T. Mammalian target of rapamycin: immunosuppressive drugs uncover a novel pathway of cytokine receptor signaling. *Curr Opin Immunol* **10**, 330-336 (1998).
23. Colombetti, S., Basso, V., Mueller, D.L. & Mondino, A. Prolonged TCR/CD28 engagement drives IL-2-independent T cell clonal expansion through signaling mediated by the mammalian target of rapamycin. *J Immunol* **176**, 2730-2738 (2006).
24. Gulen, M.F. *et al.* The receptor SIGIRR suppresses Th17 cell proliferation via inhibition of the interleukin-1 receptor pathway and mTOR kinase activation. *Immunity* **32**, 54-66 (2010).
25. Powell, J.D. & Delgoffe, G.M. The mammalian target of rapamycin: linking T cell differentiation, function, and metabolism. *Immunity* **33**, 301-311 (2010).
26. Rao, R.R., Li, Q., Odunsi, K. & Shrikant, P.A. The mTOR kinase determines effector versus memory CD8+ T cell fate by regulating the expression of transcription factors T-bet and Eomesodermin. *Immunity* **32**, 67-78 (2010).
27. Stephenson, L.M., Park, D.S., Mora, A.L., Goenka, S. & Boothby, M. Sequence motifs in IL-4R alpha mediating cell-cycle progression of primary lymphocytes. *J Immunol* **175**, 5178-5185 (2005).
28. Lee, D.F. *et al.* IKK beta suppression of TSC1 links inflammation and tumor angiogenesis via the mTOR pathway. *Cell* **130**, 440-455 (2007).
29. Inoki, K. *et al.* TSC2 integrates Wnt and energy signals via a coordinated phosphorylation by AMPK and GSK3 to regulate cell growth. *Cell* **126**, 955-968 (2006).
30. Inoki, K., Zhu, T. & Guan, K.L. TSC2 mediates cellular energy response to control cell growth and survival. *Cell* **115**, 577-590 (2003).
31. Brugarolas, J. *et al.* Regulation of mTOR function in response to hypoxia by REDD1 and the TSC1/TSC2 tumor suppressor complex. *Genes Dev* **18**, 2893-2904 (2004).
32. DeYoung, M.P., Horak, P., Sofer, A., Sgroi, D. & Ellisen, L.W. Hypoxia regulates TSC1/2-mTOR signaling and tumor suppression through REDD1-mediated 14-3-3 shuttling. *Genes Dev* **22**, 239-251 (2008).
33. Gwinn, D.M. *et al.* AMPK phosphorylation of raptor mediates a metabolic checkpoint. *Mol Cell* **30**, 214-226 (2008).
34. Budanov, A.V. & Karin, M. p53 target genes sestrin1 and sestrin2 connect genotoxic stress and mTOR signaling. *Cell* **134**, 451-460 (2008).
35. Feng, Z., Zhang, H., Levine, A.J. & Jin, S. The coordinate regulation of the p53 and mTOR pathways in cells. *Proc Natl Acad Sci U S A* **102**, 8204-8209 (2005).
36. Stambolic, V. *et al.* Regulation of PTEN transcription by p53. *Mol Cell* **8**, 317-325 (2001).
37. Oldham, S., Montagne, J., Radimerski, T., Thomas, G. & Hafen, E. Genetic and biochemical characterization of dTOR, the Drosophila homolog of the target of rapamycin. *Genes Dev* **14**, 2689-2694 (2000).
38. Zhang, H., Stallock, J.P., Ng, J.C., Reinhard, C. & Neufeld, T.P. Regulation of cellular growth by the Drosophila target of rapamycin dTOR. *Genes Dev* **14**, 2712-2724 (2000).
39. Roccio, M., Bos, J.L. & Zwartkruis, F.J. Regulation of the small GTPase Rheb by amino acids. *Oncogene* **25**, 657-664 (2006).
40. Sancak, Y. *et al.* Ragulator-Rag complex targets mTORC1 to the lysosomal surface and is necessary for its activation by amino acids. *Cell* **141**, 290-303 (2010).
41. Sancak, Y. *et al.* The Rag GTPases bind raptor and mediate amino acid signaling to mTORC1. *Science* **320**, 1496-1501 (2008).
42. Kim, E., Goraksha-Hicks, P., Li, L., Neufeld, T.P. & Guan, K.L. Regulation of TORC1 by Rag GTPases in nutrient response. *Nat Cell Biol* **10**, 935-945 (2008).
43. Zoncu, R. *et al.* mTORC1 senses lysosomal amino acids through an inside-out mechanism that requires the vacuolar H(+)-ATPase. *Science* **334**, 678-683 (2011).

44. Goberdhan, D.C., Meredith, D., Boyd, C.A. & Wilson, C. PAT-related amino acid transporters regulate growth via a novel mechanism that does not require bulk transport of amino acids. *Development* **132**, 2365-2375 (2005).
45. Heublein, S. *et al.* Proton-assisted amino-acid transporters are conserved regulators of proliferation and amino-acid-dependent mTORC1 activation. *Oncogene* **29**, 4068-4079 (2010).
46. Ogmundsdottir, M.H. *et al.* Proton-assisted amino acid transporter PAT1 complexes with Rag GTPases and activates TORC1 on late endosomal and lysosomal membranes. *PLoS One* **7**, e36616 (2012).
47. Yu, L. *et al.* Termination of autophagy and reformation of lysosomes regulated by mTOR. *Nature* **465**, 942-946 (2010).
48. Goberdhan, D.C. *et al.* Amino acid sensing and mTOR regulation: inside or out? *Biochem Soc Trans* **37**, 248-252 (2009).
49. Reynolds, B., Laynes, R., Ogmundsdottir, M.H., Boyd, C.A. & Goberdhan, D.C. Amino acid transporters and nutrient-sensing mechanisms: new targets for treating insulin-linked disorders? *Biochem Soc Trans* **35**, 1215-1217 (2007).
50. Edinger, A.L. & Thompson, C.B. Akt maintains cell size and survival by increasing mTOR-dependent nutrient uptake. *Mol Biol Cell* **13**, 2276-2288 (2002).
51. Ma, X.M. & Blenis, J. Molecular mechanisms of mTOR-mediated translational control. *Nat Rev Mol Cell Biol* **10**, 307-318 (2009).
52. Laplante, M. & Sabatini, D.M. An emerging role of mTOR in lipid biosynthesis. *Curr Biol* **19**, R1046-1052 (2009).
53. Duvel, K. *et al.* Activation of a metabolic gene regulatory network downstream of mTOR complex 1. *Mol Cell* **39**, 171-183 (2010).
54. Porstmann, T. *et al.* SREBP activity is regulated by mTORC1 and contributes to Akt-dependent cell growth. *Cell Metab* **8**, 224-236 (2008).
55. Wang, B.T. *et al.* The mammalian target of rapamycin regulates cholesterol biosynthetic gene expression and exhibits a rapamycin-resistant transcriptional profile. *Proc Natl Acad Sci U S A* **108**, 15201-15206 (2011).
56. Peterson, T.R. *et al.* mTOR complex 1 regulates lipin 1 localization to control the SREBP pathway. *Cell* **146**, 408-420 (2011).
57. Kim, J.E. & Chen, J. regulation of peroxisome proliferator-activated receptor-gamma activity by mammalian target of rapamycin and amino acids in adipogenesis. *Diabetes* **53**, 2748-2756 (2004).
58. Brugarolas, J.B., Vazquez, F., Reddy, A., Sellers, W.R. & Kaelin, W.G., Jr. TSC2 regulates VEGF through mTOR-dependent and -independent pathways. *Cancer Cell* **4**, 147-158 (2003).
59. Hudson, C.C. *et al.* Regulation of hypoxia-inducible factor 1alpha expression and function by the mammalian target of rapamycin. *Mol Cell Biol* **22**, 7004-7014 (2002).
60. Cunningham, J.T. *et al.* mTOR controls mitochondrial oxidative function through a YY1-PGC-1alpha transcriptional complex. *Nature* **450**, 736-740 (2007).
61. Kuballa, P., Nolte, W.M., Castoreno, A.B. & Xavier, R.J. Autophagy and the immune system. *Annu Rev Immunol* **30**, 611-646 (2012).
62. Bhaskar, P.T. & Hay, N. The two TORCs and Akt. *Dev Cell* **12**, 487-502 (2007).
63. Huang, H. & Tindall, D.J. Dynamic FoxO transcription factors. *J Cell Sci* **120**, 2479-2487 (2007).
64. Huang, J., Wu, S., Wu, C.L. & Manning, B.D. Signaling events downstream of mammalian target of rapamycin complex 2 are attenuated in cells and tumors deficient for the tuberous sclerosis complex tumor suppressors. *Cancer Res* **69**, 6107-6114 (2009).

65. Jacinto, E. *et al.* Mammalian TOR complex 2 controls the actin cytoskeleton and is rapamycin insensitive. *Nat Cell Biol* **6**, 1122-1128 (2004).
66. Sarbassov, D.D. *et al.* Rictor, a novel binding partner of mTOR, defines a rapamycin-insensitive and raptor-independent pathway that regulates the cytoskeleton. *Curr Biol* **14**, 1296-1302 (2004).
67. Reis e Sousa, C. Activation of dendritic cells: translating innate into adaptive immunity. *Curr Opin Immunol* **16**, 21-25 (2004).
68. Hackstein, H. *et al.* Rapamycin inhibits IL-4--induced dendritic cell maturation in vitro and dendritic cell mobilization and function in vivo. *Blood* **101**, 4457-4463 (2003).
69. Taner, T., Hackstein, H., Wang, Z., Morelli, A.E. & Thomson, A.W. Rapamycin-treated, alloantigen-pulsed host dendritic cells induce ag-specific T cell regulation and prolong graft survival. *Am J Transplant* **5**, 228-236 (2005).
70. Turnquist, H.R. *et al.* Rapamycin-conditioned dendritic cells are poor stimulators of allogeneic CD4+ T cells, but enrich for antigen-specific Foxp3+ T regulatory cells and promote organ transplant tolerance. *J Immunol* **178**, 7018-7031 (2007).
71. Turnquist, H.R. *et al.* IL-1beta-driven ST2L expression promotes maturation resistance in rapamycin-conditioned dendritic cells. *J Immunol* **181**, 62-72 (2008).
72. Woltman, A.M. *et al.* Rapamycin specifically interferes with GM-CSF signaling in human dendritic cells, leading to apoptosis via increased p27KIP1 expression. *Blood* **101**, 1439-1445 (2003).
73. Hackstein, H., Taner, T., Logar, A.J. & Thomson, A.W. Rapamycin inhibits macropinocytosis and mannose receptor-mediated endocytosis by bone marrow-derived dendritic cells. *Blood* **100**, 1084-1087 (2002).
74. Monti, P. *et al.* Rapamycin impairs antigen uptake of human dendritic cells. *Transplantation* **75**, 137-145 (2003).
75. Haidinger, M. *et al.* A versatile role of mammalian target of rapamycin in human dendritic cell function and differentiation. *J Immunol* **185**, 3919-3931 (2010).
76. Ohtani, M. *et al.* Mammalian target of rapamycin and glycogen synthase kinase 3 differentially regulate lipopolysaccharide-induced interleukin-12 production in dendritic cells. *Blood* **112**, 635-643 (2008).
77. Weichhart, T. *et al.* The TSC-mTOR signaling pathway regulates the innate inflammatory response. *Immunity* **29**, 565-577 (2008).
78. Fischer, R., Turnquist, H.R., Taner, T. & Thomson, A.W. Use of rapamycin in the induction of tolerogenic dendritic cells. *Handb Exp Pharmacol*, 215-232 (2009).
79. Reichardt, W. *et al.* Impact of mammalian target of rapamycin inhibition on lymphoid homing and tolerogenic function of nanoparticle-labeled dendritic cells following allogeneic hematopoietic cell transplantation. *J Immunol* **181**, 4770-4779 (2008).
80. Weichhart, T. & Saemann, M.D. The PI3K/Akt/mTOR pathway in innate immune cells: emerging therapeutic applications. *Ann Rheum Dis* **67 Suppl 3**, iii70-74 (2008).
81. Gomez-Cambronero, J. Rapamycin inhibits GM-CSF-induced neutrophil migration. *FEBS Lett* **550**, 94-100 (2003).
82. Lehman, J.A., Calvo, V. & Gomez-Cambronero, J. Mechanism of ribosomal p70S6 kinase activation by granulocyte macrophage colony-stimulating factor in neutrophils: cooperation of a MEK-related, THR421/SER424 kinase and a rapamycin-sensitive, m-TOR-related THR389 kinase. *J Biol Chem* **278**, 28130-28138 (2003).
83. Lorne, E. *et al.* Participation of mammalian target of rapamycin complex 1 in Toll-like receptor 2- and 4-induced neutrophil activation and acute lung injury. *Am J Respir Cell Mol Biol* **41**, 237-245 (2009).
84. Lindemann, S.W. *et al.* Neutrophils alter the inflammatory milieu by signal-dependent translation of constitutive messenger RNAs. *Proc Natl Acad Sci U S A* **101**, 7076-7081 (2004).

85. Yost, C.C. *et al.* Activated polymorphonuclear leukocytes rapidly synthesize retinoic acid receptor-alpha: a mechanism for translational control of transcriptional events. *J Exp Med* **200**, 671-680 (2004).
86. Kim, M.S., Kuehn, H.S., Metcalfe, D.D. & Gilfillan, A.M. Activation and function of the mTORC1 pathway in mast cells. *J Immunol* **180**, 4586-4595 (2008).
87. Shin, J., Pan, H. & Zhong, X.P. Regulation of mast cell survival and function by tuberous sclerosis complex 1. *Blood* **119**, 3306-3314 (2012).
88. Kuehn, H.S., Jung, M.Y., Beaven, M.A., Metcalfe, D.D. & Gilfillan, A.M. Prostaglandin E2 activates and utilizes mTORC2 as a central signaling locus for the regulation of mast cell chemotaxis and mediator release. *J Biol Chem* **286**, 391-402 (2010).
89. Smrz, D. *et al.* mTORC1 and mTORC2 differentially regulate homeostasis of neoplastic and non-neoplastic human mast cells. *Blood* **118**, 6803-6813 (2011).
90. Zhang, S. *et al.* Constitutive reductions in mTOR alter cell size, immune cell development, and antibody production. *Blood* **117**, 1228-1238 (2010).
91. Benhamron, S. & Tirosh, B. Direct activation of mTOR in B lymphocytes confers impairment in B-cell maturation andloss of marginal zone B cells. *Eur J Immunol* **41**, 2390-2396 (2011).
92. Lazorchak, A.S. *et al.* Sin1-mTORC2 suppresses rag and il7r gene expression through Akt2 in B cells. *Mol Cell* **39**, 433-443 (2010).
93. Donahue, A.C. & Fruman, D.A. Proliferation and survival of activated B cells requires sustained antigen receptor engagement and phosphoinositide 3-kinase activation. *J Immunol* **170**, 5851-5860 (2003).
94. Donahue, A.C. & Fruman, D.A. Distinct signaling mechanisms activate the target of rapamycin in response to different B-cell stimuli. *Eur J Immunol* **37**, 2923-2936 (2007).
95. Sakata, A., Kuwahara, K., Ohmura, T., Inui, S. & Sakaguchi, N. Involvement of a rapamycin-sensitive pathway in CD40-mediated activation of murine B cells in vitro. *Immunol Lett* **68**, 301-309 (1999).
96. Bretscher, P. & Cohn, M. A theory of self-nonself discrimination. *Science* **169**, 1042-1049 (1970).
97. Lafferty, K.J. & Cunningham, A.J. A new analysis of allogeneic interactions. *Aust J Exp Biol Med Sci* **53**, 27-42 (1975).
98. Gottschalk, R.A., Corse, E. & Allison, J.P. TCR ligand density and affinity determine peripheral induction of Foxp3 in vivo. *J Exp Med* **207**, 1701-1711 (2010).
99. Katzman, S.D. *et al.* Duration of antigen receptor signaling determines T-cell tolerance or activation. *Proc Natl Acad Sci U S A* **107**, 18085-18090 (2010).
100. Turner, M.S., Kane, L.P. & Morel, P.A. Dominant role of antigen dose in CD4+Foxp3+ regulatory T cell induction and expansion. *J Immunol* **183**, 4895-4903 (2009).
101. Zheng, Y. *et al.* A role for mammalian target of rapamycin in regulating T cell activation versus anergy. *J Immunol* **178**, 2163-2170 (2007).
102. Zheng, Y., Delgoffe, G.M., Meyer, C.F., Chan, W. & Powell, J.D. Anergic T cells are metabolically anergic. *J Immunol* **183**, 6095-6101 (2009).
103. Francisco, L.M. *et al.* PD-L1 regulates the development, maintenance, and function of induced regulatory T cells. *J Exp Med* **206**, 3015-3029 (2009).
104. So, T., Choi, H. & Croft, M. OX40 complexes with phosphoinositide 3-kinase and protein kinase B (PKB) to augment TCR-dependent PKB signaling. *J Immunol* **186**, 3547-3555 (2011).
105. Appleman, L.J., Berezovskaya, A., Grass, I. & Boussiotis, V.A. CD28 costimulation mediates T cell expansion via IL-2-independent and IL-2-dependent regulation of cell cycle progression. *J Immunol* **164**, 144-151 (2000).
106. Rathmell, J.C., Farkash, E.A., Gao, W. & Thompson, C.B. IL-7 enhances the survival and maintains the size of naive T cells. *J Immunol* **167**, 6869-6876 (2001).

107. Wofford, J.A., Wieman, H.L., Jacobs, S.R., Zhao, Y. & Rathmell, J.C. IL-7 promotes Glut1 trafficking and glucose uptake via STAT5-mediated activation of Akt to support T-cell survival. *Blood* **111**, 2101-2111 (2008).
108. Li, Q. *et al.* A central role for mTOR kinase in homeostatic proliferation induced CD8+ T cell memory and tumor immunity. *Immunity* **34**, 541-553 (2011).
109. Allen, A. *et al.* The novel cyclophilin binding compound, sanglifehrin A, disassociates G1 cell cycle arrest from tolerance induction. *J Immunol* **172**, 4797-4803 (2004).
110. Powell, J.D., Lerner, C.G. & Schwartz, R.H. Inhibition of cell cycle progression by rapamycin induces T cell clonal anergy even in the presence of costimulation. *J Immunol* **162**, 2775-2784 (1999).
111. Vanasek, T.L., Khoruts, A., Zell, T. & Mueller, D.L. Antagonistic roles for CTLA-4 and the mammalian target of rapamycin in the regulation of clonal anergy: enhanced cell cycle progression promotes recall antigen responsiveness. *J Immunol* **167**, 5636-5644 (2001).
112. Pearce, E.L. Metabolism in T cell activation and differentiation. *Curr Opin Immunol* **22**, 314-320 (2010).
113. Gerriets, V.A. & Rathmell, J.C. Metabolic pathways in T cell fate and function. *Trends Immunol* **33**, 168-173 (2012).
114. Powell, J.D., Pollizzi, K.N., Heikamp, E.B. & Horton, M.R. Regulation of immune responses by mTOR. *Annu Rev Immunol* **30**, 39-68.
115. Sinclair, L.V. *et al.* Phosphatidylinositol-3-OH kinase and nutrient-sensing mTOR pathways control T lymphocyte trafficking. *Nat Immunol* **9**, 513-521 (2008).
116. Kerdiles, Y.M. *et al.* Foxo1 links homing and survival of naive T cells by regulating L-selectin, CCR7 and interleukin 7 receptor. *Nat Immunol* **10**, 176-184 (2009).
117. Yang, K., Neale, G., Green, D.R., He, W. & Chi, H. The tumor suppressor Tsc1 enforces quiescence of naive T cells to promote immune homeostasis and function. *Nat Immunol* **12**, 888-897 (2011).
118. Murooka, T.T., Rahbar, R., Platanias, L.C. & Fish, E.N. CCL5-mediated T-cell chemotaxis involves the initiation of mRNA translation through mTOR/4E-BP1. *Blood* **111**, 4892-4901 (2008).
119. Araki, K. *et al.* mTOR regulates memory CD8 T-cell differentiation. *Nature* **460**, 108-112 (2009).
120. Zhang, N. & Bevan, M.J. CD8(+) T cells: foot soldiers of the immune system. *Immunity* **35**, 161-168.
121. Hand, T.W. *et al.* Differential effects of STAT5 and PI3K/AKT signaling on effector and memory CD8 T-cell survival. *Proc Natl Acad Sci U S A* **107**, 16601-16606 (2010).
122. Luckheeram, R.V., Zhou, R., Verma, A.D. & Xia, B. CD4(+)T cells: differentiation and functions. *Clin Dev Immunol* **2012**, 925135 (2012).
123. Zhu, J., Yamane, H. & Paul, W.E. Differentiation of effector CD4 T cell populations (*). *Annu Rev Immunol* **28**, 445-489 (2010).
124. Sauer, S. *et al.* T cell receptor signaling controls Foxp3 expression via PI3K, Akt, and mTOR. *Proc Natl Acad Sci U S A* **105**, 7797-7802 (2008).
125. Daniel, C., Wennhold, K., Kim, H.J. & von Boehmer, H. Enhancement of antigen-specific Treg vaccination in vivo. *Proc Natl Acad Sci U S A* **107**, 16246-16251 (2010).
126. Haxhinasto, S., Mathis, D. & Benoist, C. The AKT-mTOR axis regulates de novo differentiation of CD4+Foxp3+ cells. *J Exp Med* **205**, 565-574 (2008).
127. Cobbold, S.P. *et al.* Infectious tolerance via the consumption of essential amino acids and mTOR signaling. *Proc Natl Acad Sci U S A* **106**, 12055-12060 (2009).
128. Qin, S. *et al.* "Infectious" transplantation tolerance. *Science* **259**, 974-977 (1993).
129. Basu, S., Golovina, T., Mikheeva, T., June, C.H. & Riley, J.L. Cutting edge: Foxp3-mediated induction of pim 2 allows human T regulatory cells to preferentially expand in rapamycin. *J Immunol* **180**, 5794-5798 (2008).

130. Battaglia, M. *et al.* Rapamycin promotes expansion of functional CD4+CD25+FOXP3+ regulatory T cells of both healthy subjects and type 1 diabetic patients. *J Immunol* **177**, 8338-8347 (2006).
131. Battaglia, M., Stabilini, A. & Roncarolo, M.G. Rapamycin selectively expands CD4+CD25+FoxP3+ regulatory T cells. *Blood* **105**, 4743-4748 (2005).
132. Strauss, L., Czystowska, M., Szajnik, M., Mandapathil, M. & Whiteside, T.L. Differential responses of human regulatory T cells (Treg) and effector T cells to rapamycin. *PLoS One* **4**, e5994 (2009).
133. Strauss, L. *et al.* Selective survival of naturally occurring human CD4+CD25+Foxp3+ regulatory T cells cultured with rapamycin. *J Immunol* **178**, 320-329 (2007).
134. Zeiser, R. *et al.* Differential impact of mammalian target of rapamycin inhibition on CD4+CD25+Foxp3+ regulatory T cells compared with conventional CD4+ T cells. *Blood* **111**, 453-462 (2008).
135. Gabrysova, L. *et al.* Integrated T-cell receptor and costimulatory signals determine TGF-beta-dependent differentiation and maintenance of Foxp3+ regulatory T cells. *Eur J Immunol* **41**, 1242-1248 (2011).
136. Delgoffe, G.M. *et al.* The mTOR Kinase Differentially Regulates Effector and Regulatory T Cell Lineage Commitment. *Immunity* **30**, 832-844 (2009).
137. Kopf, H., de la Rosa, G.M., Howard, O.M. & Chen, X. Rapamycin inhibits differentiation of Th17 cells and promotes generation of FoxP3+ T regulatory cells. *Int Immunopharmacol* **7**, 1819-1824 (2007).
138. Blazar, B.R., Taylor, P.A., Panoskaltsis-Mortari, A. & Vallera, D.A. Rapamycin inhibits the generation of graft-versus-host disease- and graft-versus-leukemia-causing T cells by interfering with the production of Th1 or Th1 cytotoxic cytokines. *J Immunol* **160**, 5355-5365 (1998).
139. Delgoffe, G.M. *et al.* The kinase mTOR regulates the differentiation of helper T cells through the selective activation of signaling by mTORC1 and mTORC2. *Nature Immunology* **12**, 295-U117 (2011).
140. Lee, K. *et al.* Mammalian target of rapamycin protein complex 2 regulates differentiation of Th1 and Th2 cell subsets via distinct signaling pathways. *Immunity* **32**, 743-753 (2010).
141. Sakaguchi, S. *et al.* Foxp3+ CD25+ CD4+ natural regulatory T cells in dominant self-tolerance and autoimmune disease. *Immunol Rev* **212**, 8-27 (2006).
142. Cobbold, S.P. *et al.* Immune privilege induced by regulatory T cells in transplantation tolerance. *Immunol Rev* **213**, 239-255 (2006).
143. Sakaguchi, S., Yamaguchi, T., Nomura, T. & Ono, M. Regulatory T cells and immune tolerance. *Cell* **133**, 775-787 (2008).
144. Shevach, E.M. From vanilla to 28 flavors: multiple varieties of T regulatory cells. *Immunity* **25**, 195-201 (2006).
145. Hori, S., Nomura, T. & Sakaguchi, S. Control of regulatory T cell development by the transcription factor Foxp3. *Science* **299**, 1057-1061 (2003).
146. Hori, S. & Sakaguchi, S. Foxp3: a critical regulator of the development and function of regulatory T cells. *Microbes Infect* **6**, 745-751 (2004).
147. Shen, Z., Chen, L., Hao, F. & Wu, J. Transcriptional regulation of Foxp3 gene: multiple signal pathways on the road. *Med Res Rev* **29**, 742-766 (2009).
148. Fantini, M.C. *et al.* Cutting edge: TGF-beta induces a regulatory phenotype in CD4+CD25- T cells through Foxp3 induction and down-regulation of Smad7. *J Immunol* **172**, 5149-5153 (2004).
149. Fu, S. *et al.* TGF-beta induces Foxp3 + T-regulatory cells from CD4 + CD25 - precursors. *Am J Transplant* **4**, 1614-1627 (2004).

150. Marie, J.C., Letterio, J.J., Gavin, M. & Rudensky, A.Y. TGF-beta1 maintains suppressor function and Foxp3 expression in CD4+CD25+ regulatory T cells. *J Exp Med* **201**, 1061-1067 (2005).
151. Shevach, E.M., Davidson, T.S., Huter, E.N., Dipaolo, R.A. & Andersson, J. Role of TGF-Beta in the induction of Foxp3 expression and T regulatory cell function. *J Clin Immunol* **28**, 640-646 (2008).
152. Chen, W. *et al.* Conversion of peripheral CD4+CD25- naive T cells to CD4+CD25+ regulatory T cells by TGF-beta induction of transcription factor Foxp3. *J Exp Med* **198**, 1875-1886 (2003).
153. Davidson, T.S., DiPaolo, R.J., Andersson, J. & Shevach, E.M. Cutting Edge: IL-2 is essential for TGF-beta-mediated induction of Foxp3+ T regulatory cells. *J Immunol* **178**, 4022-4026 (2007).
154. Zheng, S.G., Wang, J., Wang, P., Gray, J.D. & Horwitz, D.A. IL-2 is essential for TGF-beta to convert naive CD4+CD25- cells to CD25+Foxp3+ regulatory T cells and for expansion of these cells. *J Immunol* **178**, 2018-2027 (2007).
155. Horwitz, D.A., Zheng, S.G., Wang, J. & Gray, J.D. Critical role of IL-2 and TGF-beta in generation, function and stabilization of Foxp3+CD4+ Treg. *Eur J Immunol* **38**, 912-915 (2008).
156. Guo, F., Iclozan, C., Suh, W.K., Anasetti, C. & Yu, X.Z. CD28 controls differentiation of regulatory T cells from naive CD4 T cells. *J Immunol* **181**, 2285-2291 (2008).
157. Scotta, C., Soligo, M., Camperio, C. & Piccolella, E. FOXP3 induced by CD28/B7 interaction regulates CD25 and anergic phenotype in human CD4+CD25- T lymphocytes. *J Immunol* **181**, 1025-1033 (2008).
158. Tai, X., Cowan, M., Feigenbaum, L. & Singer, A. CD28 costimulation of developing thymocytes induces Foxp3 expression and regulatory T cell differentiation independently of interleukin 2. *Nat Immunol* **6**, 152-162 (2005).
159. Mantel, P.Y. *et al.* Molecular mechanisms underlying FOXP3 induction in human T cells. *J Immunol* **176**, 3593-3602 (2006).
160. Tone, Y. *et al.* Smad3 and NFAT cooperate to induce Foxp3 expression through its enhancer. *Nat Immunol* **9**, 194-202 (2008).
161. Zheng, Y. *et al.* Role of conserved non-coding DNA elements in the Foxp3 gene in regulatory T-cell fate. *Nature* **463**, 808-812 (2010).
162. Kim, H.P. & Leonard, W.J. CREB/ATF-dependent T cell receptor-induced FoxP3 gene expression: a role for DNA methylation. *J Exp Med* **204**, 1543-1551 (2007).
163. Regateiro, F.S., Howie, D., Cobbold, S.P. & Waldmann, H. TGF-beta in transplantation tolerance. *Curr Opin Immunol* **23**, 660-669 (2011).
164. Long, M., Park, S.G., Strickland, I., Hayden, M.S. & Ghosh, S. Nuclear factor-kappaB modulates regulatory T cell development by directly regulating expression of Foxp3 transcription factor. *Immunity* **31**, 921-931 (2009).
165. Ruan, Q. *et al.* Development of Foxp3(+) regulatory t cells is driven by the c-Rel enhanceosome. *Immunity* **31**, 932-940 (2009).
166. Samon, J.B. *et al.* Notch1 and TGFbeta1 cooperatively regulate Foxp3 expression and the maintenance of peripheral regulatory T cells. *Blood* **112**, 1813-1821 (2008).
167. Ouyang, W. *et al.* Foxo proteins cooperatively control the differentiation of Foxp3+ regulatory T cells. *Nat Immunol* **11**, 618-627 (2010).
168. Kerdiles, Y.M. *et al.* Foxo transcription factors control regulatory T cell development and function. *Immunity* **33**, 890-904 (2010).
169. Harada, Y. *et al.* Transcription factors Foxo3a and Foxo1 couple the E3 ligase Cbl-b to the induction of Foxp3 expression in induced regulatory T cells. *J Exp Med* **207**, 1381-1391 (2010).

170. Venuprasad, K. *et al.* The E3 ubiquitin ligase Itch regulates expression of transcription factor Foxp3 and airway inflammation by enhancing the function of transcription factor TIEG1. *Nat Immunol* **9**, 245-253 (2008).
171. Lal, G. *et al.* Epigenetic regulation of Foxp3 expression in regulatory T cells by DNA methylation. *J Immunol* **182**, 259-273 (2009).
172. Yao, Z. *et al.* Nonredundant roles for Stat5a/b in directly regulating Foxp3. *Blood* **109**, 4368-4375 (2007).
173. Ouaked, N. *et al.* Regulation of the foxp3 gene by the Th1 cytokines: the role of IL-27-induced STAT1. *J Immunol* **182**, 1041-1049 (2009).
174. Huber, M. *et al.* IL-27 inhibits the development of regulatory T cells via STAT3. *International Immunology* **20**, 223-234 (2008).
175. Neufert, C. *et al.* IL-27 controls the development of inducible regulatory T cells and Th17 cells via differential effects on STAT1. *European Journal of Immunology* **37**, 1809-1816 (2007).
176. Bettelli, E. *et al.* Reciprocal developmental pathways for the generation of pathogenic effector T(H)17 and regulatory T cells. *Nature* **441**, 235-238 (2006).
177. Mangan, P.R. *et al.* Transforming growth factor-beta induces development of the T(H)17 lineage. *Nature* **441**, 231-234 (2006).
178. Veldhoen, M., Hocking, R.J., Atkins, C.J., Locksley, R.M. & Stockinger, B. TGF beta in the context of an inflammatory cytokine milieu supports de novo differentiation of IL-17-producing T cells. *Immunity* **24**, 179-189 (2006).
179. Xu, L. *et al.* Positive and negative transcriptional regulation of the Foxp3 gene is mediated by access and binding of the Smad3 protein to enhancer I. *Immunity* **33**, 313-325 (2010).
180. Maruyama, T. *et al.* Control of the differentiation of regulatory T cells and T(H)17 cells by the DNA-binding inhibitor Id3. *Nat Immunol* **12**, 86-95 (2010).
181. Fragale, A. *et al.* IFN regulatory factor-1 negatively regulates CD4+ CD25+ regulatory T cell differentiation by repressing Foxp3 expression. *J Immunol* **181**, 1673-1682 (2008).
182. Klunker, S. *et al.* Transcription factors RUNX1 and RUNX3 in the induction and suppressive function of Foxp3+ inducible regulatory T cells. *J Exp Med* **206**, 2701-2715 (2009).
183. Bruno, L. *et al.* Runx proteins regulate Foxp3 expression. *J Exp Med* **206**, 2329-2337 (2009).
184. Rudra, D. *et al.* Runx-CBFbeta complexes control expression of the transcription factor Foxp3 in regulatory T cells. *Nat Immunol* **10**, 1170-1177 (2009).
185. Kitoh, A. *et al.* Indispensable role of the Runx1-Cbfbeta transcription complex for in vivo-suppressive function of FoxP3+ regulatory T cells. *Immunity* **31**, 609-620 (2009).
186. Ono, M. *et al.* Foxp3 controls regulatory T-cell function by interacting with AML1/Runx1. *Nature* **446**, 685-689 (2007).
187. Josefowicz, S.Z., Lu, L.F. & Rudensky, A.Y. Regulatory T cells: mechanisms of differentiation and function. *Annu Rev Immunol* **30**, 531-564 (2012).
188. Huehn, J., Polansky, J.K. & Hamann, A. Epigenetic control of FOXP3 expression: the key to a stable regulatory T-cell lineage? *Nat Rev Immunol* **9**, 83-89 (2009).
189. Russel, J.S.a.D.W. Molecular Cloning, A Laboratory Manual. *Cold Spring Harbor Laboratory Press* **1-3** (2001).
190. Schmittgen, T.D. & Livak, K.J. Analyzing real-time PCR data by the comparative C(T) method. *Nat Protoc* **3**, 1101-1108 (2008).
191. Dephoure, N. & Gygi, S.P. A solid phase extraction-based platform for rapid phosphoproteomic analysis. *Methods* **54**, 379-386 (2011).

192. Cox, J. & Mann, M. MaxQuant enables high peptide identification rates, individualized p.p.b.-range mass accuracies and proteome-wide protein quantification. *Nat Biotechnol* **26**, 1367-1372 (2008).
193. Fontenot, J.D., Gavin, M.A. & Rudensky, A.Y. Foxp3 programs the development and function of CD4+CD25+ regulatory T cells. *Nat Immunol* **4**, 330-336 (2003).
194. Khattri, R., Cox, T., Yasayko, S.A. & Ramsdell, F. An essential role for Scurfin in CD4+CD25+ T regulatory cells. *Nat Immunol* **4**, 337-342 (2003).
195. Rudensky, A.Y. Regulatory T cells and Foxp3. *Immunol Rev* **241**, 260-268 (2011).
196. Apostolou, I., Sarukhan, A., Klein, L. & von Boehmer, H. Origin of regulatory T cells with known specificity for antigen. *Nat Immunol* **3**, 756-763 (2002).
197. Fontenot, J.D. *et al.* Regulatory T cell lineage specification by the forkhead transcription factor foxp3. *Immunity* **22**, 329-341 (2005).
198. Jordan, M.S. *et al.* Thymic selection of CD4+CD25+ regulatory T cells induced by an agonist self-peptide. *Nat Immunol* **2**, 301-306 (2001).
199. Mucida, D. *et al.* Oral tolerance in the absence of naturally occurring Tregs. *J Clin Invest* **115**, 1923-1933 (2005).
200. Abraham, R.T. & Weiss, A. Jurkat T cells and development of the T-cell receptor signalling paradigm. *Nat Rev Immunol* **4**, 301-308 (2004).
201. Dann, S.G., Selvaraj, A. & Thomas, G. mTOR Complex1-S6K1 signaling: at the crossroads of obesity, diabetes and cancer. *Trends Mol Med* **13**, 252-259 (2007).
202. Wullschleger, S., Loewith, R. & Hall, M.N. TOR signaling in growth and metabolism. *Cell* **124**, 471-484 (2006).
203. Ballou, L.M., Jeno, P. & Thomas, G. Protein phosphatase 2A inactivates the mitogen-stimulated S6 kinase from Swiss mouse 3T3 cells. *J Biol Chem* **263**, 1188-1194 (1988).
204. Petritsch, C., Beug, H., Balmain, A. & Oft, M. TGF-beta inhibits p70 S6 kinase via protein phosphatase 2A to induce G(1) arrest. *Genes Dev* **14**, 3093-3101 (2000).
205. Augustine, J.J., Bodziak, K.A. & Hricik, D.E. Use of sirolimus in solid organ transplantation. *Drugs* **67**, 369-391 (2007).
206. Guertin, D.A. & Sabatini, D.M. Defining the role of mTOR in cancer. *Cancer Cell* **12**, 9-22 (2007).
207. Sarbassov, D.D., Guertin, D.A., Ali, S.M. & Sabatini, D.M. Phosphorylation and regulation of Akt/PKB by the rictor-mTOR complex. *Science* **307**, 1098-1101 (2005).
208. Lamouille, S., Connolly, E., Smyth, J.W., Akhurst, R.J. & Derynck, R. TGF-beta-induced activation of mTOR complex 2 drives epithelial-mesenchymal transition and cell invasion. *J Cell Sci* **125**, 1259-1273 (2012).
209. Andrabi, S., Gjoerup, O.V., Kean, J.A., Roberts, T.M. & Schaffhausen, B. Protein phosphatase 2A regulates life and death decisions via Akt in a context-dependent manner. *Proc Natl Acad Sci U S A* **104**, 19011-19016 (2007).
210. Chen, W., Arroyo, J.D., Timmons, J.C., Possemato, R. & Hahn, W.C. Cancer-associated PP2A Aalpha subunits induce functional haploinsufficiency and tumorigenicity. *Cancer Res* **65**, 8183-8192 (2005).
211. Rodgers, J.T., Vogel, R.O. & Puigserver, P. Clk2 and B56beta mediate insulin-regulated assembly of the PP2A phosphatase holoenzyme complex on Akt. *Mol Cell* **41**, 471-479 (2011).
212. Tato, I., Bartrons, R., Ventura, F. & Rosa, J.L. Amino acids activate mammalian target of rapamycin complex 2 (mTORC2) via PI3K/Akt signaling. *J Biol Chem* **286**, 6128-6142 (2010).
213. Karin, M., Liu, Z. & Zandi, E. AP-1 function and regulation. *Curr Opin Cell Biol* **9**, 240-246 (1997).

214. Vartanian, R. *et al.* AP-1 regulates cyclin D1 and c-MYC transcription in an AKT-dependent manner in response to mTOR inhibition: role of AIP4/Itch-mediated JUNB degradation. *Mol Cancer Res* **9**, 115-130 (2010).
215. Xu, L., Kitani, A. & Strober, W. Molecular mechanisms regulating TGF-beta-induced Foxp3 expression. *Mucosal Immunol* **3**, 230-238 (2010).
216. Peng, D.J. *et al.* Noncanonical K27-linked polyubiquitination of TIEG1 regulates Foxp3 expression and tumor growth. *J Immunol* **186**, 5638-5647 (2011).
217. Yang, X.X.O. *et al.* STAT3 regulates cytokine-mediated generation of inflammatory helper T cells. *Journal of Biological Chemistry* **282**, 9358-9363 (2007).
218. Chen, Z. *et al.* Selective regulatory function of Socs3 in the formation of IL-17-secreting T cells. *Proceedings of the National Academy of Sciences of the United States of America* **103**, 8137-8142 (2006).
219. Levy, D.E. & Darnell, J.E. STATs: Transcriptional control and biological impact. *Nature Reviews Molecular Cell Biology* **3**, 651-662 (2002).
220. Bowman, T., Garcia, R., Turkson, J. & Jove, R. STATs in oncogenesis. *Oncogene* **19**, 2474-2488 (2000).
221. Zhou, L. *et al.* TGF-beta-induced Foxp3 inhibits T(H)17 cell differentiation by antagonizing ROR gamma t function. *Nature* **453**, 236-U214 (2008).
222. Kim, J.H., Yoon, M.S. & Chen, J. Signal Transducer and Activator of Transcription 3 (STAT3) Mediates Amino Acid Inhibition of Insulin Signaling through Serine 727 Phosphorylation. *Journal of Biological Chemistry* **284**, 35425-35432 (2009).
223. Yokogami, K., Wakisaka, S., Avruch, J. & Reeves, S.A. Serine phosphorylation and maximal activation of STAT3 during CNTF signaling is mediated by the rapamycin target mTOR. *Current Biology* **10**, 47-50 (2000).
224. Xu, D. & Qu, C.K. Protein tyrosine phosphatases in the JAK/STAT pathway. *Frontiers in Bioscience* **13**, 4925-4932 (2008).
225. O'Shea, J.J., Gadina, M. & Schreiber, R.D. Cytokine signaling in 2002: New surprises in the Jak/Stat pathway. *Cell* **109**, S121-S131 (2002).
226. Palmer, D.C. & Restifo, N.P. Suppressors of cytokine signaling (SOCS) in T cell differentiation, maturation, and function. *Trends in Immunology* **30**, 592-602 (2009).
227. Croker, B.A. *et al.* SOCS3 negatively regulates IL-6 signaling in vivo. *Nature Immunology* **4**, 540-545 (2003).
228. Park, Y.J. *et al.* SOCS1 induced by NDRG2 expression negatively regulates STAT3 activation in breast cancer cells. *Biochemical and Biophysical Research Communications* **363**, 361-367 (2007).
229. Fujimoto, M. *et al.* Defective thymocyte development and perturbed homeostasis of T cells in STAT-induced STAT inhibitor-1/suppressors of cytokine signaling-1 transgenic mice. *J Immunol* **165**, 1799-1806 (2000).
230. Shen, Y.H., La Perle, K.M.D., Levy, D.E. & Darnell, J.E. Reduced STAT3 activity in mice mimics clinical disease syndromes. *Biochemical and Biophysical Research Communications* **330**, 305-309 (2005).
231. Shen, Y. *et al.* Essential role of STAT3 in postnatal survival and growth revealed by mice lacking STAT3 serine 727 phosphorylation. *Mol Cell Biol* **24**, 407-419 (2004).
232. Kaptein, A., Paillard, V. & Saunders, M. Dominant negative stat3 mutant inhibits interleukin-6-induced Jak-STAT signal transduction. *J Biol Chem* **271**, 5961-5964 (1996).
233. Bromberg, J.F., Horvath, C.M., Besser, D., Lathem, W.W. & Darnell, J.E., Jr. Stat3 activation is required for cellular transformation by v-src. *Mol Cell Biol* **18**, 2553-2558 (1998).
234. Bromberg, J.F. *et al.* Stat3 as an oncogene. *Cell* **98**, 295-303 (1999).

235. Couper, K.N. *et al.* IL-10 from CD4CD25Foxp3CD127 adaptive regulatory T cells modulates parasite clearance and pathology during malaria infection. *PLoS Pathog* **4**, e1000004 (2008).
236. Sekiya, T. *et al.* The nuclear orphan receptor Nr4a2 induces Foxp3 and regulates differentiation of CD4+ T cells. *Nat Commun* **2**, 269 (2011).
237. Han, S., Wang, G., Qi, X., Englander, E.W. & Greeley, G.H., Jr. Involvement of a Stat3 binding site in inflammation-induced enteric apelin expression. *Am J Physiol Gastrointest Liver Physiol* **295**, G1068-1078 (2008).
238. Jiang, H. & English, A.M. Quantitative analysis of the yeast proteome by incorporation of isotopically labeled leucine. *J Proteome Res* **1**, 345-350 (2002).
239. Ong, S.E. *et al.* Stable isotope labeling by amino acids in cell culture, SILAC, as a simple and accurate approach to expression proteomics. *Mol Cell Proteomics* **1**, 376-386 (2002).
240. Ong, S.E., Kratchmarova, I. & Mann, M. Properties of 13C-substituted arginine in stable isotope labeling by amino acids in cell culture (SILAC). *J Proteome Res* **2**, 173-181 (2003).
241. Zhu, H., Pan, S., Gu, S., Bradbury, E.M. & Chen, X. Amino acid residue specific stable isotope labeling for quantitative proteomics. *Rapid Commun Mass Spectrom* **16**, 2115-2123 (2002).
242. Amanchy, R., Kalume, D.E., Iwahori, A., Zhong, J. & Pandey, A. Phosphoproteome analysis of HeLa cells using stable isotope labeling with amino acids in cell culture (SILAC). *J Proteome Res* **4**, 1661-1671 (2005).
243. Beausoleil, S.A. *et al.* Large-scale characterization of HeLa cell nuclear phosphoproteins. *Proc Natl Acad Sci U S A* **101**, 12130-12135 (2004).
244. Huttlin, E.L. *et al.* A tissue-specific atlas of mouse protein phosphorylation and expression. *Cell* **143**, 1174-1189 (2010).
245. Olsen, J.V. *et al.* Global, in vivo, and site-specific phosphorylation dynamics in signaling networks. *Cell* **127**, 635-648 (2006).
246. Thelemann, A. *et al.* Phosphotyrosine signaling networks in epidermal growth factor receptor overexpressing squamous carcinoma cells. *Mol Cell Proteomics* **4**, 356-376 (2005).
247. Brockmeyer, C. *et al.* T cell receptor (TCR)-induced tyrosine phosphorylation dynamics identifies THEMIS as a new TCR signalosome component. *J Biol Chem* **286**, 7535-7547 (2010).
248. Kim, H.J., Song, E.J. & Lee, K.J. Proteomic analysis of protein phosphorylations in heat shock response and thermotolerance. *J Biol Chem* **277**, 23193-23207 (2002).
249. Maguire, P.B. *et al.* Identification of the phosphotyrosine proteome from thrombin activated platelets. *Proteomics* **2**, 642-648 (2002).
250. Steen, H., Kuster, B., Fernandez, M., Pandey, A. & Mann, M. Tyrosine phosphorylation mapping of the epidermal growth factor receptor signaling pathway. *J Biol Chem* **277**, 1031-1039 (2002).
251. Gronborg, M. *et al.* A mass spectrometry-based proteomic approach for identification of serine/threonine-phosphorylated proteins by enrichment with phospho-specific antibodies: identification of a novel protein, Frigg, as a protein kinase A substrate. *Mol Cell Proteomics* **1**, 517-527 (2002).
252. Andersson, L. & Porath, J. Isolation of phosphoproteins by immobilized metal (Fe3+) affinity chromatography. *Anal Biochem* **154**, 250-254 (1986).
253. Neville, D.C. *et al.* Evidence for phosphorylation of serine 753 in CFTR using a novel metal-ion affinity resin and matrix-assisted laser desorption mass spectrometry. *Protein Sci* **6**, 2436-2445 (1997).

254. Ikeguchi, Y. & Nakamura, H. Determination of organic phosphates by column-switching high performance anion-exchange chromatography using on-line preconcentration on titania. *Analytical Sciences* **13**, 479-483 (1997).
255. Ikeguchi, Y. & Nakamura, H. Selective enrichment of phospholipids by titania. *Analytical Sciences* **16**, 541-543 (2000).
256. Pinkse, M.W.H., Uitto, P.M., Hilhorst, M.J., Ooms, B. & Heck, A.J.R. Selective isolation at the femtomole level of phosphopeptides from proteolytic digests using 2D-nanoLC-ESI-MS/MS and titanium oxide precolumns. *Analytical Chemistry* **76**, 3935-3943 (2004).
257. Wolf-Yadlin, A., Hautaniemi, S., Lauffenburger, D.A. & White, F.M. Multiple reaction monitoring for robust quantitative proteomic analysis of cellular signaling networks. *Proceedings of the National Academy of Sciences of the United States of America* **104**, 5860-5865 (2007).
258. Nuhse, T.S., Stensballe, A., Jensen, O.N. & Peck, S.C. Large-scale analysis of in vivo phosphorylated membrane proteins by immobilized metal ion affinity chromatography and mass spectrometry. *Molecular & Cellular Proteomics* **2**, 1234-1243 (2003).
259. Gruhler, A. *et al.* Quantitative phosphoproteomics applied to the yeast pheromone signaling pathway. *Molecular & Cellular Proteomics* **4**, 310-327 (2005).
260. Villen, J., Beausoleil, S.A., Gerber, S.A. & Gygi, S.P. Large-scale phosphorylation analysis of mouse liver. *Proceedings of the National Academy of Sciences of the United States of America* **104**, 1488-1493 (2007).
261. Rigbolt, K.T.G. *et al.* System-Wide Temporal Characterization of the Proteome and Phosphoproteome of Human Embryonic Stem Cell Differentiation. *Science Signaling* **4** (2011).
262. Yu, Y.H. *et al.* Phosphoproteomic Analysis Identifies Grb10 as an mTORC1 Substrate That Negatively Regulates Insulin Signaling. *Science* **332**, 1322-1326 (2011).
263. Wilson-Grady, J.T., Villen, J. & Gygi, S.P. Phosphoproteome analysis of fission yeast. *Journal of Proteome Research* **7**, 1088-1097 (2008).
264. Villen, J. & Gygi, S.P. The SCX/IMAC enrichment approach for global phosphorylation analysis by mass spectrometry. *Nature Protocols* **3**, 1630-1638 (2008).
265. Thingholm, T.E. & Larsen, M.R. TiMAC - A new phosphoproteomic strategy for the separation of mono-from multiply phosphorylated peptides combined with optimized tandem MS mass spectrometric analysis. *Molecular & Cellular Proteomics* **6**, 34-34 (2007).
266. Hsu, P.P. *et al.* The mTOR-regulated phosphoproteome reveals a mechanism of mTORC1-mediated inhibition of growth factor signaling. *Science* **332**, 1317-1322 (2011).
267. Okamura, H. *et al.* Concerted dephosphorylation of the transcription factor NFAT1 induces a conformational switch that regulates transcriptional activity. *Mol Cell* **6**, 539-550 (2000).
268. Liu, B., Tahk, S., Yee, K.M., Fan, G. & Shuai, K. The ligase PIAS1 restricts natural regulatory T cell differentiation by epigenetic repression. *Science* **330**, 521-525 (2010).
269. Mizushima, N. The role of the Atg1/ULK1 complex in autophagy regulation. *Curr Opin Cell Biol* **22**, 132-139 (2010).
270. Wu, M.Y., Eldin, K.W. & Beaudet, A.L. Identification of chromatin remodeling genes Arid4a and Arid4b as leukemia suppressor genes. *J Natl Cancer Inst* **100**, 1247-1259 (2008).
271. Xiong, Y. *et al.* Polycomb antagonizes p300/CBP associated factor (PCAF) to silence FOXP3 in a Kruppel like factor (KLF)-dependent manner. *J Biol Chem* (2012).
272. Liu, Q., Thoreen, C., Wang, J., Sabatini, D. & Gray, N.S. mTOR Mediated Anti-Cancer Drug Discovery. *Drug Discov Today Ther Strateg* **6**, 47-55 (2009).

273. Ma, J., Ding, Y., Fang, X., Wang, R. & Sun, Z. Protein kinase C-theta inhibits inducible regulatory T cell differentiation via an AKT-Foxo1/3a-dependent pathway. *J Immunol* **188**, 5337-5347 (2012).
274. Buckner, J.H. Mechanisms of impaired regulation by CD4(+)CD25(+)FOXP3(+) regulatory T cells in human autoimmune diseases. *Nat Rev Immunol* **10**, 849-859 (2010).
275. Martin, F., Ladoire, S., Mignot, G., Apetoh, L. & Ghiringhelli, F. Human FOXP3 and cancer. *Oncogene* **29**, 4121-4129 (2010).
276. Acuto, O. & Michel, F. CD28-mediated co-stimulation: a quantitative support for TCR signalling. *Nat Rev Immunol* **3**, 939-951 (2003).
277. Acuto, O., Di Bartolo, V. & Michel, F. Tailoring T-cell receptor signals by proximal negative feedback mechanisms. *Nat Rev Immunol* **8**, 699-712 (2008).
278. Soligo, M. *et al.* CD28 costimulation regulates FOXP3 in a RelA/NF-kappaB-dependent mechanism. *Eur J Immunol* **41**, 503-513 (2011).
279. Constant, S.L. & Bottomly, K. Induction of Th1 and Th2 CD4+ T cell responses: the alternative approaches. *Annu Rev Immunol* **15**, 297-322 (1997).
280. Iezzi, G., Scotet, E., Scheidegger, D. & Lanzavecchia, A. The interplay between the duration of TCR and cytokine signaling determines T cell polarization. *European Journal of Immunology* **29**, 4092-4101 (1999).
281. Purvis, H.A. *et al.* Low-strength T-cell activation promotes Th17 responses. *Blood* **116**, 4829-4837 (2010).
282. Ichiyama, K. *et al.* Foxp3 inhibits ROR gamma t-mediated IL-17A mRNA transcription through direct interaction with ROR gamma t. *Journal of Biological Chemistry* **283**, 17003-17008 (2008).
283. Zhang, F.P., Meng, G.X. & Strober, W. Interactions among the transcription factors Runx1, ROR gamma t and Foxp3 regulate the differentiation of interleukin 17-producing T cells (vol 9, pg 1297, 2008). *Nature Immunology* **10**, 223-223 (2009).
284. Bernardo, D. *et al.* T-cell proliferation and forkhead box P3 expression in human T cells are dependent on T-cell density: physics of a confined space? *Human Immunology* **73**, 223-231 (2012).
285. Fox, C.J., Hammerman, P.S. & Thompson, C.B. The Pim kinases control rapamycin-resistant T cell survival and activation. *J Exp Med* **201**, 259-266 (2005).
286. Liu, Z. *et al.* Deletion of CD98 Heavy Chain in T Cells Results in Cardiac Allograft Acceptance by Increasing Regulatory T Cells. *Transplantation* **93**, 1116-1124 (2012).
287. Chen, W., Liang, X., Peterson, A.J., Munn, D.H. & Bruce, B.R. The indoleamine 2,3-dioxygenase pathway is essential for human plasmacytoid dendritic cell-induced adaptive T regulatory cell generation. *Blood* **110**, 404a-405a (2007).
288. Chung, D.J. *et al.* Indoleamine 2,3-dioxygenase-expressing mature human monocyte-derived dendritic cells expand potent autologous regulatory T cells. *Blood* **114**, 555-563 (2009).
289. Hill, M. *et al.* IDO expands human CD4(+)CD25(high) regulatory T cells by promoting maturation of LPS-treated dendritic cells. *European Journal of Immunology* **37**, 3054-3062 (2007).
290. Manches, O. *et al.* HIV-activated human plasmacytoid DCs induce Tregs through an indoleamine 2,3-dioxygenase-dependent mechanism. *Journal of Clinical Investigation* **118**, 3431-3439 (2008).
291. Mellor, A.L. *et al.* Specific subsets of murine dendritic cells acquire potent T cell regulatory functions following CTLA4-mediated induction of indoleamine 2,3 dioxygenase. *International Immunology* **16**, 1391-1401 (2004).
292. Munn, D.H. *et al.* Inhibition of T cell proliferation by macrophage tryptophan catabolism. *Journal of Experimental Medicine* **189**, 1363-1372 (1999).

293. von Bubnoff, D. *et al.* Fc epsilon RI induces the tryptophan degradation pathway involved in regulating T cell responses. *Journal of Immunology* **169**, 1810-1816 (2002).
294. Stockwell, B.R. & Schreiber, S.L. TGF-beta-signaling with small molecule FKBP12 antagonists that bind myristoylated FKBP12-TGF-beta type I receptor fusion proteins. *Chemistry & Biology* **5**, 385-395 (1998).
295. Wang, T.W. *et al.* The immunophilin FKBP12 functions as a common inhibitor of the TGF beta family type I receptors. *Cell* **86**, 435-444 (1996).
296. Song, K.Y., Wang, H., Krebs, T.L. & Danielpour, D. Novel roles of Akt and mTOR in suppressing TGF-beta/ALK5-mediated Smad3 activation. *Embo Journal* **25**, 58-69 (2006).
297. Foster, D.A. Regulation of mTOR by phosphatidic acid? *Cancer Research* **67**, 1-4 (2007).
298. Josefowicz, S.Z. *et al.* Extrathymically generated regulatory T cells control mucosal T(H)2 inflammation. *Nature* **482**, 395-U1510 (2012).
299. Samstein, R.M., Josefowicz, S.Z., Arvey, A., Treuting, P.M. & Rudensky, A.Y. Extrathymic Generation of Regulatory T Cells in Placental Mammals Mitigates Maternal-Fetal Conflict. *Cell* **150**, 29-38 (2012).
300. Andersen, K.G., Nissen, J.K. & Betz, A.G. Comparative Genomics Reveals Key Gain-of-Function Events in Foxp3 during Regulatory T Cell Evolution. *Front Immunol* **3**, 113 (2012).
301. Trowsdale, J. & Betz, A.G. Mother's little helpers: mechanisms of maternal-fetal tolerance. *Nature Immunology* **7**, 241-246 (2006).
302. Kropf, P. *et al.* Arginase activity mediates reversible T cell hyporesponsiveness in human pregnancy. *Eur J Immunol* **37**, 935-945 (2007).
303. Cathomen, T. & Joung, J.K. Zinc-finger nucleases: the next generation emerges. *Mol Ther* **16**, 1200-1207 (2008).
304. Shalek, A.K. *et al.* Vertical silicon nanowires as a universal platform for delivering biomolecules into living cells. *Proc Natl Acad Sci U S A* **107**, 1870-1875 (2010).